Orpheus

Life on Venus?

Group 11

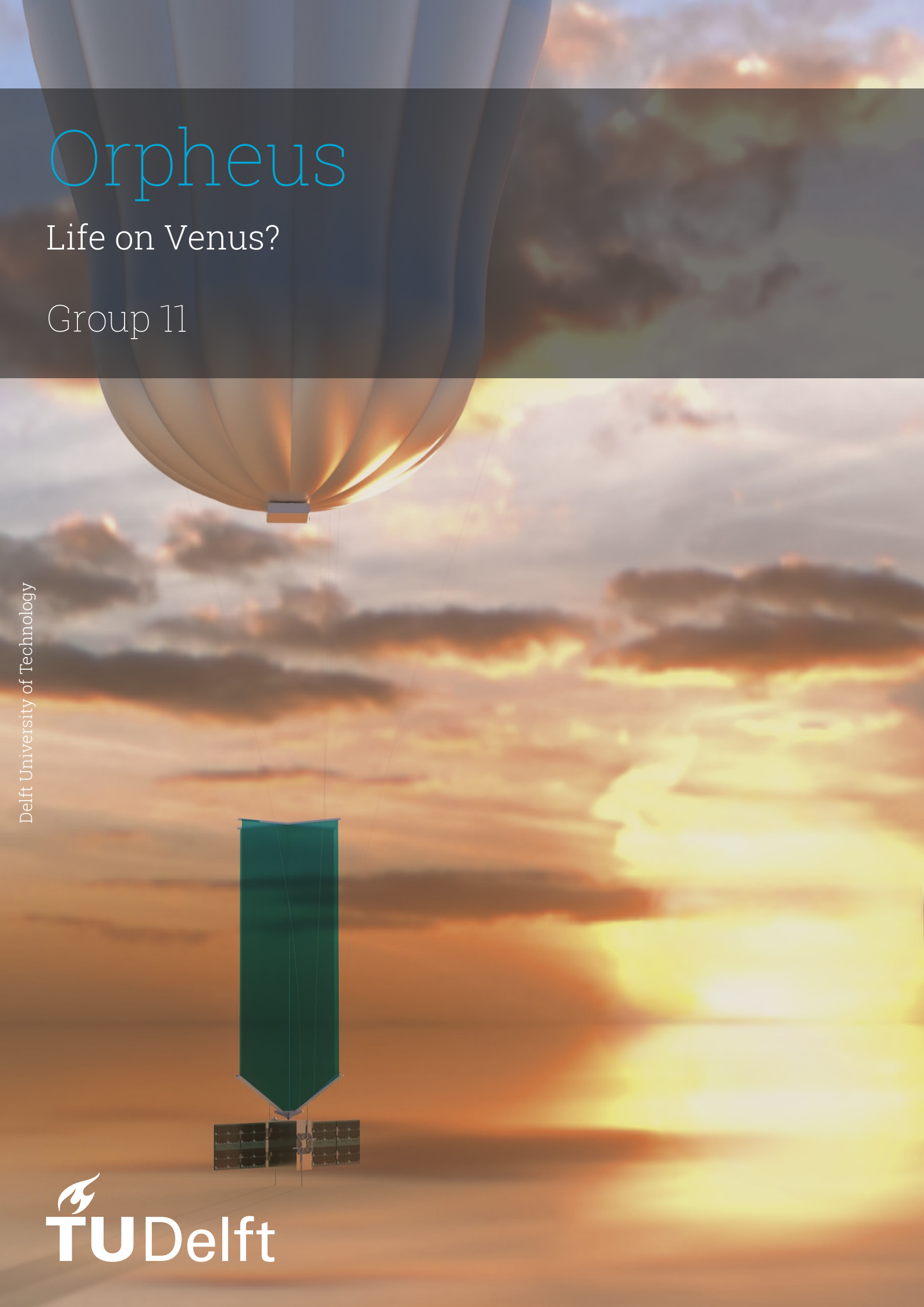

Delft University of Technology

TU Delft

Orpheus

Life on Venus?

by

Group 11

Student Name	Student Number
Alphan Umman	5691869
Carla Alcántara Collado	5698405
Carlos Pérez Bravo	5693829
Firine Bugenhagen	5720214
Giulio Ruiz de Cardenas	5698073
Peter de Mandt	5777925
Thijs van den Heuvel	5593174
Tristan Souillart	5713366
Ward Depoorter	5760089
Wout Schaerlaecken	5780802

Principle Tutor:	Sijme-Jan Paardekoper
Expert:	Niels Ligterink
Coaches:	Johannes Algera, Aneek Chakraborty
Project duration:	April 2025-June 2025
Faculty:	Faculty of Aerospace Engineering, Delft
Cover:	Own work

TU Delft

Executive Overview

Mission Motivation & Goal

Many interplanetary missions with the goal of finding extraterrestrial life have been conducted in the past and more are planned for the future. However, a key gap remains: no long-duration mission has yet explored the clouds of Venus, despite this environment being a promising location to search for signs of life. Orpheus addresses this market gap with the following project objective statement:

"Design a mission from launch to end-of-life to deploy the LMC_{OOL} in the Venusian clouds at an altitude of 40-60 km and detect signs of potential life, by 10 students in 10 weeks."

The mission is defined by the primary payload, the Origin of Life Marker Chip LMC_{OOL}. The integrated photonic biosensor is a lab-on-a-chip instrument for detecting the presence of chemicals. In the Orpheus Mission it is used to analyse samples from the sulphuric acid clouds for a total of 40 different functional groups and biomarkers. The targeted molecules—including amino acids, nucleobases, lipids, and polycyclic aromatic hydrocarbons— were chosen because they serve as fundamental building blocks for life as we know it and they are capable of surviving Venus' harsh cloud environment. These characteristics make them ideal candidates to provide evidence for the proof of the existence of life within Venus.

A secondary payload, a gas sensor array, is used to complement LMC_{OOL} analysis that is based on liquid samples.

Mission Overview

The mission includes a probe operating in the Venusian clouds. It consists of a gondola with the scientific payload, supported by a variable altitude balloon. A spacecraft is designed for transfer to Venus and communication between the probe and Earth.

Concept Selection

During the previously conducted conceptual design phase, several design options were explored to complete the mission objectives [1]. A trade-off analysis was performed between four feasible concepts: a variable-altitude balloon, a swarm of falling capsules, a glider and a spaceplane. The variable-altitude balloon was selected and is now the focus of the detailed design phase. Its key advantages are its reliability and wide horizontal coverage.

Mission Timeline

The mission time line includes a design and assembly phase until the launch on the 06.12.2032, provided by the Rocket Factory Augsburg (RFA). The launcher will provide an insertion burn into the transfer orbit. Transfer from Earth to Venus takes 160 days. At Venus, the entry capsule with the probe will separate from the spacecraft and enter the Venusian atmosphere, while the spacecraft conducts an insertion burn into an orbit around Venus. The spacecraft acts as a relay station from the probe to the ESTRACK deep space ground system on Earth. The entry capsule releases the probe and the balloon is deployed. The scientific mission on Venus lasts at least 49 days, circling Venus multiple times with the help of strong atmospheric winds. Once the probe stops operating, end of life procedures are conducted. An overview of the mission operation is shown in Figure 1.

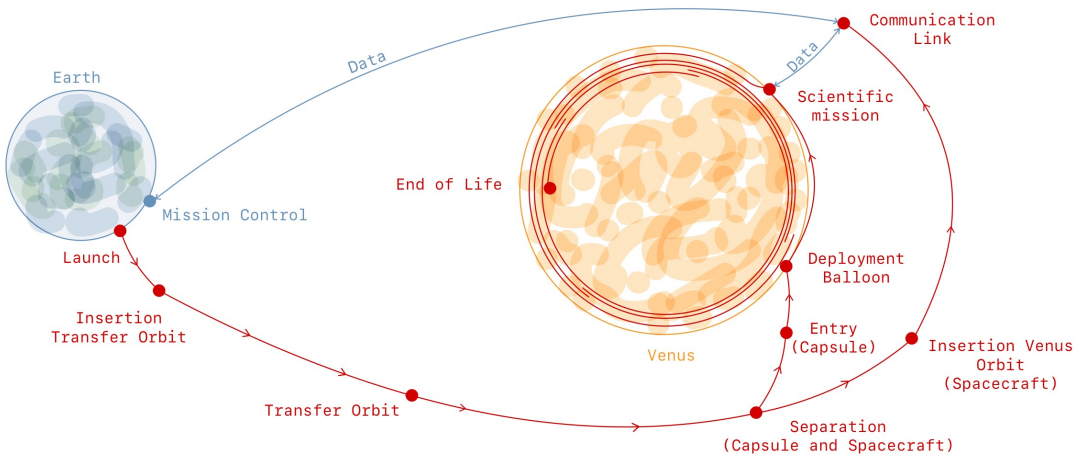

Figure 1: Mission overview.

Sustainability Approach

The sustainable development strategy addresses environmental and societal sustainability, planetary protection, and enforcement. For environmental sustainability materials are selected carefully. However, essential materials such as helium, batteries, and PTFE are required due to their unique properties, despite their negative environmental impact. The launch poses one of the main environmental impacts. The chosen launch provider, RFA, pursues a strong sustainability policy. Planetary protection is ensured by following COSPAR guidelines. Societal sustainability is supported through fair production practices and alignment with the European Autonomy Strategy. All measures are overseen by the sustainability and life-cycle officers.

Journey to Venus

The journey to Venus includes the launcher selection, transfer orbit, spacecraft design and entry into the Venusian atmosphere.

Launcher and Astrodynamic Characteristics

The launcher selected is the RFA One, complying with the European Autonomy Strategy. Its main advantage is the low launch costs of 3M EUR. The transfer trajectory from Earth to Venus is optimized to minimize the ΔV needed for the spacecraft insertion burn into Venus orbit. The optimal trajectory requires a launcher ΔV of 3.32 $km \cdot s^{-1}$ and a spacecraft ΔV of 1.39 $km \cdot s^{-1}$. The preferred launch date is the 06.12.2032, but the spacecraft is designed such that a launch window is available approximately every two years.

The target orbit of the spacecraft around Venus has a pericenter at an altitude of 300 km and an apocentre at 20,000 km that lies on the line connecting Venus with the sun. The high eccentricity and orbit orientation allows for optimal communication and power production properties and reduces the ΔV budget.

Spacecraft Design

The main functions of the spacecraft are the transport of the probe to Venus and to enable communication between the probe and Earth. A model of the spacecraft is shown in Figure 2.

The Attitude Determination and Control System (ADCS) consists of six sun sensors, three rate gyros and 12 thrusters (10 N) to enable 3-axis-control. The main propulsion system used for the insertion burn consists of a single 200 N thruster. All thrusters use the same bi-propellant, Hydrazine and Oxides of Nitrogen. The thermal system is mainly passive, using Multi-Layer Insulation (MLI). The propellant tanks require active thermal patches during transfer. The power system of the spacecraft

consists of a solar array with secondary batteries for operation during eclipse. For communication with Earth a high-gain antenna and a low-gain antenna are selected for transmitting and receiving, respectively. Communication with the probe is supported by a low-gain patch antenna. A performance overview of the spacecraft is given in Figure 1.

Characteristic	Value
ADCS	
Pointing accuracy	0.5 °
Propulsion	
Max. Thrust	200 N
ΔV	1.84 $km \cdot s^{-1}$
Thermal system	
Passive temperature range	$-20.9°C$ to $23.1°C$
Power	
Peak Solar Power (1 AU)	66 W
Energy storage	30 Wh
Communication	
Downlink data rate (to probe)	2900 bit/s
Downlink data rate (to Earth)	1400 bit/s

Table 1: Performance analysis of the spacecraft.

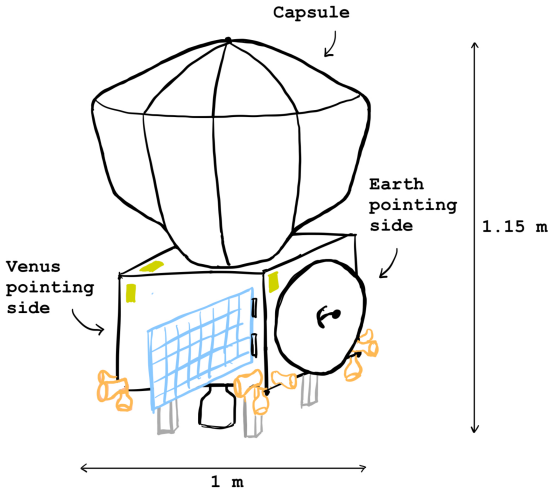

Figure 2: Spacecraft model.

Entry and Balloon Deployment

In order to safely deploy the probe into the atmosphere, it is housed in an atmospheric entry capsule. A trajectory is carefully planned out and the mechanical loads that the probe subsystems have to be able to survive are assessed. To survive the intense heat of entry, a heat shield made of PICA is installed. After the main deceleration phase is over, parachutes are deployed from the capsule and a deployment sequence is set in motion in order to inflate the balloon within an allowed altitude range, and remove all unnecessary hardware afterward.

Probe Design

Once the deployment sequence has been carried out successfully, the probe, consisting of the balloon and the gondola, will float through the Venusian clouds and carry out the operations. A performance analysis of the probe is given in Figure 2.

Figure 3: Balloon render.

Gondola

The gondola is a Cubesat-like pressurize cuboid with dimensions of $20 \times 20 \times 10\ cm$. It is made out of Ti-6Al-4V and it houses the scientific payload, batteries, and communication and data handling system components. Power is provided by solar panels during the day and secondary batteries during eclipse. The entire gondola, including solar panels and supporting structure, is coated in Teflon® in order to resist the harsh sulphuric acid environment. Figure 4 provides a render of the gondola with one of the sidepanels removed showing the layout of the gondola. The LMC_{OOL} assembly can be seen in the top left unit, the transceiver together with the Command and Data Handling (C&DH) subsystem below and on the bottom right the battery system is located.

Variable-Altitude Balloon

The variable altitude balloon controls the operational height of the gondola between 50 and 55.5 km, allowing collection of samples in a wide range of altitudes. Cruising along the Venusian winds, the

balloon will circumnavigate Venus roughly 8 times over the 49 day mission duration. A render of the balloon accompanied by the gondola can be seen in Figure 3.

Characteristic	Value
Power	
Peak Solar Power (55 km, noon)	80 W
Energy storage	100 Wh
Communication	
Uplink data rate (to spacecraft)	2900 bit/s
Altitude Control	
Altitude range	50-55.5 km
Ascent time	12 hours
Descent time	10 hours
Lifetime	58 days

Table 2: Performance analysis of the probe.

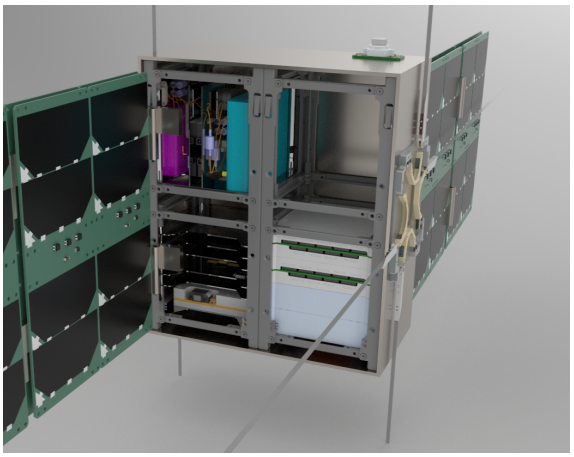

Figure 4: 3D render of the probe, it will be sealed, but it is open to show the internal configuration.

In Figure 2, the ascent and descent time refer to the time that the balloon needs to go up or down through the whole operating altitude range. It can also be noted that the lifetime is 58 days, whereas the mission duration is only 49 days. This is due to the fact that the balloon can still float within the operating range at 58 days, but is not controllable and becomes unstable when it is nearing the end of its lifetime.

Instrument Design and Operation

The instrument design includes the primary payload, consisting of LMC_{OOL} and the sampling system, and the secondary payload, including a camera and a gas sensor array.

An optimised scientific timeline is established and the four payload subsystems are designed: the Sampling System, Microfluidic Network, LMC_{OOL} Assembly, and Secondary Payloads.

Scientific Operations Timeline

To deliver the best scientific data, the balloon path is optimised with a script which aims to maximise the number and diversity of samples, all while aligning with power constraints that forbid low altitude flights during the Venusian night. This culminates in the scientific operations timeline shown in Figure 5.

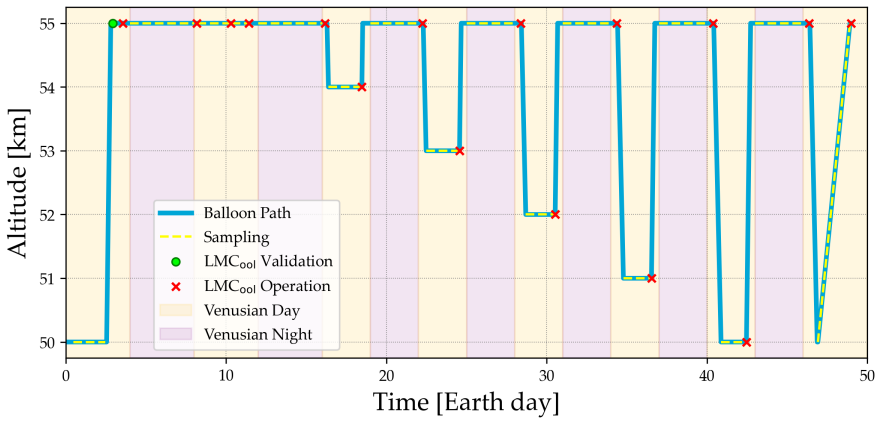

Figure 5: Timeline of scientific operations.

After validating the LMC_{OOL} instrument in-situ, the scientific mission starts by securing two clean, uncontaminated samples at the boundaries of the flight envelope, one at 50 km during the day and one at 55 km during the night. Following this, targeted sampling at specific altitudes is conducted over six days, providing insight into the vertical distribution of Venus' atmospheric composition. Finally, a concluding sample is acquired during one last ascent, capturing the complete spectral profile of the atmosphere's composition.

Instruments Design

The Sampling System consists of a mesh which can passively capture sulphuric acid aerosols from the Venusian environment, without altering their chemical composition. Strategically placed on the cable connecting the balloon with the gondola, it can achieve a sampling rate of $1mL$ per day. The collected samples coalesce and trickle down the mesh towards the gondola, where they are secured by a funnel. The strength of this system lies in its integrated design which makes it the perfect passive collector, allowing it to sample even during the night.

The Microfluidic Network safely carries the collected sample to the LMC_{OOL}. It consists of a loading chamber, a validating chamber, a disposal tank, and the LMC_{OOL} Assembly, who are all connected together in a redundant fluidic architecture. This compact, lightweight, low-power and cost-effective design fits in a $10 \times 10 \times 10cm^3$ CubeSat, making it a reusable design ready to operate in any relevant mission.

At the heart of the Microfluidic Network sits the LMC_{OOL} Assembly. It comprises of a Peltier Thermoelectric Cooler and an Aerogel Thermal Barrier, acting like a small fridge, and protecting 16 LMC_{OOL} chips from the harsh Venusian temperatures. In this secure environment, the immunoassay science can safely operate. Over the course of 49 days, 16 samples from 6 different altitudes are tested and cross-checked. All raw data, sampled at 0.5 Hz, is sent back to Earth without any loss. This complete mission architecture will unambiguously answer the controversial question of life on our sister planet, and could pave the way for future extraterrestrial life-seeking strategies.

Mission Performance

The mission performance evaluates the Orpheus mission's compliance with requirements, resource allocation, risk assessment, and RAMS (Reliability, Availability, Maintainability, and Safety) characteristics.

Mass budget

The total mission mass amounts to 118.14 kg, comprising 56.9 kg for the spacecraft, 39.6 kg for the entry capsule, and 21.6 kg for the probe.

Compliance with Requirements

The mission successfully meets nearly all of the technical and operational requirements established in the Baseline Report [2]. With conservative margins applied to each subsystem, the total mission mass amounts to **118.1** kg, well below the requirement of **320** kg. Preliminary cost estimates indicate total mission expenditures of approximately **€65M**, comfortably within the **€150M** budget constraint.

The following requirements are currently unmet and require further design efforts:

- Not all components align with the European Autonomy Strategy. It is proposed to accept this deviation and use European products and services where feasible.
- The targeted reliability of 95% has not yet been achieved. Additional testing, particularly of the LMC_{OOL} assembly and the sampling system, is necessary.
- The probe's batteries cannot operate in the temperature range of the gondola when operating in the Venusian atmosphere. Implementing an active temperature control system is a potential solution.

Sampling performance of the probe
During the scientific mission phase the sampling system collects a total of 49 ml of sulphuric acid, which is more than double the 20 ml requirement, whilst covering an altitude range between 50 and 55 km.

RAMS Analysis
The mission's RAMS (reliability, availability, maintainability, and safety) evaluation highlights both strengths and areas for improvement. While the total mission reliability of **75%** currently falls below the the target due to unvalidated components, the design incorporates redundancy in critical systems such as propulsion, communications, and pressure regulation to provide fault tolerance. Availability is ensured through contentious autonomous operations and the aforementioned redundancies. The safety protocols adhere to COSPAR Category II planetary protection standards to minimize contamination risks.

Risk analysis
The thorough risk assessment identifies potential failure modes throughout the missions operations, from manufacturing anomalies to Venus entry and scientific operations.The most critical risks, such as sampling system malfunctions and LMC_{OOL} performance degradation, are mitigated through redundancy, rigorous testing, and design improvements. Post-mitigation analysis confirms that no catastrophic risks remain.

Future Mission Development
The present report started the detailed design phase. Recommendations for the future mission development are given.

A critical part of the future plan is how the different systems of the mission are going to be manufactured. As this is an expensive process, off-the-shelf components will be used where possible to increase reliability and decrease cost. The spacecraft and the capsule are going to be assembled by TU Delft's own aerospace lab whilst outsourcing the production of the propulsion subsystem. The entry capsule provides a significant challenge, especially with the production of the toroidal helium tanks used for the balloons deployment, which requires the collaboration of a specialized firm MT Aerospace. The balloon manufacturing utilises techniques from similar NASA projects, especially concerning the bonding of acid-resistant materials. Regarding the LMC_{OOL} instrumentation, MIPs manufacturing and deposition require sequential functional monomers dispensing accompanied by laser photopolymerisation, which requires submicron precision.

Several critical areas require attention in future design phases. First, extensive balloon material testing must be conducted under Venusian conditions to verify performance. The pyrotechnic separation systems also need refinement to ensure reliable operation. Additionally, debris mitigation strategies should be developed along with detailed debris impact estimations. Finally, establishing industry and academic partnerships for specialized European-sourced components will be essential for mission success.

List of Symbols

Symbol	Description	Unit	Symbol	Description	Unit
A	Cross-sectional area	m^2	α	Solar absorptivity	–
A	Amplitude	$^\circ$	β	Sideslip angle	$^\circ$
B	Buoyancy	N	α	Angle of attack	$^\circ$
b	Width	m	ΔV	Velocity change	kms^{-1}
C	Heat capacity	JK^{-1}	ϵ	Emissivity	–
C_D	Drag coefficient	–	γ	Specific heat ratio	–
			γ	Flight path angle	$^\circ$
C_d	Discharge coefficient	–	ν	Poisson's ratio	–
C_m	Virtual mass coefficient	–	ϕ	Hoop angle	$^\circ$
D	Drag	N	μ	Gravitational parameter	m^3s^{-2}
d	Diameter	m	ρ	Density	kgm^{-3}
d	Distance from the sun	AU	σ	Stress	Pa
$\frac{d}{dt}$	Time derivative	–	σ	Stefan–Boltzmann constant	$Wm^{-2}K^{-4}$
E	Young's modulus	Pa	θ	Solar incidence angle	$^\circ$
E_b/N_0	Energy per bit to noise ratio	-	δ	Direction of rotation	$^\circ$
F	Force	N	η	Efficiency	–
g	Gravitational acceleration	ms^{-2}	–	–	–
h	Heat transfer coefficient	$Wm^{-2}K^{-1}$	–	–	–
h	height	m	-	-	-
I	Current	A	–	–	–
I_{sp}	Specific impulse	s	-	-	-
L	Length	m	–	–	–
m	Mass	kg	–	–	–
M	Molar mass	$kgmol^{-1}$	–	–	–
n	Amount	–	–	–	–
P	Power	W	–	–	–
P	Pressure	Pa	–	–	–
$\dot{Q}$	Heat flux	Wm^{-2}	–	–	–
Q^*	Heat of ablation	Jkg^{-1}	–	–	–
r	Cross-sectional radius	m	–	–	–
R	Radius	m	–	–	–
R	Ideal gas constant	$Jmol^{-1}K^{-1}$	–	–	–
Rx	Receiving	–	–	–	–
r	Reliability	–	–	–	–
S	Solar flux	Wm^{-2}	–	–	–
S	Surface area	m^2	–	–	–
$\dot{s}$	Heat shield recession rate	-	-	-	-
T	Temperature	K	–	–	–
t	Thickness	m	–	–	–
Tx	Transmitting	–	–	–	–
u	Rotational velocity	$^\circ\, s^{-1}$	-	-	-
V	Velocity	ms^{-1}	–	–	–
V	Voltage	V	–	–	–
V	Volume	m^3	–	–	–

List of Abbreviations

Abb.	Meaning	Abb.	Meaning
ADCS	Attitude Determination and Control System	aMZI	Asymmetric Mach-Zehnder Interferometer
LCA	Life Cycle Assessment	ESA	European Space Agency
AU	Astronomical Unit	LMC_{OOL}	Life Marker Chip (Origin of Life)
bps	bits per second	RNA	Ribonucleic acid
C&DH	Command and Data Handling	MIP	Molecular Imprinted Polymer
COSPAR	Committee on Space Research	MIT	Massachusetts Institute of Technology
DNA	Deoxyribonucleic acid	MLI	Multi-Layer Insulation
EIRP	Effective isotropic radiated power	FSK	Frequency Shift Keying
EMS	Environmental Management Systems	PAH	Polycyclic Aromatic Hydrocarbon
EoL	End of Life	PCB	Printed Circuit Board
EPS	Electrical Power System	PDCU	Power Distribution and Control Unit
FEA	Finite Element Analysis	PET	Polyethylene terephthalate
FEP	Fluorinated Ethylene Propylene	PFA	Perfluoroalkoxy Alkane
GCM	General circulation model	PFAS	Polyfluoroalkyl Substances
HMT	Hexamethylenetetramine	P&ID	Piping & Instrumentation Diagram
RAMS	Reliability, Availability, Maintainability, and Safety	PMD	Power management and distribution system
kbps	kilo bits per second	PPE	Personal Protective Equipment
GWP	Global Warming Potential	PRS	Pressure Regulation System
LMC	Life Marker Chip	PTFE	Polytetrafluoroethylene - Teflon®
LOD	Limit Of Detection	ppb	part per billion
R&D	Research and Development	IMU	Inertial Measurement Unit
EU	European Union	RFA	Rocket Factory Augsburg
VCSEL	Vertical Cavity Surface Emmitting Laser	NASA	National Aeronautics and Space Administration
RX	Receiving	SP	Superpressure
DSE	Design Synthesis Exercise	TRL	Technology Readiness Level
DSN	Deep Space Network	TX	Transmitting
DC	Direct Current	UTJ	Ultra Triple Junction
NTC	Negative Temperature Coefficient	UV	Ultra-violet
STEM	Science, Technology, Engineering and Mathematics	VIRA	Venus International Reference Atmosphere
CSG	Centre Spatial Guyanais	XTR	Extreme Temperature Resistant
TEC	Thermoelectric Cooler	ZP	Zeropressure
PICA	Phenolic-Impregnated Carbon Ablator	ESTEC	European Space Research and Technology Centre
FFD	Functional Flow Diagram	FBS	Functional Breakdown Structure
COTS	Commercial Off-The-Shelf	PEEK	Polyetheretherketone
LEO	Low Earth Orbit	MMH	Monomethyl hydrazine
MON	Mixed Oxides of Nitrogen	SMAD	Space Mission Analysis and Design
BER	Bit Error Rate	BPKS	Binary Phase Shift Keying
HPBW	Half-Power Beam Width	UHF	Ultra-High Frequency
HG	High Gain	LG	Low Gain
RF	Radio Frequency	CFD	Computational Fluid Dynamics
DOF	Degrees of Freedom	HEEET	Heatshield for Extreme Entry Environment Technology
PID	Proportional - Integral - Derivative	IC	Inflation Configuration

Table of Contents

1 Introduction

The possibility of life on Venus has been a topic of interest in the scientific community for many years. Past missions have demonstrated that the high temperature and pressure at the surface make the presence of life unrealistic. However, in the Venusian clouds, at altitudes between 40 and 60 km, the atmospheric pressure is similar to that on the surface of Earth. Additionally, temperatures in this region range from 0 to 50 ° [3], which has led researchers to consider the sulphuric acid clouds as a potentially habitable environment [4]. The objective of project Orpheus is to design a mission to deploy the Origin of Life Marker Chip LMC_{OOL} in the Venusian clouds and detect signs of potential life. LMC_{OOL} is an integrated photonic biosensor capable of detecting a range of biosignatures that might suggest the possibility of life, such as amino acids or DNA strands.

The aim of this report is to present a full mission design for project Orpheus, including launch, interplanetary flight, flight through the Venusian atmosphere, collection and transmission of scientific data and end-of-life operations. The main focus of the mission design is to support the scientific payload during operation in the clouds of Venus with a variable altitude balloon. This project is carried out as part of the Design Synthesis Exercise at Delft University of Technology by a team of 10 bachelor students over a period of 10 weeks.

The mission motivation and goal is explained in chapter 2 and a mission overview is given in chapter 3. The initial phase of the mission, covering the transfer from Earth to Venus and the design of the spacecraft serving as a communication relay for the probe, is described in chapter 4. The design of the probe, comprising the gondola with its scientific payload and the balloon supporting it, is presented in chapter 5. Chapter 6 outlines the Instrument Design and Operations in the Venusian clouds. The mission performance is summarized in chapter 7 and a plan for the future mission development is given in chapter 8.

2 Mission Motivation & Goal

You might know Orpheus as a prophet and musician from classical Greek mythology, where he famously was able to charm anyone with the notes coming from his golden lyre. As the story goes, his wife Eurydice tragically died when she fell into a nest of vipers during their wedding. In an attempt to retrieve her, Orpheus went on a journey to the underworld to charm Hades and try to revive Eurydice.

Analogously, the presented mission 'Orpheus' is an attempt to find signs of biotic chemistry in the hellish atmosphere of Venus, the solar system's most hostile planet. With surface temperatures reaching 480°C and pressures 92 times higher than Earth's, the term 'underworld' is not very far-fetched.

This chapter provides strong justification for the necessity of the Orpheus mission. This is shown by identifying the key market gaps left by other similar missions and defining the mission objective of Orpheus. Notably, it highlights the mission's ability to break through the mysteries of complex, life-related astrobiology through the use of a remarkable and novel instrument, the LMC_{OOL} biosensor.

Section 2.1 explores the market of interplanetary missions and defines the key market gap that the Orpheus mission will fill. Moving on, section 2.2 presents the mission objective, the stakeholders and their top-level requirements. Moreover, section 2.3 introduces the primary scientific payload, the LMC_{OOL} instrument and section 2.4 describes the specific astrobiology aspect of the mission.

2.1. Market Analysis

A market analysis is conducted to identify the maximum potential of mission Orpheus.

Market Overview

As explored in the Baseline Report [2], the market for interplanetary, life-seeking missions is extremely dense, and has experienced a sudden growth in the recent decades. Understanding this market is crucial to determine the strengths, but also limitations of the Orpheus mission. Also, from a cost efficiency point of view, it will help in finding the most recent models and tools to use, and obtain a maximal amount of resources available from past missions and research. Figure 2.1 documents an extensive list of relevant past and future interplanetary missions.

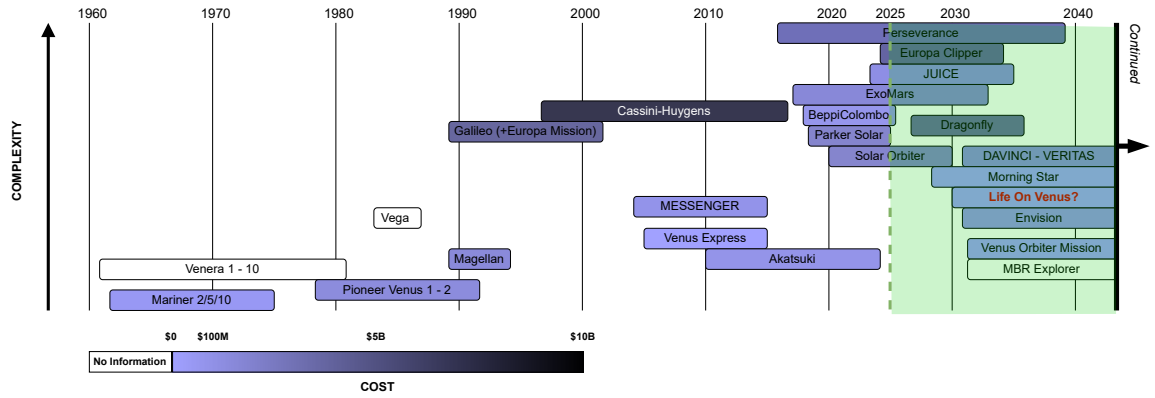

Figure 2.1: Timeline of similar past missions including the cost and complexity of each mission showing a clear increase in interest for related missions.

In general, this recent increase of interplanetary missions is characterised by three factors. Firstly, a shift towards "life-seeking" missions. Secondly, the emergence of private, ambitious companies and

university-led mission initiatives which introduce a more cost-effective approach to interplanetary missions. Thirdly, novel technologies that improve feasibility by decreasing mission complexity. Orpheus aligns with these trends and more importantly, fills in key gaps left by other missions.

Venus as Home for Life

The shift towards life-seeking missions is driven by a better understanding of our nearby celestial bodies. After over half a century of pioneering missions and then more specialised missions to other planets in the solar system, scientists have a better understanding of the composition and processes occurring at other planets. This allows the targeted exploration of specific regions where life is prone to emerge.

Mars, for instance, has become a focal point of interest due to the increasing evidence of ancient water activity. This has led to missions such as Exomars[1] and Perseverance[2], aimed at specific regions believed to hold clues of habitability. However, Mars is saturated with ongoing and planned missions and it becomes increasingly hard to find innovative research ideas to explore the red planet.

Venus, on the other hand, is relatively unexplored, despite it being a potential home for life. In the early era of solar system exploration, it was rapidly disregarded and lacked interest due to its apparent extreme inhospitability, characterised by its abundance of sulphuric acid. However, interest in the planet is rapidly growing due to the recent, and much debated, discovery of phosphine in its atmosphere [5]. On Earth, the only known biological production of phosphine is attributed to anaerobic life. It is seen as a biosignature molecule, a chemical that could indicate the presence of biotic chemistry. It was detected using the James Clerk Maxwell and Atacama Large Millimeter/submillimeter Array telescopes, but this needs in-situ confirmation.

Next to phosphine, new research has shown other biosignatures like amino acids, nucleobases, and lipids to be stable in concentrated sulphuric acid [4, 6–8]. Further emphasising the possibility of complex, carbon-based chemistry, a carbon cycle has been proposed that in theory could be sustained in the Venusian environment [9].

Fortunately, despite it being generally left out, Venus has just the necessary exploration heritage to understand its mechanics and design a successful mission. The initial Venusian exploration phase (1960-90) demonstrated the ability for spacecraft to reach the planet. The next missions (1990-2010) focused on imaging of Venus using orbiters, thus determining the general composition of the planet. The last phase (2010-now) has consisted of investigating in more detail the dynamics of its atmosphere.

All these advancements are recent, making it important to act rapidly and take advantage of them. Orpheus meets this urgency with a planned launch in 2033.

A TU Delft Initiative

While NASA and ESA are still leading the space exploration market, private companies seem to take more and more territory on the production line of recent missions. Sometimes used to outsource specific subsystems and other times for full mission design, they tend to be more efficient and cheaper than the public institutions, which are characterised by unnecessarily lengthy and costly procedures.

A good example of this is the Morning Star mission [10]. Led by the Massachusetts Institute of Technology (MIT), it aims to detect life signs on Venus across three separate missions. Impressively, the researchers were able to propose a promising spacecraft cost estimation of $\$25M$[3].

Similarly, Orpheus is led by the Delft University of Technology, using the strengths of this private approach and offering a low spacecraft cost of $€150M$. However, in contrast to the Morning Star

[1] https://www.esa.int/Science_Exploration/Human_and_Robotic_Exploration/Exploration/ExoMars, [Accessed 02/05/2025]

[2] https://science.nasa.gov/mission/mars-2020-perseverance/, [Accessed 02/05/2025]

[3] https://www.morningstarmissions.space/ Accessed 02/05/2025

mission, Orpheus is a European-led initiative, a necessary step towards strengthening Europe's independence and presence in the space exploration sector.

A Novel Instrument: LMC_{OOL}
To set itself apart from the similar Morning Star mission, Orpheus makes use of a highly precise, yet extremely lightweight instrument as its main payload, which is the Origin of Life - Life Marker Chip (LMC_{OOL}).

The LMC_{OOL} is an innovative lab-on-a-chip technology with outstanding reliability. Specific biosignatures can be targeted using an immunoassay strategy, and their concentration is determined with high accuracy. A more detailed description of the instrument can be found in section 2.3.

The focus of the mission design will be put on taking advantage of the low mass of the payload, for example by choosing a lightweight gas sensor array as secondary payload. This lightweight approach will in turn reduce the complexity of the mission. Overall, this light and less complex design will allow Orpheus to stand out as a very feasible mission, making it a competitor in the interplanetary mission market.

Limitations
The highly specific nature of LMC_{OOL} imposes constraints on the extent of the chemical analysis. Although certain broader groups of molecule and particle cycles will be indicated by detecting specific biomarkers, Orpheus will be incapable of completing a full analysis of the chemical spectrum, like a mass spectrometer would be able to. This targeted approach, while efficient and compact, may limit the ability to detect unexpected or novel compounds. Additionally, due to the nature of LMC_{OOL} (see section 2.3), targeting the same molecule in multiple locations will be challenging. Still, even a single detection of a life-indicating molecule would constitute a major breakthrough.

Politically, as a European-led mission, Orpheus must navigate through a limited production line and infrastructure access compared to other competitors. This is further complicated by a tense and shifting international political climate, which may impact collaboration and funding stability. Despite these challenges, the mission offers a crucial step toward European autonomy in planetary science.

Market Gap
In conclusion, Orpheus is a solution proposition to answer the recently opened debate on the presence of life on Venus. It is a private, European, and cheap solution, which makes use of a high-accuracy, innovative, and low-weight payload. These points make it a strong fit for investment in the crowded interplanetary mission market, and justifies the thorough level of design presented in this paper.

2.2. User Requirements & Constraints

Following from the defined market gap, the mission is formulated in a *mission need statement* and *project objective statement*, that explain the scope of the project in a single statement.

Mission Need Statement

"Determine whether there are signs of life in the clouds of Venus."

Project Objective Statement

"Design a mission from launch to end-of-life to deploy the LMC_{OOL} in the Venusian clouds at an altitude of 40-60 km and detect signs of potential life, by 10 students in 10 weeks."

Furthermore, the client and the LMC_{OOL} scientists have compiled a set of user requirements, shown in Table 2.1. They are unchanged as given in the project guide [3], with the exception of the launch mass requirement **R-BGT-01**. The initial value of 100 kg was deemed unfeasible and therefore increased to 320 kg, following from an initial mass estimation in the baseline report [2].

Table 2.1: Overview of the mission requirements.

ID	Category	Requirement Description
R-SCI-01	Science	The mission shall be able to use the Life Marker Chip to unambiguously detect biomolecules in the clouds of Venus.
R-SCI-02	Science	Additional instruments shall support LMC_{OOL} measurements.
R-SCI-03	Science	Measurements shall be taken at at least two locations in the Venusian cloud deck, which are separated by 100 km.
R-PRF-01	Performance	At least 3 ml of fluid (concentrated sulphuric acid) from the clouds shall be collected onto the Life Marker Chip.
R-PRF-02	Performance	Collection altitude shall be between 40-60 km.
R-PRF-03	Performance	All science data shall be transmitted to Earth.
R-REL-01	Reliability	Reliability of the complete system shall be at least 95%.
R-REL-02	Reliability	The probe shall handle the corrosive H_2SO_4 clouds of Venus for the duration of its mission, using existing coating and protection techniques.
R-REL-03	Reliability	The mission shall support European Strategic Autonomy.
R-SUS-01	Sustainability	Clear end-of-life strategy; the mission shall comply with COSPAR Policy on Planetary Protection, minimizing impact on potential Venusian ecosystems.
R-BGT-01	Budget	A launch mass of 320 kg is provided, which needs to account for cruise vehicle, probe(s), and fuel.
R-BGT-02	Budget	Engineering designs need to complement and enhance the core strengths of the LMC_{OOL} instrument, primarily its compact and lightweight footprint.
R-CST-01	Cost	Spacecraft cost shall not exceed €150M. This includes the spacecraft (e.g., cruise vehicle, probe(s), etc) and scientific instrument(s), but excludes launch and operations. A launch mass of up to 320 kg is provided.

Stakeholders

As mentioned, these requirements are given by the client and LMC_{OOL} scientists, and it is important to keep them updated across the whole mission design and operations on the advancements and compliance of these requirements. At the end of this report, in section 7.1, a requirement compliance matrix, with more detailed subsystem requirements, is presented for this purpose. On top of this, it is essential to identify all other stakeholders of the project. They are displayed in Figure 2.2. Each stakeholder has their own interests, and it is important to understand them to satisfy their needs and to ensure efficient communication and negotiation across the project duration. The key stakeholders are all the ones with important influence on the project outcome. Those are the ones placed in the *Manage Closely* and *Keep Satisfied* boxes.

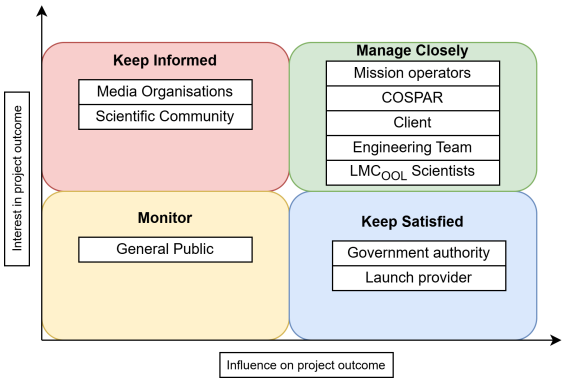

Figure 2.2: Interest-influence diagram of the stakeholders.

2.3. Origin of Life Marker Chip LMC$_{OOL}$

Since the scientific payload drives the rest of the mission, it is important to have a solid understanding of how it works, its strengths and weaknesses, and what supporting equipment is needed for its

operation. This section aims to present this innovative instrument.

LMC_{OOL} is an integrated photonic biosensor, a lab-on-a-chip instrument for analysing chemicals. It takes advantage of silicon-based photonic integrated circuits and selective surface chemistry. It is a further development of the Life marker Chip (LMC), which was initially one of the instruments to be carried by ESA's ExoMars rover [11]. While it was later discarded, the technology has advanced since then, and has reached a Technology Readiness Level (TRL) between 3-4.

The working principle of LMC_{OOL} is based on an asymmetric Mach-Zehnder Interferometer (aMZI): it detects the phase difference between two light waves, a reference wave and one whose refractive index has been modified by the presence of an analyte. If no phase difference is measured, there is no detection. But if there is a difference, it proves the presence of the target molecule, and its concentration in the sample is proportional to the measured difference.

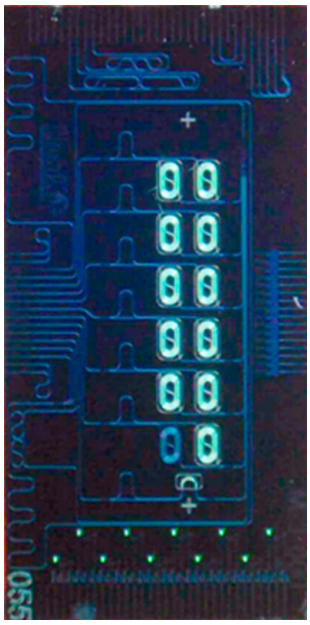

Figure 2.3: One LMC_{OOL} chip with 2×6 interferometer arrays, total dimensions: $10 \times 5\ mm$.

The chip is made of a silica (SiO_2) substrate and silicon-nitride (Si_3N_4) waveguides running through it (the dim blue lines on Figure 2.3). These waveguides have the capacity to excite and "guide" light, nominally chosen at 850 nm, essentially creating paths for light to propagate through the chip. It can be seen as a miniature Printed Circuit Board (PCB), but instead of electrons running through electrical paths, there are photons running through silicon-nitride paths.

One chip of $5 \times 10\ mm$ can detect 6 molecules by the use of immunoassay.
For one molecule, one light wave first exits from a laser and propagates in a Si_3N_4 path before entering the aMZI configuration: the light splits at a Y-junction into a reference arm and a sensing arm. On both of these paths, the SiO_2 cladding is locally removed and thus exposes the waveguide to the sample liquid during operations, as shown by the 6 pairs of coil path on Figure 2.3 (the "0s"). While the reference path is left untouched, the sensing path gets modified: antibodies specific to the chosen target molecule are chemically bonded to its surface. Now, when pumping sample liquid over the chip, if a target molecule comes into contact with an antibody, it chemically bonds to it and slightly alters the local energy of the system, ever so slightly disturbing the refractive index of the light through the waveguide underneath. After this, the reference light wave and sensing light wave remerge in a new Y-junction, closing the aMZI configuration. Further away, the reunited light wave reaches a photodiode, where the difference in refractive index can be measured in the light's phase shift difference. The higher the concentration of target molecules in the sample, the more analytes bond, the higher the refractive index difference, and the higher the detected phase shift.

In practice, a sample liquid is smeared over the chip at a slow rate, around 5 $\mu L\ min^{-1}$, and the measured phase shift is small, in the order of picometers pm. The results of a lab experiment where LMC_{OOL} was tested for the detection of Phenylalanine at 3 micromolar is shown in Figure 2.4. The linear trend of the graph is expected and simply reflects the natural phase shift of the undisturbed waves over time. What matters is the dip of 10 pm after 100 s, this is what characterises the detection of Phenylalanine. The nominal state is then retrieved at 300 s, when a buffer liquid is pumped on the chip, cleaning it and removing the analytes.

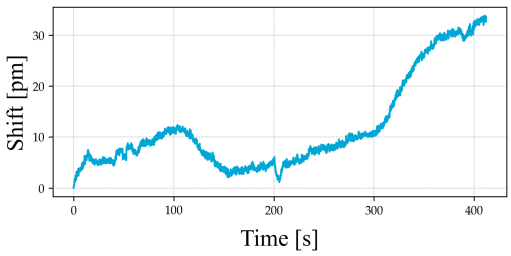

Figure 2.4: Phenylalanine measurements at a 3 μM concentration.

The Origin of Life - Life Marker Chip shows great aerospace-worthy advantages in comparison to

the typical instruments used for life detection. First, its ability to unambiguously target specific molecules with the use of antibodies makes it a highly reliable instrument. Next, its immunoassay inspired technology in combination with the photonic chip configuration make it an ultra lightweight, low-power instrument, contrasting with typical aerospace-grade instruments which usually weigh over at least one kilogram and require extensive power supply. Additionally, it requires only a minute amount of sample to operate (around 100 μL per cycle) and still does not lose in performance compared to other instruments, safely achieving a Limit Of Detection (LOD) down to part per billion (ppb). On top of this, it does not require any sample pre-processing or pressure vacuum condition.

Some limitations include that LMC_{OOL} can only detect target molecules present in liquid sample, so molecules that can dissolve. Next, the receptors each need to be custom made for each molecule, which can be costly in research. These antibodies also need to be resistant to the sample liquid, which can sometimes be corrosive. Finally, the LMC_{OOL} cannot survive hot temperatures above 60°C and must operate around room temperatures of 25°C to avoid noise alterations.

2.4. Scientific Overview: The Choice of Molecular Targets

This section outlines Orpheus' scientific strategy: to search for signs of life within Venus' atmosphere. This search starts from the fundamental question of how to define life in the first place. NASA defines it as the following[4] : *'Life is a self-sustaining chemical system capable of Darwinian evolution.'* Every planet is different, and thus there is no reason for life to rely on the same principles as it does on Earth. Despite that, the discovery of amino acids and nucleobases into meteoritic samples drive the theory that terrestrial life, or at least its building blocks, have initially come from outer space.

Rather than adopting a speculative approach, Orpheus extends that hypothesis to Venus, assuming that Venusian lifeforms originate from these same building blocks, adapted to the sulphuric acid-rich environment. The mission will focus on looking for a set of 40 carefully selected biosignatures: organic molecules, equilibria and cycles that support metabolism. These biomarkers, such as DNA/RNA, amino acids, and gases like phosphine or ammonia, offer a starting point that is better suited for a highly specific instrument like LMC_{OOL}. As a result, the detection of any of the target molecules does not directly prove the presence of life; instead it provides information about the existence of complex organic chemistry in the Venusian atmosphere.

2.4.1. Target Molecules

Orpheus' core scientific mission is to collect sulphuric acid samples from the Venusian cloud deck for in-situ analysis by LMC_{OOL}. Following a detailed literature study considering many biosignatures, a total of 40 target molecules in 10 groups are selected. Additionally, 6 gases are chosen to be investigated by the secondary payload, a gas sensor array. Table 2.2 shows the final list of biosignatures.

Table 2.2: List of selected biosignatures for Orpheus.

Functional Groups					
1	Phosphate group	2	Trimethylamine	3	Sulfate Group
4	Pyrimidine	5	Purine		
Biogenic Amino Acids					
6	Alanine	7	Arginine	8	Asparagine
9	Aspartic acid	10	Glutamine	11	Glutamic acid
12	Glycine	13	Histidine	14	Isoleucine
15	Leucine	16	Lysine	17	Phenylalanine
18	Proline	19	Serine	20	Threonine
21	Valine				

Continued on next page

[4] `https://astrobiology.nasa.gov/research/life-detection/about/` Accessed on: 15/06/2025

Sulph(on)ated Biogenic Amino Acids					
22	Sulphonated Phenylalanine	23	O-sulphated Serine		
24	O-sulphated Threonine				
Canonical Nucleobases					
25	Adenine	26	Cytosine	27	Guanine
28	Thymine	29	Uracil		
Other Nucleobases					
30	Hypoxanthine	31	Xanthine		
Nucleosides					
32	Adenosine	33	Guanosine		
Lipid and Fatty Acid					
34	Ether phospholipid	35	Caprylic acid		
Polycyclic Aromatic Hydrocarbons (PAHs)					
36	Naphthalene	37	1-Naphthalenesulphonic Acid	38	Phenanthrene
Prebiotic Molecules					
39	Di-ethylether	40	Hexamethylenetetramine (HMT)		
Gases					
1	Ammonia	2	Carbon Monoxide	3	Formaldehyde
4	Hydrogen Sulfate	5	Phosphine	6	Sulfur Dioxide

LMC, LMC_{OOL}'s heritage instrument from ExoMars, was configured with a focus on biomarkers indicating extinct life. On Mars, due to the high radiation environment, this makes sense. On Venus however Orpheus will focus mostly on biomarkers indicating **extant life**. This choice is made based on the fact that radiation is much more reduced due to Venus' thick atmosphere. Additionally, it is assumed extinct life would not stay afloat, but rather descend and end up on the surface over time.

Selecting Target Molecules

As mentioned earlier, the list is built up starting from terran biomarkers. From a statistic point of view, due to the high specificity of LMC_{OOL} a speculative approach by 'guessing' a set of molecules that can sustain life is likely not successful. For such an approach, a less selective instrument like a mass spectrometer or even a microscope would provide more valuable information. On the contrary, Orpheus assumes that complex Venusian (biotic) chemistry originates from similar building blocks as on earth i.e. amino acids, nucleobases, lipids, etc. Additionally, where possible the selection builds upon research that looked into how these molecules are chemically altered in an acidic environment.

The final list is set up such that it provides scientists with data about the selected molecules, but also gives clues about the chemistry between them. One way this is achieved is by including different 'levels' of biomarkers. As an example, take DNA. It is a sequence of nucleotides, built up from a phosphate group bound to a nucleoside. Breaking up a nucleoside even further results into a nucleic base and a deoxyribose molecule. Using this hierarchical structure, the list includes a phosphate functional group, some nucleosides and many nucleotides. Note that, to increase the chances of positive measurements, as molecular complexity goes down a bigger variety of targets is included. Now a detailed look into each molecule class follows.

Functional Groups

The first category in the list is the functional groups. This category differs from the other ones since it does not target a specific biosignature, but rather certain functional groups. Functional groups are structural units within organic compounds that are defined by specific bonding arrangements between specific atoms[5]. The five functional groups that were chosen to be analysed are phosphates, sulfates,

[5] https://chem.libretexts.org/Courses/SUNY_Potsdam/Book%3A_Organic_Chemistry_I_(Walker)/01%3A_Introduction/1.06%3A_Functional_Groups Accessed 17/06/2025

trimethylamines, pyrimidines and purines.

Phosphates, sulphates and trimethylamines are 3 common functional groups occurring as the hydrophobic head of lipids. Since lipids are important building blocks for cell membranes, they are considered biosignatures. Additionally, they are related to fats, which act as energy storage molecules in biological systems. Dudzevich et al. [8] has shown that all three lipid types are stable in sulphuric acid, and even form cell-like structures due to their hydrophobic heads.

Next to lipids, phosphates are a common functional group that occur in nucleotides as well. A recent phosphine detection [5] suggesting the presence of phosphorus molecules, makes them an interesting group to analyse. Sulphates are interesting because of the common sulphation and sulphonation reactions of organic chemistry when subjected to a sulphuric acid solution. Examples include amino acids[4] and PAHs [12]. Sulphates are chosen over sulphonates since the instrument is by design limited to 40 target molecules, and sulphates are more common in literature. Still, some sulphonated molecules are included (ID 22 and 38 in Table 2.2). One concern for phosphate and sulphate functional groups, is that both are small and finding receptors for them might prove challenging. No existing MIPs have been found, thus more research is needed to confirm if they are a realistic target.

Finally, pyrimidine and purine are included as well. Pyrimidines are a class of single-ring nucleobases, the canonical nucleobases C, T, and U are part of this class, as well as other non-canonical nucleobases. Similarly, purines refer to the double-ring nucleobases (like A and G). By including a receptor for both fundamental nucleobases structures, more context is provided to the measurement. It also increases overall detection chances since non-canonical nucleobases can be detected as well.

Biogenic Amino Acids

The next and largest category in Table 2.2 are biogenic amino acids. It is a subgroup of 20 amino acids which make up the standard genetic code for life as we know it. Since they are crucial for protein synthesis, amino acids are considered an important extant biomarker. Typically, they do not survive long within Earth's fossil record [13], let alone the Venusian environment. Thus, a detection would suggest that something, biological or not, is responsible for sustained production of amino acids.

Only 16 out of the 20 are included as target. To compile a well-rounded list with 40 targets, the 4 amino acids whose presence is least likely are omitted. This is decided by using a ranking scheme based on the amino acid's stability in sulphuric acid, polarity[6] and detection in meteoritic samples. Polarity is included, as it determines solubility. The results are seen in Table 2.3. Seager et al. investigates the stability in concentrated sulphuric acid [4]. Recently published research by Galvin et al. shows the presence of various amino acids in a sample brought back from asteroid Bennu by NASA's OSIRIS-REx mission[14]. Supporting this further, meteorite samples from earth confirm this as well [15, 16].

An interesting observation to be made is the L/D chirality distribution; in all known samples from space, a more or less 50/50 distribution was found. On earth, life is known to prioritize L-chirality. It is not used as a ranking metric in Table 2.3, since no assumption can be made that Venusian life also exhibits this same preference for L-chirality. LMC_{OOL} is however able to detect chirality, thus depending on the data, Orpheus might offer a new point of view in this discussion.

Table 2.3 Shows the outcome, with a rank from A-D assigned to each molecule. The red-coloured amino acids rank as the worst candidates, and will not be studied. Notice how some of the selected amino acids are stable after they are modified by the acid. Three of the modified versions will also be carried and are listed under **Sulp(on)ated Biogenic amino acids**. [4] shows that Phenylalanine becomes sulphonated, and Serine and Threonine undergo sulphation in the acid medium. Note that this links back to the sulfate functional group as well.

[6] https://ecampusontario.pressbooks.pub/bioc2580/chapter/bioc2580-lecture-2-amino-acid-properties-polarity-and-ionization/ Accessed: 03/06/2025

Table 2.3: Ranked amino acids based on stability, polarity and their presence in meteoric samples. The amino acids in red will not be targeted.

Amino Acid	Stable in H_2SO_4?	Polarity?	Meteoric sample?	Rank
Alanine	yes	polar	confirmed	A
Arginine	yes	pos. charged	no	B
Asparagine	yes	neg. charged	confirmed	A
Aspractic acid	yes	polar	confirmed	A
Cysteine	modified	weak	no	C
Glutamine	modified	pos. charged	no	B
Glutamic acid	yes	polar	confirmed	A
Glycine	yes	weak	confirmed	A
Histidine	yes	pos. charged	no	B
Isoleucine	yes	apolar	confirmed	B
Leucine	yes	apolar	confirmed	B
Lysine	yes	pos. charged	no	B
Methionine	modified	apolar	uncertain	D
Phenylalanine	modified	weak	confirmed	B
Proline	yes	weak	confirmed	A
Serine	modified	polar	confirmed	B
Threonine	modified	polar	confirmed	B
Tryptophan	no	hydrophobic	no	D
Tyrosine	modified	hydrophobic	uncertain	C
Valine	yes	apolar	confirmed	B

Nucleobases

A small selection (5) of the large nucleobase group are known as canonical nucleobases, and occur in terran DNA/RNA as base pairs. Parnell et al. places them in the highest priority category of biomarkers [13], since DNA/RNA are responsible for reproduction and thus contribute to the 'self-sustaining' aspect of NASA's life definition. Much like amino acids, all five have also been found in the previously mentioned Bennu sample [14]. Nucleobase sulphuric acid stability is confirmed by Seager et al. [6].

Supporting the earlier statement that life in Venus could look significantly different, non-canonical nucleobases are also included as target. Specifically, Xanthine and Hypoxanthine are chosen. They are known to occur both on Earth, as degradation product of purines, and in outer space, as confirmed by [15]. Next to these two specific non-canonical nucleobases,the general class of purines and pyrimidines will be analysed as well (ID 4&5 in Table 2.2)

Nucleosides

Zooming out from the basic nucleobase structures, the next step in nucleic acid assembly involves the formation of nucleosides. Built up from a nucleic acid bound to a sugar molecule, these are larger molecules generally considered to be less stable than the previously covered nucleobases [6, 13]. While the probability is lower, a detection would be a very strong indicator of the presence of complex chemistry. For this reason Orpheus will carry two common nucleosides. Adenosine and guanosine, the nucleosides corresponding to adenine and guanine, were selected as representative targets.

Lipids

Lipids have already been introduced under the functional groups, but two specific targets are chosen as well. Due to the enormous chemical variety among lipids, differing in headgroups, tail lengths, degrees of saturation, and backbone linkages, it is a challenging class to tackle and covering many specific molecules would not be efficient use of resources. Instead, the approach is to focus on the functional groups were added to cover a large amount of possible lipids.

On top of the foundation of the functional groups, the two complete lipid molecules are an ether phospholipid and a small fatty acid (caprylic acid). The ether phospholipid is chosen since ethers are generally very stable molecules, with good resistance against hydrolysis and oxidation. In addition, phospholipids are known to spontaneously form vesicle-like structures in both aqueous and acidic solutions [8].

Complementing the larger phospholipid, caprylic acid was included to represent the fatty acid subgroup. Caprylic acid is a common and simple fatty acid that appears in both biotic and prebiotic chemical chemistry [17]. Much like the phospholipids, short-chain fatty acids are known to form vesicles [18], which are thought to be an early form of cell membranes. Next to that, caprylic acid is also a degradation product of larger lipids. This makes them a good candidate to analyse.

Polycyclic Aromatic Hydrocarbons

PAHs are a class of molecules well-known for their chemical stability, which is largely attributed to their aromatic ring structures. This structure allows them to persist in harsh environments such as interstellar space and acidic solutions like sulphuric acid. Their presence is not directly linked to biological processes, but it would confirm the existence of complex carbon-based chemistry. For example, like the proposed carbon cycle from Spacek et al. [9]. The paper suggests synthesis of larger carbon-based molecules from atmospheric gases like formaldehyde, hydrogen sulphide and carbon monoxide. Combined with the fact that PAHs are known to degrade under UV radiation, a detection would indicate the existence of a steady source on Venus (UV is limited due to the thick atmosphere, but the argument still holds). Furthermore, PAHs are common in other space samples [14–16]. Three compounds were selected: naphthalene, phenanthrene, and a modified, sulphonated derivative: 1-naphthalenesulphonic acid.

Out of the many known variants, 2 and 3 ring PAHs are considered since they are the simplest and most likely to be found. Naphthale is a 2-ring PAH, while phenanthrene is a 3-ring PAH, with a bent structure. Phenanthrene was chosen over the linear 3-ring Anthracene, since it tends to be more stable[19]. Finally, as an attempt to predict naphtalene's behaviour in sulphuric acid, a sulphonated version is included: 1-naphthalenesulphonic acid.

Prebiotic Molecules

The final category consists of two prebiotic molecules: hexamethylenetetramine (HMT) and di-ethyl ether. Both are relatively small molecules and are linked to the gases selected for the gas sensor array.

HMT is an apolyheterocyclic organic molecule, and a reaction product of formaldehyde and ammonia. The compound is assumed to be a signature for prebiotic chemistry [20]. Vinogradoff et al. [21] shows purely thermally synthesised HMT from ammonia and Formaldehyde (both of which are targets for the gas sensor array) and [15] confirms its presence in a meteoric sample. This is significant since HMT is the first step to synthesise more complex organic molecules from atmospheric gases [8, 20].

Diethyl ether, a small ether, is known for its resistance to acid hydrolysis and oxidation. Implying that it could survive in harsh atmospheric environments like planetary cloud layers better than esters or alcohols. Diethyl ether can plausibly form through recombination of small hydrocarbons and oxygen-bearing species in gas-phase. Next to that, on earth microbial life in harsh environments has evolved to use ether-linked lipids for enhancing thermal membrane stability[7] di-ethylether was included for this reason, although it is generally less studied in meteoritic samples.

Gases

Next to the 40 targets for LMC_{OOL}, 6 gases are selected for further analysis by the secondary payload. They are listed on the bottom of Table 2.2. With the exception of phosphine, these gases are thought to play an important role in the proposed Venusian carbon cycle [8]. On top of that, they are known

[7] `https://biologyinsights.com/adaptations-of-microbial-life-in-extreme-environments/`, [Accessed:18/06/2025]

to be a part of the carbon and sulphur cycles on earth as well. In addition, several of the selected gases directly relate to the solid-phase biomarkers (ID 1-40). Formaldehyde and ammonia link to HMT, Phosphine links to phosphates in lipids and nucleic acids. Carbon monoxide, formaldehyde and hydrogen sulphide link to the production of PAHs.

Phosphine is the only of the 6 gases considered to be a biomarker, since on earth it is only produced by biological sources [5]. The other 5 are not direct biomarkers, but are analysed to give more context, and investigate how complex organic chemistry can exist on Venus.

2.4.2. Receptors

As mentioned in section 2.3, the LMC_{OOL} lab-on-a-chip is based on receptor molecules, which use molecular recognition to identify targeted biosignatures. This requires each sensing element to be set up with receptors for its target molecule. Three main types exist: antibodies, Molecular Imprinted Polymers (MIPs) and aptamers. While al three work well in combination with LMC_{OOL}, for Orpheus' purposes MIPs will be used. The reason is simple; it is the only receptor type to have shown good stability in acidic environments.

Antibodies

The traditional method used for molecular recognition in biotechnology is the use of antibodies. Biologically, plasma cells are responsible for antibody production. In turn, these antibodies selectively bind to antigens like viruses and bacteria to protect the body. Bioscience exploits them to be used in receptor technology. Historically, antibodies are the preferred method for molecular recognition, and are the most mature technology. Unfortunately, some downsides prevent them from being used for Orpheus' purposes. The main reason is their chemical instability. They are protein structures, large 3D molecules built up from amino acids and folded in a certain way. The folds are held together by rather weak hydrogen bonds, responsible for protein denaturation when exposed to temperature or acidity changes [22, 23]. Besides their chemical instability, antibody development is challenging and has high production costs.

Aptamers

Aptamers are artificial receptors based on the same chemical structure as DNA. They differ from antibodies, which are protein structures and therefore consist of amino acids. Compared to antibodies, they are chemically a bit more stable since they do not rely on weak hydrogen bonds. Aptamers build upon protonation to bind to target molecules. This means that in media with a pH lower than pK_A, the binding mechanism is prevented due to an effect called binding-linked protonation [24]. This makes them unusable in the highly acidic Venusian environment.

Molecular Imprinted Polymers

Finally, MIPs are another type of receptor that has become increasingly interesting over the past years. Next to lower production costs than antibodies and aptamers, MIPs have been shown to exhibit very little change in binding capacity in a large range of acidic and basic environments [25]. Thus MIPs are preferred over antibodies or aptamers, whose chemical stability is known to degrade in acidic environments [22, 24] below a pH of 4.0.

The choice for MIPs sets the new LMC_{OOL} apart from the original LMC, which was planned to use antibodies instead [26]. Back then, it was decided against using MIPs due to their low TRL. Since then the technology has become more common, and is deemed mature enough to be used for the instrument. One issue persists though, which is that MIPs are not yet available for all the target molecules. While MIPs exist for common molecules in biotech research, like biogenic amino acids and canonical nucleobases, for some less common target molecules little research was found. For this reason, more effort should be put towards for developing MIPs for the resulting biosignatures. On top of that, testing should be done for all chosen receptors to ensure their stability in space and in highly acidic environments.

3 Mission Overview

Before delving into the detailed design of every system, a mission overview is provided here for the reader to have a point to come back to whenever a general question is raised. It summarises the considered concepts and how the balloon was chosen in the end in section 3.1. Following, a description of the operations and logistics of the mission is given in section 3.2. This summarises the basic timeline of the mission and introduces the design and assembly considerations, and the mission operation procedures. In section 3.3, the diagrams outlining all the functions that the system must perform in order to achieve a successful mission are presented. Finally, the sustainability strategy followed is explained in section 3.4.

3.1. Concept Trade-off Summary

The trade-off analysis was conducted in the previous phase, the conceptual design, after careful consideration of multiple feasible concepts. Four different options were studied: a variable altitude balloon, a swarm of falling capsules, a glider, and a spaceplane. If the reader wants to get a deeper overview of any of the conceptual designs, please refer to the Midterm Report [1]. Table 3.1 presents the final trade-off table with its corresponding criteria and weights, as well as the scores given for each design. As can be read from the last row, the balloon was the selected concept, and thus it will be further developed in the present report.

Table 3.1: Orpheus probe design trade-off. Red = 0-0.1, orange = 0.1-0.2, yellow = 0.2-0.3, blue = 0.3-0.4, green = +0.4.

Level 1	Level 2	Weight	Balloon	Capsul.	Glider	Spacepl.
Reliability 0.310	Communications Reliability 0.516	**16%**	0.451	0.119	0.261	0.169
	Operations Reliability 0.484	**15%**	0.351	0.351	0.189	0.109
Scientific Payload 0.280	Payload Mass 0.500	**14%**	0.160	0.277	0.095	0.467
	Sampling Volume 0.500	**14%**	0.240	0.085	0.523	0.152
Coverage & Control 0.180	Vertical Control 0.389	**7%**	0.385	0.087	0.385	0.143
	Horizontal Coverage 0.611	**11%**	0.415	0.293	0.185	0.107
Total Cost 0.130	Manufacturing Cost 0.310	**4%**	0.239	0.434	0.239	0.089
	R&D Cost 0.690	**9%**	0.301	0.494	0.145	0.060
Sustainability 0.100		**10%**	0.095	0.467	0.277	0.160
		100%	**30.0%**	**26.9%**	**25.4%**	**17.7%**

The balloon emerged as the best candidate due to its strengths being aligned with what is required for the mission. Because of its long operational life, low speed, and multiple opportunities to establish communication with the orbiter, in addition to being a previously proven concept with a high technology readiness level, its reliability is strong. The design is not outstanding at enabling and

enhancing the scientific payload, however, its coverage and control capabilities outweigh this fact by allowing the payload to sample from a wide range of locations, increasing the diversity. The cost is assumable, as it does not require much development. However, the sustainability of this design is low because of its large surface area, which must be coated with environmentally harmful materials to withstand the harsh conditions of the Venusian atmosphere.

The swarm of capsules ranked second. Their simple design and extensive flight heritage minimize both manufacturing and R&D expenses, making them a budget-friendly option. From a sustainability perspective, capsules are favorable, as they are already widely produced and do not require additional complex subsystems. While their operational lifetime is short and communication windows are narrow, the inclusion of redundancy through swarm deployment enhances reliability. Finally, their sampling capability is limited due to their short lifespan, but they can obtain sampling diversity when dropping the capsules at different points of Venus.

The glider followed closely. Its ability to include a cyclonic collector allows for high-efficiency sampling, and its control surfaces provide good vertical control, even if the horizontal coverage is limited by its dependence on solar power. It also ranks lower in reliability due to a lack of Venus-specific aerodynamic data, which reduces its technology readiness level. Its cost is moderate, requiring more development than the capsule or balloon, and its sustainability is low due to the inclusion of multiple subsystems like avionics and batteries.

Finally, the spaceplane came last. Being a stand-alone system without the need for a cruise vehicle or an orbiter, it has a high payload potential. However, the design is complex, novel, and requires significant research and development, resulting in a low technology readiness level, reliability, and cost. Sample collection would be limited due to its poor horizontal and vertical control and the risk of sample degradation from the heat exposure. Moreover, its sustainability is poor, given the extensive use of materials and systems needed to survive and operate in Venus' atmosphere.

3.2. Operations and Logistics Concept

The Operations and Logistics Concept describes the operations of the system during the preparation and conduction of the mission and how it is linked to existing infrastructure. It is divided into two phases, the design and assembly phase and mission operation including transfer from Earth to Venus and the scientific mission on Venus. A time line of the mission is shown in Figure 3.1, and will be expanded upon throughout the report.

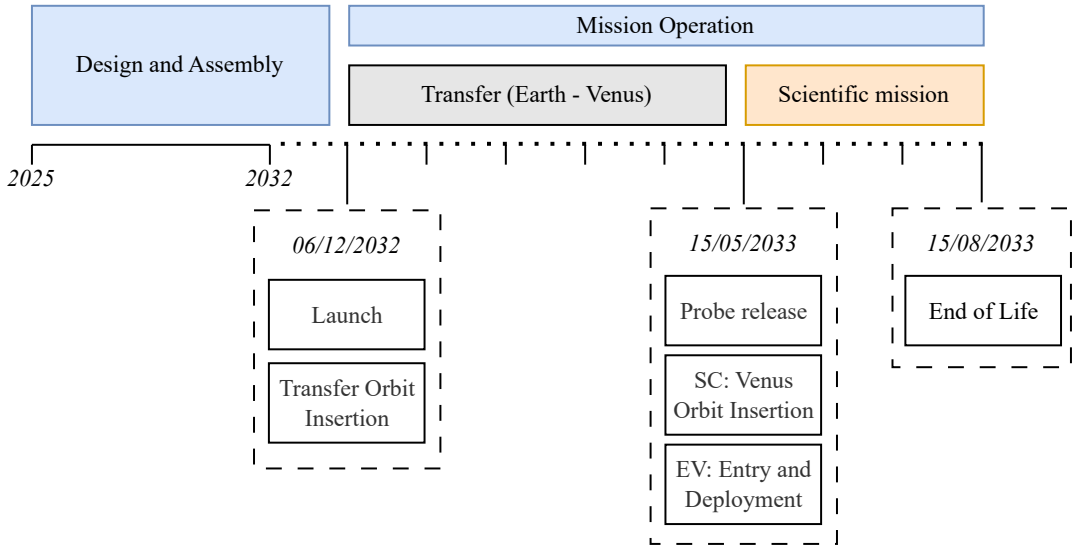

Figure 3.1: Timeline of the Orpheus mission.

Design and Assembly

The design and assembly is divided into the spacecraft, the entry capsule and the probe. As many subsystems as possible are designed, manufactured, and assembled in the facilities of Delft University of Technology. When no suitable facilities are available, subsystems are outsourced to other companies. The objective during the entire design is to use space-rated off-the-shelf components where possible and verify and validate their use for operation under the expected conditions. This reduces mission cost, design time, and improves development sustainability; using compatible off-the-shelf components also makes the assembly easier.

Spacecraft and Capsule

For the spacecraft and entry capsule, TU Delft offers multiple laboratories that could be used for testing, but assembly would have to be outsourced. These include the Satellite Communication and Orbital Mechanics Laboratory, and the Space Instrumentation Laboratory. Potentially, collaboration with Delfi Space Laboratory could be arranged, as it provides extensive infrastructure and experience in the assembly and integration of small satellites. However, for the propulsion system a subcontractor would be needed, as proper infrastructure to store and handle the propellant is necessary. For that purpose, Air Liquide Advanced Technologies from France is chosen due to its expertise with helium tanks and the possibility of testing their services. As a backup company, Nammo Space from Norway is considered. It is critical to properly communicate between the teams to ensure a fitting interface between all the subsystems of the mission.

Probe

The probe design, assembly and final integration is conducted by the team at the Delft University of Technology in the Delft Planetary Laboratories. The LMC_{OOL} instrument itself will also be assembled at TU Delft. One of the most critical components that is not available off the shelf is the pump to inflate the probe. The team has reached out to companies specialised in pumps, investigating the possibility of developing a pump for the Orpheus mission. The main issue with commercially available pumps is that the materials of the components cannot withstand the high temperatures and sulphuric acid environment of the Venusian atmosphere. Schwarzer Precision, a German company, aligning with the European Autonomy Strategy, has offered to adjust a pump design to the Orpheus mission requirements [Carsten Treichel, Schwarzer Precision, personal communication, 5 June 2025]. An alternative partner would be the Dutch company KNF Verder B.V. [Mark Hommersen, KNF Verder B.V., personal communication, 6 June 2025]

Instruments

To prepare LMC_{OOL} for operating in the Orpheus mission, MIPs have to be developed that can detect the target biomarkers presented in section 2.4. During Verification and Validation of the MIPs, it is especially important to test their stability in sulphuric acid and to investigate their lowest concentration detection.

For the secondary payload, involving cameras and a gas sensor array, off the shelf space rated components exist, but they would have to be tested for operation in the Venusian environment. In particular, the membrane included in the gas sensor must be tested for highly concentrated sulphuric acid environment.

Verification and validation

For performing verification and validation, the most logical choice is the ESA ESTEC (European Space Research and Technology Centre), due to its proximity and the company's ongoing collaboration with the university in *Fly your satellite!* programme. Partial funding could be achieved through the Open Space Innovation Platform [1]. For a more extensive test campaign, collaboration with other projects,

[1] `https://technology.esa.int/page/funding-your-ideas` [Accessed 13/06/2025]

such as Team 12 from DSE, who are designing a similar mission, could be used to share and decrease costs. An alternative test facility could be the National Test Facility in the UK, however, costs would most likely increase due to the facility being outside the EU. On the other hand, to verify and validate the system entering Venus, such as the LMC_{OOL} system, the Delft Planetary Laboratory could be used, as they can recreate environments similar to other planets. This is an important factor, as for example, the microfluidics system from the LMC_{OOL} is a novel design and should be tested under representative conditions. They also sustain collaboration with other partners like the Netherlands Platform for Planetary Science and ESA.

Mission Operation

Mission operation includes the launch from Earth, transfer to Venus, conducting the scientific mission at Venus and finally the End of Life procedures. The concept of operations is visualized in Figure 3.2.

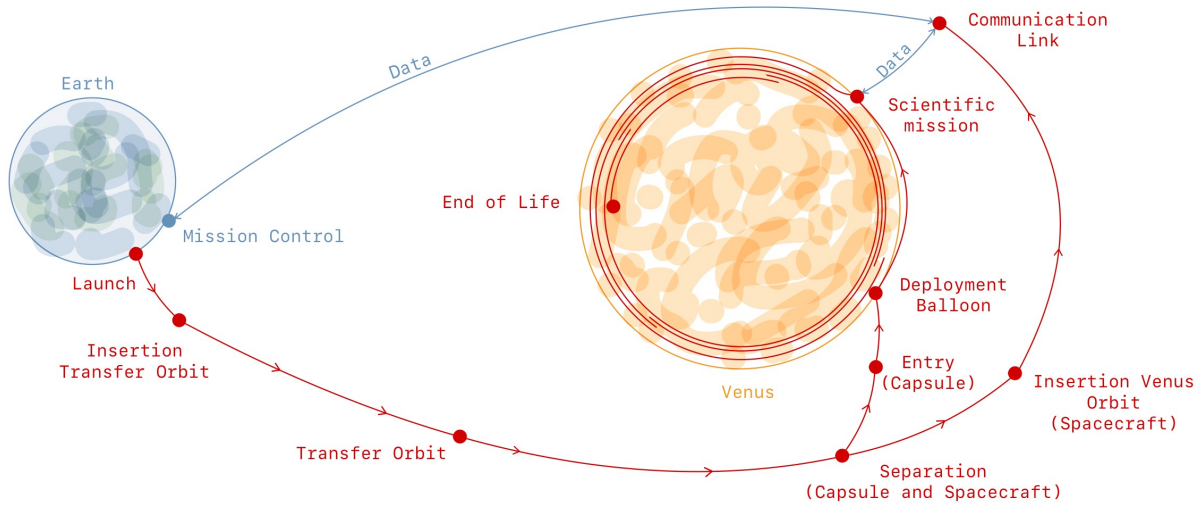

Figure 3.2: Concept of operations.

The launch of the system on 6^{th} of December 2032 is provided by Rocket Factory Augsburg (RFA). Once in space, the same launcher provides an insertion into the transfer orbit. A journey of 160 days lies ahead of the spacecraft from this point. About 30 minutes before the insertion burn into Venus orbit, the probe is released and put on its own way to the Venusian atmosphere. Once in the correct position, on the 15^{th} of May 2033, the spacecraft performs the burn and gets into an elliptical orbit of 300 km perigee and 20,000 km apogee around Venus.

At an altitude of around 50 km, the capsule will release and inflate the balloon, its gondola, and drop the helium tanks. The balloon-gondola system will then enter a stable buoyant flight, carried by the Venusian winds, designed to last 60 days (up to the 16^{th} of July 2033). There, the scientific mission can operate, with the gondola transporting instruments through the cloud deck. These include a *Sampling System*, a *Fluidic Network*, the LMC_{OOL} *Assembly*, and *Secondary Payloads*, all detailed in chapter 6. To maximise sample diversity, the scientific operations aim to collect and test samples from different target altitudes between 50 and 55 km, and at different segments of the Venusian time cycle, including the night. These operations are designed to last 45 days, up to the 1^{st} of July 2033, leaving a 15 days buffer to assess potential mission extension.

Data from the probe will be transmitted to Mission Control, using the spacecraft as a relay. Data has to be stored by the probe until the next link to the spacecraft is possible.

During the mission, communication between the ground station and the spacecraft is required for telemetry, tracking, and transmission of scientific data. The most evolved systems for deep space monitoring with a global network of large and sensitive antennas are NASA's DSN and ESA's ESTRACK

[2]. With respect to **Req-EXT-3.2**, which specifies that any service shall be provided by European-based organisations, ESTRACK is chosen for the Orpheus mission.

On July 16^{th} 2033, depending on the orbiter and balloon viability, a decision will be made to either extend the mission duration or call the mission shutdown. Regardless of when mission shutdown happens, appropriate End of Life (EoL) procedures will be activated to align with the Committee on Space Research (COSPAR) regulations set as of 2025 (see section 3.4). Essentially, the balloon will vent out and descent to the Venusian surface, where it will be crushed and destroyed by the extreme conditions. In parallel, the orbiter will slowly descent and burn up in the high Venusian atmosphere. Both procedures will destroy any potential contaminants or foreign material, preventing disruption of the Venusian environment.

3.3. Functional Diagrams

The Functional Flow Diagram (FFD), Figure 3.3 (next page), shows the time-dependent flow of one function to the next, it serves as a guide to know if functions must be performed in parallel or series, and whether any iterations are needed.

The Functional Breakdown Structure (FBS), Figure 3.4 (page 21), while not showing the tasks in chronological order, gives an overview of the hierarchy of the functions. As it can be seen, the FBS has functions one lower level than the FFD, this serves as an overview of the lower-level functions that have to be performed to carry out the tasks in the FFD. It is these lower-level functions from which the requirements are obtained.

Additionally, in both the FFD and the FBS the system(s) that must perform the function have been identified, the legend is given in the FFD, but it is the same as for the FBS.

3.4. Sustainable Development Strategy

Considering the concerning international climate, both environmental and political, it is essential that space missions are developed with a strong commitment to sustainability, responsibility, and long-term impact. This section presents a strategy for the sustainable development of the Orpheus mission, structured across four key dimensions: environmental sustainability on Earth, planetary protection on Venus, societal considerations, and enforcement.

Environmental Sustainability

It becomes increasingly hard to justify space missions in the current global warming crisis, especially considering the excessive pollution produced during launch and the rare metals and infrastructure necessary for manufacturing. During the earlier concept trade-off [2], the balloon option was chosen despite it having the lowest score in the environmental sustainability criteria. During the current detailed design phase, thorough effort is put on design choices to minimise the environmental impact of the Orpheus mission.

To assess the environmental and broader sustainability impact of the mission, a Life Cycle Assessment (LCA) approach should be conducted. Unfortunately, this requires an amount of time and qualification that exceeds the resources of the current design phase, including the absence of a complete LCA database. Still, general LCA principles are mimicked to guide design choices and prioritize alternatives. This includes defining a proper functional unit: *One complete Venus mission, from component manufacturing to launch, operations, and end-of-life*; and defining specific impact categories such as *Global Warming Potential* (GWP).

[2] `https://flypix.ai/blog/deep-space-monitoring/` [Accessed 20/05/2025]

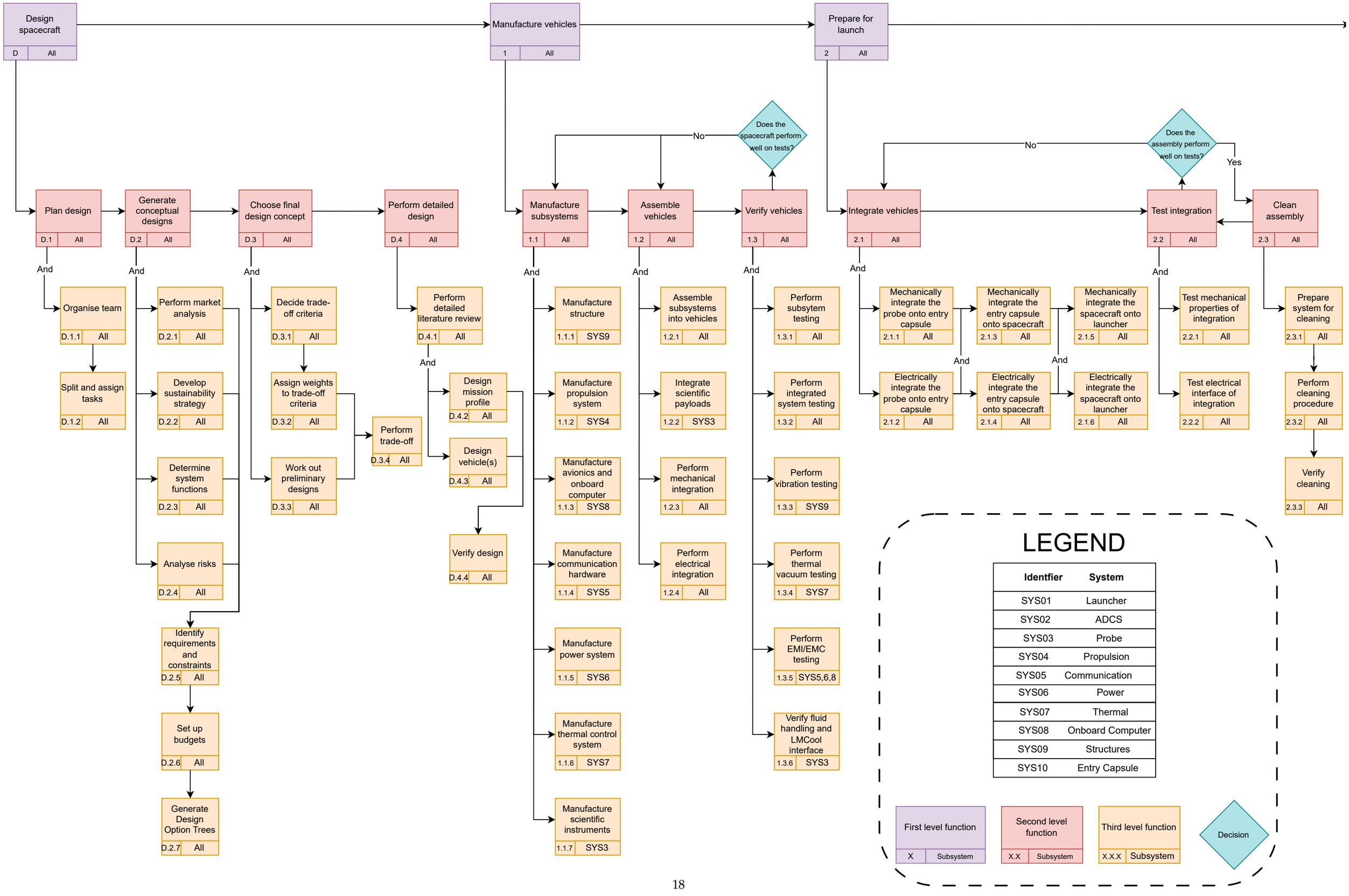
Design spacecraft
D All
Manufacture vehicles
1 All
Prepare for launch
2 All
Plan design
D.1 All
Generate conceptual designs
D.2 All
Choose final design concept
D.3 All
Perform detailed design
D.4 All
Manufacture subsystems
1.1 All
Assemble vehicles
1.2 All
Verify vehicles
1.3 All
Does the spacecraft perform well on tests?
No
Integrate vehicles
2.1 All
Test integration
2.2 All
Clean assembly
2.3 All
Does the assembly perform well on tests?
No
Yes
And
Organise team
D.1.1 All
Split and assign tasks
D.1.2 All
Perform market analysis
D.2.1 All
Develop sustainability strategy
D.2.2 All
Determine system functions
D.2.3 All
Analyse risks
D.2.4 All
Identify requirements and constraints
D.2.5 All
Set up budgets
D.2.6 All
Generate Design Option Trees
D.2.7 All
Decide trade-off criteria
D.3.1 All
Assign weights to trade-off criteria
D.3.2 All
Work out preliminary designs
D.3.3 All
Perform trade-off
D.3.4 All
Perform detailed literature review
D.4.1 All
Design mission profile
D.4.2 All
Design vehicle(s)
D.4.3 All
Verify design
D.4.4 All
Manufacture structure
1.1.1 SYS9
Manufacture propulsion system
1.1.2 SYS4
Manufacture avionics and onboard computer
1.1.3 SYS8
Manufacture communication hardware
1.1.4 SYS5
Manufacture power system
1.1.5 SYS6
Manufacture thermal control system
1.1.6 SYS7
Manufacture scientific instruments
1.1.7 SYS3
Assemble subsystems into vehicles
1.2.1 All
Integrate scientific payloads
1.2.2 SYS3
Perform mechanical integration
1.2.3 All
Perform electrical integration
1.2.4 All
Perform subsytem testing
1.3.1 All
Perform integrated system testing
1.3.2 All
Perform vibration testing
1.3.3 SYS9
Perform thermal vacuum testing
1.3.4 SYS7
Perform EMI/EMC testing
1.3.5 SYS5,6,8
Verify fluid handling and LMCool interface
1.3.6 SYS3
Mechanically integrate the probe onto entry capsule
2.1.1 All
Electrically integrate the probe onto entry capsule
2.1.2 All
Mechanically integrate the entry capsule onto spacecraft
2.1.3 All
Electrically integrate the entry capsule onto spacecraft
2.1.4 All
Mechanically integrate the spacecraft onto launcher
2.1.5 All
Electrically integrate the spacecraft onto launcher
2.1.6 All
Test mechanical properties of integration
2.2.1 All
Test electrical interface of integration
2.2.2 All
Prepare system for cleaning
2.3.1 All
Perform cleaning procedure
2.3.2 All
Verify cleaning
2.3.3 All
LEGEND
Identfier System
SYS01 Launcher
SYS02 ADCS
SYS03 Probe
SYS04 Propulsion
SYS05 Communication
SYS06 Power
SYS07 Thermal
SYS08 Onboard Computer
SYS09 Structures
SYS10 Entry Capsule
First level function
X Subsystem
Second level function
X.X Subsystem
Third level function
X.X.X Subsystem
Decision

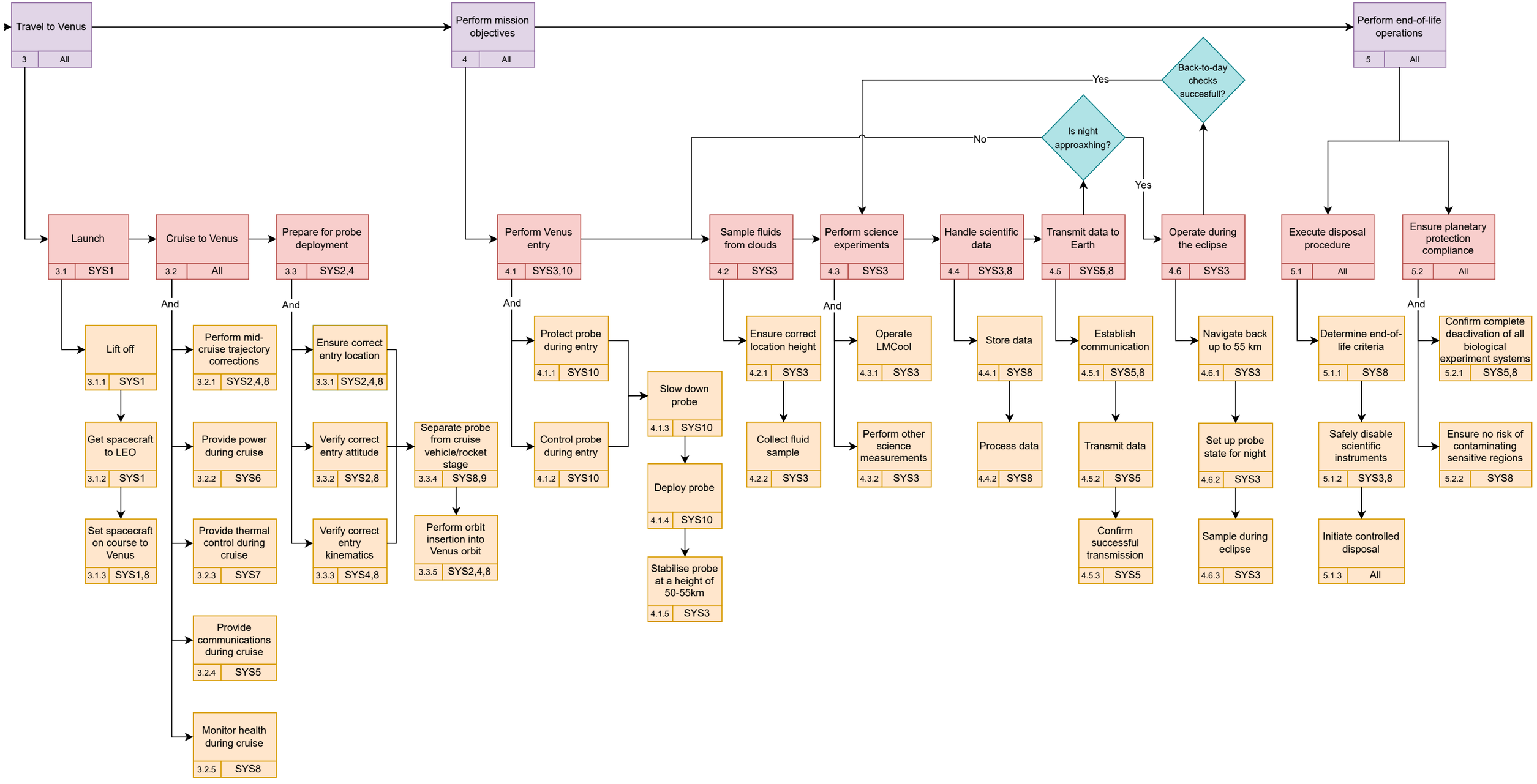

Figure 3.3: Functional Flow Diagram for the mission.

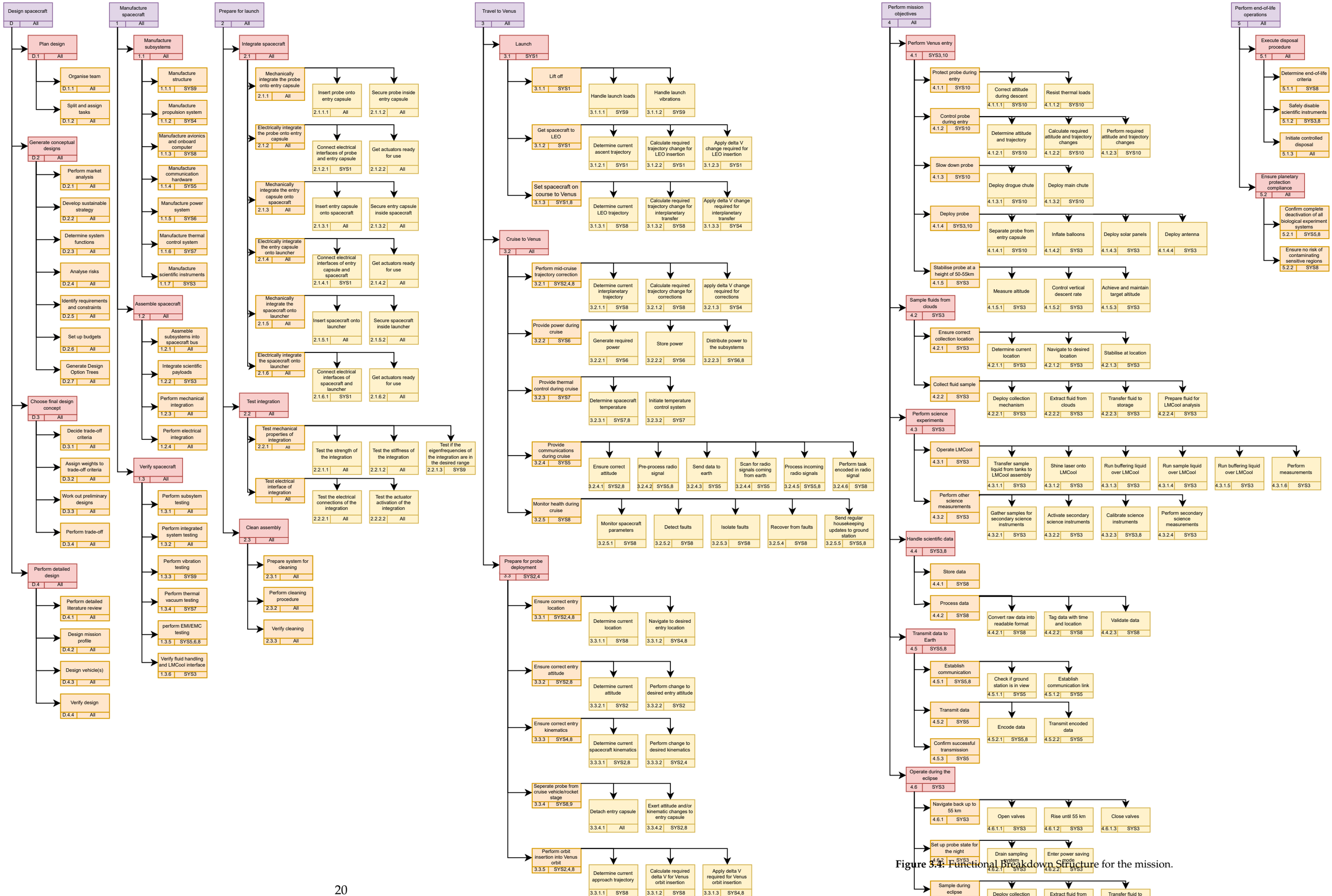

Figure 3.4: Functional Breakdown Structure for the mission.

Manufacturing
First of all, The use of Commercial Off-The-Shelf (COTS) components is highly prioritised. COTS reduce the need for resource-intensive custom manufacturing. By leveraging existing, mass-produced components, material waste, energy consumption, and associated emissions during production are significantly minimised. COTS availability also facilitates reuse, refurbishment, and recycling at end-of-life, aligning with circular economy principles.

Furthermore, preference is given to materials with low environmental impact. Also, components and parts should be sourced from manufacturers with proper environmental management strategies, manufacturers with established Environmental Management Systems (EMS), like ISO 14001, are prioritized. Local manufacturers are also preferred to reduce transport emissions.

A specific concern is the use of helium. Its extraction and processing have notable environmental impacts, and as a non-renewable and scarce resource on Earth, it cannot be artificially produced. Alternative gases were evaluated: hydrogen was deemed too flammable and hazardous, with costly and polluting storage needs; nitrogen, while safer, proved too heavy, resulting in an unfeasible design. Ultimately, helium remains the only viable option, and measures will be taken to use it efficiently and responsibly.

Another important concern is the use of high density batteries. They typically represent an important part of manufacturing impact, and several alternatives to classical polluting batteries will be observed in the detailed design. This includes solid-state batteries (less flammable, less toxic materials), batteries with recycling agreements, modular batteries, and low-cobalt batteries like $LiFePO_4$ if energy density is acceptable.

Lastly, Polytetrafluoroethylene (PTFE) and Fluorinated Ethylene Propylene (FEP), commonly known as Teflon®, serve as the primary coating material for many probe components: the full large-area balloon, the exposed sampling system, and the fluidic network. PTFE and FEP are essential due to their resistance to concentrated sulphuric acid and very beneficial because of their lightweight properties. However, its production involves hazardous chemicals and generates significant environmental pollution. Alternatives have therefore been explored, but without success. One such option is Perfluoroalkoxy Alkane (PFA), which offers similar performance. Yet, like PTFE and FEP, it belongs to the infamous group of Polyfluoroalkyl, substances known as PFAS, or "forever chemicals". These substances owe their durability in harsh environments to the same extreme chemical stability that also makes them persistent, non-degradable pollutants. To limit any damage, strict handling protocols will be implemented, including adequate ventilation and provision of personal protective equipment (PPE).

Testing
Testing is a crucial step to ensure the spacecraft's reliability, but it can also be approached sustainably. Where possible, digital twin simulations and hardware-in-the-loop tests are employed to minimize the need for full-scale physical prototypes. This reduces material use and avoids the energy-intensive manufacturing of multiple products.

For environmental tests that remain unavoidable such as vibration, thermal vacuum, and electromagnetic compatibility, consolidated testing campaigns are scheduled to maximize efficiency and reduce facility usage time. The adoption of shared ESA testing facilities, already optimized for sustainability[3], further limits the footprint of the verification phase.

Launch & Transfer
The launch contributes the most to the mission's environmental footprint. Accordingly, much effort is put to effectively choose a launcher with sustainable considerations and a transfer orbit that minimises the required fuel. As will be explained in section 4.1, the RFA One rocket is selected as the launcher

[3] https://www.esa.int/About_Us/ESTEC/ESA_signs_contract_to_modernise_ESTEC_campus

for Orpheus. RFA one's consideration and stances on sustainability are assessed.

RFA notably plans on completing ten launches per year on the developing SaxaVord Spaceport, which provided an Assessment of Environmental Effects in 2023 [27], which has for example extensive considerations on local bird biodiversity and harm, as well as more general animal habitats preservation. The proximity of the SaxaVord Spaceport in the UK is highly advantageous, as it allows spacecraft assembled at ESA's ESTEC facility in Noordwijk to avoid the long journey to French Guiana, which is typically ESA's sole launch site. This significantly reduces transportation-related emissions, making the launch process more sustainable and environmentally friendly.

Furthermore, RFA One is designed with partial reusability in mind, contributing to a further reduction in its environmental impact. Specifically, the rocket's first stage is engineered for recovery and refurbishment, allowing it to be reused in subsequent launches [28]. By avoiding the need to manufacture entirely new stages for every mission, material consumption, manufacturing emissions, and waste generation are substantially decreased. This reusability approach aligns with broader industry trends aiming to make space access more sustainable.

Considering the transfer orbit, fuel need can be minimised by optimising the orbit for minimal ΔV. In future stages of the design process, complex manoeuvrers such as gravity assists and aerodynamic breaking will be considered. On top of this, the fuel collection should be monitored to ensure it incorporates sustainable practices.

Operations
Operational sustainability focuses on minimizing the mission's environmental footprint during its active lifetime, this mainly concerns the activity of ground stations. Ground stations powered with renewable power and energy efficient technologies are prioritised. All data transmissions are scheduled such that the ground station needs activation only at specific times. Additionally, this can be coordinated with other missions to avoid redundant infrastructure use.

The storage of data will be done in green data centres. TU Delft's North C Data center[4], which aligns with tier 3 data center standards and is certified 100% green energy, is an evident choice.

Planetary Protection

The international agreements about planetary protection are summarised in COSPAR's planetary protection protocols. Celestial bodies are separated into categories of increasing sensitivity. Venus has been categorised as a category II celestial body, with the following description:

> *"bodies where there is significant interest relative to the process of chemical evolution and the origin of life, but where there is only a remote chance that contamination carried by a spacecraft could compromise future investigations."* [29]

At mission end, the gondola's biological instruments are disabled, and the balloon descends to the surface, where extreme pressure crushes it. If contact is lost, an automatic safe mode ensures proper disposal. All components are sterilized before launch to prevent biological contamination.

During controlled aerobraking, the spacecraft burns up in the atmosphere. Any complex molecules that survive will degrade under Venus' extreme pressure and temperature, breaking into simpler molecules already present in the atmosphere, further limiting contamination.

Societal Sustainability

Some aspects of sustainable development that are generally overlooked are societal considerations. It is challenging to account for the satisfaction of all individual and societal stakeholders with respect to the mission, whether directly involved or more distantly affected. This is split up into socio-economic, political and ethical considerations.

[4] https://www.northcdatacenters.com/en/northc-datacenters/delft/

Socio-Economic
The key socio-economic considerations are the development of multi-purpose technology, STEM education and workforce development and the the economically sustainable use of materials. Firstly, during the development of this mission, new developed technologies could have a dual earth based applications. This can create new jobs and the technology could be used to benefit society. Secondly, this mission will inspire new generations of STEM students and boost the education level of the work force. This is done by sharing the mission progress globally and sharing the attained knowledge to educational institutions. Finally, the sourcing of materials will be done in an economically sustainable way such that the suppliers are not exploited.

Political
Considering the current tense international politics, effort is made to adhere to European strategic autonomy as per requirement **STK-9** [2]. The Orpheus mission will demonstrate European corporation and space independence by reducing reliance on non-European partners. This is done by prioritising the use of European made off-the-shelf components and using European infrastructure for manufacturing, assembly, launch stations and ground operations. Furthermore, the origins of goods or services used that are not available within Europe will be monitored and alternate providers are listed for rapid replacement. Finally, the scientific findings will be published to the rest of the world promoting global scientific collaboration and avoiding the perception of space colonisation. This will present an example of democratic, peaceful and sustainable space exploration.

Ethical
The main ethical considerations of the Orpheus mission are the incentives behind the mission and the labour practices. Firstly, the incentives behind the mission are solely to attain a greater scientific understanding of our solar system and the Venusian cloud layer. Every effort will be made to ensure full transparency with the general public regarding scientific findings, emissions, and supply chains. Lastly, fair humane labour practices and proactive management strategies will be implemented to have an ethical work environment.

3.4.1. Enforcement
In order to ensure that these rules are enforced, a sustainability officer has been appointed (Alphan) who is responsible for the implementation of the aforementioned guidelines.

The life-cycle engineer (Ward) oversees the specifics of environmental sustainability, and is concerned with how the requirements with regard to the Venusian environment will be fulfilled exactly.

4 Journey to Venus

The mission begins with the transfer of the probe from Earth to Venus. For this purpose, a spacecraft is designed to facilitate the transfer and later function in orbit around Venus as a communication relay between the probe and Earth. The launcher selection is presented in section 4.1 and the astrodynamic characteristics of the transfer trajectories are detailed in section 4.2. The spacecraft design is outlined in section 4.3 and the probe's entry into the Venusian clouds is described in section 4.4.

4.1. Launcher

The selection of a launcher drives the mission design as it defines the initial conditions for the orbital trajectory and the mass budget. First, launcher selection criteria are chosen to narrow down the extensive list of launch options available (subsection 4.1.1). Subsequently, a study is presented that investigates various launcher options that meet the criteria. The selected launcher for the Orpheus mission is the **RFA One** rocket. Vega-C is chosen as backup option (subsection 4.1.2).

4.1.1. Launcher Considerations

This section provides argumentation for the criteria and considerations on which the launcher choice is based. A literature study was done but unfortunately each manufacturer states its launcher performance using different metrics, making a numerical comparison difficult. The payload user guide is not publicly available for all options either, further complicating a numerical study. Thus, the following four criteria were set up to narrow down the options qualitatively.

- **Small Launchers** The first criterion is that the launcher should fall into the small-lift vehicle category($< 2000\ kg$). This stems from the fact that interplanetary missions require very specific trajectories which are not of high interest for other missions, limiting rideshare options. On top of that, missions like this have tight launch windows, limiting the options even further. Thus a dedicated launch is preferred. Next to that, with sustainability and cost in mind the launcher picked should not over-perform too much.
- **European Autonomy** Driven by **Req-EXT-3**, the launch should be executed by a European provider. Since the only operational small-lift European launcher is Vega-C, also launchers under development are being considered. This leads to the next criterion, the TRL.
- **Technology Readiness Level (TRL)** A lot of smaller European privately funded companies and start-ups are developing new launchers. It should be kept in mind that making a launch company profitable is very hard, and that it is not uncommon for young companies to go bankrupt. It is therefore not without extra risk. To mitigate this, it was decided that only companies that have done successful testing and have a finalised design will be considered.
- **Launch site** The launch site is an important consideration, since it is closely connected to the mass a rocket can deliver to the required orbit. Launch sites close to the equator offer two advantages for interplanetary launches. Firstly, interplanetary missions have inclinations close to 0. Thus equatorial launches are beneficial to minimise ΔV for inclination changes. Next to that, earths rotational speed is largest at the equator, further maximising the launcher's capabilities. For these reasons, Europe's Centre Spatial Guyanais (CSG) is therefore the best candidate. Other European spaceports like Esrange, Andøya or Saxavord are all located at higher latitudes. The recent decision to allow private launches from CSG is therefore ideal for Orpheus.

Next to these criteria, two other metrics are considered. These are launch cost and sustainability. These are not used in an absolute sense, but will rather be used as trade-off criteria to compare the final

options relative to each other.

- **Launcher performance** While all can deliver the mission, the performance is still an important factor. A more powerful launcher reduces the ΔV that the spacecraft has to provide itself, therefore reducing the mass of the spacecraft and in particular the propellant system.
- **Cost** Even though no user requirement on the launch cost is provided, it is still deemed an important factor in the launcher choice. Especially compared to the estimated mission cost in subsection 7.2.2, it should not be neglected. The new European launch providers aim to offer competitive pricing to gain market traction.
- **Sustainability** Sustainability is an important factor to be considered, both from an environmental and operational standpoint. It includes the launcher propellant type, but also the companies general sustainability approach. This includes reusability, usage of COTS components, materials and manufacturing processes.

4.1.2. Selected Launcher and Backup

From a comprehensive list of launcher options, the options that fall within the 4 specified criteria are further compared on Cost and Sustainability. Table 4.1 lists the 4 final launchers. Note that the payload capacity to LEO is used to compare the options, but Orpheus' launch mass will be significantly lower, since it requires insertion into an interplanetary transfer trajectory. The fuel type used in the first stage is also included, since this is an important measure to consider for sustainability.

Table 4.1: Launcher options for Orpheus.

Company and name	Fuel type	Payload to LEO [kg]	Launch cost [EUR]
Avio Vega-C	Solid	2300	37M
PLD Space Miura 5	RP-1/LOX	1080	12M
RFA One	RP-1/LOX	1600	3M
Isar Aerospace Spectrum	Propane/LOX	1000	10M

From these four options, the **RFA One** rocket is selected as the launcher for Orpheus. The main reason for this choice is the pricing of RFA, which is an order of magnitude cheaper than the others. While an optimistic estimate from the company, they have repeatedly mentioned that they are using COTS parts where possible, and that their design is purely driven by a low-cost requirement. Even if a launch would triple in price, it is still the cheapest option. Considering the fuel type, RFA uses RP-1/LOX, a refined version of kerosene. While Isar's use of propane is slightly less polluting, the difference is small and it was deemed not to weigh up against the cost argument. Next to that, the use of COTS components aligns with Orpheus' design philosophy and is positive for sustainability. PLD space's Miura 5 launcher was discarded due to higher cost, and the fact that its TRL is lower than both RFA and Isar. Vega-C is selected as backup option, since it is the only option in the list with flight heritage.

4.1.3. Launcher Performance

No data is publicly available about the RFA One rocket's performance regarding a Venus transfer orbit. In particular, payload mass and corresponding ΔV performance are needed to evaluate the maximum mass that the launcher can insert into transfer orbit. However, it is known that the launcher can place a payload of 300 kg into lunar transfer orbit [1]. A ΔV of approximately 3.0 $km \cdot s^{-1}$ can be assumed for insertion into Lunar Transfer Orbit from Earth orbit[2]. The optimal launch date (subsection 4.2.2) requires a ΔV provided by the launcher of 3.32 $km \cdot s^{-1}$. For a total mission mass of less than 120 kg it is assumed, that the launcher can provide the required performance. In case a different launch window is used, the ΔV requirements for insertion can increase. For further development, a collaboration with RFA is needed.

[1] `https://www.rfa.space/rfa-one/` Accessed:18/06/2025

[2] `https://en.wikipedia.org/wiki/Delta-v_budget`[Accessed: 17/06/2025]

4.2. Astrodynamic Characteristics

Travelling from Earth to Venus is a demanding task, that requires precise trajectory design to keep the fuel consumption as low as possible. Every kilogram saved on propellant allows for more structural and payload mass, while still adhering to the tight mass budget. This section presents the strategy followed to optimise the transfer trajectory and the mission timing to ensure maximising the scientific return.

Subsection 4.2.1 explains the general trajectory approach, including the two main burns into transfer orbit and into target orbit at Venus, along probe handling and launch date considerations. Subsection 4.2.2 gives numerical values for the ΔV based on possible launch windows. Finally, subsection 4.2.3 describes the final orbit around Venus of the spacecraft and its influence on the subsystems designs.

4.2.1. Interplanetary Transfer Approach

The launch date must be analysed to identify the optimal timeframe that results in the minimum required ΔV possible. Since this is a computationally intensive process, the search must be constrained to a practical range of years to avoid evaluating launch windows that are either too soon or unnecessarily far in the future. For this reason, the analysis is limited to the period between 2030 and 2040. This timeframe is driven by two key factors: the readiness of the mission design and the availability of the selected launch vehicle. On one hand, the spacecraft design still requires further development and extensive testing, making a launch within the next few years unfeasible. On the other side, the launcher is not commercially operative yet, again restricting the next few years. Therefore, 2030 is considered a realistic starting point for viable launch windows. 2040 is selected as the upper boundary to prevent excessive delays to the mission timeline. The exact launch windows with backup dates are presented in subsection 4.2.2.

As explained in section 4.1, the launcher has been selected such that the spacecraft is brought into transfer orbit without having to perform the insertion burn by itself. Once released into transfer orbit, the journey to Venus takes about 160 days depending on the launch date. The transfer trajectory can be seen in Figure 4.1.

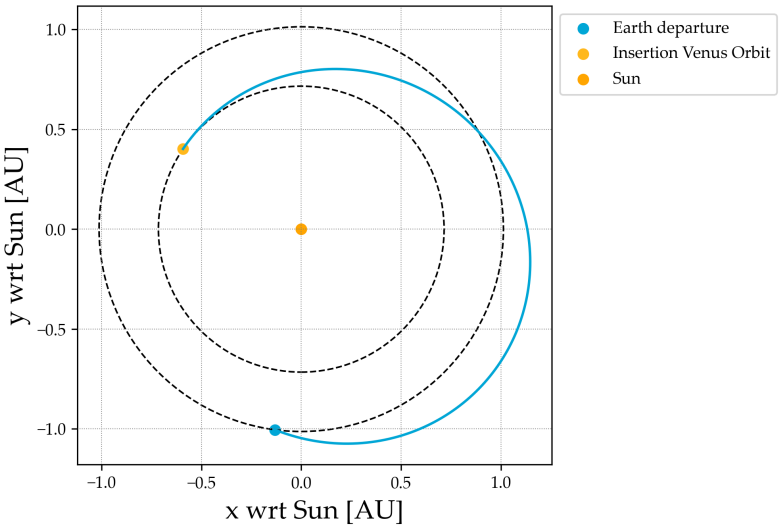

Figure 4.1: Interplanetary transfer trajectory from Earth to Venus.

The probe is separated from the spacecraft before reaching Venus due to the positive effect on the ΔV required for the target orbit insertion burn, as anticipated in the Midterm Report [1]. Not having the mass of the probe onboard while performing the insertion burn into Venus' orbit considerably reduces the amount of propellant needed, allowing more payload and structural mass for other systems.

Hence, this strategy is pursued. The timing of the probe release is considered to be 30 min before the insertion of the orbiter around Venus. This assumption is derived from the Venus Life Finder mission [30], as this is the strategy investigated in their paper. Additionally, it is preferred to keep the probe connected to the spacecraft for as long as possible as the spacecraft delivers the power to the probe during transfer. However, further refinement must be done to verify that 30 min would also be satisfactory for the Orpheus mission, and is thus included in the post-DSE activities in section 8.3.

Once the spacecraft approaches Venus, the insertion is performed at the point that will be the pericenter of the final orbit (subsection 4.2.3). The probe enters the Venusian atmosphere and the scientific mission can start.

4.2.2. Trajectory Simulation

To find the optimal transfer, a model has been set up using the TU Delft Astrodynamics Toolbox (tudat), a set of Python libraries for astrodynamics and space research [3]. The trajectory approach explained above is simulated. The launch frame from 2030 - 2040 is split up into chunks of five days, for which an optimisation problem is run. The optimisation is based on minimising the ΔV required for the insertion burn from the transfer trajectory into orbit around Venus. The launcher picked will likely not be shared with other payload, since the Orpheus has a very specific trajectory that might not be needed by other possible clients. The Orpheus mission is also lighter than what the launcher could transport. Thus, the insertion burn from LEO into the transfer trajectory, provided by the launcher, is not critical and the optimisation problem can focus on minimizing the insertion burn from transfer into Venus orbit provided by the spacecraft. This minimizes the propellant and propulsion system mass required onboard the spacecraft and allows for higher structural and payload mass. The required ΔV for orbit insertion at Venus based on the launch date is shown in Figure 4.2. The required ΔV varies because the approach velocity depends on the specific transfer orbit, which in turn is determined by the relative positions of the planets at a given time.

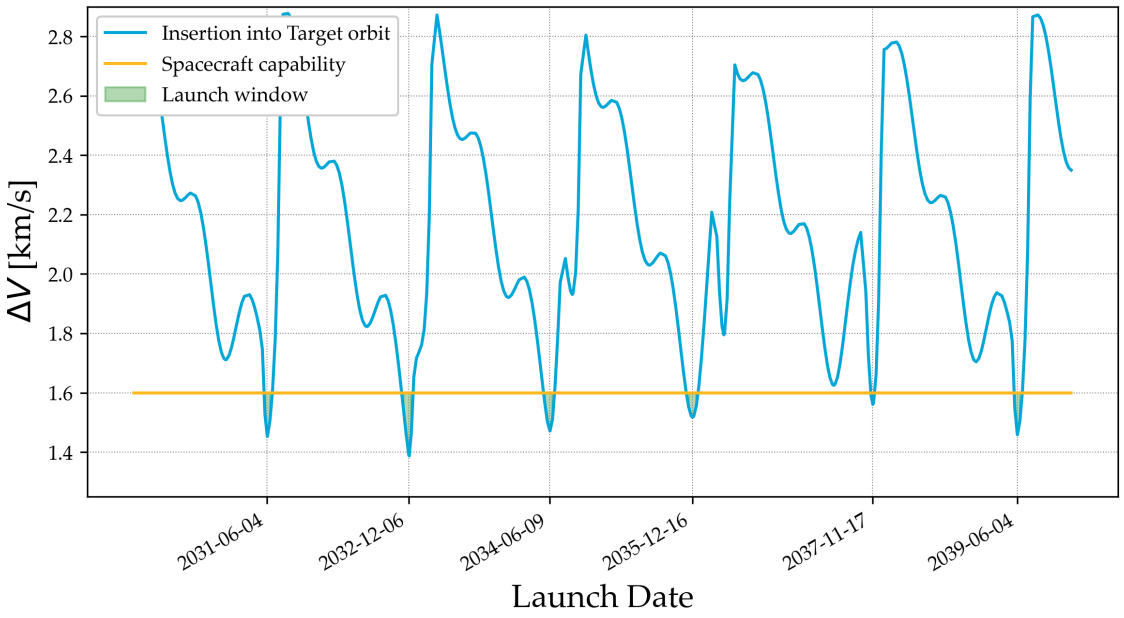

Figure 4.2: Spacecraft ΔV required for insertion burn from transfer trajectory into orbit around Venus based on launch date from 2030 - 2040.

The optimal launch date would be the 09.12.2032 with a spacecraft ΔV of 1.39 $km \cdot s^{-1}$. It is desired to have backup launch dates in case of mission delays. Figure 4.2 shows that there is a local minimum for

[3] `https://docs.tudat.space/en/latest/`, [Accessed 16/06/2025]

the required ΔV, approximately every 2 years. To have sufficient alternative backup launch dates, the spacecraft is designed for an insertion ΔV of 1.6 $km \cdot s^{-1}$. Increasing the available ΔV for the insertion burn at Venus also increases the launch window length of each launch opportunity, which allows for rescheduling in case the weather conditions make a launch impossible at a certain moment. For the optimal launch window in December 2032, for instance, the launch window would have a length of about 47 days for a ΔV of 1.6 $km \cdot s^{-1}$. A summary of possible launch dates and corresponding launch windows are shown in Table 4.2.

Table 4.2: Launch windows.

Optimal launch date	ΔV Budget [$km \cdot s^{-1}$]			Launch window	
	Launcher	Spacecraft	Total	Start	End
06.12.2032 (Optimal)	3.32	1.388	4.71	08.11.2032	24.12.2032
09.06.2034	3.80	1.47	5.28	15.05.2034	27.06.2034
16.12.2035	5.08	1.52	6.53	22.11.2034	07.01.2035
17.11.2037	4.93	1.56	6.49	09.11.2037	25.11.2037
04.06.2039	3.68	1.46	5.91	21.05.2039	22.06.2039

Verification and Validation

The code is verified by simulating an extensive example from the official tudat page [4] and comparing the results. Furthermore, when simulating the transfer to Venus, results from NASA's optimised transfer trajectories database [5] are used for comparison. While NASAs predicted ΔV requirements differ because different models and assumptions are used, the dates of the local minima of insertion burns coincide.

4.2.3. Target Orbit of Spacecraft around Venus

The orbit of the spacecraft has an influence on multiple subsystems that have to be all taken into account to select a final orbit.

Influence of Target Orbit on Design

The target orbit design has an effect on the ΔV needed for the insertion burn from transfer, the power generation by the solar panels of the spacecraft and the communication to the probe and to Earth.

To minimize the ΔV for the insertion burn, a highly elliptic orbit is desired. The lower the pericenter and the higher the apocenter, the lower the ΔV requried. A circular orbit around Venus is unfeasible for a low mass mission like Orpheus, since it requires a very high ΔV. For comparison, an orbit at an altitude of 400 km would require an optimised ΔV of 3.28 $km \cdot s^{-1}$ while an elliptical orbit with an apocenter at 20,000 km and pericenter at 300 km can be optimised for a ΔV of 1.38 $km \cdot s^{-1}$.

The power for the spacecraft is provided by a solar array. Thus, it is desired to maximise the time of the spacecraft in the sun and to minimize the time in eclipse. For an elliptical orbit it would be optimal to have the pericenter, where the spacecraft moves fastest, in the eclipse.

The communication with the probe differs based on whether the probe is operating on the day or night side of Venus. System telemetry data is produced during the entire mission, but scientific data is only produced during the day time (subsection 4.3.7). It is desired to transmit scientific data as fast as possible and minimise the time it is stored by the probe to reduce data loss when the probe fails. Thus

[4] `https://docs.tudat.space/en/latest/examples/tudatpy-examples/mission_design/cassini1_mga_optimization.html`, [Accessed 16/06/2025]

[5] `https://trajbrowser.arc.nasa.gov/`, [Accessed: 14/06/2025]

it is wanted that the probe has longer contact times when on the day side compared to the night side. Again, it is preferred to have the pericenter of the spacecraft orbit in eclipse.

For communication with Earth, it is optimal to have the pericenter in the part of the orbit where Venus blocks communication with Earth, because the spacecraft moves fastest at pericenter. Placing it in the no-contact zone minimizes the time spent without contact, while maximizing communication time near apocenter, where the spacecraft moves more slowly and is visible from Earth. The desired pericenter location depends on the relative position of Earth and Venus during mission operation.

Target Orbit Characteristics

The different subsystem preferences are taken into account when designing the final target orbit of the spacecraft. The selected orbit at arrival at Venus is shown in Figure 4.3.

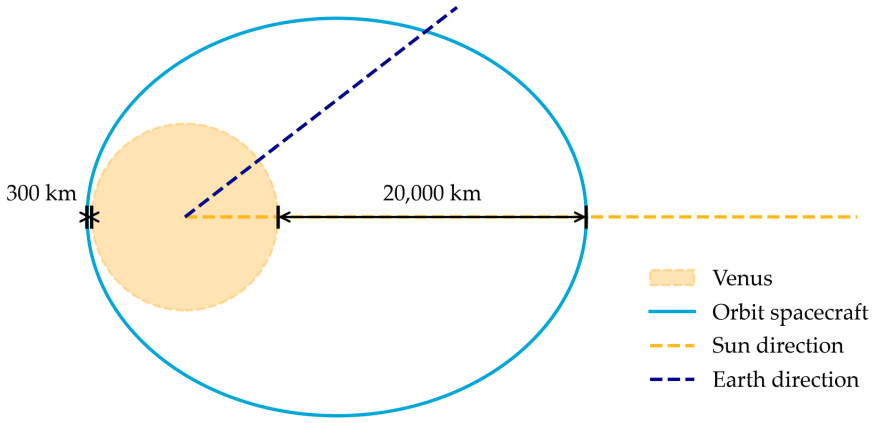

Figure 4.3: Spacecraft orbit around Venus at arrival.

The pericenter altitude is minimised and the apocenter alitude is maximised based on the desired orbit characteristics for the different systems mentioned above. The pericenter is chosen to be at an altitude of 300 km, which is a typical pericenter altitude for scientific Venus missions [31, p. 51]. At a lower pericenter, the atmospheric influence that leads to orbit circularisation increases significantly. The altitude of the apocenter is chosen to be 20,000 km. The limiting factor is the communication system of the probe. A higher apocenter requires more power than available for transmitting data from the probe to the spacecraft, decreasing the reliability of communication.

The orbit is equatorial since the probe is operating mostly close to the equator. Furthermore, this minimises the required ΔV related to inclination change during transfer.

The orbit will be oriented such that the apocenter lies on the line connecting Venus and the Sun, and the pericenter is located in the eclipse. This allows for a maximum time in the Sun for the power system and long communication windows with the probe when operating on the day side. Based on the relative position of Earth and Venus at arrival (15.05.2033) for the selected launch date (06.12.2032), this orientation also provides sufficient transmission periods to Earth. Throughout the mission, the apocenter will propagate out of the ideal position due to the orbital motion of Venus around the Sun. This effect is taken into account when sizing the power and communication subsystems of the spacecraft in later sections.

4.3. Spacecraft Design

The trajectory design sets the path to reach Venus, but a capable vehicle is needed to facilitate the journey. With the transfer orbit and timing defined, the next step is to ensure that the spacecraft can support the journey. A set of requirements for the spacecraft was defined in the Baseline Report [2],

and the following analysis will complete the still unknown values in the requirements, while designing for them. A completed list can be seen in Table 4.3. These set the baseline for the choice of components.

Table 4.3: Requirements table. EVT: Earth-Venus Transport, VEE: Venus Entry, SCM: Scientific Mission, INT: Internal Constraints, EXT: External Constraints, SAR: Safety and Reliability.

Requirement ID	Requirement
Earth-Venus Transport	
Req-EVT-1	The system shall be compatible with the launcher.
Req-EVT-1.1	The system shall withstand the vibrations during launch as specified by the launch provider.
Req-EVT-1.2	The system shall withstand the loads during launch specified by the launch provider.
Req-EVT-1.3	The dimensions of the system shall comply with the fairing dimensions of the RFA One launch vehicle.
Req-EVT-2	The system shall comply with the set engineering budget during the transfer to Venus.
Req-EVT-2.1	The system shall have a maximum mass of 320 kg.
Req-EVT-2.2	The spacecraft shall provide a ΔV of at least 1.6 $km \cdot s^{-1}$.
Req-EVT-2.3	The spacecraft shall provide a power of at least 47 W at 1 AU.
Req-EVT-2.4	The spacecraft shall provide a downlink transmission data rate of 1.4 $kbps$
Req-EVT-3	The spacecraft shall comply with the minimum required performance parameters.
Req-EVT-3.1	The spacecraft shall provide a thrust of at least 200 N.
Req-EVT-3.2	The spacecraft shall achieve a pointing accuracy higher than 0.5° (3σ) in all axes during the transfer to Venus.
Req-EVT-3.3	The spacecraft shall achieve orbital insertion with an altitude error of no more than <TBD> km relative to the target orbit.
Req-EVT-3.4	The spacecraft shall achieve orbital insertion with an inclination error of no more than <TBD> degrees relative to the target orbit.
Req-EVT-3.5	The spacecraft shall achieve orbital insertion with a right ascension of the ascending node error of no more than <TBD> degrees relative to the target orbit.
Req-EVT-4	The system shall withstand the operational environment during the transfer to Venus.
Req-EVT-4.1	The system and its components shall be able to withstand the radiation of the space environments.
Req-EVT-4.2	The system shall withstand the thermal environment.
Req-EVT-4.2.1	The system shall withstand a total temperature range of [243, 333 K] for the duration of the transfer to Venus.
Req-EVT-4.2.2	The system shall withstand the thermal load during for the duration of the transfer to Venus.
Req-SCM-6	The spacecraft shall provide the necessary operational support functions to enable full execution of the scientific payloads' measurement.
Req-SCM-6.1	The spacecraft shall provide an average power of at least 55.5 at 0.72 AU.
Req-SCM-6.2	The spacecraft shall provide a data rate of at least 1 kbps to transmit scientific data.
Req-SCM-6.3	The spacecraft shall be able to store at least 25 MB of data in between transmission periods.

Subsection 4.3.1 gives an overview of the general parameters of the spacecraft along with its configuration. Following, the attitude determination and control system and the propulsion system are

presented in subsection 4.3.2 and 4.3.3, respectively. An explanation for the simulation tool used in the spacecraft design is given in subsection 4.3.5. The power and communication strategies are outlined in subsection 4.3.6 and subsection 4.3.7, respectively.

4.3.1. Configuration and Structure

The main body of the spacecraft consists of a cubic shape of 40 x 50 x 50 cm sides. The Earth-pointing side has a parabolic antenna, used to transmit data back to Earth. Each one of the cube sides has a sun sensor, shown in Figure 4.4 on the top corner of each side. On the opposite face, the Venus-pointing one, another antenna is used to receive scientific data from the probe. The solar panels are attached to the sides and can be deployed, revealing the components attached to the structure. The main thruster is placed on the bottom face, surrounded by four supports that protect it when standing on the floor on Earth. On each corner of the same side, three small thrusters are placed, used to desaturate the ADCS and as a backup. On the top side, the capsule is attached by means of an adapter. The outside spacecraft configuration can be seen in Figure 4.4.

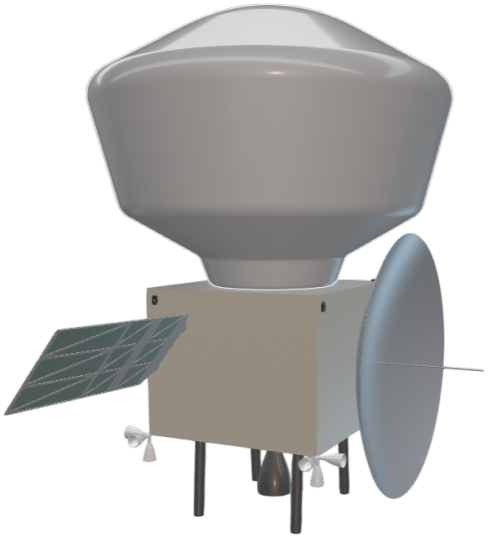

Figure 4.4: Spacecraft configuration

The fairing of the selected launcher, the RFA One, is 30 m in height and 2 m in diameter. Hence, the design complies with **Req-EVT-1.3**, as its maximum dimensions are 1.15 m in height and 1 m in diameter. All the other components, which are listed in Table 4.4, are placed inside the spacecraft.

Table 4.4: Spacecraft components.

Component	Amount	Total Mass [kg]	Power [W]	Section
Sun sensors	6	0.024	0.05	subsection 4.3.2
Rate Gyros	3	0.165	3.6	subsection 4.3.2
Reaction wheels	3	0.438	2.4	subsection 4.3.2
ADCS Thrusters	12	4.2	-	subsection 4.3.3
MON-3 tank	1	1.73	-	subsection 4.3.3
MMH-3 tank	1	1.73	-	subsection 4.3.3
Helium tank	1	2.06	-	subsection 4.3.3
MON-3 propellant	-	16.47	-	subsection 4.3.3
MMH propellant	-	9.98	-	subsection 4.3.3
Helium	-	0.04	-	subsection 4.3.3
Valves & Mount	-	1.104	32	subsection 4.3.3
Main Thruster	1	1.9	-	subsection 4.3.3
Patch heater MON-3 tank	1	0.04	15	subsection 4.3.4
Patch Gain Uplink Antenna	1	0.017	50	subsection 4.3.7
Parabolic High Gain Antenna	1	4	-	subsection 4.3.7
UHF Dipole Antenna	1	0.055	1.5	subsection 4.3.7
IRIS Radio	1	1.1	35	subsection 4.3.7
Onboard Computer	1	0.25	3.5	subsection 4.3.7
Cabling	-	0.4	-	subsection 4.3.7
Solar Panels	6	0.888	66	subsection 4.3.6
Battery	1	0.268	30 Wh	subsection 4.3.6

Continued on next page

Continued from previous page

Component	Amount	Total Mass [kg]	Power [W]	Section
PMD	1	0.35	-	subsection 4.3.6
Propellant Management Device (PMD)	1	0.35	-	subsection 4.3.6
Structures	-	0.62	-	subsection 4.3.1
Electrical Power System	-	0.93	2.5 - 28	subsection 4.3.1
Contingencies	-	1.66	-	subsection 4.3.1

All the components shown in Table 4.4 are off-the-shelf, except the structures, electrical components and contingencies (last three rows). These are general parts of the spacecraft that connect all of the components, plus margins for uncertainties. Their masses have been obtained from empirical relations [32]: 3% of the dry mass for structures, 4.5% for the electrical power system and 8% for contingencies.

The following subsections show the process to choose all the components in more detail, together with the analysis to make sure that they comply with the requirements.

4.3.2. Attitude Determination and Control System

The attitude determination and control system (ADCS) from the spacecraft ensures that the orientation of the orbiter is as desired, which is crucial for the Orpheus mission to communicate between the different systems. Sensors are needed to determine the attitude, and actuators to control it. The ADCS architecture can be seen in Figure 4.5, together with the interrelations between the systems.

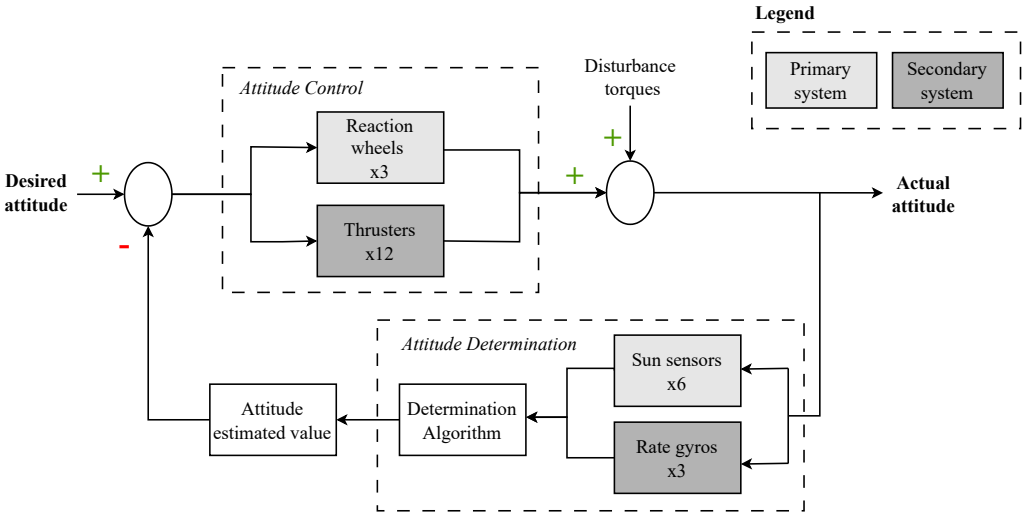

Figure 4.5: ADCS Block Diagram.

Sensors

Six Sun sensors and three rate gyros are chosen for the design. Because the spacecraft structure is cubic, one Sun sensor is needed on each side to ensure that multiple sensors can detect the Sun, regardless of the spacecraft's orientation. Off-the-shelf components are selected in order to reduce development and testing costs and increase reliability. The *NanoSSOC-A60* from Solar MEMS Technologies [6] is chosen due to its low weight, power consumption, and high flight heritage. Moreover, its pointing accuracy is higher than 0.5°, complying with **Req-EVT-3.2**.

Moreover, for redundancy and to reduce the calculation load of the onboard computer, three rate gyros are added as secondary devices. They measure the angular rate of rotation about one axis, hence

[6] `https://www.satcatalog.com/component/nanossoc-a60/`, [Accessed 15/06/2025]

one is needed for each of the three axes. The *STIM202* from Safran Sensing Technologies [7] is chosen, again due to its low weight and required power.

Sun sensors and gyros naturally complement each other due to the nature of their measurements. Sun sensors are not as reliable with high roll rates, so gyros can be used to measure the relative attitude. Additionally, measurement errors for the gyros accumulate over time, so sun sensors can be used to "reset" the error by obtaining the absolute attitude.

Actuators

Once the attitude is determined by the sensors, actuators are needed to move the spacecraft to the desired orientation. For this, three reaction wheels, the *RW20* from comat [8], are chosen because of their high momentum storage capability. However, they still have a maximum storage capacity, so thrusters are needed for desaturation purposes. Thrusters can also be a secondary actuator system, so twelve are chosen, as that is the minimum for full 3-axis control [33, p. 171]. 10 N thruster from ArianeGroup are selected, as is further explained in subsection 4.3.3.

In order to properly size the reaction wheels, information about the mass moment of inertia of the spacecraft is necessary, as it dictates the torque that the wheels need to provide. Because this information will change with every future iteration of the design, a conservative reaction wheel has been chosen for now. However, this needs further refinement and is thus included in the post-DSE activities in section 8.3.

4.3.3. Propulsion System

To perform the insertion burn into Venusian orbit and to act as an attitude control actuator, a propulsion system must be designed. For orbit insertion, the 200 N liquid bi-propellant thruster from the Ariane Group is chosen to meet **Req-EVT-3.1** [34]. This thruster is qualified to use monomethyl hydrazine (MMH) as a fuel and Mixed Oxides of Nitrogen (MON-3) as an oxidiser. This fuel-oxidiser combination is also used for the 10 N thruster from the same family, which has a single seat valve. Twelve of these thrusters are integrated into the propulsion system to perform attitude changes of the spacecraft and desaturate the reaction wheels as explained in subsection 4.3.2.

The reasons for choosing these propellants are summarized below:

- The propellants are hypergolic, eliminating the need for an ignition system, simplifying design and reducing failure points.
- The propellants support restarts and throttling.
- Using the same propellants for both main and ADCS thrusters simplifies the tank and plumbing system, reducing overall mass and complexity.
- The propellants are well-characterized and widely used, ensuring robust, reliable performance.
- Both are storable at ambient conditions; only MON-3 requires mild heating to avoid freezing which is discussed in subsection 4.3.4.

The propulsion system architecture is shown in Figure 4.6. Pressurised helium is stored in a third tank which pressurises the fuel and oxidiser as these tanks empty during burns. The propellants are stored in tanks with a flexible diaphragms separating the helium from the propellant preventing sloshing within the tanks. The separate pressure regulators and pressure transducers allow the fuel and oxidiser pressure to be controlled independently. All pyrogenic valves that are normally closed have a redundant one in parallel to improve reliability. The fuel and oxidiser are kept separate until they meet at the thrusters to prevent explosion hazards. The main thruster and the ADCS thrusters are turned on and off by solenoid valves.

[7] https://www.satcatalog.com/component/stim202/, [Accessed 15/06/2025]
[8] https://satcatalog.s3.amazonaws.com/components/1381/SatCatalog_-_COMAT_-_RW20_-_Datasheet.pdf

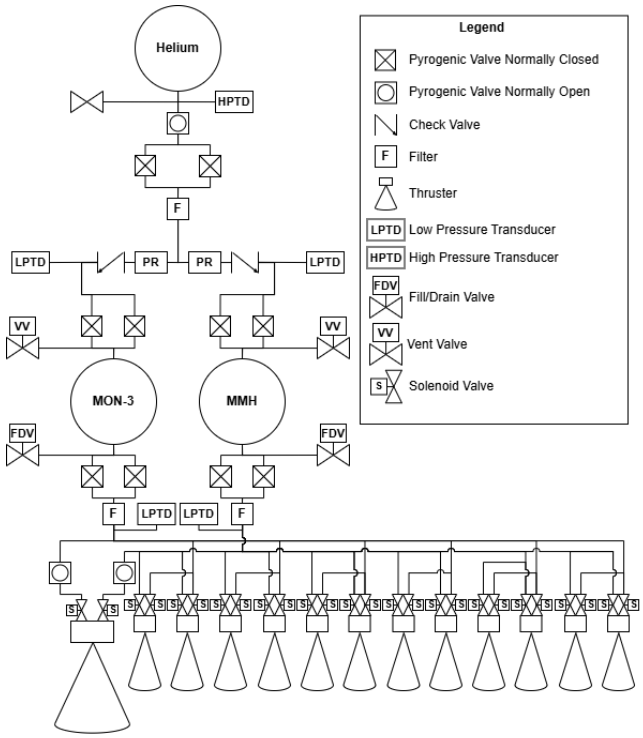

Figure 4.6: Spacecraft propulsion system diagram.

The propulsion system is sized to provide a total velocity change (ΔV) of 1840 $m \cdot s^{-1}$ to meet **Req-EVT-2.2**. 1600 $m \cdot s^{-1}$ is required for orbit insertion as explained in subsection 4.2.2, then a margin of 15% is included to account for Venus orbit maintenance, frequent attitude changes for communication links and minor transfer orbit adjustments.

The propellant mass can be estimated using the rocket equation described in Equation 4.1. The nominal specific impulse (I_{sp}) of the main thruster is 270 s [34] and g_0 is 9.81 $m \cdot s^{-2}$. The spacecraft dry mass (m_{dry}) is 23.97 kg, resulting in a required propellant mass of 26.46 kg after applying a 10% safety factor to account for propellant leakage and the inability to fully drain the tanks.

$$m_{\text{propellant}} = m_{\text{dry}} \cdot \left(\exp\left(\frac{\Delta V}{I_{\text{sp}} \cdot g_0}\right) - 1 \right) \tag{4.1}$$

The oxidiser to fuel ratio is 1.65 and the densities of MMH and MON-3 are 875 and 1440 $kg \cdot m^{-3}$ at 293K respectively, leading to 11.41 litres of MMH and 11.44 litres of MON-3 [34, 35]. Using the propellant volumes, the tank mass can be estimated with the statistical relationship shown in Equation 4.2, derived from qualified diaphragm tanks [35]. Here V is the propellant volume in litres and this leads to a mass of 1.73 kg for the MMH tank and the MON-3 tank.

$$m_{\text{tank}} = 2.36 \cdot 10^{-7} V^3 - 2.32 \cdot 10^{-4} \cdot V^2 + 0.131 \cdot V + 0.264 \tag{4.2}$$

The pressurant Helium gas mass (m_{He}) can be calculated based on the minimum inlet pressure for the thrusters of 10 bar [34] according to Equation 4.3. Here the ideal gas law is assumed, which holds well for Helium as it is a monatomic gas. Additionally, at the beginning of life, before the first spacecraft burn, the pressure tank is assumed to be at 323 K and 27.6 Mpa where the Helium density (ρ_{He}) is 36.78 $kg \cdot m^{-3}$ [35]. At the end of life, it is assumed that both the MMH and MON-3 tank volume ($V_{\text{propellant}}$) are completely filled with helium at 10 bar (P_{EOL}) and at 293 K (T_{EOL}) [35]. Here R_{He} is the

gas constant for helium, equal to 2078.615 $J \cdot kg^{-1} \cdot K^{-1}$. This results in a Helium mass of 0.04 kg with a tank volume of 1.07 litres.

$$m_{\text{He}} = \frac{P_{\text{EOL}} \cdot V_{\text{propellant}}}{R_{\text{He}} \cdot T_{\text{EOL}} - P_{EOL}/\rho_{\text{He}}} \tag{4.3}$$

Similarly to Equation 4.2, the statistical relationship shown in Equation 4.4 based on qualified pressurised Helium tanks can be used to estimate the helium tank mass [35]. The term PV represents the product of the pressure in Mpa and the volume in m^3 of the full helium tank at the beginning of life. This leads to a helium tank mass of 2.06 kg.

$$m_{\text{pressure tank}} = 5.4548 \cdot (PV)^2 + 6.6092 \cdot (PV) + 1.862 \tag{4.4}$$

Finally, the mass required for all the valves and the propellant tank mounting structures is accounted for by adding a mass equal to 20% of the mass of the propellant and pressurant gas tanks [36]. This is equal to 1.1 kg, leaving the total propulsion system mass at 35.05 kg, including the propellant mass.

Thermal control of the propellant tanks should be analysed; while the propellants are liquid at room temperature, the temperature in space can vary a lot. Thus it is important to ensure the propellant does not freeze. This is considered in the following subsection.

4.3.4. Thermal System

Thermal control is requried during the transfer from Earth to Venus to ensure that all components stay within their acceptable temperature range. The thermal control of the spacecraft is a mostly passive system, utilizing Multi-Layer Insulation (MLI) blankets. The exception is the addition of 3 small patch heaters for the MON-3 propellant tank, to prevent the propellant from freezing.

Thermal Simulation

A simplified thermal model of the spacecraft is set up to simulate its temperature behaviour, depending on the solar flux it receives based on the distance from the sun. The solar flux at any distance from the sun is given by the Equation 4.5.

$$S = S_0 \cdot \left(\frac{1\text{AU}}{d}\right)^2 \tag{4.5}$$

Where d is the distance from the sun in AU, S_0 the solar constant at earth($1367 W/m^2$) and S the local solar flux. The spacecraft is modelled as a cube with an edge of $0.5m$. Furthermore, the simulation assumes that radiation is received on one side of the cube, while radiating out to space using its total outside surface area. Note that this is a first order estimation, and it needs further refinement. Next to that, it is assumed that 30 W of heating is generated inside of the spacecraft, due to electrical components. Under these assumptions, a thermal balance is set up using Equation 4.6.

$$\alpha_{\text{s}} \cdot \ \text{A}_{\text{s}} \cdot \ \text{S} + \text{Q}_{\text{int}} = \varepsilon \cdot \text{A}_{\text{ext}} \cdot \sigma \cdot \ \text{T}^4 \tag{4.6}$$

Here, α_s is the solar absorptivity constant, A_S is the area receiving solar flux, S is the solar flux from Equation 4.5. On the right side of Equation 4.6, ϵ is the emissivity constant, A_{ext} the external area of the spacecraft, σ the Stefan-Boltzmann constant and T the equilibrium temperature. Both emissivity and absorptivity constants are assumed to be equal to 0.04, as taken from[36]. These values are given for well-established MLI blankets used in the space industry.

From Equation 4.6, the equilibrium temperature of the spacecraft, covered with MLI blankets can be calculated as a function of the local solar flux during transfer orbit. As a result of the simulation,

the temperature ranges from $-20.9°C$ at 1 AU (Earth), to $23.1°C$ at 0.72 AU (Venus). Since this range complies with **Req-EVT-4.2.1**.

As mentioned before, small heaters are needed for the first part of the transfer orbit to ensure the MON-3 propellant does not freeze, which happens below $-11.2°C$. To size the tank heater, Equation 4.7 is used.

$$P_{radiated} = \epsilon \cdot \sigma \cdot A \cdot \left(T^4 - T_{env}^4\right) \tag{4.7}$$

Where $P_{radiated}$ is the radiated power, ϵ is the emissivity constant, σ the Stefan-Boltzmann constant, A the radiated area, T the temperature and T_{env} the temperature from the environment. Assuming that the fuel tank stays at a temperature of $0°C$, and the tank has a low-emissivity coating applied ($\epsilon = 0.04$), it is found to radiate 5.3 W. This means that to keep the tank at a temperature of $0°C$, 5.3W of heating should be applied. Since this is only a first order estimation a total heating power of 10 $W$is assumed to pick the heating components. Next to that, redundancy is added by having multiple small patch heaters. In particular, the final tank heater system will consist of three 5 W patch heaters.[9]

4.3.5. Spacecraft Simulation Tool for Operation in Venus Orbit

For the operation of the spacecraft as a relay satellite between the probe and Earth, a simulation has been developed. It is used to size the power, communication and data storage subsystems.

The positions of the Sun, Venus, and Earth are determined using the tudat library. Based on the starting date of the mission, their positions can be propagated over the mission duration. The spacecraft's position is calculated using its orbital elements, assuming a two-dimensional Keplerian orbit for motion propagation. The probe's motion around Venus is modelled using a fixed orbital period of 8 days, representing the time required to complete one full rotation at the equator, as given by the general circulation model (subsection 4.4.3). This value is chosen as it results in the longest duration spend on the night side during the mission representing the most critical case.

Based on the relative position of the probe, the spacecraft and Earth, communication links can be represented, which allows to design for requirements regarding data rates of communication links and data storage size of the probe and the spacecraft in subsection 4.3.7.

Furthermore, operational conditions for each subsystem can be defined, allowing the simulation to calculate the power requirements throughout the mission. This enables a detailed and realistic design of the spacecraft's solar array and secondary batteries. The theoretical background and justification for the power system simulation are provided in subsection 4.3.6.

The simulation evaluates the conditions at each moment during the mission in time steps of 5 s. An example of the simulation interface can be seen in Figure 4.7. It shows the probe operating on the day side, communicating with the spacecraft and transmitting data. The spacecraft has already spend enough time in the sun since the last eclipse to fully recharge the batteries. At the shown state it is operating on energy directly delivered from the solar panels.

[9] https://www.satcatalog.com/component/flexible-heater-for-space/ Accessed: 04/06/2025

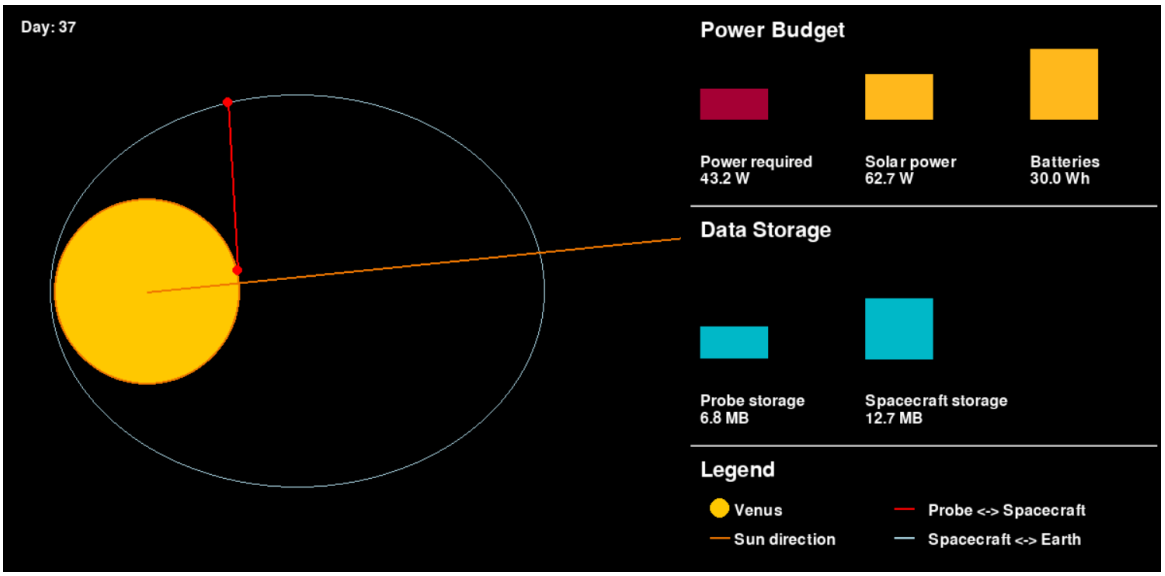

Figure 4.7: Interface of the spacecraft simulation.

Verification and Validation

The simulation is primarily verified through its user interface. Visual inspection ensures that key input parameters, such as the orbital periods of the spacecraft and probe, the maximum battery charge, and data storage capacities, are correctly applied.

The code regarding power subsystem computations are checked manually using the theory from subsection 4.3.6. Likewise, the data storage evaluation is compared with manual computations.

The position of celestial bodies, obtained from tudat, is compared to available online tools like TuTiempo [10] based on the mission date simulated.

At this stage of the design process, the assumption of a 2D Keplerian orbit for the spacecraft orbit is considered valid. However, it simplifies the dynamics by assuming a two-body problem and neglecting perturbative effects from the Sun and other celestial bodies. Safety margins are thus still applied when using the simulation outcome for designing mission parameter.

Sensitivity Analysis

The sensitivity analysis is conducted for each subsystem separately. For the power budget it is verified that increasing the solar array area and decreasing the solar incidence angle, do increase the power delivered by the solar panels. It is also observed that adjusting the power requirements of individual subsystems influences the power required at a given moment during the mission, in expected ways.

For the data storage sensitivity analysis, the data rates are adjusted, ensuring that decreased data rates lead indeed to less data transmitted.

To verify the orbital computations of the spacecraft, orbital parameters are changed and it is confirmed that the orbital representation changes accordingly. For instance, a higher pericenter altitude does lead to a lower velocity at pericenter.

4.3.6. Power System

The power system for the spacecraft consists of solar arrays in combination with secondary batteries, ensuring functionality during eclipse periods. It has to provide power during the Earth-to-Venus transfer and while in orbit around Venus. The most critical scenario is identified for sizing the solar array and batteries.

[10] `https://en.tutiempo.net/astronomy/astronomical-view/solar-system/` [Accessed 14/06/2025]

Power System Architecture

The spacecraft is powered by solar arrays together with secondary batteries that are used for operation during eclipse periods. This power architecture is common for planetary missions in the inner solar system, where high solar flux is available. Alternative space graded power systems, such as radioisotope thermoelectric generators or fuel cells are used for missions with higher power requirements or when the solar flux is insufficient for power generation with a feasible solar array size [33]. Additionally, the use of solar arrays, being a renewable energy source, allow a potential mission extension in case the probe operates after the planned mission end.

The power system concept can be seen in Figure 4.8. The power conditioning unit controls the power flow of the solar array and the secondary battery. The power generated by the solar array is handled by the solar array regulator. The power flow in and out of the battery, based on the solar array output and the momentary system power requirement is controlled by the battery charge and discharge regulators. The power distribution unit then supplies the power to the different subsystems and their components. The power required per subsystem differs between the transfer and orbiting phase and the operating conditions.

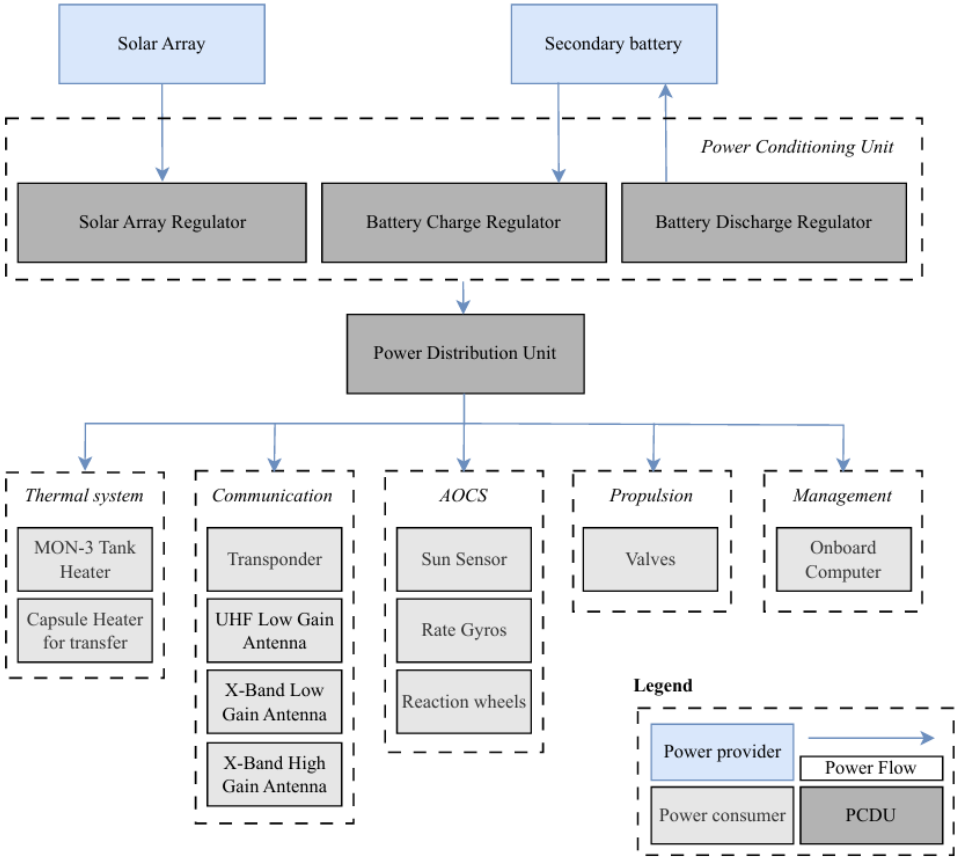

Figure 4.8: Spacecraft power system architecture.

Power Requirements during Earth-to-Venus Transfer

During the transfer period the communication system, C&DH, ADCS, EPS and the thermal system consume power. The spacecraft power system also provides the capsule with power for heating, since the probe power system, relying on solar arrays, cannot operate inside of the capsule. The propulsion system requires power once for opening the valves right before the insertion burn into Venus orbit, which is negligible and not included in the power budget. The power consumed by EPS is incorporated

in the power budgets by applying efficiencies to the different subsystem power requirements. When operating in the sun, an efficiency of 0.8 is assumed. During operation in the eclipse, the power consumed had to be stored in the batteries, which decreases the efficiency to 0.6 [33, p. 125].

The power requirements are assumed to be constant during the entire transfer based on the worst-case scenario for each subsystem, leading to a conservative power budget. The communication system consumes the most power near the end of the transfer, when the spacecraft is farthest from Earth and free-space losses are at their highest. The thermal system reaches peak power at a maximum distance from the Sun, at the beginning of the transfer. During transfer a power system efficiency of 0.8 can be assumed [33, p. 124]. Based on the power requirements of the other subsystems, the power system efficiency can be translated to a power requirement of 8.8 W. An overview of the power requirements and operating conditions of the subsystems is given in Table 4.5. A total power of 46.3 W has to be provided continuously during transfer to Venus.

Table 4.5: Power budget for the spacecraft operating in Venus orbit.

Subsystem	Function	Power [W]	Operating condition
Communication	Earth link (rx + tx) with telemetry data	10.0	Continuously
C&DH	Onboard Computer	3.5	Continuously
ADCS	6x Sun Sensor	0.05	Continuously
Thermal	MON-3 Tank Heater	5.0	Continuously
	Capsule Heater	19.0	Continuously
EPS	-	8.8	Continuously
Total		46.4	Continuously

Power Requirements in Orbit around Venus

While orbiting Venus, power is required for the communication system, C&DH and ADCS. The active thermal control system is not required since the solar flux at Venus is high enough to allow for passive thermal control. The communication system has a significantly higher power demand compared to the transfer phase, as it must handle increased data transmission and maintain links with both Earth and the probe. An overview of the power requirements and operating conditions of the subsystems is given in Table 4.6.

Table 4.6: Power budget for the spacecraft operating in Venus orbit.

Subsystem	Function	Power [W]	Operating condition
Communication	Earth link (rx)	10.3	Whenever there is a link possible to Earth
	Earth link (rx + tx)	33.6	Whenever there is a link possible to Earth and no communication link to the probe
	Probe link (rx + tx)	15.0	Whenever there is a link possible to the probe
C&DH	Onboard Computer	3.5	Continuously
ADCS	6x Sun Sensor	0.05	Continuously
	3x Rate Gyros	3.6	Continuously
	3x Reaction Wheels	2.4	Continuously
EPS	-	2.5 - 28	Continuously, Power required depends on momentary power requirement of the other subsystems
Total		55.5	Maximum average from critical orbit determined by spacecraft simulation

The power requirements and operating conditions are incorporated into the spacecraft simulation (subsection 4.3.5) to determine the total energy required per orbit. This energy varies slightly depending

on the duration of the communication link with the probe and Earth and the time spend in eclipse. The power required from the solar arrays increases slightly throughout the mission duration. At the beginning of the mission the orbit is oriented such that the time in the eclipse is minimised but during the mission, the apocenter propagates such that eclipse time increases and time in the sun decreases (subsection 4.2.2), which leads to a more critical solar array requirement.

The peak power that has to be provided by the solar array is determined by dividing the required energy by the available time in the sun to generate power. The most critical orbit yields a power requirement of 55.5 W.

An example of the power demand distribution across different subsystems during a single orbit is illustrated in Figure 4.9.

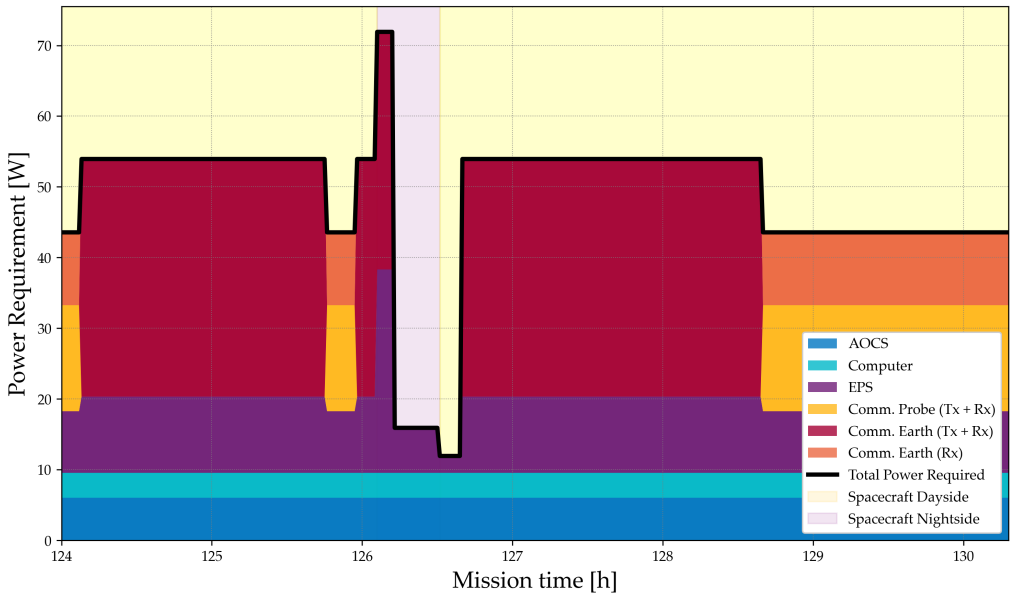

Figure 4.9: Power requirement Spacecraft during one orbit based on subsystem power requirements.

It can be seen the same functions have a higher power consumption during the night than during the day, since the efficiency of the power system decreases as mentioned above. While ADCS and Computer operate continuously, the communication switches between two main modes. When the spacecraft communicates with the probe, signals from Earth are only received but not transmitted. As soon as there is no link opportunity to the probe, the power for Earth communication increases since the spacecraft starts transmitting data to Earth.

Solar Array Sizing

For sizing the solar arrays, the maximum power required is compared to the power that can be provided by the solar arrays. The most important parameter is $P_{peak} \cdot n$, where P_{peak} represents the peak power produced per panel at 1 AU and n is the number of solar panels. Once, that value is determined, components can be selected. Different solar panels available on the market have different P_peak values and thus a different number of solar panels is needed. It is desired to select a solar panel that can provide with an even number of solar panels enough power, such that two same-sized solar arrays can be formed.

The solar arrays are sized based on the power they are able to provide, P, that is determined as follows:

$$P = P_{peak} \cdot n \cdot cos(\theta) \cdot \frac{1}{d^2} \tag{4.8}$$

where P_{peak} represents the peak power produced per panel at 1 AU, n the number of panels, θ the solar incidence angle and d the operating distance of the solar panels to the sun in AU. θ is the angle between the normal of the panel and the solar flux. It is assumed to be 10° since the orientation of the solar panels can be adjusted by rotating the panels themselves independently of the probe and thus a value close to the optimum of 0° can be assumed [33, p. 124].

$P_{peak} \cdot n$ drives the solar array design. Equation 4.8 is used to determine whether the transfer period or the operation in Venus orbit requires a higher $P_{peak} \cdot n$. Table 4.7 shows the corresponding computations.

Table 4.7: Requirement of power generated by solar arrays during Transfer and in Venus orbit.

	P [W]	θ °	d [AU]	($P_{peak} \cdot n$) [W]
Transfer	46.4	10	1	47.0
Venus orbit	55.5	10 °	0.72	29.2

It can be seen that although the power consumed by the subsystems is higher at Venus, operation during transfer is more critical for sizing the solar array. This is related to the fact that the transfer starts at a distance of the sun of 1 AU, where the solar flux available for power generation is significantly lower than at Venus.

The power budget shown in (Table 4.5) is already conservative as mentioned above. Additionally, for sizing the solar arrays a safety factor of 1.25 is applied. With Equation 4.8 a requirement for $P_{peak} \cdot n$ of 58.8 W for zero incidence angle is found.

The Core-04 panels from 2NDSpace are chosen [37]. They are produced by an Italian company, complying with the European Autonomy Strategy, that produces CubeSat technology already for more than 30 years [11]. The array consists of 6 panels with a total peak power of 66 W at 1 AU under a zero ° incidence angle. Their dimensions fit well into the spacecraft design. With a length of 0.4 m matching the spacecraft's 0.4 m width, integration is straightforward and enhances a compact spacecraft design.

When operating during transfer, taking an average sun incidence angle of 10 ° into account, an average power of 65 W is provided, complying with **Req-EVT-2.3**. In orbit around Venus, considering the distance to the sun of 0.72 AU, the solar incidence angle of 10 ° and the longest time spend in eclipse of 6.3 % of the orbit period, an average power of 115.7 W can be provided, complying with **Req-SCM-6.1**. For eclipse operation, batteries are required.

Battery Sizing

To size the secondary battery, the highest energy requirement during eclipse is found from the spacecraft simulation, to be 12.4 Wh. Taking the Depth of Discharge and the level of detail of the current design stage into account, a safety factor of 2 is applied. It follows a required minimum capacity of 24.8 Wh. The OPTIMUS-30 with a capacity of 30 Wh is chosen. It is produced by AAC Clyde Space, a European company. Testing conducted by NASA and many operations on space missions in the past 20 years proof the reliability of the component. In the temperature range of -20 to +20 ° according to **Req-EVT-4.2.1**, a minimum lifetime of 1 year is ensured, sufficient for the transfer from Earth to Venus and operation in Venus orbit taking a design maximum of less than 8 months from launch till end of life.

An overview of the power consumption, solar array output, and battery usage during a representative orbit is presented in Figure 4.10.

Since the solar arrays are sized for the transfer phase, they are oversized for operation at Venus. As a result, when the spacecraft is exposed to sunlight, the solar arrays generate excess power, indicated in green. During eclipse periods, the required power is supplied by the batteries, shown in red. The

[11] `https://www.2ndspace.eu/` [Accessed 13/06/2025]

figure also illustrates that the orbit design and orientation optimize power generation by minimizing eclipse duration.

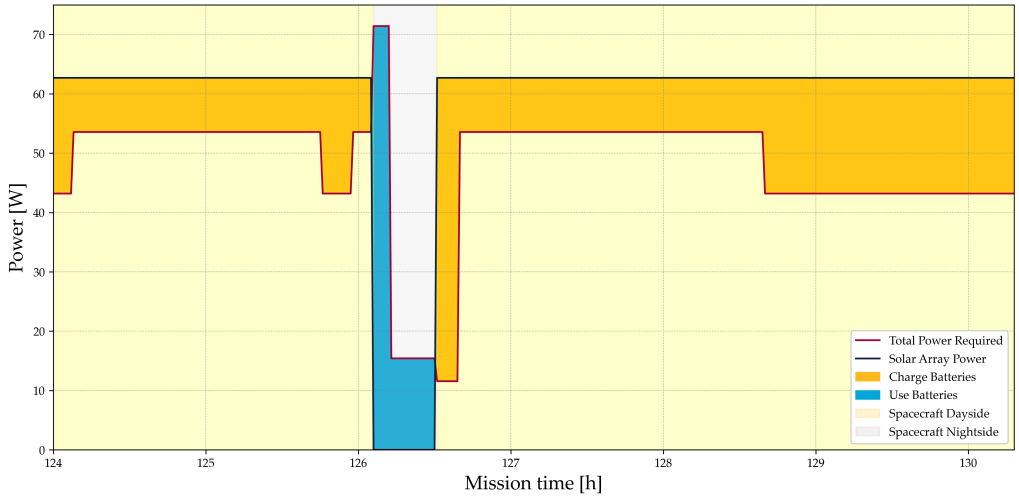

Figure 4.10: Power requirements Spacecraft and power produced during one orbit.

4.3.7. Communication and Data Operation

To size the data handling subsystem, first, the data produced by the probe and by the spacecraft are determined. Combined with contact times, they lead to data rates needed for communication from the probe to the spacecraft and the spacecraft to Earth. The data rates are a basis for establishing the link budgets that are then used to select components for the communication subsystem.

Communication System Architecture

The communication system architecture is shown in a hardware and software diagram in Figure 4.11. The main components for communications payload is a transponder to handle and process and handle the RF signals for both downlink and uplink connections. For this mission the transponder will handle both the Earth to Spacecraft link and the Spacecraft to Probe link.

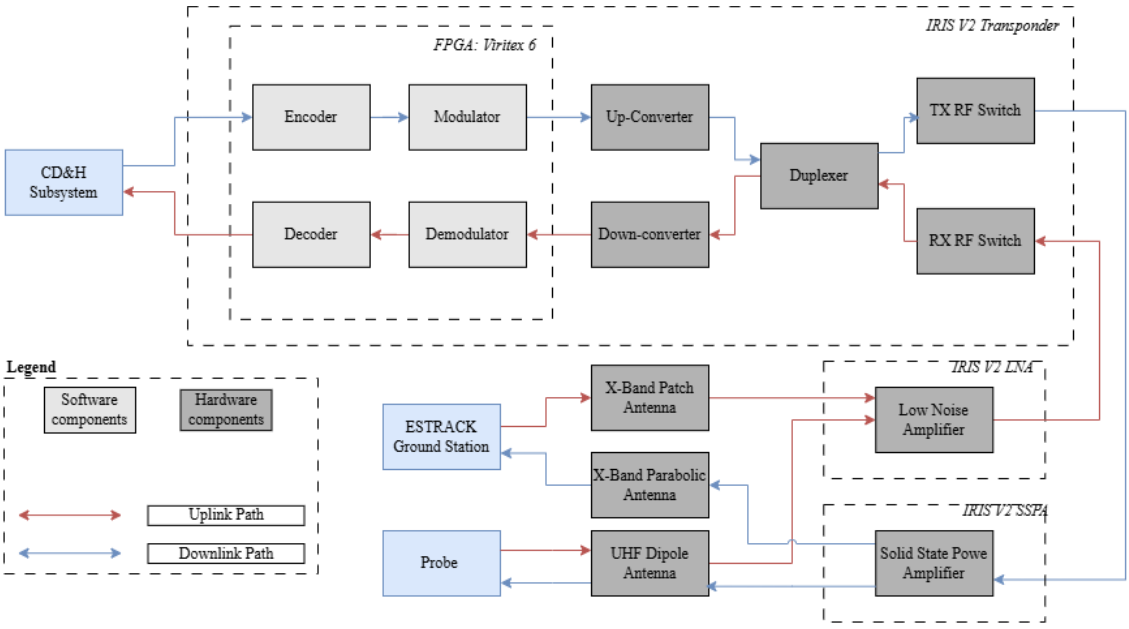

Figure 4.11: Hardware/Software diagram of the communications subsystem onboard the spacecraft.

Data production: Probe and Spacecraft

An overview of the data produced by the probe and the spacecraft is shown in Table 4.8. The data produced by the probe has to be transmitted to the spacecraft first and then to Earth, the data produced by the spacecraft is transmitted directly to Earth. The system telemetry data rates for the probe are estimated in detail in subsection 5.2.4. For the spacecraft the telemetry data rate is calculated by considering the number of telemetry points for a similarly sized spacecraft [12] [33] .

Table 4.8: Data produced by probe and spacecraft during Venus orbit.

System	Data	Data rate [$bits \cdot s^{-1}$]	Operating condition
Probe	Telemetry	258	Continuously
	LMC_{OOL}	1770	Every 2 days (Day side only) for 2 hours
	Camera	1.2e6 [13]	Every 2 hours on the day side
Spacecraft	Telemetry	480	Continuously

Data Rate Requirements

The data produced per system is combined with the time available for data transmission to determine the data rate required for the link between the probe and the spacecraft, and the spacecraft and Earth, respectively. This is done using the spacecraft simulation (subsection 4.3.5).

The communication time available between the systems depends on the relative position of the probe, the spacecraft and Earth. For communication between the probe and the spacecraft, the spacecraft has to be at an elevation between 0 and 45°. Below 0°, the link is blocked by Venus and above 45° the balloon is restricting. When a link is possible, the spacecraft and probe receive and transmit data at the same time. Communication between the spacecraft and Earth is physically possible whenever Venus does not obstruct the connection and there is a direct line of sight and. Additionally, it is assumed that the probe does not transmit significant amounts of data when operating on the night side due to the power limitations of the probe. Data will only be send if access power is available that is not needed for surviving the night.

Transmitting data to Earth requires high pointing accuracy, as does communication with the probe. This creates a potential conflict in attitude control. To resolve this, communication with the probe is given higher priority. This is because contact durations with the probe are generally shorter than those with Earth, and prioritizing the probe enhances the overall reliability of data transmission. The probe operates under extreme conditions and is at higher risk of failure than the spacecraft. Therefore, transmitting scientific data from the probe to the spacecraft as quickly as possible is critical, minimizing the amount of data stored onboard the probe in case of failure.

For the simulation, it is conservatively assumed that the spacecraft transmits data to Earth only when there is no active connection with the probe. Receiving data from Earth, however, is assumed to be possible whenever a physical link exists, as it requires lower pointing accuracy.

For conservative estimates the data rate is estimated taking into account that per orbit, one physical link opportunity cannot be used for data transmission. This could for instance happen when the winds in the Venusian atmosphere move the orientation gondola such that the antennas cannot transmit data to the spacecraft,

Simulating the data production characteristics and communication time with the spacecraft simulation tool (subsection 4.3.5) allows for determining the minimum required data rates for the links. For the communication between the probe and the spacecraft, a data rate, including telemetry, of 2900 $bits \cdot s^{-1}$ is found, leading to **Req-SCM-1.1**. For communication between the spacecraft and Earth a data rate of 1400 $bits \cdot s^{-1}$ is required, completing **Req-EVT-2.4**. Even though, more data has to be

[12] Assuming each telemetry point is sampled at a frequency of 0.1 Hz at 16 $bits$ per sample

transmitted from the spacecraft to Earth than from the probe to the spacecraft, the data rate required is significantly lower since the link windows are longer.

Link Budget: Communication Spacecraft and Earth

From the requirement **Req-EVT-2.4** the link budget for the Venus Earth link is calculated based on procedure from the SMAD textbook [35]. The ESTRACK ground station system is selected, complying with the European Autonomy Strategy. ESTRACK supports frequencies in the X and K band [38]. The X band is selected because it covers a lower frequency range, which decreases the free space loss, while providing sufficient bandwidth for transmitting the required data rate. The central frequency taken for transmission is 8.45 GHz according to the allowed frequency for the ESTRAK ground station [38]. A modulation scheme with low required energy per bit to noise power ratio (E_b/N_0) for a low bit error rate (BER) is essential to ensure that the system remains within the stringent power requirements. A cutting edge BPSK turbo code with a code rate of $1/2$ is chosen [39]. Based on SMAD, a number of conservative assumptions are made regarding losses in the transmission chain [35]. A summary of gains and losses along with brief explanations for the downlink is shown in Table 4.9.

Table 4.9: Communication link budget for Earth-to-Venus downlink.

Name	Gain/Loss (dB/dBw)	Explanation
Spacecraft System		
RF Transmission Power	5.79	3.8 W converted to decibels. RF output of IRIS V2 Transponder.
TX Gain	31.84	Calculated from high-gain antenna sizing from SMAD with 0.55 efficiency assumed [35].
Line Loss	-2	Conservative assumption from SMAD [35, p. 480].
Back-off Loss	-2	Conservative assumption from SMAD [35, p. 480].
EIRP	33.63	Effective Isotropic Radiated Power: sum of TX Power, TX Gain, and losses.
Transmission Path		
Space Loss	-278.18	SMAD equation based on maximum transmitting distance.
Atmospheric Loss	-0.28	SMAD p. 475: Zenith absorption at X-band. For 10° elevation, scales with 1/sin(10°).
Pointing Loss TX	-0.009	Based on 0.1° pointing accuracy of the ADCS system [40].
Pointing Loss RX	-0.28	Based on ground system pointing offset [38, 40].
Ground System		
G/T (Gain over Temperature)	50.8	Value taken from ground station performance table [38].
Modulation Path		
Required E_b/N_0	-1.8	BPSK with Turbo coding, code rate 1/2 [39].
Final Margin		
Carrier-to-Noise Ratio (C/N)	34.26	Sum of EIRP, G/T, and total losses.
Transmitted E_b/N_0	2.8	C/N minus data rate in dB (31.46 dB).
Margin	1	Transmitted minus required E_b/N_0.

For the uplink, the frequency of 7.19 GHz is based on ESTRACK and the modulation scheme is kept identical to the downlink [38]. The link budget for the transmission from the spacecraft to Earth is shown in Table 4.10.

Table 4.10: Communication link budget for Earth-to-Spacecraft uplink, assuming a maximum data rate of 4 kbps.

Name	Gain/Loss (dB/dBW)	Explanation
Spacecraft Receiving System		
Receiver Gain	8	Patch antenna gain specification.
Total Noise System Temperature	-22.72	Calculated using SMAD equation on p. 477 [35], based on noise figure, feed loss (from transponder specs), and antenna noise temperature[14].
Transmission Path		
Space Loss	-276.88	SMAD equation for maximum transmission distance.
Atmospheric Loss	-0.28	Zenith absorption at X-band from SMAD p. 475. Scaled for 10° elevation using $1/\sin(10°)$.
Pointing Loss (TX)	-0.28	Based on 0.1° pointing accuracy of the ADCS system [40].
Ground System		
EIRP	107	Value from ground station performance table [38].
Modulation Path		
Required E_b/N_0	-1.8	BPSK with Turbo coding, code rate 1/2 [39].
Final Margin		
Carrier-to-Noise Ratio (C/N)	43.51	Sum of EIRP, receiver gain, and total losses.
Data Rate	-36.02	4 kbps expressed in dB.
Transmitted E_b/N_0	7.49	C/N minus data rate in dB.
Margin (Maximum Gain)	5.59	Transmitted minus required E_b/N_0.
Margin (Half-Power Beamwidth)	2.59	Link margin at 65° receiving angle where antenna gain is halved.
Margin (110°)	0.09	Maximum receiving angle at which link budget still closes, based on specified gain drop specified by datasheet [15].

According to Table 4.10, the maximum uplink data rate possible is 4 $kbps$. For comparison, the Venus Express mission, which is significantly larger and more complex, had a maximum data rate of just 2 $kbps$ [16]. The data rate of 4 $kbps$ also complies with **Req-EVT-2.4**.

In cases where a lower uplink data rate is sufficient, the signal can be received over a much wider angle. For example, using the same tool and specifications provided by the antenna manufacturer, it has been calculated that at 1 $kbps$ the reception angle can increase to as much as 160°. This enhanced capability is primarily due to the extremely high EIRP of the ground system, which uses 20 kW of DC power solely for RF signal generation, combined with the large 34 m diameter of the high-gain antenna [38].

Sizing of Antennas and Transceiver

The component selection is performed based on the link budget. For communication with Earth, a high gain antenna is selected to satisfy the data rate required for downlink. However, it requires a high pointing accuracy as from Table 4.9. During certain operations the pointing of the antenna might conflict with higher priority tasks like pointing during orbital insertion or when communicating with the probe, as explained above. For this reason a second low gain antenna with larger beamwidth

[14] This value represents the weighted average of the temperatures of the objects within the antenna beam's radiation pattern. Only Earth and the Sun are considered in the calculation.

[16] `https://sci.esa.int/web/venus-express/-/33877-engineering?section=communications` Accessed 06/06/25

antenna is selected for uplink operations receiving key commands from Earth in critical mission phases and possibly transmitting limited amount of data.

The high-gain parabolic antenna's gain is calculated based on its diameter, which is considered as an input of the link budget. The diameter itself is maximized to fit within the spacecraft body constraints. Even though the antenna selected should be deployable so it does not cause any problems during launch it can interfere with the capsule harbouring the probe which is slightly wider than the spacecraft body. A diameter of 0.7 m is deemed suitable.

For the uplink a low-gain patch antenna is selected, primarily for meeting the required gain while offering a sufficiently wide half-power beamwidth (HPBW) to ensure reception under less favourable pointing conditions.

The resulting off-the-shelf components are one low-gain patch antenna and one high-gain parabolic antenna, both operating in the X-band.

For communication with the probe a UHF Cross Dipole Antenna is chosen. The corresponding link budget and component selection is shown in subsection 5.2.4. An overview of the antennas of the spacecraft is given in Table 4.11.

Table 4.11: Characteristics of the three antennas, HG = High gain, LG = low gain, UHF = ultra-high frequency.

Type	Name	Mass [kg]	Dimensions [mm]	Temp. Range
HG Parabolic	HRT Reflector Antenna[17]	4	700 (diameter)	NA [18]
LG Patch	SAM-7127220865-SF-L1[19]	0.055	27.94×27.94×16.2	-40 to 85 °C
UHF Cross Dipole	SAM-UHF/VHF[20]	0.017	98×98×9	-40 to 85 °C

Next to the antennas, a transceiver is selected to provide transmission power and ensure encoding, modulation and uplink/downlink switching. This component needs to accommodate at least 3 TX paths and 2 RX paths, while providing sufficient power for the link budget to close [21]. The IRIS V2 transceiver has been identified to fulfil all requirements, a summary of the characteristics of the component is given in Table 4.11.

Table 4.12: Characteristics of the transceiver.

Component	Name	Mass (kg)	Dimensions (mm)	Temperature Range
Transceiver	IRIS V2[22]	1.1	114.3×101×56 mm	-20 to +50 °C

It is important to note that the quoted transceiver power represents the peak consumption during the most critical case, a simultaneous uplink and downlink using the high-gain antenna at the maximum distance from Earth during the mission. This value may be lower under different operational modes or mission phases, especially during transfer.

[17] https://satcatalog.s3.amazonaws.com/components/710/SatCatalog_-_L3Harris_Technologies_-_1m_Ka-Band_High_Compaction_Ratio_Reflector_Antenna_-_Datasheet.pdf Accessed: 10/06/2025

[18] https://satcatalog.s3.amazonaws.com/components/710/SatCatalog_-_L3Harris_Technologies_-_1m_Ka-Band_High_Compaction_Ratio_Reflector_Antenna_-_Datasheet.pdf Accessed: 10/06/2025

[19] https://sftp.eravant.com/content/datasheets/SAM-7127220865-SF-L1.pdf Accessed: 10/06/2025

[20] https://satcatalog.s3.amazonaws.com/components/1696/SatCatalog_-_Spacemanic_CZ_-_SAM_-_Small_Antenna_Module_UHFVHF_-_Datasheet.pdf Accessed: 10/06/2025

[21] 1 TX and 1 RX paths are in the UHF band in communication with the Venus probe, this component should also accommodate this

[22] https://satcatalog.s3.us-west-1.amazonaws.com/components/1076/SatCatalog_-_Space_Dynamics_Laboratory_-_IRIS_v2.1_-_Datasheet.pdf Accessed: 11/06/2025

Data Storage Design

The required memory size for data storage depends on the communication links between the systems. The amount of data stored in each system during the probe's initial operational days is illustrated in Figure 4.12.

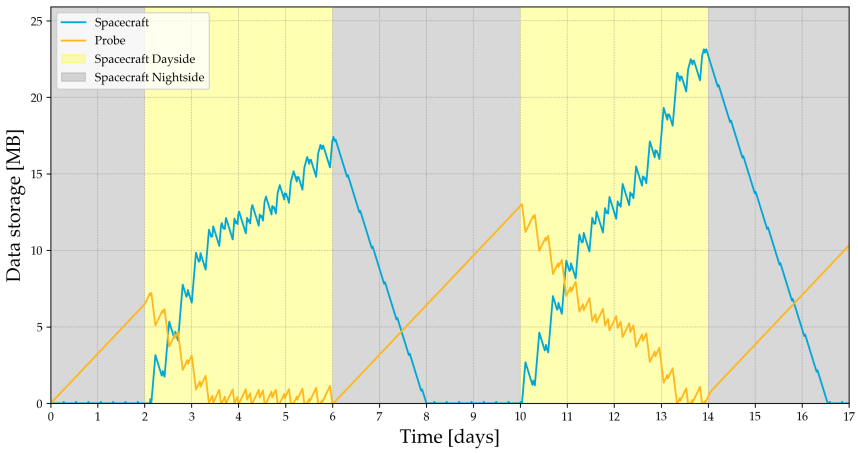

Figure 4.12: Data storage of the Probe and Spacecraft during Mission operation at Venus.

For the probe, shown in orange, data accumulation increases while operating on the nightside. Telemetry is generated continuously, but the window for transmitting data to the spacecraft is short, as the spacecraft is near pericenter during these contacts. The peak in stored data during the first night is shorter than in subsequent nights, as the probe begins operating only after atmospheric entry, which occurs midway through the night. When the probe transitions to the dayside, the stored data begins to decrease. On the dayside, the probe has access to more power, resulting in an increased data production rate due to the addition of scientific data alongside telemetry. However, as the spacecraft moves toward apocenter and slows down, the duration of communication windows increases. This allows the probe to transmit data faster than it is generated, enabling a complete offload of stored data. A memory size for data that is transmitted to the spacecraft of 25 MB is found, including a safety factor of 2, complying with **Req-SCM-6.3**.

The amount of data stored on the spacecraft is shown in blue in Figure 4.12. As the probe enters the day side, the spacecraft's stored data begins to increase for two main reasons. First, the probe starts transmitting scientific data to the spacecraft. Second, downlink opportunities to Earth are reduced because priority is given to receiving data from the probe. The spacecraft can only downlink its own data when it is not receiving from the probe. When the probe enters the night side, the data stored on the spacecraft decreases again. The highly eccentric spacecraft orbit and relative position of Earth and Venus during the mission (subsection 4.2.3), physically enable a link to Earth almost at all times. This guarantees that the storage is cleared in time before new data from the probe begins to accumulate again when entering dayside. A memory size for data that is transmitted to the spacecraft of 50 MB is found, including a safety factor of 2, complying with **Req-SCM-6.3**.

Command and Data Handling

The spacecraft shall be able to perform complex logic operations throughout the lifetime of the mission. Therefore, the selection of a suitable onboard computer is critical to ensure reliable data processing and operational control. This subsystem is responsible for a range of key functions, such as: executing command sequences from ground control, managing onboard timing and scheduling, processing

sensor and actuator data and handling fault detection and safety mode routines. The ZeroCube [23] onboard computer was deemed more than suitable for these tasks with the capability of handling mega-bit per second processing speeds with giga-bits of non volatile memory storage. More than enough to satisfy the requirements of the mission whilst easily remaining within the stringent power and mass budgets.

A detailed schematic representing the data handling architecture of the spacecraft is shown in Figure 4.13.The flow of different types of data is highlighted by the different colours as shown in the legend.

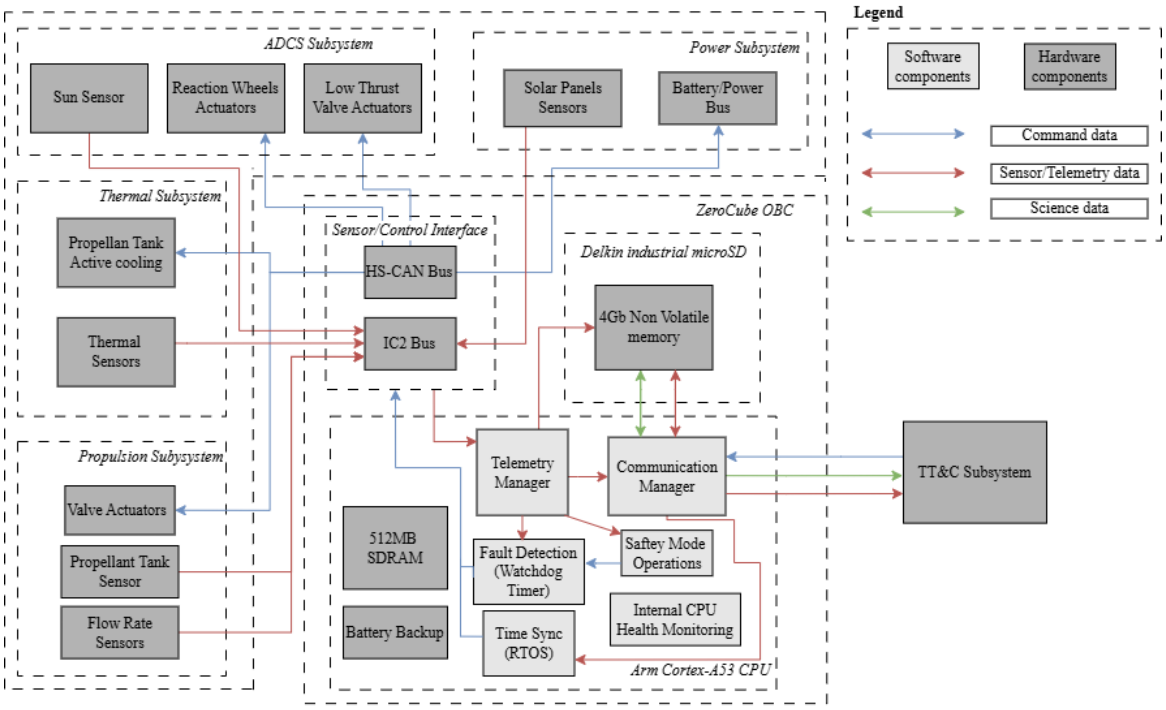

Figure 4.13: Command and Data handling software and hardware diagram.

Verification and Validation

One of the main benefits of selecting off the shelf components is that they have been already tested extensively to comply and withstand the harsh environment of space. In many cases, like the IRIS V2, for example these components have already been mission tested. This allows us to decrease time required extensive validating procedures which can cause delays and increase costs.

From a perspective of software in this section, the link budget tool has been validated by performing sensitivity analysis. Changing parameters that intuitively affect the calculation like the transmitted power move the margin towards a direction that was expected. Furthermore since quite often the conversion between numerical values and decibels is utilised multiplying input values by multiples of ten predictably adds or subtracts by the same multiple in decibels from the final link margin.

The data rate analysis is performed with the spacecraft simulation, verified in subsection 4.3.5.

Sensitivity Analysis

The RF link between Earth and Venus demonstrates robust performance characteristics. However, there are several factors that could potentially influence it. The narrow beamwidth of the high gain antenna requires accurate pointing , in the case where accurate pointing is not possible this will significantly

[23] `https://satcatalog.s3.amazonaws.com/components/2819/SatCatalog_-_TakeMe2Space_-_ZeroCube_-_Datasheet.pdf` Accessed: 11/06/2025

hinder the transmission capabilities of the spacecraft, maybe even making the downlink of scientific data impossible. However, the inherent redundancy incorporated into the attitude determination and control system means that this situation is extremely unlikely. On the other hand atmospheric effects introduce a more certain layer of variability. While X band is absorbed less than other higher frequencies, weather variations which change the amount of water vapour, could reduce the margin significantly by attenuating the signal. This would require providing more power to enable a secure transmission margin which could lead to having larger solar panels in terms of design.

Operational contingencies such as ground station unavailability or temporary safe mode operations could impact data communication schedule assumed by the simulation. However, the spacecraft is equipped with onboard data storage significantly exceeding expected needs. With 4 GB of available storage, the system can buffer more than 120 hours of continuous data, providing ample margin to accommodate delays in data downlink and ensuring mission continuity.

4.4. Entry

During the transfer orbit, the capsule disconnects from the spacecraft by use of pyrotechnics, and continues on a path to intersect Venus. To withstand the heat and loads that come with atmospheric entry, the probe is shielded in an entry capsule. This chapter outlines the progression of the entry, the loads that have to be withstood, and the external and mechanical design of the entry vehicle to withstand them. A more internal design of the entry capsule, as well as the deployment sequence after decelerating is given in section 5.1. The requirements for the entry vehicle are outlined in Table 4.13

Table 4.13: Relevant requirements for the entry phase. VEE: Venus Entry, EXT: External Constraints, SAR: Safety and Reliability.

Requirement ID	Requirement
Venus Entry	
Req-VEE-1	The system shall perform a controlled entry.
Req-VEE-1.1	The capsule shall remain in an orientation with the heat shield facing the flow.
Req-VEE-1.2	The capsule shall not tumble uncontrollably.
Req-VEE-1.3	The system shall not enter via a flight path angle that causes excessive thermal or mechanical loads.
Req-VEE-2	The system shall withstand the operating environment during entry.
Req-VEE-2.1	The system shall withstand the peak heat flux during entry.
Req-VEE-2.2	The system shall withstand the total heat load during entry.
Req-VEE-2.3	The system shall withstand peak entry deceleration loads.
Req-VEE-2.4	The system shall withstand the vibrations during entry into the Venusian atmosphere.
Req-VEE-2.5	The system shall withstand gust loads due to atmospheric wind.
External Requirements	
Req-EXT-3	The mission shall support European Strategic Autonomy.
Req-EXT-3.1	Any goods shall be purchased from European-based organisations.
Req-EXT-3.2	Any service shall be provided by European-based organisations.
Safety and Reliability	
Req-SAR-1	Reliability of the complete system shall be at least 95%.
Req-SAR-2	The system shall include safety measurements.
Req-SAR-2.1	The system shall be able to detect anomalies during all mission phases to a degree of accuracy of 95%.
Req-SAR-2.2	The system shall be able to autonomously resolve detected anomalies within <TBD> where possible.

Continued from previous page

Requirement ID	Requirement
Req-SAR-2.3	The system shall autonomously enter a predefined safe mode within upon detection of a critical anomaly that cannot be resolved within <TBD> minutes.

The design steps of the capsule are outlined in the following subsections, and the final relevant capsule parameters are a diameter of 0.98 m, a height of 0.75m and a mass of 24.4kg, where the mass includes the aluminium shell, heat shield an insulation.

4.4.1. Trajectory Simulation

In order to know what type of loads the entry vehicle will have to survive, a 3-DOF trajectory simulation was written in Python:

$$\dot{V}_y = \frac{D\sin(-\gamma)}{m} - g + \frac{B}{m}, \qquad \dot{V}_x = \frac{D\cos(-\gamma)}{m}, \qquad \dot{h} = V_y, \qquad \dot{x} = V_x$$

With the following state-dependent functions:

$$\gamma(V_y, V_x) = -atan\left(\frac{V_y}{V_x}\right) - 90, \qquad D(V_y, V_x, h) = \frac{1}{2}C_D\rho(h)S(V_x^2 + V_y^2), \qquad g(h) = \frac{\mu_{Venus}}{(R_{Venus} + h)^2}$$

And the initial parameters:

Table 4.14: Trajectory simulation input parameters.

Initial parameters	Capsule parameters	Parachute parameters
h_{entry}	m_{caps}	$C_{D,para}$
V_{entry}	R_{caps}	R_{para}
γ_{entry}	$R_{n_{caps}}$	

Where V is velocity, D is the drag force, B is the buoyant force, x and y represent horizontal and vertical directions, ρ is density, S is reference area, γ is flight path angle, g is the gravitational acceleration, μ is the gravitational parameter, R represents the objects base radius, and R_n is the nose radius of curvature of the capsule which is relevant for the heat analysis. $V_{x,t=0}$, $V_{y,t=0}$ are calculated using V_{entry} and γ_{entry}. The capsule mass includes the mass of the parachute.
The equations of motion are then solved for V_y, V_x, h, x using the fourth-order Runge-Kutta method with a time-step of 0.01 seconds as the results converge at around 0.05 seconds.

The third degree of freedom, the angle-of-attack angle of the vehicle was semi-fixed by having the vehicle follow the trim angle of attack determined from the aerodynamic database as described in subsection 4.4.2. Assuming an entry velocity of $11.5kms^{-1}$, as with the Pioneer probes [41], the entry angle is iterated using a trade-off between maximum g-load, and total heat load. An entry angle of $-5.5°$ is selected and the baseline trajectory can be determined and analysed.

After the main deceleration phase is over, the extreme loads have passed and the the further progression of the trajectory is determined by the exact moment of parachute deployment, parachute size, and the inflation progression of the balloon. This is included in the same trajectory program, and the relevant parameters are iterated in order to be able to efficiently and safely inflate the balloon. This iterative procedure is discussed in subsection 5.1.1 and mainly concerns the deployment phase rather than the entry phase.

The atmospheric model used in this simulation is covered in section subsection 4.4.3, and the assumptions are covered in subsection 4.4.6.

4.4.2. Aerodynamic database

In order to facilitate the entry trajectory, the capsule aerodynamics are analysed by use of CFD, performed using OpenFOAM. In an attempt to obtain the complete set of 6 aerodynamic coefficients (3 forces and 3 moments) on the body axes while taking into account all aerodynamic angles and rates, a method to obtain relevant CFD data is experimented with.

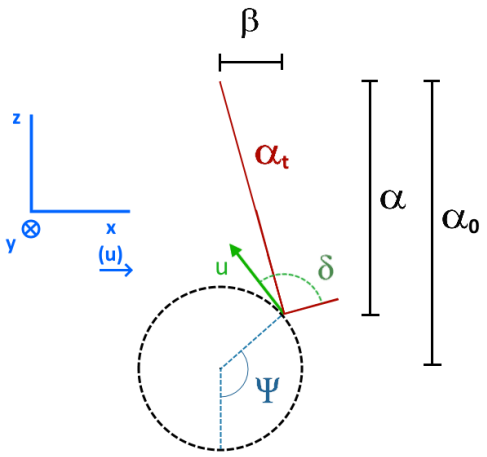

Figure 4.14: Angle definitions during dynamic CFD. Left in blue: Intermediate frame, where the y-axis aligns with the body longitudinal axis (pointing into the nose) and the x-axis aligns with the rotational direction.

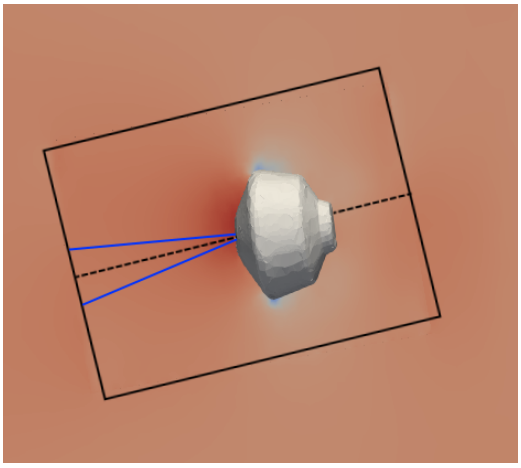

Figure 4.15: Visualisation of capsule rotation. The rectangular box represents the border of the cylindrical section in which the vehicle is fixed.

The data is obtained by rotating the vehicle around an axis at angle α_0 with a constant rotational rate and amplitude (A). As the vehicle rotates, it traverses a range of total angles of attack (the angle between the longitudinal axis of the body and the airspeed, α_t). The vehicle experiences varying angle of attack (α) and sideslip (β) rates during this rotation, with a constant total rotational rate (u). This rotational can be expressed by the total angle of attack, rotational rate, and an angle between the direction of rotation and the the total angle of attack (δ in Figure 4.14).

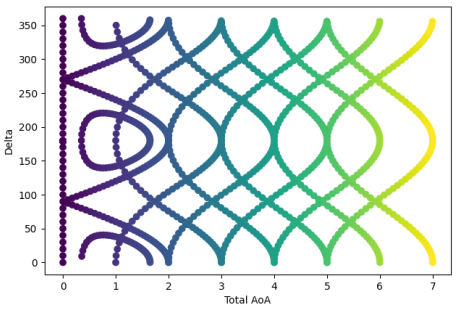

Figure 4.16: CFD coverage between α_t[0-7°] and δ[0-360°] obtained by performing 7 rotations with amplitude 1° and α_0 of (0.7,1,2,3,4,5,6)

The idea is then that the rotation of an axisymmetric vehicle during any moment in a 6-DOF entry simulation can be expressed in the intermediate frame shown in blue in Figure 4.14 and defined by a total angle of attack, a total rotational rate and the direction of rotation with respect to the total angle of attack (δ). The aerodynamic coefficients can then be interpolated from CFD data that has been transformed to the same frame as described in table 4.17. A sample coverage of α_t and δ achieved by running seven dynamic simulations with varying α_0 can be seen in Figure 4.16.

The angles required to define the CFD grid and the frame transformation from the CFD frame to the intermediate frame

Figure 4.17: Counter-clockwise-positive frame transformations between CFD-intermediate and intermediate-body frames

frame	axis	angle
CFD	z	β
-	x	α
-	y	$-\delta$
Intermediate		
Intermediate	x	$-\alpha_t$
-	y	$-\omega$
-	x	$-90°$
Trajectory	x	$-\sigma$
Aerodynamic	z	$-\beta$
-	y	$-\alpha$
Body		

are defined as follows:

$$\alpha = \alpha_0 + Asin(\Psi) \tag{4.9}$$
$$\beta = Acos(\Psi) \tag{4.10}$$
$$\alpha_t = cos^{-1}(cos(\alpha)cos(\beta)) \tag{4.11}$$
$$\delta = \Psi - tan^{-1}\left(\frac{\beta}{\alpha}\right) \tag{4.12}$$

Where all angles are visualised in Figure 4.14. On the receiving end, the angles necessary for data interpolation and to transform from the intermediate frame to the body frame can be calculated using the output from a 6-DOF using spherical coordinates [42] as such:

$$\tau = tan^{-1}\left(\frac{\dot{\alpha}}{\dot{\beta}}\right) \tag{4.13}$$
$$\omega = -tan^{-1}\left(\frac{\alpha}{\beta}\right) \tag{4.14}$$
$$\delta = 90 + hoek1 + hoek2 \tag{4.15}$$
$$\alpha_t = cos^{-1}(cos(\alpha)cos(\beta)) \tag{4.16}$$
$$\tag{4.17}$$

For brevity, no diagram is included to visualise ω and τ, but they can be described as the angles between the α_t offset and the horizontal, and the angle between the horizontal and the rotational direction respectively.
Note that in this case, α and β are defined by the simulation state. After this, the force- and moment coefficients can be interpolated form the database using α_t, δ, Mach number and rotational speed, and transformed into the body frame as shown in the second half of table 4.17.
Once in the body frame, the moments only have to be scaled by using the body forces and location of center of mass, and can then be used.
The database required for a full 6-DOF entry simulation would contain coverage plots as shown in Figure 4.16 in a grid between Mach number, rotational rate, and amplitude (the contribution of amplitude is dependent on the angular position of the vehicle at previous timesteps, but this analysis has not been considered in this report). Due to a combination of lack of computer time and difficulties with dynamic-supersonic CFD, this database has only been generated for a velocity of Mach 0.2. The results are however scaled according to α_t and Mach number by correcting by comparison to static coefficients which have been generated over the full angle-of-attack range shown in table 4.15.

Table 4.15: Aerodynamic database for the entry capsule. Cells show CD, CL respectively.

AoA, Mach	1.5	2.0	2.5	3.0	4.0
0°	1.39, 0.00	1.40, 0.00	1.40, 0.00	1.36, 0.00	1.38, 0.00
5°	1.39, 0.14	1.39, 0.087	1.40, 0.08	1.37, 0.076	1.39, 0.075
10°	1.38, 0.23	1.37, 0.18	1.36, 0.16	1.35, 0.15	1.37, 0.148
15°	1.36, 0.3	1.35, 0.26	1.33, 0.24	1.32, 0.22	1.34, 0.21

The implementation of this method into a 6-DOF trajectory was attempted but not finished in the timespan of this report. Instead, the data is used in the 3-DOF trajectory simulation described in subsection 4.4.1 with the angle of attack fixed at its trim value for a certain Mach number and location of center of mass. The 6-DOF trajectory that was created, with the rotational terms set to zero, support the findings of the 3-DOF trajectory. In order to investigate the attitude progression over the entry the rotational dynamics need to be implemented.

4.4.3. Atmospheric model

There are two atmospheric models that are widely used throughout the design process, and for brevity they are outlined in this section.

VIRA

The Venus International Reference Atmosphere (VIRA) is an atmospheric model based on the data collected by the Venera 10, 12 and 13 landers, as well as the Pioneer Venus probes and orbiter. The data is composed into a comprehensive set of tables and published in 1985[24]. The benefit of this model is the simplicity, as it is static and independent of location of the planet for low altitudes. The drawback is the reduced accuracy.

General Circulation Model (GCM)

GCM's are computer-solved atmospheric behaviour simulations, and are currently the most accurate models of the Venusian atmosphere available. Although they are highly complex to produce, the data of a GCM ran over the timespan of 1 Venusian day has been made public by Dr. Cohen[25], who kindly extended the team a lecture on how it works and the invitation to use it for this project.

The data consists of various atmospheric properties and wind velocities in three directions with a spatial and temporal resolution. In order to use it, an interpolation scheme is written in Python. This data is mainly used in the flight simulation of the trajectory that the balloon will follow throughout its operation.

As the duration of the entry is significantly shorter than the timestep of the GCM model (25 minutes vs. 28 hours), and as the model does not extend above 100 km altitude, it is decided to use VIRA for the entry simulation.

4.4.4. Heat Load

A driving requirement of the entry vehicle design is the material selection and sizing of the heat shield. Methods used to determine the required size, mass and material are outlined in this section.

There are generally two types of atmospheric heating acting on an entry vehicle: convective heating and radiative heating, the former of which making up the majority of the experienced heat flux. In this analysis, the convective heating is approximated using the Sutton-Graves method [43–45]:

$$\dot{q}_{conv} = K\sqrt{\frac{\rho}{R_n}}V^3 \tag{4.18}$$

Where V is the velocity in $m \cdot s^{-1}$, ρ is the atmospheric density in $kg \cdot m^{-3}$, R_n is the nose radius in m and K is a constant dependent on the planet of entry. K is given as $1.8960 \cdot 10^{-4}\ m\sqrt{kg}$ for Venus [44]. As the trajectory simulation solves for velocity and altitude, the convective heat flux is easily found at each timestep. A similar engineering relation for radiative heat flux, also by Tauber and Sutton, is shown [43, 45, 46]:

$$\dot{q}_{rad} = C \cdot f(v) \cdot R_n^a \cdot \rho^b \tag{4.19}$$

Where C is an atmosphere-dependent constant, f(V) is a function of velocity and atmospheric conditions, and the exponents a and b being either constant or functions of velocity and density [46]. For Venus, the values dependent on instantaneous velocity are displayed in table 4.16

[24] https://www.sciencedirect.com/journal/advances-in-space-research/vol/5/issue/11
[25] https://doi.org/10.21954/ou.rd.c.7292911.v1 [Accessed 19/05/2025]

Table 4.16: Radiative Heat flux equation coefficients.

	v ($km \cdot s^{-1}$) < 10.028	**10.028 < v ($km \cdot s^{-1}$) < 12**
C·f(v)	$2.195 \cdot 10^{-22} \cdot v^{7.9}$	$8.497 \cdot 10^{-63} \cdot v^{18}$
a	0.49	0.49
b	1.2	1.2

Meaning that, like the convective heat flux, the radiative heat flux can be integrated in the trajectory simulation using the nose radius, local free-stream density and the velocity.

The total heat flux at any moment then equals the sum of the convective and radiative heat flux, and the result from the trajectory simulation a heat flux profile which is used in this analysis.

The values of interest that can be derived from the heat flux profile are the maximum heat flux in order to determine allowable materials, and the total heat load, taken as the time-integral of the heat flux at the stagnation point, in order to determine a conservative heat shield mass. The required heat shield mass can be estimated using the following equation [45, 46]:

$$\dot{s} = \frac{\dot{Q}}{\rho_{TPS} \cdot Q^*} \tag{4.20}$$

Where $\dot{s}$ is the heat shield recession rate, ρ_{TPS} is the density of the heat shield material, $\dot{Q}$ is the heat flux, and Q^* is the heat of ablation. The heat of ablation is a material property used to estimate the heat a material can absorb. Relevant material properties in the heat shield trade-off are given in table 4.17. Equation 4.20 can be rearranged using the density and heat shield area S_{TPS}, and then integrated over time, resulting in:

$$m_{TPS} = \frac{Q \cdot S_{TPS}}{Q^*} \tag{4.21}$$

Table 4.17: Heat shield material properties.

	Density [$kg \cdot m^{-3}$]	Q^* [$J \cdot kg^{-1}$]	**max. Flux** [$W \cdot m^{-2}$]
PICA[26] [47]	236	$1.15 \cdot 10^8$	$1.5 \cdot 10^7$
carbon-phenolic[48][49]	1390	$1.60 \cdot 10^8$	$3.0 \cdot 10^8$
HEEET [47]	1000	-	$3.5 \cdot 10^7$

Since the mass is only dependent on the heat of ablation, the density only makes a difference in the final heat shield volume. Although the heat of ablation of HEEET (Heatshield for Extreme Entry Environment Technology) could not be found, according to [47] PICA (Phenolic-Impregnated Carbon Ablator) is always more mass-effective below a heat flux of $1.5 \cdot 10^7\ W \cdot m^{-2}$.
Since, from the trajectory simulation, the maximum heat flux predicted for the vehicle is $5.0 \cdot 10^6\ W \cdot m^{-2}$, all materials are possible options, with carbon-phenolic having the highest mass-efficiency. However, because of the high thermal conductivity and low thickness of the material due to the high density, carbon-phenolic requires a proportionally very large mass of insulation [50], whereas PICA acts as its own insulator. For this reason, and the fact that simply a lot more data is available for PICA, it is selected for this mission and heat shield mass can now be estimated.

The trajectory simulation returns a total heat load of Q = 69.4 MJ. With a heat shield area of 0.98 m^2, density and heat of ablation of PICA and Equation 4.21, the total heat shield mass and thickness can be calculated. With a 100% margin to provide reliability and additional insulation, the heat shield mass and thickness are calculated to be 1.2 kg and 9.00 mm respectively.
To provide additional insulation, the entire capsule is covered in a 1cm layer of Solimide® [27] between

[26] `https://tpsx.arc.nasa.gov/Material?id=43` [Accessed 16/05/2025]
[27] `https://ntrs.nasa.gov/api/citations/20020064720/downloads/20020064720.pdf`

the capsule shell and the heat shield. This amounts to a mass of roughly 700 grams.

4.4.5. Mechanical Design and Loads

The structural integrity of the entry capsule must be sufficient to withstand the mechanical loads imposed upon during entry. The relevant values to estimate the structural effect are the maximum deceleration of the probe (78 g) and the total aerodynamic pressure acting on the heat shield (49 kN). In order to test the capability of the entry capsule to withstand these loads, a finite-element analysis is performed using ANSYS.

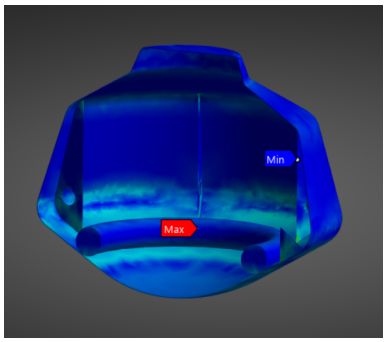

Figure 4.18: Finite element analysis of Aeroshell.

As the only internal component in direct contact with the capsule is the Helium tank (see Figure 5.2), the internals were estimated as a toroid with the same outer radius as the helium tank, sized to have mass of all the internal subsystems in order to simulate the inertia.

For the material, aerospace grade Aluminium 7075-T6 is chosen for its widespread use and favourable material characteristics. By investigating the maximum stress occurring on the vehicle and comparing it to Aluminium 7075's yield strength (503 MPa[28]), it is decided to add 6 flanges. The thickness of both the capsule shell and flanges are iterated in order for the maximum stress to stay below 15% of the yield strength. Even with this margin, the resultant thickness for the shell and the flanges are 3 mm and 4 mm respectively.
The FEM model results are shown in Figure 4.18. The maximum stress can be seen to occur at the flange base and has a value of 53.5 MPa. The general CAD model of the capsule is shown in Figure 4.19. This figure does not include the heat shield or any mechanisms. The resulting capsule shell has a mass of 22.6 kg.

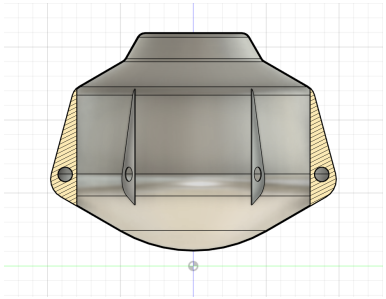

Figure 4.19: CAD model of entry capsule.

4.4.6. Verification and Validation

Atmospheric Model

The main assumptions of the VIRA model covered in subsection 4.4.3 that affect the project are the following:

- Local time-based effects are neglected.
- Ideal gas
- Static atmosphere (dynamic effects neglected)

However, the VIRA model is widely used in literature and the best available atmospheric model without the need for high-level implementation. The assumptions are suitable for design decisions with no specific time and location requirement, as the balloon moves.

Entry Simulation Besides the assumptions made in the atmospheric model that is used for the entry simulation, the simulation itself makes a number of assumptions:

- Flat, non-rotating Venus.
- Perfectly spherical gravity field.
- Currently winds are not taken into account.
- Capsule-parachute interaction is neglected.
- Change in shape and mass due to ablation is neglected.
- Ballistic entry with constant 0° angle of attack.

A main use of the entry phase of the simulation is to get the heat profile and mechanical loads of an atmospheric entry. At hypersonic speeds the drag coefficient decreases due to decreased pressure

[28] https://asm.matweb.com/search/specificmaterial.asp?bassnum=ma7075t6[Accessed 17/06/2025]

drag and ballistic entry also neglects the lifting properties of the capsule. These effects overestimate deceleration and heat loads, sacrificing trajectory accuracy to ensure conservative heat shield sizing.

CFD data The static aerodynamic coefficients obtained using OpenFOAM are validated by running the same OpenFOAM setup on the Orion capsule. The gathered coefficients are compared to wind tunnel data [51] and show a good correlation, validating the setup.

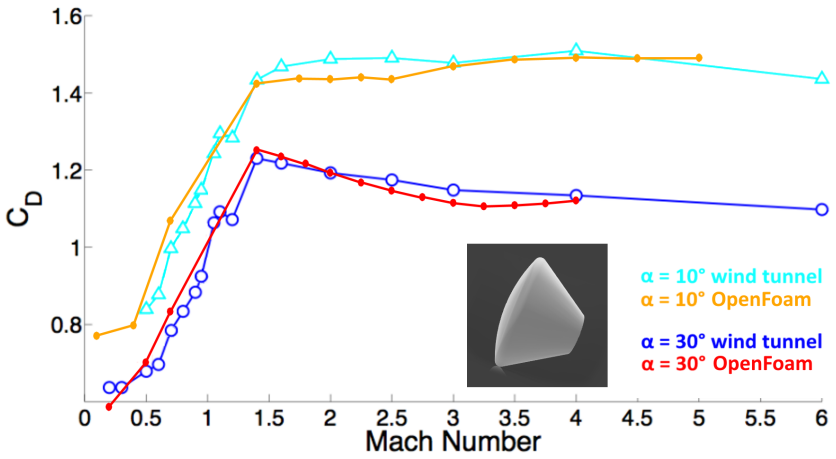

Figure 4.20: OpenFOAM data compared to wind tunnel data for the Orion capsule.

It should be noted that the Orion coefficients are gathered for an Earth atmosphere, while the coefficients used in this project are gathered assuming an atmosphere made out of pure carbon dioxide. Although there is little validation data for Venus entry vehicles, the chemical composition is similar enough to that of Mars that Mars entry capsules could be used as further validation in future work.

Heat analysis The heat analysis is validated using the Stardust entry capsule. The Stardust capsule entered the Earth's atmosphere at 12.9 $km \cdot s^{-1}$ and used PICA for a heat shield. A set of aerodynamic coefficients similar to Table 4.15 is generated for the Stardust geometry and used in the trajectory simulation. The atmospheric model is switched to Earth's, and the same heat analysis used for the Orpheus entry capsule is used, and the resultant prediction of heat shield recession is $0.84cm$. The true value is measured to be $0.57cm$ [52], meaning the model is conservative. More validation cases would be desired to build fidelity. Finding entry capsules with published information on heat shield recession is challenging, however.

5 Probe Design

With the Orpheus mission now approaching Venus, it will undergo one of the harshest and most critical phases of the mission, namely the entry of the Venusian atmosphere. Once within the operating altitude range, the balloon will start inflating marking the start of the scientific mission. The chapter will start with the deployment sequence and the design of the entry capsule in section 5.1, after which the gondola and its subsystems designed to support LMC_{OOL} conduct its mission objectives. will be discussed in section 5.2. The design of the balloon that will carry the gondola around Venus, together with the pressure regulations system responsible for the altitude control will be discussed section 5.3.

5.1. Deployment

When the capsule has slowed down to subsonic velocities, the atmospheric entry is over and the deployment phase begins. For the deployment phase, the requirements listed in Table 5.1 have to hold:

Table 5.1: Relevant requirements for the deployment phase. VEE: Venus Entry, EXT: External Constraints, SAR: Safety and Reliability.

Requirement ID	Requirement
Venus Entry	
Req-VEE-2	The system shall withstand the operating environment during entry.
Req-VEE-2.3	The system shall withstand peak entry deceleration loads of at least 78 g.
Req-VEE-2.4	The system shall withstand the vibrations during entry into the Venusian atmosphere.
Scientific Mission	
Req-VEE-3	The capsule shall successfully deploy the probe in an operational state.
Req-VEE-3.1	The system shall deploy two parachutes without damage.
Req-VEE-3.2	The system shall open the balloon up to the atmosphere at a velocity no higher than 16 $m \cdot s^{-1}$.
Req-VEE-3.4	The system shall vent no less than 99.5 % of stored Helium into the balloon before reaching 50 km altitude.
Req-VEE-3.5	The system shall dismount from the probe without any further contact.
External Requirements	
Req-EXT-3	The mission shall support European Strategic Autonomy.
Req-EXT-3.1	Any goods shall be purchased from European-based organisations.
Req-EXT-3.2	Any service shall be provided by European-based organisations.
Safety and Reliability	
Req-SAR-1	Reliability of the complete system shall be at least 95%.
Req-SAR-2	The system shall include safety measurements.
Req-SAR-2.1	The system shall be able to detect anomalies during all mission phases to a degree of accuracy of 95%.
Req-SAR-2.2	The system shall be able to autonomously resolve detected anomalies within <TBD> where possible.
Req-SAR-2.3	The system shall autonomously enter a predefined safe mode within upon detection of a critical anomaly that cannot be resolved within <TBD> minutes.

Although terminal velocity is reached at around 68.4 km, the deployment is chosen to begin at 60 km altitude. The terminal velocity at this altitude is lower which means a smaller parachute is required

for a safe balloon deployment, while the altitude is high enough to ensure enough time to inflate the balloon passes before reaching 50 km.

The steps of the deployment are described, with the time passed since the previous steps in parenthesis below. The sequence is also visualised in Figure 5.1:

1. The parachute cap releases.
2. (+2s) Drogue mortar fires.
3. (+12s) Main parachute is pulled out.
4. (+15s) Heat shield and gondola configuration lowers.
5. (+0s) Inflation begins.
6. (+10m) Aeroshell release.
7. (+1m) Inflation ends, Heat shield and Helium tank are dropped.

The design decisions of the deployment sequence are discussed in more detail in the following subsections. Finally, a detailed deployment sequence including the required mechanisms is given in subsection 5.1.6. A schematic layout of the capsule contents is shown in Figure 5.2.

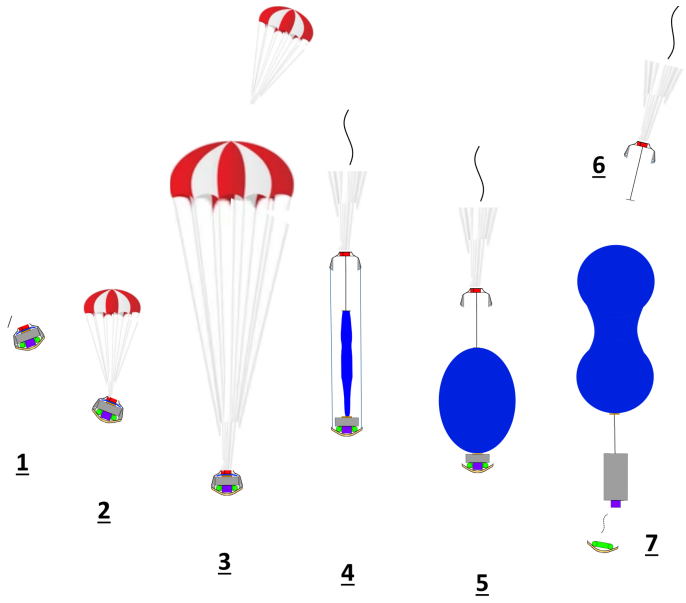

Figure 5.1: Deployment sequence.

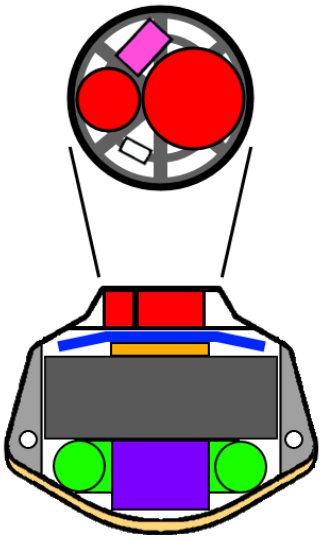

Figure 5.2: Entry capsule layout. Blue: Balloon, red: Parachutes, orange: PRS, grey: Sampling mesh, green: Helium tank, purple: Gondola, pink: EPS and control computer.

5.1.1. Deployment Iteration

Throughout the deployment sequence, a range of velocities and altitudes is traversed. Assuming a short parachute and balloon deployment duration, the descent can be modelled using the change in terminal velocity as the balloon inflates. Venting begins as soon as the valves between tank and balloon open, and the inflation rate is determined by the difference in pressure and the density inside the balloon. These values depend both on altitude and moles of Helium in the tank. To model the descent, the balloon inflation equations developed in subsection 5.3.4 are integrated with the trajectory simulation outlined in subsection 4.4.1.

Out of the altitude and velocity requirements for the balloon to inflate, the effect of the balloon on drag and the desire for the lightest possible parachute, an iterative process arises which can be characterised by the parameters to be varied, the requirements to hold and the optimization parameter:

Parameters:

- Parachute deployment altitude
- Parachute area

Requirements:

- The parachute deployment speed shall be below Mach 0.3
- The balloon deployment speed shall not supersede 16 $m \cdot s^{-1}$
- The balloon shall be fully inflated before reaching 50 km.
- The balloon volume shall not supersede 25 m^3 at any time

Optimize:

- Parachute size (minimize)

Complications include but are not limited to:

- The instantaneous volume of the balloon affects the drag.
- If the balloon were to start venting at a high altitude, there is a limited time before the balloon over-expands.
- Due to the increase in atmospheric pressure during the descent, the balloon volume first increases and then decreases before reaching 50 km.
- Although starting to vent at a high altitude affords a longer venting time, it requires a larger parachute to adhere to the minimum balloon deployment speed.
- The balloon drag does not affect the parachute drag.
- The balloon has a peanut-shape throughout the descent, the cross-sectional surface area estimated using a peanut-volume equation.
- The drag coefficient of a peanut-shaped balloon equals 0.4.
- The Helium is directly vented into the zero-pressure balloon.

After integrating the effects of balloon inflation on the descent, and the effects of the descent on balloon inflation, the optimization parameters are manually iterated to reach the final sequence.
Using this sequence, the parachute deployment speed is Mach 0.16, the balloon deployment speed is 16 ms^{-1}. From here the descent takes 22 minutes to reach 50 km, at the end of which all but 1.4 moles of Helium (99.7%) will have been vented (Figure 5.3). The total parachute area (drogue and main) is 14.64m^2

5.1.2. Inflation Configuration (IC)

The inflation configuration consists of the following parts:

- Heat shield & insulation
- Aluminium bottom cover
- Helium tank
- Gondola
- Sampling mesh & tether
- PRS

The location and connection points of the various subsystems are described below:
The Heat shield, insulation and aluminium bottom cover can be regarded as a solid piece and will henceforth be referred to as simply "the heat shield".
The heat shield is secured to the Helium tank by means of bolted clamps. This provides both rigidity to the capsule during the intense entry loads, and not ejecting the heat shield entirely allows for various mechanisms needed during the later deployment sequence to be located on the inner heat shield.
In turn, the Helium tank is secured to the PRS by means of 4 pipes, with releasable pipe sections. The

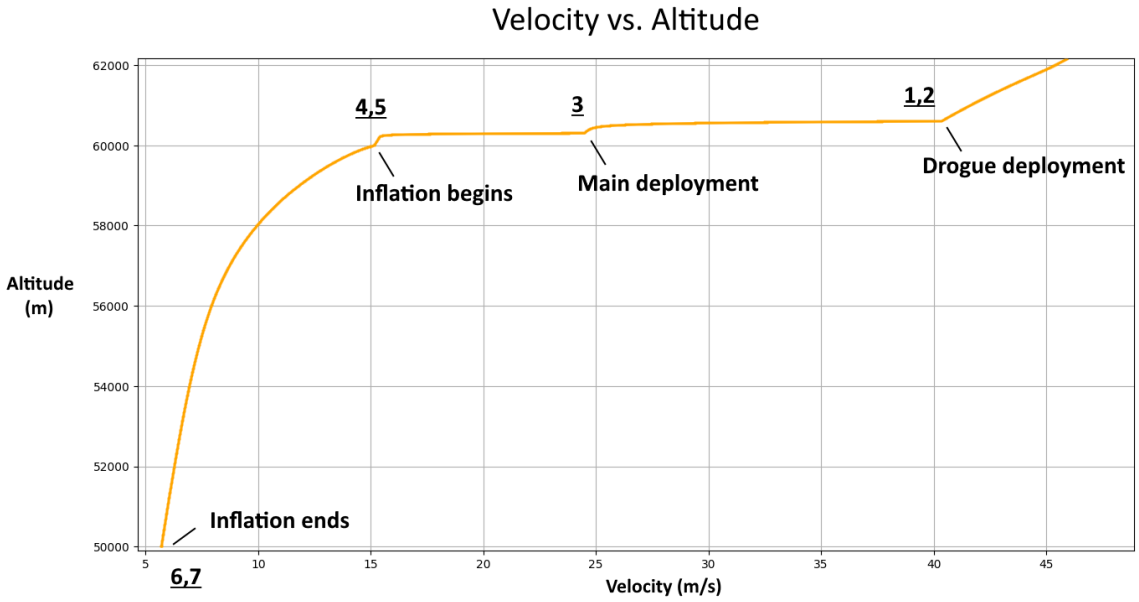

Figure 5.3: Deployment altitude vs. velocity graph.

purpose for these pipes is to vent Helium from the tank to the balloon, as well as to support the weight of the entire IC below the PRS. As soon as the helium is depleted, these pipes will disconnect (step 7). The exact disconnection mechanism is outside the scope of this paper.
The compressed mesh, with the coiled tether on top is located in between the PRS, the pipes and the Helium tank. Having a larger diameter than the tank, the mesh is kept in place.
The gondola, being attached to the mesh, is positioned within the inner circumference of the tank.

5.1.3. Helium tank

Throughout the journey to Venus, the Helium is stored in a pressure tank located in the re-entry capsule. To make optimal use of the limited space available within this re-entry capsule, the Helium pressure tank is toroidal (or donut-shaped) in form as can be seen in Figure 5.4. To calculate the hoop stress occurring in a toroidal pressure tank, Equation 5.1 can be used where σ_ϕ is the hoop stress, p is the pressure, r is the cross-sectional radius, ϕ is the hoop angle and R is the centreline radius [53].

$$\sigma_\phi = \frac{pr}{2t}\left(\frac{2R + r\cos(\phi)}{R + r\cos(\phi)}\right) \tag{5.1}$$

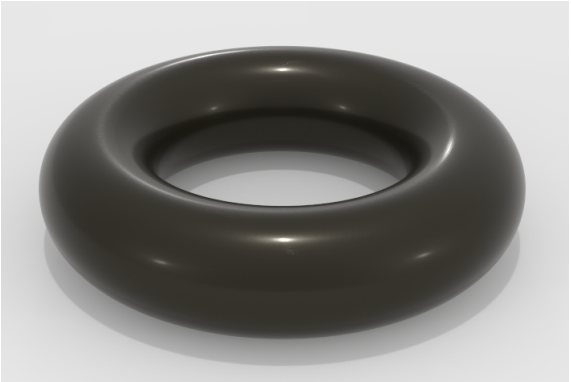

Figure 5.4: Render of the toroid helium tank.

In order to store the 461.94 moles of helium at a pressure of 300 bars[1] required for the balloon (section 5.3, together with another 1.41 moles of Helium that are left in the tank after inflation), the pressure tank will need a volume of 38.52 litres. To allow for adequate space for the gondola in the middle of the toroid, the toroid has a centreline radius of 26.57 cm and a cross-sectional radius of 8.57 cm [2]. As mass is limited, a type IV Composite overwrapped pressure vessel is used to handle the high pressures. A type IV pressure

[1] https://www.isatec-aachen.de/en/glossary/cfrp/composite-pressure-vessel
[2] https://www.geeksforgeeks.org/how-to-calculate-the-surface-area-and-volume-of-a-torus/ [accessed 09/06/2025]

vessel consists of a non-metallic liner, surrounded by composite materials [54]. Using a conservative yield strength of 1200 MPa [3][54] for the pressure tank results in a maximal wall thickness according to Equation 5.1 of 2.65 mm. This results in a total mass of 4.3 kg using a density of 1800 $kg \cdot m^{-3}$ [3] [55]. A factor of 1.5 will be applied to the mass in order to account for additional reinforcements required for holes and other elements causing higher local stress concentrations resulting in a tank mass 6.45 kg.

5.1.4. Aeroshell

The aeroshell consists of the following parts:

- Main capsule body + insulation
- Structural support
- Parachute cap
- Parachute bay
- Aeroshell tether
- Control computer and EPS
- Two spring spools

The location and connection points of the various subsystems are as follows:
The structural support is welded to the main capsule body.
The aluminium aeroshell, insulation and PICA heat shield are connected via the HT-424 bonding agent [56].
The parachute bay is the region between the diaphragm and the parachute cap. The content consists of two cylindrical aluminium canisters, one of which acts as a mortar, and the Control Computer and EPS shown in pink in Figure 5.2. The parachute canisters contain the parachutes and parachute bags and are welded to the diaphragm. The position and sizes of these subsystems are as shown in Figure 5.2.
The aeroshell tether is connected to the diaphragm, and to the top of the balloon via a sown region on the balloon.

5.1.5. Parachutes

A drogue parachute, designed to decelerate the capsule to a speed of 20 $m \cdot s^{-1}$ at 60 km altitude is deployed. The deployment of the drogue parachute is done via mortar. The drogue is expected to unfold and decelerate to the new terminal velocity within 10 seconds. The connection point is a hook on the diaphragm, which can disconnect via pyrotechnics. At the signal given by the control computer, the hook disconnects, releasing the cord. The cord then extends to the main parachute bag, which gets pulled, and the main parachute is released. Another 15 seconds are selected to unfold and decelerate to 16 $m \cdot s^{-1}$. The main parachute is connected to the aeroshell via the diaphragm as well.
The shape of the parachutes are chosen to be a ribbon-chute for the drogue parachute, and a disk-gap-band for the main parachute as this is one of the most stable and flight-proven parachute designs. This follows the design decisions of the Pioneer Venus mission [50].
The material selected for both parachutes is Nylon, following the Pioneer large probe. The aerial density of a Venus-grade Nylon parachute is determined empirically by examining past cases such as Pioneer and determined to be on the order of 0.2828 $kg \cdot m^{-2}$ (4.7 kg / 16.62 m^2) [50], taken as 0.35 $kg \cdot m^{-2}$ as to be conservative. This includes the mass of the shrouds and so indirectly selects the shroud length. To specify this for this mission is outside the scope of this report.

The total packing density of a nylon parachute and parachute bag system can be taken as 684 $kg \cdot m^{-3}$ [57]. Together with the parachute masses and a 15% margin, the size of the parachute canisters displayed in Figure 5.2 is calculated. The bags are stored in an aluminium shell of 1 mm thickness. The mass of these shells are taken into account in the aeroshell design.
The total parachute dimensions are shown in Table 5.2

[3] `https://www.matweb.com/search/datasheet_print.aspx?matguid=39e40851fc164b6c9bda29d798bf3726` [accessed 09/06/2025]

Table 5.2: Parachute dimensions and mass.

	Diameter (m)	**Area (m^2)**	**Mass (kg)**	**Volume (cm^3)**
Drogue	2.05	3.30	1.16	1469
Main	3.8	11.34	3.97	5046

5.1.6. Mechanisms and Deployment Sequence

The detailed deployment sequence, and the required mechanisms are outlined in this subsection.
At an altitude of 68.4 km above the surface of Venus, the capsule reaches a terminal velocity of 80 $m \cdot s^{-1}$. The capsule coasts for 128 seconds until it reaches 60.1 km altitude, at which point the deployment begins.

Step 1. Parachute cap ejection.
Mechanism: Pyrotechnic ejection
After withstanding the heat of entry, the parachute cap is ejected by use of pyrotechnics. The cap flies away and afterward, a delay of 5 seconds before parachute deployment is permitted to ensure the parachute will not interact with the cap. The parachute canisters are without any other cap, and the parachute bags are kept in place by their expansion force only.

Step 2. Drogue mortar.
Mechanism: Mortar shot
The drogue parachute is deployed by firing the bag from the parachute bag canister. The bag is pulled from the canopy by a "slug" moving ahead of the bag. The exact design of this mortar is outside of the scope of this report.
In order for the drogue parachute to decelerate the capsule before being used to pull out the main parachute (15 seconds is allocated), an attachment point to the capsule is required. This connection point is a metal attachment hook secured to the diaphragm and is the mechanism in the next step.

Step 3. Main parachute deployment.
Mechanism: Hook release
Upon successful deployment, unfolding and deceleration of the drogue parachute, the drogue attachment hook disconnects by use of pyrotechnics. The chord extends to its next connection point, which is the main parachute bag.
The main parachute, densely packed into the parachute bag, is pulled out of the container with the bag until the drogue chord is fully extended again, at which point the bag is pulled from the main canopy and the drogue and main parachute fly away.
Another 15 seconds is allocated for the main parachute to fully unfold and decelerate the vehicle to its new terminal velocity of 16 $m \cdot s^{-1}$. The altitude at this point is around 60 km.

Step 4. IC deployment.
Mechanisms: Aeroshell release pyrotechnics, spring spools
Holding together the two capsule segments, the IC and the Aeroshell, are 6 pyrotechnic release blocks located on the connecting edge.
Shortly after reaching a velocity of 16 $m \cdot s^{-1}$, the blocks are given the release signal by the control computer, and the two segments are severed.
At the moment of disconnection, the weight of the IC causes it to drop from below the aeroshell. Connecting the IC and the Aeroshell is the folded-up balloon, which is now being unfolded. The balloon is attached to the IC via the PRS, and to the aeroshell via the Aeroshell tether as described in 5.1.4.
On the inside of the balloons, a tether runs from the PRS to the sown patch on the top of the zero-pressure balloon. The purpose of this tether is to carry the weight of the IC during the inflation phase, and is hence sized to be slightly shorter than the maximum diameter the balloon is expected to experience. This is determined to be 3.6 m by the deployment analysis outlined in subsection 5.1.1.

To reduce the rate of fall and the jerk imposed on the balloon tether, a set of spring spools is employed. These spools work by imposing a upward force on the IC by means of two tethers, simply connected to the heat shield. The spools themselves are located on the aeroshell. The exact design of these spools is outside the scope of this report.
At a height of 10 centimetres before the IC has reached this fully extended state, the spool chords run out and descent, hanging idly below the heat shield as not the block the balloon from inflating. A slight drop occurs at this moment which is considered to be small.
After they have been extended fully, the chords run out and release from the spool, dangling from the heat shield. This allows for the space for the balloon to inflate.

Step 5. Inflation.
Mechanism: Helium tank valves
The Helium tank valves are opened, controlled by the gondola on-board computer. Once opened, the valves can not be closed, and for the next 10 minutes the balloon inflates with varying rates as the altitude and tank pressure decrease.

Step 6. Aeroshell release.
Mechanism: Pyrotechnic release
At 51 km altitude, the aeroshell is released from the balloon. Since the complete IC mass is still attached to the balloon, the upward force of the aeroshell configuration is higher than that of the balloon and IC. As a result, the balloon falls safely away from the aeroshell.
The disconnection is triggered by the Control Computer in the parachute bay of the Aeroshell as it detects the proper altitude via barometer. The signal travels through an electrical wire downward through the Aeroshell tether. At about 10 cm above the balloon sown path, a pyrotechnic cutter is activated and the tether is severed.

Step 7. Heat shield & tank release.
Mechanism: Valve release, spring spools
Near 50 km altitude, the buoyancy of the balloon is sufficient to carry the weight of the gondola. At this moment, the gondola on-board computer triggers for the Helium valves to release the tank. Upon release, the heat shield and tank configuration descent under their own weight. Again, a set of spring spools are used to decrease the jerk, as the gondola and mesh are descending with the tank and heat shield. After a couple seconds the cord runs out, the mesh and tether are unfolded and the probe is deployed.

5.1.7. Validation and Verification
As a possible method of validation, the parachute deployment sequence can be performed either in-flight or in a wind tunnel test. All mechanisms can and should be manufactured and tested before the production of the final design.

5.2. Gondola Design
Once deployment is complete, operations start. In order to house the payload and provide essential functions such as environmental protection, communication, and power, a gondola is designed. The design of the gondola is driven by a number of requirements, which are shown in Table 5.3.

Table 5.3: Relevant requirements for the gondola. VEE: Venus Entry, SCM: Scientific Mission, EXT: External Constraints, SAR: Safety and Reliability.

Requirement ID	Requirement
Venus Entry	
Req-VEE-2	The system shall withstand the operating environment during entry.
Req-VEE-2.3	The system shall withstand peak entry deceleration loads of at least 78 g.

Continued from previous page

Requirement ID	Requirement
Req-VEE-2.4	The system shall withstand the vibrations during entry into the Venusian atmosphere.
Scientific Mission	
Req-SCM-1	The platform shall provide the necessary operational support functions to enable full execution of the scientific payloads' measurement.
Req-SCM-1.1	The system shall transmit 2.9 $kbps$ of data to the orbiting spacecraft.
Req-SCM-1.2	The platform shall achieve a pointing accuracy higher than <TBD> degrees (3σ) in all axes.
Req-SCM-1.4	The platform shall be autonomously controlled throughout the duration of the scientific mission.
Req-SCM-1.5	All scientific payload components shall be accommodated within the allocated volume and interfaces of the platform.
Req-SCM-4	The system shall withstand the conditions of the Venusian atmosphere for the entire mission duration.
Req-SCM-4.1	The system shall withstand the H_2SO_4 clouds for the entire mission duration.
Req-SCM-4.1.1	During measurement phases critical components inside the system shall be protected.
Req-SCM-4.2	The system shall withstand all trace elements of the Venusian atmosphere for the entire mission duration.
Req-SCM-4.3	The system shall withstand a temperature range of 280-350 K for the entire mission duration.
Req-SCM-4.5	The system shall withstand the UV radiation at and above the target altitude of the Venusian atmosphere for the entire mission duration.
Req-SCM-4.6	The system shall withstand the pressure at the target altitude of the Venusian atmosphere for the entire mission duration.
Req-SCM-5	The system shall comply with the set engineering budget during the mission on Venus.
Req-SCM-5.1	The platform and payload combined shall have a maximum mass of 20 kg.
Req-SCM-5.2	The platform shall provide a power of at least 35 W.
Req-SCM-5.3	The platform shall be able to store at least 12.5 MB of data in between transmission periods.
Req-SCM-5.4	The platform shall have an energy storage capacity of at least 80 Wh.
External Requirements	
Req-EXT-3	The mission shall support European Strategic Autonomy.
Req-EXT-3.1	Any goods shall be purchased from European-based organisations.
Req-EXT-3.2	Any service shall be provided by European-based organisations.
Safety and Reliability	
Req-SAR-1	Reliability of the complete system shall be at least 95%.
Req-SAR-2	The system shall include safety measurements.
Req-SAR-2.1	The system shall be able to detect anomalies during all mission phases to a degree of accuracy of 95%.
Req-SAR-2.2	The system shall be able to autonomously resolve detected anomalies.
Req-SAR-2.3	The system shall autonomously enter a predefined safe mode within upon detection of a critical anomaly.

5.2.1. Configuration

The gondola is a cuboid with size 20 x 20 x 10 cm, in other words, it is a 4U cubesat (1U = $10 \times 10 \times 10$ cm) in a square configuration, as opposed to the "traditional" line configuration. The gondola is made out of Ti-6Al-4V, a high-strength, aerospace-grade titanium alloy, due to its high strength, the

thickness is only 2.1 mm. The power is generated by 8 solar panels during the day, and provided by 2 secondary batteries during the night.

The gondola is pressurized in order to maintain a stable environment inside it and prevent sulphuric acid leaks. The gondola is connected to the balloon by means of 5 cables, one through the middle and one through each corner. All surfaces (gondola, solar panels, cables, etc) are coated with Teflon® to make them resistant to sulphuric acid. An overview of the components that make up the gondola, their mass, and their power, is shown in Table 5.4.

Table 5.4: Gondola components.

Component	Amount	Total Mass [kg]	Power [W]	Section
Solar panels	8	1.184	80.25 (peak)	subsection 5.2.3
Battery + PDCU	2	0.720	100 Wh	subsection 5.2.3
Argon gas	-	0.007	0	subsection 5.2.2
Microprocessor	1	-	0.050	subsection 5.2.4
Flash storage	1	-	0.050	subsection 5.2.4
Electrical cables	20 m	0.617	0.26	subsection 5.2.4
Supporting cables	15 m	0.075	0	subsection 5.2.2
Teflon® coating	0.84 m^2	0.054	0	subsection 5.2.2
Structure	-	1.489	0	subsection 5.2.2
Structural integration	-	0.170	0	subsection 5.2.1
Electrical integration	-	0.254	0	subsection 5.2.1
Contingency	-	0.455	0	subsection 5.2.1
Transponder	1	0.125	8	subsection 5.2.4
UHF Antenna	2	0.11	0.04	subsection 5.2.4

Internally, the gondola houses two batteries and PDCUs; however, this is assembled in a single component of size 1U [58]. The LMC_{OOL} assembly was designed in order to fit in a 1U package as well, as will be shown in chapter 6. Furthermore, the communications subsytem fits in less than 1U, subsection 5.2.4. This leaves over 1U for mechanical integration, cables, and networks to transport samples to LMC_{OOL}. The configuration of the gondola can be seen in Figure 5.5 below:

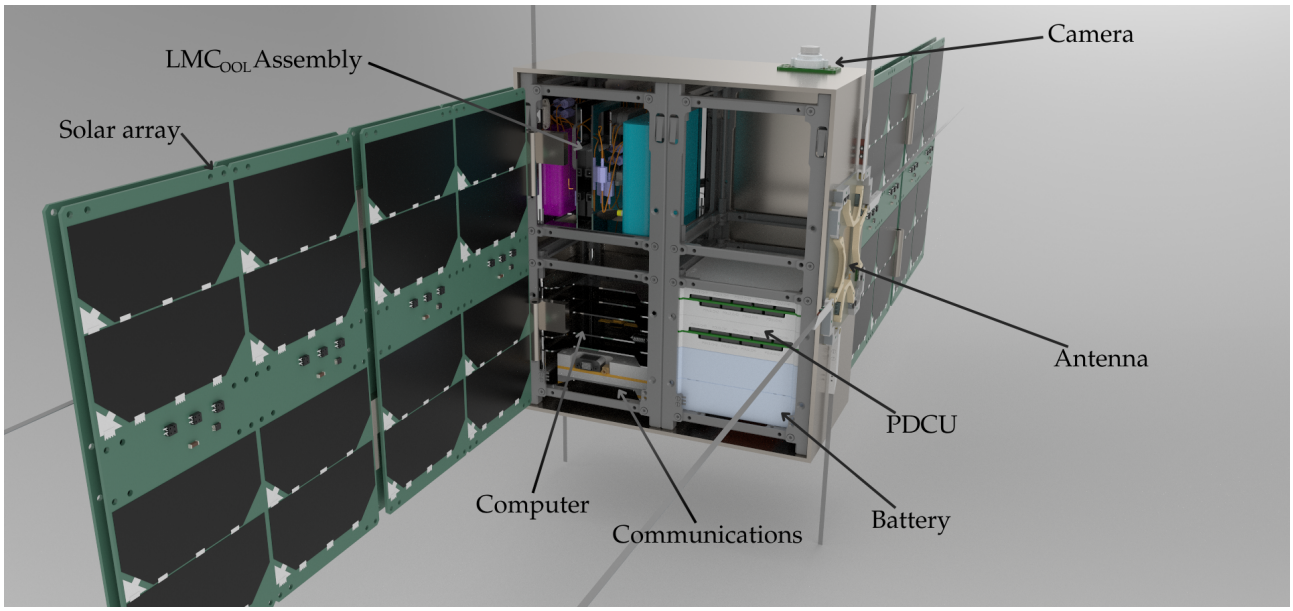

Figure 5.5: 3D render of the final gondola configuration. The gondola will be sealed but it is open to show the internal configuration.

The integration and contingency masses in Table 5.4 are obtained from the same empirical relations as for the spacecraft [32], 3.5% of the total mass for structural integration, 4% for electrical integration, and an 8% margin added to the final mass, note that the "total mass" also includes payload, which will be explored in chapter 6. Although the relations are for a satellite, they were deemed appropriate due to the cubesat-like nature of the gondola. In the following subsections, the design process for the gondola will be explained.

5.2.2. Structure

It is decided to make the gondola a cubesat-like probe, this is done to exploit the availability of off-the-shelf components for cubesats. In addition to this, the gondola is pressurized to the highest pressure that will be encountered in Venus. By doing this, the overpressure (with respect to the environment) will prevent sulphuric acid from entering the gondola in case of a small leak.

With this in mind, three shapes are considered for the gondola: a cuboid, a cylinder, and a sphere. The sphere is the most appropriate shape for a pressurized vessel, while the cuboid has the advantage of easier integration, the cylinder is a middle-ground between both. The concept of a pressurized cylinder cubesat was already carried out by NASA with the GeneSat-1 [59], the cylinder was encaged in a cubesat frame for integration. After considering all three concepts, it is found that, although the cuboid requires a thicker wall, hence leading to a heavier vessel, the need for a frame for the other two concepts makes them heavier overall, so the cuboid configuration is chosen.

Based on internal components, power system requirements (presented in subsection 5.2.3), and entry capsule size, it is decided to make the gondola a $20 \times 20 \times 10\ cm$ cubesat.

Pressure loads

The lowest altitude the probe is expected to drop down to in the worst case scenario (downwind at night) is 48.25 km. This is a conservative estimate, as the mission is designed to spend the night at high altitudes. At 48.25 km, the pressure is around 133 kPa and the temperature is around 365 K, as given by VIRA[4]. The number of moles inside the gondola are obtained using the ideal gas law (Equation 5.2):

$$PV = nRT \tag{5.2}$$

Where P is pressure, V is volume, n is number of moles, R is the ideal gas constant (R = 8.3145 $J \cdot mol^{-1} \cdot K^{-1}$), and T is temperature. The number of moles inside the gondola is 0.176, argon is the chosen gas to pressurize the gondola, as it is an inert gas, and it is less prone to leaking than Helium due to its bigger size. Using the molar mass of argon of 39.9 $g \cdot mol^{-1}$[5], it is found that the mass of the argon inside the gondola will only be 7 grams.

Knowing the number of moles inside the gondola, the maximum pressure it needs to withstand can be calculated. It is found that the most critical case is the highest temperature during cruise, 60 $°C$ is assumed conservatively, although the maximum expected temperature is 23 $°C$, as stated in subsection 4.3.4. During cruise the outside pressure is still 0, leading to the highest net inside pressure. Under these conditions, using Equation 5.2, the gondola will need to withstand an internal pressure of 122 KPa.

As opposed to spheres or cylinders, pressurizing a cuboid is a novel concept, so obtaining the stresses due to pressure is not a trivial task. Each face of the cuboid is modelled as a flat plate clamped in all sides, in this case the "clamps" are the other faces of the cuboid. Under this assumption, the maximum stress on the plate is given by Equation 5.3 below [60, p. 508]:

$$\sigma_{max} = \frac{\beta_1 P L^2}{t^2} \tag{5.3}$$

[4] https://www.sciencedirect.com/journal/advances-in-space-research/vol/5/issue/11

[5] https://pubchem.ncbi.nlm.nih.gov/compound/Argon Accessed 12/06/2025

Where P is the pressure acting on the plate, L is the length of the short edge of the plate, and t is the thickness of the plate, β_1 is equal to 0.3078 for a square plate, and 0.4974 for a plate with one side twice as long as the other. Note that in the case of a clamped flat plate, the maximum stress happens at the centre of the long edge (this is also the case for the cuboid). To account for the effect of the edges of the cube, a stress concentration factor of 2.5 [60, p. 793] will be added to the stress predicted by Equation 5.3.

Several materials are studied, namely titanium alloys, aluminium alloys, magnesium alloys, and fibres. The choice of material is heavily influenced by the manufacturing method. Welding is chosen due to the need for the gondola to be airtight and the lack of extra mass from components like bolts of rivets. It is decided to use Ti-6Al-4V because of its excellent strength retention after welding, with the yield strength even being improved by over 10% in some cases [61]. Al5456-H343 comes in second due to its low strength compared to titanium, leading to a higher overall mass. Al5456-H343 has excellent weldability [62], being one of the aluminium alloys with higher strength after welding, so it is kept as a backup in case complications arise with Ti-6Al-4V upon manufacturing. Taking a Ti-6AL-4V yield strength of 880 MPa and density of 4430 $kg \cdot m^{-3}$[11], the thickness of the gondola comes out to 2.1 mm, and the mass of the structure to around 1.489 kg.

Entry Loads

Aside from the pressure, entry loads are considered for sizing the gondola. It is assumed that the peak loads during entry are 78 gs, as stated in subsection 4.4.5, and that the gondola must carry a mass of 10 kg. This is a conservative estimate, as it will be shown later that the entire platform assembly, including the sampling and pressure regulation systems, is less than 10 kg. Both axial loads (Equation 5.4), and skin buckling (Equation 5.5, [63]) are taken into account:

$$\sigma_y = \frac{F}{A} \tag{5.4}$$

$$\sigma_{cr} = C\frac{\pi^2 E}{12(1-\nu^2)}\left(\frac{t}{b}\right)^2 \tag{5.5}$$

Where σ_y is the yield stress, F is the entry load, A is the cross-sectional area, σ_{cr} is the critical buckling stress, C is a constant dependent on the aspect ratio (b/t), C is taken as 4 conservatively [63], E is the Young's modulus, ν is the Poisson's ratio, t is the thickness, and b is the width. It is found that, with the thickness of 2.1 mm as already stated, neither failure mode is a concern (**Req-VEE-2.3**). Due to the lightweight nature of the gondola, even the high entry loads are not critical for the structure. Due to the limited time, the vibrations during entry could not be analysed, so the compliance with **Req-VEE-2.4** is left for further design stages.

Deployment and Environmental Protection

To size the supporting cables the gondola will hang from, a similar analysis as for the entry loads is performed. Once again, due to the lightweight mass of the gondola, it is found that the rope strength is not an issue for high-performance ropes. The V-Plus-XTR rope manufactured by LIROS is chosen [64], this rope, manufactured 100% in Germany, is made out of Vectran® and has a XTR (extreme temperature resistant) coating, which allows it to survive temperatures up to 200 $°C$. This XTR coating also improves UV resistance, shielding the weakest point of the assembly against it (**Req-SCM-4.5**). A total of 5 ropes will be used to ensure the stability of the gondola, each with a length of around 3 m. The V-Plus-XTR weights 7 $g \cdot m^{-1}$ when its diameter is 3 mm, so the total mass of the ropes is 105 g.

As for the Teflon® coating, the entire gondola structure and solar panels have to be coated resist the H_2SO_4 (**Req-SCM-4.1**, **Req-SCM-4.1.1**). The area of the gondola is simple to calculate due to its cuboid shape, 0.16 m^2. For the solar panels, although they are assembled with the backsides of two panels together, it is conservatively assumed that the seal is not perfect, and thus both sides need to be coated for both panels. The area of each panel is assumed to be 20 x 20 cm, which when multiplied by the 16 faces of the panels gives an area of 0.64 m^2. A 5% margin is added to the total area of 0.8 m^2 to account for the cables and hinges. Using an areal density of 64.2 $g \cdot m^{-2}$ for the Teflon® and the

adhesive combined [65], the mass of the coating is 54 g. The Teflon® coating also resists most trace elements in the Venusian atmosphere, like HCl or H_2S, complying with **Req-SCM-4.2**.

It is decided not to apply any insulation to the gondola, as it is rendered useless due to the length of the mission. The approach taken is to pick components that are rated for the maximum expected temperature of 350 K, or to cool the components that are a must-have for the mission (LMC_{OOL}). The most critical component is the batteries, as they are rated only for 333 K. Extra work will need to be put into making them more temperature resistant in order to comply with **Req-SCM-4.3**.

5.2.3. Power

Power System Architecture

Due to the expected lifetime of the probe exceeding 45 Earth days, solar panels are chosen as the main power source. For energy during the night, two secondary batteries are used. The two secondary batteries are mounted in the same assembly as 2 power distribution and control units (PDCU). Each PDCU has 4 inputs, so the 8 solar panels are distributed evenly between both. An overview of the power flow in the gondola can be seen in Figure 5.6 below.

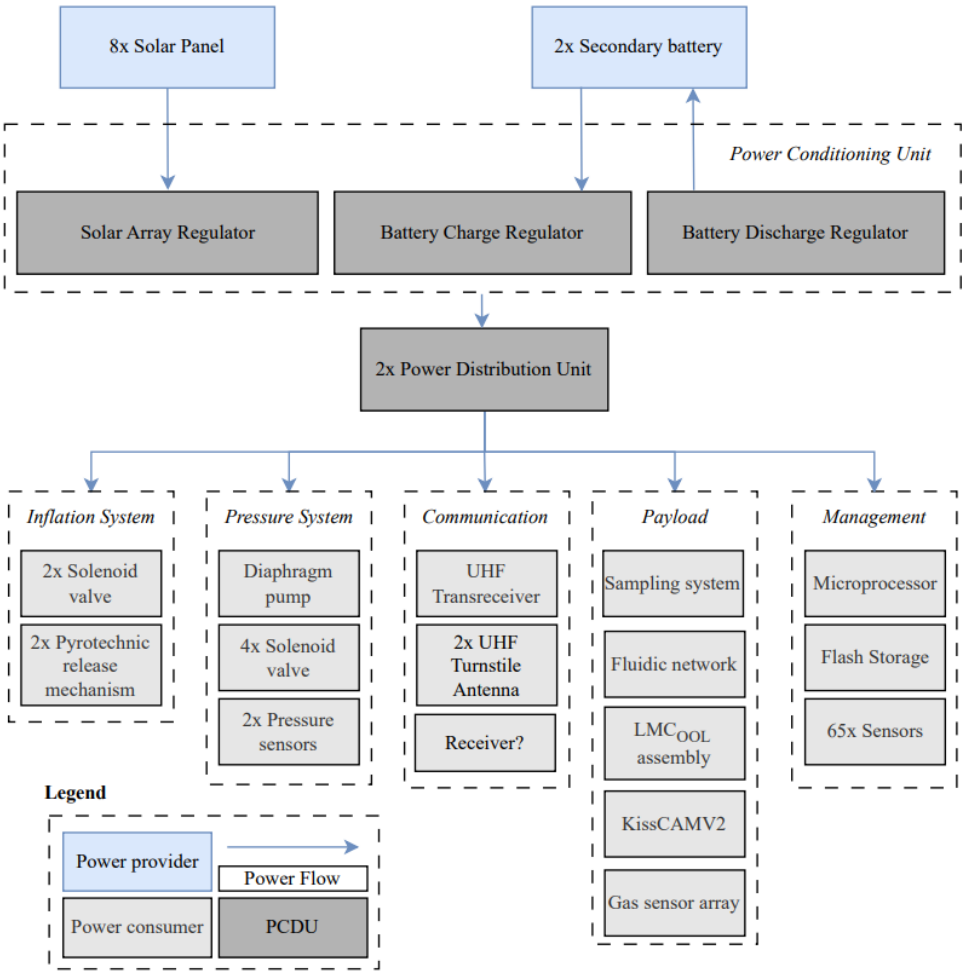

Figure 5.6: Electrical block diagram for the gondola.

Power requirements

An overview of the power requirements and operating conditions of the spacecraft subsystems during the operations is given in Table 5.5.

Some considerations about the required power are made:

Table 5.5: Power consumption of the gondola.

Subsystem	Function	Power [W]	Operating condition
Communication	Receiving	0.23	Continuously
	Transmitting	8	Continuously during day
C&DH	Onboard Computer	0.1	Continuously
	Cable loss	0.26	Continuously
Payload	Sampling	0.05	Active on demand
	LMC_{OOL} operation	4	Active on demand
	LMC_{OOL} cooling	11 (nominal)	Continuously if below 55 km
		18 (peak)	Continuously if below 55 km and operating LMC_{OOL}
	Secondary payload	2	Active on demand
Pressure regulation	Pump	6.6	Active on demand
	2x Valves	16	Active on demand, power needed for 0.2 s
Housekeeping	61x Sensors	0.1	Continuously
	4x IMUs	0.132	Continuously during day

- Solar panel and antenna deployment are handled by the battery, which will be charged by the orbiter shortly before the arrival to Venus.
- The PDCU efficiency is 92%[58], this will be accounted for by dividing all power values over 0.92 when doing the calculations.
- 4 IMUs are carried on the solar panels to check the deployment; however, after deployment, they will only be operated during the day to save battery power.
- The 61 sensors are comprised of 43 temperature sensors, 4 pressure sensors, 9 accelerometers, 4 capacitors, and 1 acidity sensor. They are all assumed to consume 0.00165 W, as that is the consumption of the thermal sensors in the solar panels [37].

An overview of the required power, based on the mission timeline, can be found in Figure 5.7a below, while the required power for the most critical day-night cycle can be observed in Figure 5.7b, where the breakdown per subsystem can be better observed.

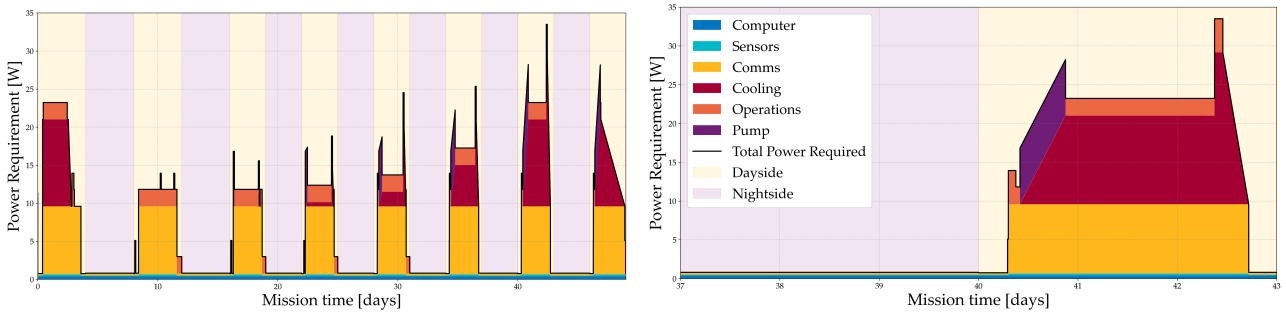

(a) Power required by the gondola throughout the mission.

(b) Power required by the gondola during the most intense cycle.

Figure 5.7: Power requirements of the gondola across the full mission and during the most intense cycle.

Figure 5.7 highlights how the power consumption depends on the scientific timeline. The peak power consumption occurs late in the mission, as the probe will descend deeper into the atmosphere, requiring more cooling power. Furthermore, two spikes can be observed each day, one for the pumping to descend, and one for the increase in cooling combined with the power to run the LMC_{OOL} assembly. The detailed timeline for the mission can be found in section 6.2. An important remark is that there is no transmitting power during the night; however, the probe will be able to communicate with the

spacecraft while operating with the battery, as will be shown later. Additionally, it is assumed that during the day the probe is always transmitting, this is an overestimation, but it guarantees that the probe will be able to transmit data during the day no matter the situation.

Solar Array Sizing

To obtain the power generated by the solar panels, taking into account the Venusian conditions is essential. The solar flux varies with altitude, latitude, time of day, and time of year. A simulation based on the data of the Venera probes [66] that takes into account these 4 factors is created to obtain the solar flux that the panels receive at all times during the mission. The details of this simulation can be found in the Midterm Report [1].

Solar panels become less efficient as the temperature rises, while this is not too important in an orbit, the probe will experience temperatures up to 80 $^{\circ}C$ inside the Venusian atmosphere. The decrease in power can be obtained by knowing the change in current and voltage, as shown by Equation 5.6 below:

$$\frac{dP}{dT} = I \cdot \frac{dV}{dT} + V \cdot \frac{dI}{dT} \tag{5.6}$$

Where P is power, T is temperature, I is current, and V is voltage. Using this, the drop in power for Ultra Triple Junction (UTJ) solar cells can be calculated. Using Spectrolab's numbers [67], the percentage decrease in power for UTJ cells is 0.27 $\% \cdot K^{-1}$, while the nominal temperature is 28 $^{\circ}C$. The higher temperature at low altitudes, combined with the lower solar flux, make the low altitude case more critical for power generation.

Two additional remarks need to be made with respect to the power generation. Due to the small size of the gondola compared to the balloon, the balloon could cast a shadow on the panels, rendering the face facing the top useless. For this reason the panels will be facing the sides, to account for this, it is assumed that all the flux hitting the panels is due to atmospheric scattering (only 80% of the nominal flux reaches the panels [68]). The second remark is with regards to the coating. The panels need to be coated with Teflon® to be sulphuric acid resistant, and Teflon®, while transparent, only lets 95% of light through [69], so a 5% decrease is applied to the power generated.

The panels chosen for the gondola are the same as those for the spacecraft, the Core-04 panels from 2NDSpace [37]. For the case of the gondola, a total of 8 solar panels will be used; however, instead of the 1U×4U configuration used in the spacecraft, a 2U×2U configuration will be used in the gondola to fit within its dimensions. Using 8 panels of 11W nominal power (at 1AU) each, the power requirement is reached, as shown in Figure 5.8.

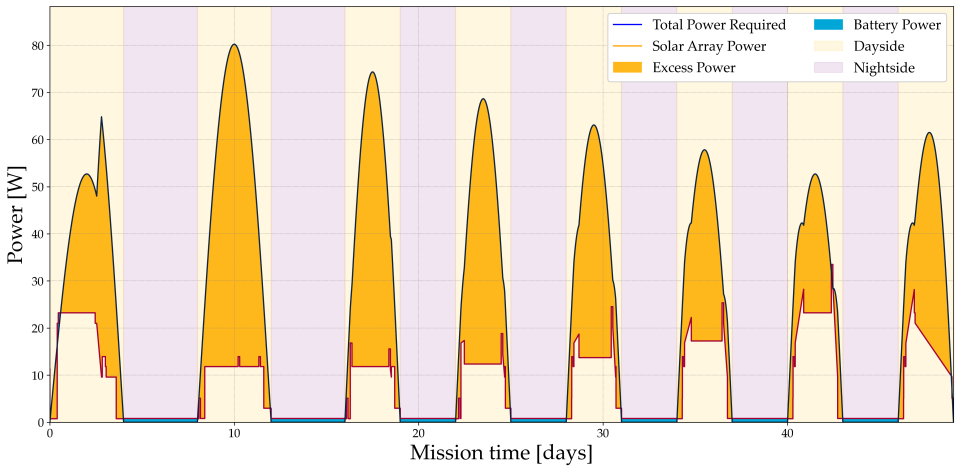

Figure 5.8: Power generated vs power required by the gondola.

As it can be observed, there is a lot of excess power at noon; however, as the probe enters/exits eclipse, the power constraint becomes higher. The panels are sized such that there is enough power at the more constraining times, complying with **Req-SCM-5.2**. As already stated, the initial power deficit is made up via the pre charged battery.

Battery Sizing

During the night, power is consumed by the following components: 0.23 W by the receiver, 0.1 W by the computer, 0.26 W due to cable loss, 0.05 W by the sampling system, and 0.1 W due to the 61 sensors; for a total of 0.74 W. Taking into account the 92% efficiency of the PDCU, the total power needed continuously during the night rises to 0.805 W. The longest night occurs at the equator, where it lasts 96 hours, so a total energy consumption of 77.29 Wh is obtained, **Req-SCM-5.4** is derived from this number.

The chosen battery is the SOLO-EPS X8 by 2NDSpace [58]. Using a battery manufactured by the same company as the solar panels ensures easier integration and compatibility. The SOLO-EPS X8 offers an energy storage capacity of 100 Wh, and it has 2 PDCU units integrated. It is decided to use 2 PDCU units as each one has 4 input channels for solar panels and the probe has 8 solar panels. The probe will use the 22.71 Wh remaining during the night to communicate with the spacecraft when a link is possible. With a transmitting power of 8.70 W (8/0.92), it is possible to transmit for a total of 2.61 hours during the eclipse in the worst case scenario. As the balloon goes up in latitude and the night becomes shorter, the transmitting time will increase, and depending on the power, there exists the possibility of operating the secondary payload or LMC_{OOL} for short periods during the night.

5.2.4. Data Handling and Communications

Data Generation

To obtain an accurate estimate of the data generated by all instruments and sensors, assumptions regarding the sampling frequency and the number of bits generated per reading have been made. This information is summarized in Table 5.6.

To correctly interpret data received from multiple sensors, each transmitted sample must include not only the measured value but also metadata identifying its source and time of acquisition. These metadata fields are referred to as the *identifier bits* and *time bits*, respectively, and are included in the total number of bits generated per sample.

The number of identifier bits required depends on the total number of distinct sensors N:

$$b_{\text{id}} = \lceil \log_2(N) \rceil$$

The number of time bits depends on the desired temporal resolution ΔT and the total time span T that must be represented. For this analysis, a mission duration of 45 days is assumed. The required number of time bits is calculated as:

$$b_{\text{time}} = \left\lceil \log_2 \left(\frac{T}{\Delta T} \right) \right\rceil$$

Whilst sensor data is assumed to be generated at a constant rate at all times, instruments like LMC_{OOL} and the camera are only active during specific times, to come up with a data rate that they each generate for transmission the total data is divided by the time spent on the illuminated portion of the planet during which a link can be established. This yields 148 bps required to be transmitted from LMC_{OOL} and 167 bps generated by the camera.

Table 5.6: Sensor data generation rates for orbiter transmission (rounded up to nearest bit per second).

Sensor	# Sensors	Freq. [Hz]	Time Bits	ID Bits	bps Gen.
Temperature	43	0.05	18	6	86
Pressure	4	0.2	20	2	44
Accelerometers (3x3 axis)	9	0.2	20	4	72
Capacitors (Sulphuric Acid Volume)	4	0.05	18	2	8
Solar Panel IMU	4	0.2	20	2	22
Acidity Sensor	1	0.2	20	0	7
Total	–	–	–	–	**239**

Data Storage

For the probe, the orange line in Figure 4.12 represents the total amount of data generated, it accumulates during the night time when transmission is assumed to be not possible, this is a conservative estimate, as it has been shown in subsection 5.2.3 that some communication is possible. Telemetry is generated continuously, but the window for transmitting data to the spacecraft is short, as the spacecraft is near pericenter during these contacts. The peak in stored data during the first night is shorter than in subsequent nights, as the probe begins operating only after atmospheric entry, which is assumed to occur midway through the night. This represents the worst-case scenario, as the probe is generating data without transmitting from the start. When the probe transitions to the dayside, the stored data begins to decrease. On the dayside, the probe has access to more power, resulting in an increased data production rate due to the addition of scientific data alongside telemetry. However, as the spacecraft moves toward apocenter and slows down, the length of the windows increases. This allows the probe to transmit data faster than it is generated, enabling a complete offload of stored data. A memory size for data that is transmitted to the spacecraft of 25 MB is found, including a safety factor of 2, complying with **Req-SCM-6.3**.

Command and Data Handling

The data storage unit must be selected to comply with the requirement described above .Since the required processing rates are even smaller for the probe than for the spacecraft modern microprocessing chips and storage units are more than capable of handling the subsystems demands. The driving requirements on the system are imposed by the data rate generated by LMC_{OOL} instrument which must be compressed to enable transmission, the compression protocol selected is CCSDS121 a standard for most space application [70]. The data handling unit must also be able to to handle sensor data, schedule operations onboard of the probe, send data to the storage system and handle incoming commands from the spacecraft.

Link Budget and Transmission

After running the simulation described in subsection 4.3.7 that estimates the contact time with the orbiting spacecraft a value for the required transmission bit rate is calculated and described in **Req-SCM-1.1**. This is then the driving input to determine the margin for the link between the spacecraft and the orbiter. Since the largest loss in any link budget results from free-space path loss , which increases with both signal frequency and transmission distance, a lower frequency helps to reduce this loss. Additionally, lower frequencies experience less atmospheric attenuation on Venus. For these reasons, a frequency of 380MHz has been chosen.

Assuming that the bit rate required for science and telemetry data from the probe is far higher than the commands revived for the budget and that the downlink and uplink will be performed with the same antenna, the a detailed command uplink budget is deemed unnecessary as it will definitely have a higher margin than than in the downlink case. The modulation scheme is selected based on the transceiver's capabilities, which are limited to FSK. To improve performance, it is assumed that FSK can be combined with Turbo error correction coding to reduce the required E_b/N_0 for the link [71].

The atmospheric attenuation is calculated using data from a referenced paper, which provides a value of 0.004 $dB \cdot km^{-1}$ at an altitude of 50 km [72]. Assuming a worst-case scenario—where the signal is transmitted toward the horizon—a simple geometric estimate gives a signal path length through the atmosphere of 1047 km. Multiplying these values yields an estimate of the total signal attenuation in decibels. The same source also reports scattering losses, but these are of a smaller order of magnitude. To remain conservative, an additional loss equal to half the absorption value is included. The resulting link budget is presented in the following section. Table 5.7

Table 5.7: Communication link budget for Venus to Orbiter, required data rate of 2900 bps.

Name	Gain/Loss (dB/dBW)	Explanation
Probe transmission path		
Transmission gain	2.3	UHF Antenna specification
Transmission power	6.989	5 W transciever output RF power
EIRP	5.289	Effective Radiated Power
Spacecaft Receiving System		
Receiver Gain	2.3	UHF Antenna specification
Total Noise System Temperature	-23.01	Calculated using SMAD equation on page 477 [35], based on noise figure, feed loss (from transponder specs), and antenna noise temperature[6].
Transmission Path		
Space Loss	-170.64	Calculated using SMAD equation for maximum transmission distance during orbiter elliptical orbit. [35]
Atmospheric absorption loss	-4.29	[72]
Atmospheric absorption loss	-2	[72]
Modulation Path		
Required E_b/N_0	-5	For FSK with Turbo coding, code rate 1/2 [71].
Final Margin		
Carrier-to-Noise Ratio (C/N)	43.51	Sum of EIRP, G/T, and total losses.
Data Rate	-34.62	2.9 $kbps$ expressed in dB.
Transmitted E_b/N_0	10.2	C/N minus data rate in dB.
Margin (Maximum Gain)	5.2	Transmitted minus required E_b/N_0.
Margin (Half-Power Beamwidth)	2.20	Link margin at 90 ° receiving angle where radiation power is halved.

Component Selection

To decrease the number of bits to be transmitted the antennas need to be able to establish a link for as long as possible whilst there can be contact between the orbiter considering that the antennas will not be able to be pointed from the gondola but their orientation will rotate frequently. Therefore the choice of two low gain dipole antennas each pointing in opposite directions will maximise the transmission radiation pattern, completely reducing the need for any active control of the gondola body. The antenna selected is the SAM UHF cross dipole antenna described in Table 4.11 its half power beamwidth is not specified in the data sheet provided but a conservative assumption is 90° in the vertical plane [73]. Even at this large angle transmission is possible as shown in Table 5.7 the link budget allows for a connection with a reasonable margin. A very useful property of cross dipole antennas that when the individual dipoles are fed with 90° phase difference then the antennas produce an omnidirectional pattern in the horizontal plane meaning that motions that change the orientation of the balloon will not affect the communications between the probe and the spacecraft [73].

One major difference between the antennas on the probe and those on the spacecraft is that they are subjected to a harsher environment compared to the spacecraft, especially concerning the sulphuric acid significantly damaging the antenna system. For this reason a coating of gold could be used to protect the transmitting rods which are the most exposed to environment. Whilst not significantly increasing the weight, gold plating keeps the electrical conductivity of the rods essentially unchanged to avoid signal degradation and it it is used often for RF components where corrosion and degradation are an issue. At the same time the central part of the antenna which houses the deployment mechanism and the electrical interface shall be enclosed by a protective housing made of PTFE (polytetrafluoroethylene), which provides excellent resistance to the corrosive sulfuric acid environment of Venus while remaining transparent to radio frequencies to ensure uninterrupted communication.

Selecting a transceiver dedicated to UHF frequencies unlike on the spacecraft where it handled a wide range of frequencies allows for higher DC power to RF output characteristics. Indeed the performance of the TRX-U[7] transponder is shown in Table 5.8.

Table 5.8: Specifications of the TRX-U transciever.

Parameter	**DC Power In** $[W]$	**RF Power Out** $[W]$	**Mass** $[kg]$	**Temp. Range** $[°C]$
Value	8	5	0.126	-35 to 80

The microprocessor and storage unit were selected to be tolerant radiation whilst enabling the data rate and and functions required for the probe to function. The microprocessor selected is the SAMD21RT [8] a radiation tolerant, low power chip . For storage the SST26LF064RT [9], a 64 $mbit$ chip with radiation resistance and non-volatile flash memory, is chosen.

Diagrams showing the flows and interactions of both the communications and data handling subsystem are shown in Figure 5.9 and Figure 5.10.

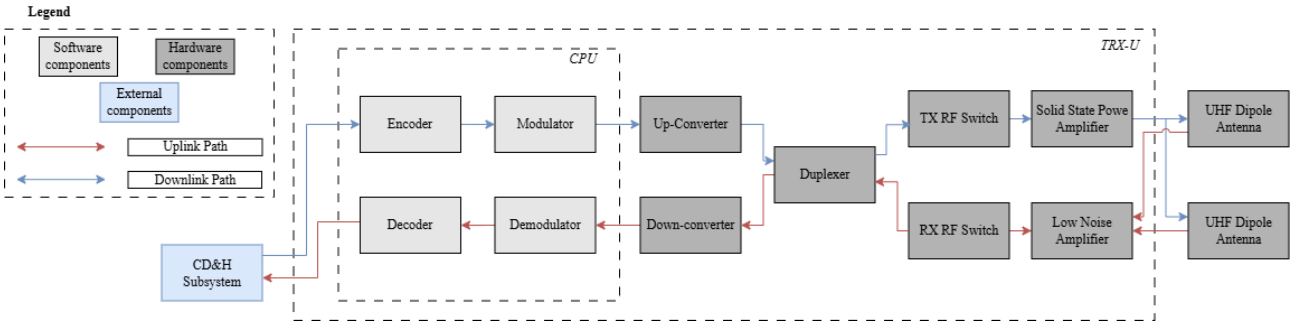

Figure 5.9: Sofware/Hardware block diagram of the communications subsystem of the probe.

[7] https://www.aac-clyde.space/wp-content/uploads/2021/11/TRX-U-datasheet.pdf Accessed 09/06/2025

[8] https://ww1.microchip.com/downloads/aemDocuments/documents/AERO/ProductDocuments/DataSheets/SAMD21RT_Datasheet_DS50003677.pdf Accessed: 09/06/2025

[9] https://ww1.microchip.com/downloads/en/DeviceDoc/00004443.pdf Accessed: 09/06/2025

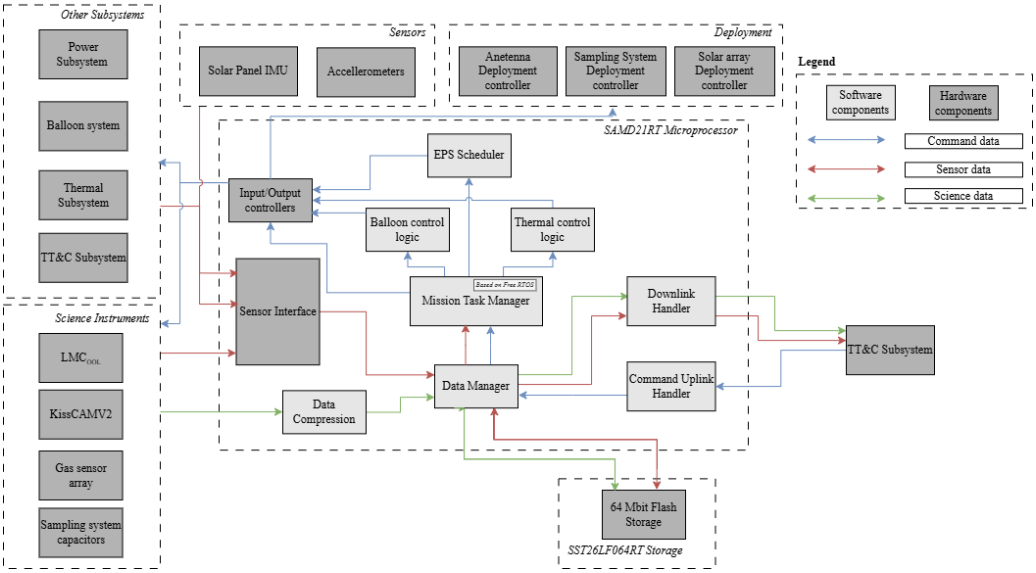

Figure 5.10: Sofware/Hardware block diagram of the command and data handling subsystem of the probe.

5.2.5. Verification and Validation

The method of computing the maximum stress on a cuboid is verified by means of a finite element analysis (FEA), the FEA is performed using Siemens NX[10], the solver used is NX Nastran. Due to time constraints, the FEA could not be performed for the final design of the gondola, but it was performed for an earlier design iteration to verify that the stress calculation is conservative. The outcome is shown in Figure 5.11, it can be seen that the maximum stress occurs at the centre of the edges. Additionally, the maximum stress of 137.49 MPa is quite lower than the yield stress of Al 6061 (276 MPa)[11], complying with **Req-SCM-4.6**. It must be noted that the stress concentration factor used for Figure 5.11 was 3, upon noticing the large margin in pressure, it was reduced to 2.5 for the rest of the design. For the entry load stresses, the code output was compared to hand calculations to ensure it is correct; however, due to the time constraint, and entry loads not being critical (required thickness for the pressure is over 3 times as high as that of the entry loads), proper unit tests were not written for them. They should be written in the future to ensure the code works as intended.

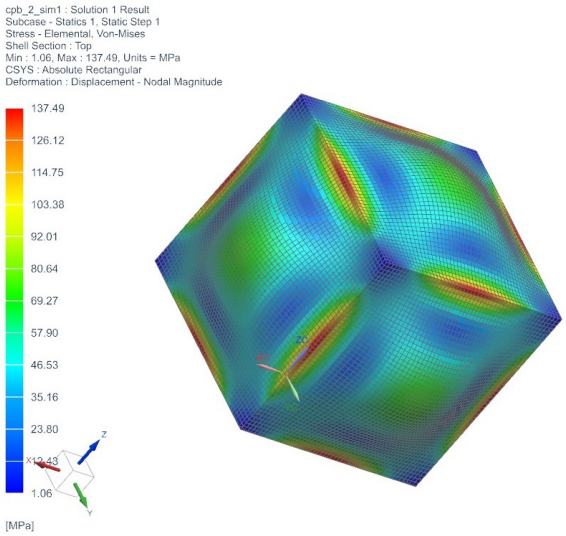

Figure 5.11: FEA for a cube of Al 6061 with side length 20 cm, 121300 Pa of internal pressure, 3 mm thickness.

As for the power, a similar situation arises due to time constraints. The plots were manually checked to ensure that they make sense, and some of the parameters were varied and checked as a sensitivity analysis, with the outcomes behaving as expected. In the future, proper unit and system tests should be done for the power consumed and generated, including the solar flux simulation.

5.3. Balloon design

The balloon will be a crucial part of the mission, as it will carry the gondola across a wide range of altitudes and locations around Venus. A set of requirements was defined in the Baseline Report [2], of

[10] `https://plm.sw.siemens.com/en-US/nx/` Accessed 05/06/2025
[11] `https://www.matweb.com/` Accessed 12/06/2025

which the ones that apply to the balloon can be found in Table 5.9

Table 5.9: Requirements table. SCM: Scientific Mission, BFM: Balloon Fabric Material, PRS: Pressure Regulation System.

Requirement ID	Requirement
Scientific Mission	
Req-SCM-1	The probe shall provide the necessary operational support functions to enable full execution of the scientific payloads' measurement.
Req-SCM-1.3	The probe shall remain at an altitude range of 47-58 with an accuracy of 0.25km.
Req-SCM-1.4	The probe shall be autonomously controlled throughout the duration of the scientific mission.
Req-SCM-2	The payload shall collect samples of the clouds.
Req-SCM-2.3	At least two of the samples shall be separated by a distance of at least 100km.
Req-SCM-2.4	The samples shall be taken within an altitude range of 50-55.5 km with an accuracy of 0.25 km.
Req-SCM-2.7	The samples shall be disposed of in a manner.
Req-SCM-4	The system shall withstand the conditions of the Venusian atmosphere for the entire mission duration.
Req-SCM-4.1	The system shall withstand the H_2SO_4 clouds for the entire mission duration.
Req-SCM-4.2	The system shall withstand all trace elements of the Venusian atmosphere for the entire mission duration.
Req-SCM-4.3	The system shall withstand a temperature range of 280-350 K for the entire mission duration.
Req-SCM-4.4	The system shall withstand wind gusts up to 2 $m \cdot s^{-1}$ at the target altitude for the duration of the whole mission.
Req-SCM-4.5	The system shall withstand the UV radiation at and above the target altitude of the Venusian atmosphere for the entire mission duration.
Req-SCM-4.6	The system shall withstand the pressure at the target altitude of the Venusian atmosphere for the entire mission duration.
Req-SCM-4.7	The system shall have a lifetime of at least 30 days.
Balloon Fabric Material	
Req-BFM-1	The material of the superpressure balloon shall endure a super pressure of at least 50 000 Pa.
Req-BFM-2	The balloon material shall accommodate integrated openings for venting, pumping, and inflating the lifting gas.
Req-BFM-3	The balloon shall not tear due to dynamic pressure loads during deployment.
Req-BFM-4	The balloon shall not leak more Helium than 900 $cm^3 \cdot m^{-2} \cdot day^{-1}$.
Req-BFM-5	The balloon material shall have a solar absorptivity of 0.15 or less.
Req-BFM-6	The balloon material shall have an infrared emissivity of 0.5 or more.
Pressure Regulation System	
Req-PRS-1	The altitude control system shall allow the balloon to descent the whole range within at most 12 hours
Req-PRS-2	The altitude control system shall allow the balloon to ascent the whole range within at most 12 hours
Req-PRS-3	The pressure system shall have a total mass of less than 2 kg
Req-PRS-4	The pressure system shall be able to handle a temperature range of 280-350 K
Req-PRS-5	The pressure system shall be able to handle a pressure difference between the superpressure and zeropressure balloon of at least 50 000 Pa

The overall design of the balloon is briefly discussed in subsection 5.3.1, after which more detail on the material, altitude control, pressure system, thermal effects, and the balloon simulations can be seen in subsection 5.3.2, 5.3.3, 5.3.4, 5.3.5, and 5.3.6 respectively.

5.3.1. Balloon Architecture

To comply with the requirements seen in Table 5.9, a balloon-in-balloon system is designed consisting of a superpressure balloon with a diameter of 1.84 m and a zeropressure balloon with a diameter of 3.68 m. A quick overview of the principles of this concept can be seen in Figure 5.12, showing the venting of helium from the superpressure to the zeropressure balloon to increase the volume and therefore buoyancy of the balloon allowing it to increase in altitude. To decrease the altitude, helium is pumped back into the superpressure balloon in order to decrease the volume and thus the buoyancy. The pressure regulation system designed in subsection 5.3.4 allows for a descent from 55.5 km down to 50 km within 12 hours, and an ascent back to 55.5 km once again within 12 hours. The pressure regulation system consists of a series of pumps and valves, has a total mass of 1.2 kg and will hang right below the balloon. Due to the material designed in subsection 5.3.2, the balloon is capable of flying within the operating range for around 2 months allowing it to circumnavigate the planet roughly 10 times. This all results in a zeropressure balloon mass of 7.63 kg, a superpressure balloon mass of 1.19 kg, and a total of 461.93 moles or 1.85 kg of helium. A render of the balloon can be seen in Figure 5.13.

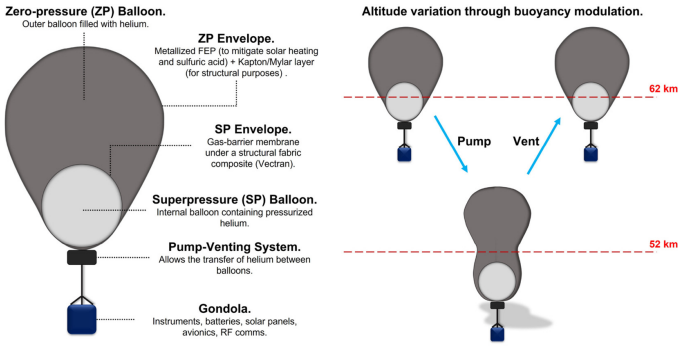

Figure 5.12: Overview of the balloon-in-balloon concept [74], showing the venting and pumping process in order to ascent and descent respectively.

Figure 5.13: Render of the balloon in the clouds, accompanied by the gondola hanging below.

5.3.2. Material

The wide range of technical requirements for the balloon material quickly leads to a laminate design. The balloon must survive the transfer to Venus, the entry and the Venusian environment as described in **Req-EVT-4**, **Req-VEE-2** and **Req-SCM-4**. More specific requirements are defined in Table 5.9 under the label **Req-BFM**. Note that the leakage rate of 900 $cm^3 \cdot m^{-2} \cdot day^{-1}$ in Req-BFM-4 is driven by **Req-SCM-4.7**, which requires a probe lifetime of 45 days. It is estimated that with a leakage rate of 900 $cm^3 \cdot m^{-2} \cdot day^{-1}$, the balloon operates within the required altitude range for 45 days.

Laminate Architecture

To meet these different requirements, a laminate design is required which is shown in Figure 5.14. For the zeropressure balloon, the design consists of an outer Fluorinated Ethylene Propylene (FEP) film. Driven by **Req-SCM-4.1**, this protects the other materials from the sulphuric acid aerosols. It is aluminized with a 30 nanometre layer of aluminium with the purpose of reflecting solar radiation and meeting **Req-BFM-5** and **Req-BFM-6**. Then there is an aluminized polyimide (Kapton®) film barrier with the purpose of providing UV radiation shielding (**Req-SCM-4.5**), thermal insulation (**Req-BFM-5**) and preventing helium leakage (**Req-BFM-4**). Thirdly, to meet **Req-BFM-1** and **Req-BFM-3**, there is a Vectran® fabric layer which ensures the balloon is strong enough to sustain super pressures and prevents tearing during deployment. Finally, there is a layer of Aliphatic Urethane which enables bonding of the different fabric parts to manufacture the balloon. The FEP film, aluminised polyimide gas barrier and Vectran® fabric layers are bonded together by adhesives. The masses of the adhesive layers are estimated based on a prototype balloon developed by the Jet Propulsion Laboratory, California Institute of Technology, and NASA. These are: 9.9 $g \cdot m^{-2}$ for the bond between the FEP coating and the Kapton® film, and 17 $g \cdot m^{-2}$ for the bond between the Kapton® film and the Vectran® fabric [65]. For the superpressure balloon, the laminate design is the same except for the FEP coating. Since the superpressure balloon is not exposed to the Venusian atmosphere, this does not require the coating which is reflected in Figure 5.14. To accomodate integrated openings for venting, pumping and inflating the balloons with Helium and meet **Req-BFM-2**, a concept design is discussed in section 8.1.

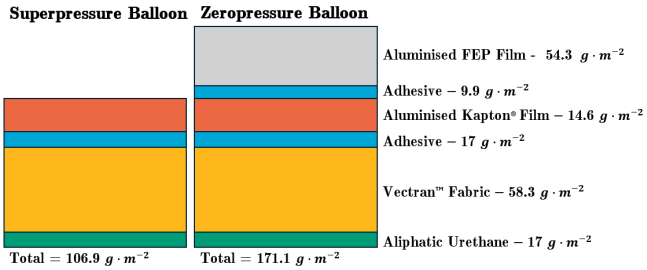

Figure 5.14: Material diagram of the balloon (not to scale).

Aluminised FEP Coating

Teflon® states in their FEP Properties Bulletin: "Teflon® FEP film is chemically inert and resistant to virtually all chemicals, except molten alkali metals, gaseous fluorine, and certain complex halogenated compounds, such as chlorine trifluoride, at elevated temperatures and pressures."[69]. This makes it an excellent coating for protecting other materials from the corrosive Venusian environment. Furthermore, Dunmore can manufacture a version of the film with an aluminium layer which reduces the solar heating of the balloon by reflecting solar radiation [75]. FEP itself is transparent and lets through 96% of solar radiation making it an excellent coating for the solar array as well [69]. A prototype designed and tested by the Jet Propulsion Laboratory, California Institute of Technology and NASA used an aluminised FEP film coating with a thickness of 25.4 micrometers at 54.3 $g \cdot m^{-3}$ with a 30 nanometre aluminium layer [65]. In this stage of the material design, these values will be assumed but in post-DSE project phases, this will be refined in coordination with European manufacturing partners.

Aluminised Kapton® Barrier

To form a barrier which limits the helium permeability through the balloon an aluminised polyimide (Kapton®) film is used. In the paper by Hall, it was found that their Venus balloon prototype with an aluminised Mylar gas barrier did not have any significant Helium leakage after 13.5 days [65]. The fact that an aluminium layer is great in preventing gas permeability is further supported by an experiment from Haeyong Jung stating that permeability "through the Al-metallized film are measured to be only about 4.1% of those through uncoated PET film" for a range of gases [76]. This paper also states that multiple layers of aluminium improve the barrier performance due to manufacturing imperfections causing small holes within the layer [76]. For this reason there is one aluminium layer in the FEP coating and another one in this polyimide layer.

A polyimide film is chosen because it has excellent chemical resistance to almost all chemicals including sulphuric acid [77]. However at high concentrations and hot temperatures, it will degrade which is why the FEP coating is still included [78]. Furthermore, the material is a space-grade insulator with a

thermal range between -250 °C to 290 °C [12]. Dunmore could manufacture an aluminised Kapton® film at a thickness range of 7.6-127 micrometers and hence at this stage to limit mass, a thickness of 10 micrometers is chosen [12]. With a thickness of 10 micrometers and a density of 1.46 $g \cdot cm^{-3}$ stated by Saint-Gobain Tape Solutions, this leads to 14.6 $g \cdot m^{-2}$ for this layer [79].

Vectran® Fabric

The Vectran® fabric is chosen to carry the dynamic and static pressure loads during deployment procedures and when inflated. The fabric is based on the fabric used in the prototype built by Jet Propulsion Laboratory, California Institute of Technology and NASA which has 100 denier, 1-3-1 ripstop weave pattern, and 25 yarns per cm in the warp and fill direction [65]. This ripstop weave pattern prevents tares from growing by having 15% thicker yarns every 3 yarns. Vectran® fabric has a Young's modulus of 75 GPa and a maximum elongation of 3.8% [80]. The specific mass (μ_{fabric}) can be calculated as shown in Equation 5.7.

$$\begin{aligned} \text{yarn mass} &= \frac{1+1.15+1}{3} \cdot \frac{\text{denier}}{9000} = 1.05 \cdot \frac{100}{9000} = \frac{7}{600} \ \left[\text{g} \cdot \text{yarn}^{-1}\right] \\ \mu_{\text{fabric}} &= \text{yarn mass} \cdot \text{yarns per square meter} = \frac{7}{600} \cdot (2500+2500) = 58.33 \ \left[\text{g} \cdot \text{m}^{-2}\right] \end{aligned} \tag{5.7}$$

Aliphatic Urethane

The material is fully covered by aliphatic urethane on the interior. This flexible thermoplastic layer allows Vectran® based structural tape to be thermally welded to it. This is done to join the different material parts into a balloon shape as described in section 8.1. Furthermore, it acts as a thermoplastic matrix which helps to distribute the loads equally across the Vectran® fabric, preventing stress concentrations and improving the material durability.

Material Performance

To determine if the design meets the driving requirements, preliminary predictions of key material performance parameters have been made. These will be validated through extensive testing of the laminate and the assembled balloon in future design phases.

To check if the laminate design meets **Req-BFM-4**, the Helium leakage is estimated. This is based on tests performed on the prototype built by Jet Propulsion Laboratory, California Institute of Technology and NASA [81]. It is found that the Helium permeability increases with temperature and with how wrinkled the laminate is. At 50 °C, it is found that 662 $cm^3 \cdot m^{-2} \cdot day^{-1}$ of Helium would permeate and at 23 °C, 253 $cm^3 \cdot m^{-2} \cdot day^{-1}$ [81]. For the heavily wrinkled samples it is 860 $cm^3 \cdot m^{-2} \cdot day^{-1}$ at 23 °C and 4009 $cm^3 \cdot m^{-2} \cdot day^{-1}$ at 50 °C [81]. However the wrinkling here is exaggerated and in reality the creasing is believed to be significantly less. Furthermore, permeability is directly proportional to the super pressure in the balloon and this experiment was done at 3000 Pa super pressure [81]. The super pressure that the outer zeropressure balloon experiences is negligible as explained in subsection 5.3.6 and the Helium that permeates from the superpressure balloon can be pumped back using the PRS. Hence the value of 700 described in Table 5.10 is very conservative. Assuming this constant Helium leakage, it takes 58.32 days until the balloon cannot climb above 50 km altitude and the mission is over. At this time, there is no pressure difference between the zeropressure and superpressure balloon and a small downward wind would cause the balloon to drop down below 50 km in altitude. Here the atmospheric pressure increases and the balloon shrinks resulting in less buoyancy and further loss in altitude. This meets **Req-SCM-4.7** but extensive helium leakage tests should be done to verify this.

The solar absorptivity and Infrared (IR) emissivity of the material is taken from the values based on the previously mentioned prototype with the same aluminised FEP coating. The testing on different laminate samples with different degrees of wrinkling suggest 0.15 and 0.51 are accurate values for modelling as stated in Table 5.10 [81].

[12] `https://www.dunmore.com/products/aluminized-polyimide-film.html`, accessed 16/06/2025

The strength of the balloon laminate material is calculated assuming that only the Vectran® fabric carries the loads. This is a conservative assumption, as the other layers in the laminate will carry some of the load. As stated in Equation 5.7, the average yarn mass including the ripstop weave pattern is $\frac{7}{600} \approx 0.01167\ g \cdot \text{yarn}^{-1}$, and the material properties state a density of 1400 $kg \cdot m^{-3}$ [80]. The strength of the fabric can be calculated according to Equation 5.8, where the maximum stress ($\sigma_{\max}$), maximum strain ($\epsilon_{\max}$), tensile modulus (E_{Vectran}) and density (ρ_{Vectran}) are used. The result of 59375 $N \cdot m^{-1}$ is in line with the tests performed on the similar Vectran® based laminate of the mentioned prototype balloon, which resulted in a strength of 71 $kN \cdot m^{-1}$ and 57 $kN \cdot m^{-1}$ in the warp and fill directions respectively [65].

$$\begin{aligned} \text{Strength} &= \sigma_{\max} \cdot A_{\text{yarn}} \cdot (\text{yarns per meter}) \\ &= \epsilon_{\max} \cdot E_{\text{Vectran}} \cdot \frac{\text{mass per yarn}}{\rho_{\text{Vectran}}} \cdot (\text{yarns per meter}) \\ &= 0.038 \cdot 75 \cdot 10^9 \cdot \frac{\frac{7}{600} \cdot 10^{-3}}{1400} \cdot 2500 = 59375\ \left[\text{N} \cdot \text{m}^{-1}\right] \end{aligned} \tag{5.8}$$

The assumption that the load is only carried by the Vectran® fabric suggests that the superpressure balloon laminate and the zeropressure balloon have the same strength. Using thin membrane theory, the maximum super pressure that the balloons can sustain is calculated according to Equation 5.9 [65]. A radius of 0.92 m and 1.84 m for the superpressure and zeropressure balloon respectively leads to the maximum super pressures stated in Table 5.10. Further finite element analysis (FEA) will be performed to in the next design stages to account for the stress concentrations due to the Helium Tube fittings and gore to gore joints. Hall suggests that the maximum burst pressure for the prototype according to the FEM is half that suggested by the thin membrane theory [81]. Nevertheless, at half the super pressure, **Req-BFM-1** is met. With this high strength, low mass and ripstop-weave pattern, it is predicted that the laminate materials will not tare during deployment meeting requirement **Req-BFM-3**.

$$P = \frac{2 \cdot \text{Strength}}{\text{radius}} \tag{5.9}$$

Table 5.10: Material properties of the balloon.

Parameter	Performance	Unit
Helium Leakage	700	$cm^3 \cdot m^{-2} \cdot day^{-1}$
Balloon Lifetime	58.32	days
Solar Absorptivity	0.15	N/A
IR Emissivity	0.51	N/A
Strength	59375	$N \cdot m^{-1}$
Super Pressure Superpressure Balloon	129076	Pa
Super Pressure Zeropressure Balloon	64538	Pa
Superpressure Balloon Specific Mass	106.9	$g \cdot m^{-2}$
Zeropressure Balloon specific Mass	171.1	$g \cdot m^{-2}$

5.3.3. Altitude Control

The altitude of the balloon can be controlled by venting or pumping helium between the zeropressure and superpressure balloon. To increase the altitude of the balloon, helium will be vented from the superpressure balloon to the zeropressure balloon, and thus increasing the overall volume and therefore buoyancy of the system. To go down, the volume of the balloon needs to be decreased, which can be achieved by actively pumping helium from the zeropressure to the superpressure balloon.

In order to predict how the balloon moves, a simulation is created in Python to model its behaviour.

The equation of motion of the balloon in the vertical direction is shown in Equation 5.10 [82] below. It takes into account gravity, buoyancy, and drag. Thermodynamic effects are accounted for by means of varying the volume based on the temperature, as will be explained in subsection 5.3.5.

$$(m + \rho V_{zp} C_m) \cdot \frac{d^2h}{dt^2} = (V_{sp} + V_{zp}) \cdot \rho_{atm} g - mg - \frac{1}{2} \rho_{atm} C_D A \cdot \left(\frac{dh}{dt} - w\right) \left|\left(\frac{dh}{dt} - w\right)\right| \tag{5.10}$$

Where m is the total mass that needs to be lifted, ρ is density, V is volume, C_m is the virtual mass coefficient, which is used to account for the fluid the balloon accelerates when it itself is accelerated. A virtual mass coefficient of 0.5 is taken [83], as the balloon is modelled as a sphere travelling through an inviscid fluid. Continuing with the formulas, g is the gravitational acceleration, A is the cross-sectional area of the balloon, once again modelled as a sphere, w is the wind speed, defined as positive in the upwards direction. The wind term does not appear in the original equation in [82], it is added to be able to investigate the response of the balloon to continuous winds or strong gusts. Finally, a drag coefficient C_D of 0.5 is assumed for the balloon [82].

5.3.4. Pressure Regulation System

In order to allow for a better altitude control, a requirement is set for the time needed to ascend/descend the full altitude range (50-55.5 km). It is decided that the balloon shall be able to traverse this distance in around 12 hours, whether it is ascending or descending. This length is chosen because it allows for moderately fast travel, while not being too fast to avoid excessive forces or sudden thermal changes. This requirement is used to size both the valve and the pump. The mass flow through a pump is given by Equation 5.11, while the mass flow through a valve is given by Equation 5.12, both formulas were taken from [84].

$$\dot{m}_{pump} = \rho_{zp} \cdot \dot{V}_{pump} \tag{5.11}$$

$$\dot{m}_{vent} = C_d \cdot \frac{\pi}{4} \cdot d^2 \sqrt{2 \cdot (P_{sp} - P_{atm}) \cdot \rho_{sp}} \tag{5.12}$$

Where ρ is the density of the helium gas, $\dot{V}_{pump}$ is the volumetric flow rate of the pump, C_d is the discharge coefficient of the valve, d is the diameter of the valve, and P is the pressure. The subscripts "zp", "sp", and "atm" refer to the helium inside the zeropressure balloon, the helium inside the superpressure balloon, and the atmosphere, respectively.

The simulation allows to time the balloon movement, and to investigate its movement when pumping or venting. Using this, the volumetric flow rate of the pump should be 3.5 $L \cdot min^{-1}$, while the diameter of the vent diameter should be in the order of 0.35 mm. After a extensive search, it is decided to choose the Schwarzer Precision SP 620 EC-DV pump [85], as it is lightweight and fulfils all requirements for this mission. While this German company produces pumps for a range of industries, they are not graded for use in space, so testing and development will be needed to ensure the SP 620 EC-DV will operate reliably on Venus. In general, the pump is also not suitable for the high temperatures it will have to endure in the Venusian clouds, however a modified version can be developed capable of operating at 80°C, and withstanding periods of up to 110 °C before the elastomers start to break down according to Carsten Treichel (Schwarzer Precision, personal communication, 5 June 2025) and Mark Hommersen (KNF Verder B.V., personal communication, 6 June 2025). As for the valve, the Marotta MV602L latching solenoid valve is chosen [86]. Once again, it is lightweight and fulfils all requirements, the latching nature of the valve makes the power requirement low, as it only needs to be powered for 0.2 s to be opened/closed. Marotta Controls is a trusted company with experience in the space industry, and the MV602L valve has been flight qualified on ESA's LISA Pathfinder and Aeolus[13].

In addition to the main pump and valve, there are two other types of valves in the pressure system. Check valves are used to ensure that helium flows in the right direction, and a pressure relief valve is

[13] `https://marotta.com/products/flow-controls/solenoid-valves/miniature-solenoid-valves//`, [Accessed 06/06/2025]

added to be able to vent helium to the atmosphere in case the pressure inside the zeropressure balloon grows too much (for example, due to a leak in the superpressure balloon). Both types of valves are manufactured by The Lee Company, an American company that specializes in micro fluid control. The check valve selected is the 187 Zero-leak check valve[14], while the pressure relief valve is the 187 Zero-leak PRI® pressure relief valve[15].

The P&ID (Piping and Instrumentation Diagram) for the probe is shown in Figure 5.15 below. It is composed of two parts: the pressure regulation system (dashed box), and the inflation system.

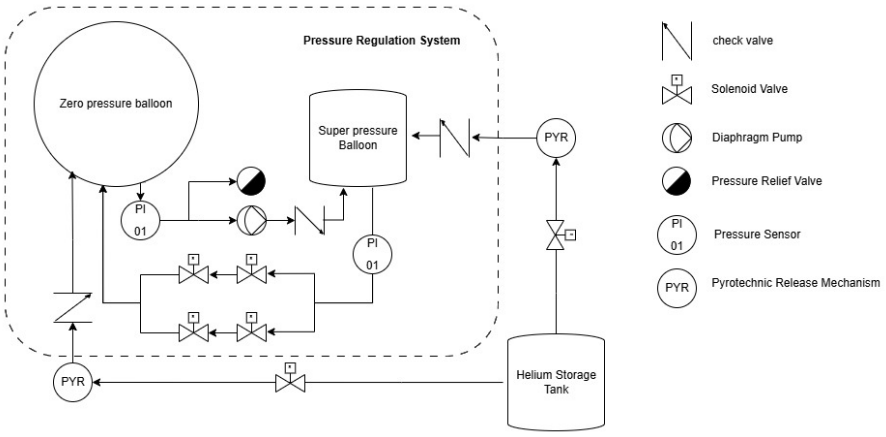

Figure 5.15: P&ID of the balloon pressure regulation system, including the initial inflation system.

The inflation system consists of two valves and two check valves, they will move the helium from the tank to the balloons during entry. After the deployment is done, the inflation system will be dropped through the use of pyrotechnics. For the pressure regulation system, an array of 4 valves will vent helium from the superpressure to the zeropressure balloon, having 4 valves not only adds redundancy, it also allows to vent through 2 valves in parallel at the same time, essentially cutting the ascent time by half. To pump helium back into the superpressure balloon, a pump is used in combination with a check valve, to prevent back pressure. Finally, as already stated, a pressure relief valve is added for safety.

For the tubing of the pressure regulation system, standard 1/4 inch stainless steel pipes [16] can be used resulting in a fluid velocity of roughly 10 $m \cdot s^{-1}$ and a piping mass of 200 grams for roughly 1 meter of piping[17]. Similarly, the inflation pipes will use standard 1.1/4 inch stainless steel pipes [16] resulting in just below 400 grams for roughly 30 cm of pipes.

5.3.5. Thermal Effects

Throughout its mission, the balloon will encounter a wide range of conditions and temperatures ranging from close to 0° C at the maximum operating altitude, all the way to 80° C at its lowest altitude. Apart from the wide temperature range, the balloon will encounter intense sunlight during day-time, and long periods of darkness during the night. These constantly changing conditions, together with the balloon-in-balloon system results in an intricate play of temperatures between the balloon films and helium within. This behaviour can all be captured by Equation 5.13 to 5.16, taken and modified to fit the balloon-in-balloon concept from "Thermodynamic Study for Venus Balloon" [87]. In these equations, m is the mass, C is the heat capacity, T is the temperature, h is the heat transfer coefficient, S is the surface area, α is the solar absorptivity, A is the projected area, Q is the solar flux, ϵ is the

[14] https://www.theleeco.com/product/187-zero-leak/, [Accessed 07/06/2025]
[15] https://www.theleeco.com/product/187-zero-leak-pri/, [Accessed 07/06/2025]
[16] https://www.mcmaster.com/products/pipe/pipe-and-pipe-fittings~/standard-wall-steel-unthreaded-pipe-nipples-and-pipe/ [accessed 11/06/2025]
[17] https://asm.matweb.com/search/specificmaterial.asp?bassnum=mq304a [accessed 11/06/2025]

infrared emissivity, σ is the Stefan-Boltzmann constant, M is the molar mass, g_{Venus} is the gravitational acceleration of Venus, γ is the specific heat ratio, and SP is the superpressure in the balloon. In Equation 5.13 to 5.16, subscripts are used where f indicates the balloon film/material, sp indicates the superpressure balloon, He refers to helium, ext refers to the outside, up refers to the solar flux coming from above, down refers to the solar flux reflected due to the albedo effect and atm refers to the atmospheric conditions.

$$m_{f_{sp}} C_{sp} \frac{dT_{f_{sp}}}{dt} = h_{He_{sp}}(T_{He_{sp}} - T_{f_{zp}})S_{sp} - \epsilon\sigma(T_{f_{sp}}^4 - T_{He_{zp}}^4)S_{sp} \tag{5.13}$$

$$m_{f_{zp}} C_{zp} \frac{dT_{f_{zp}}}{dt} = \Big(h_{He_{zp}}(T_{He_{zp}} - T_{f_{zp}}) + h_{ext_{zp}}(T - T_{f_{zp}})\Big)S_{zp} + \alpha A(Q_{up} + Q_{down}) - \epsilon\sigma(T_{f_{zp}}^4 - T^4)S_{zp} \tag{5.14}$$

$$m_{He_{sp}} C_{He} \frac{dT_{He_{sp}}}{dt} = h_{He_{sp}}(T_{f_{sp}} - T_{He_{sp}})S_{sp} - \frac{M_{atm}\, m_{He_{sp}}\, T_{He_{sp}}\, g_{Venus}}{T_{He_{zp}}\, M_{He}} + T_{He_{sp}} \left(\frac{\gamma - 1}{\gamma}\right)\left(\frac{dSP/dt}{SP}\right) \tag{5.15}$$

$$m_{He_{zp}} C_{He} \frac{dT_{He_{zp}}}{dt} = h_{He_{zp}}(T_{f_{zp}} - T_{He_{zp}})S_{zp} - \frac{M_{atm}\, m_{He_{zp}}\, T_{He_{zp}}\, g_{Venus}}{T\, M_{He}} \tag{5.16}$$

Equation 5.13 is composed of inner gas natural convection and outwards heat radiation, Equation 5.14 is composed of the inner gas natural convection, the forced convection due to the moving air around the balloon, the received solar radiation and the outwards heat radiation. Equation 5.15 consists of natural convection and the first law of thermodynamics plus a factor taking into account the isochoric heating as the volume of the superpressure balloon will be constant. Equation 5.16 is the same as Equation 5.15 minus the last term as it does not have a constant volume.

In the equations above, the helium heat transfer coefficients are a function of the Nusselt number, the thermal conductivity and the characteristic length. The Nusselt number then depends on the Prandtl and Grashof number where the Grashof number is dependent on the temperatures, characteristic length, expansion coefficient and viscosity [87]. The expansion coefficient is defined as $\frac{1}{T}$ [18], and both the thermal conductivity and viscosity values depend on temperature and were interpolated using values found on [19] and [20] respectively. Lastly, the external heat transfer coefficient is a function of the Reynolds number [87].

5.3.6. Balloon Simulation

Using the equations, principles and pressure system from subsection 5.3.3, subsection 5.3.4 and subsection 5.3.5, a simulation can be set up to analyse the balloon's performance. Throughout the mission, certain key critical phases can be analysed and are shown in the graphs below. One major challenge that the balloon will experience throughout its life, is vertical winds. According to the outputs of the GCM discussed in subsection 4.4.3, the maximum vertical wind gust are roughly 1 $m \cdot s^{-1}$ both up and down. In order to ensure that the balloon is adequately designed to handle the vertical winds, and due to the uncertainty in the wind model, the balloon is designed to handle continuous winds of 2 $m \cdot s^{-1}$.

Downward Wind

When the balloon faces a downward wind, it will descent and face higher atmospheric pressures. This increase in pressure around the balloon will decrease the volume of the zero-pressure balloon, further decreasing the buoyancy of the balloon. Apart from the loss of buoyancy, a decrease in altitude will

[18] https://phys.libretexts.org/Bookshelves/Thermodynamics_and_Statistical_Mechanics/Heat_and_Thermodynamics_(Tatum)/13:_Expansion_Compression_and_the_TdS_Equations/13.03:_Pressure_and_Temperature [accessed 06/06/2025]

[19] https://www.engineersedge.com/heat_transfer/thermal-conductivity-gases.htm [accessed 06/06/2025]

[20] https://www.engineeringtoolbox.com/gases-absolute-dynamic-viscosity-d_1888.html [accessed 06/06/2025]

result in a decrease in superpressure as the pressure in the superpressure balloon stays constant, while the ambient pressure increases. This poses a major risk to the balloon, as a loss of superpressure would mean a loss of control sending the balloon into an unrecoverable descent. These effects are most pronounced when the balloon is at its lowest operating altitude and during the night as solar heating creates an upwards effect. This effect can be seen in Figure 5.16.

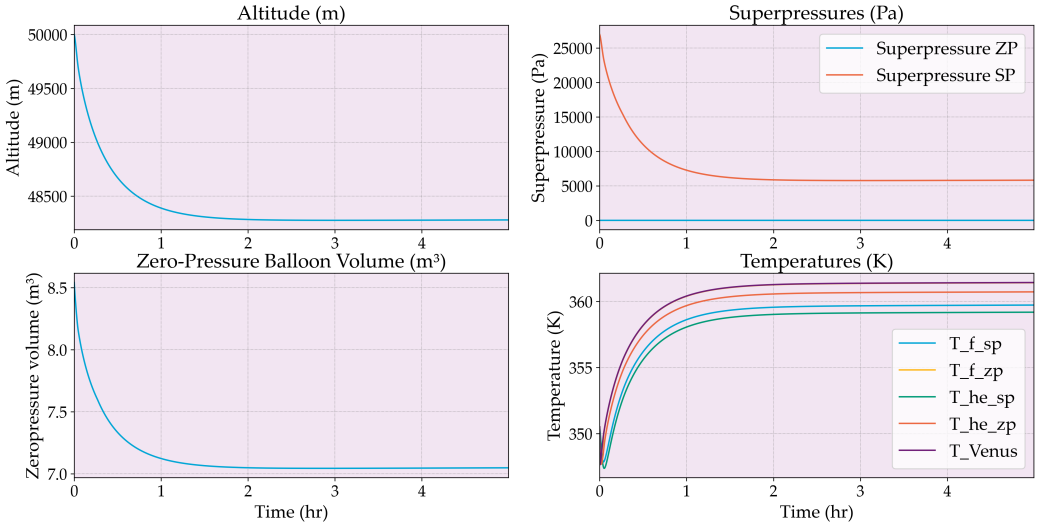

Figure 5.16: Balloon simulation starting at 50 km altitude, with a 2 $m \cdot s^{-2}$ downward wind during nighttime at the start of the mission, showing the altitude, superpressures, zeropressure balloon volume and temperatures over time.

From Figure 5.16, it is clear that even under a 2 $m \cdot s^{-1}$ downward wind, the balloon stabilises itself after going about 1800 m. While this results in a significant drop in superpressure, it is clear that the balloon keeps enough superpressure to keep control even during a continuous 2 $m \cdot s^{-1}$ downward wind.

Upward Wind

Another scenario that the balloon should be able to handle is sustained upward winds. The effect of an upward wind are the exact opposite as the downward wind discussed previously, and will subsequently be most pronounced when the balloon is flying at its maximum operating altitude during the daytime. Plots of this effect can be seen in Figure 5.17.

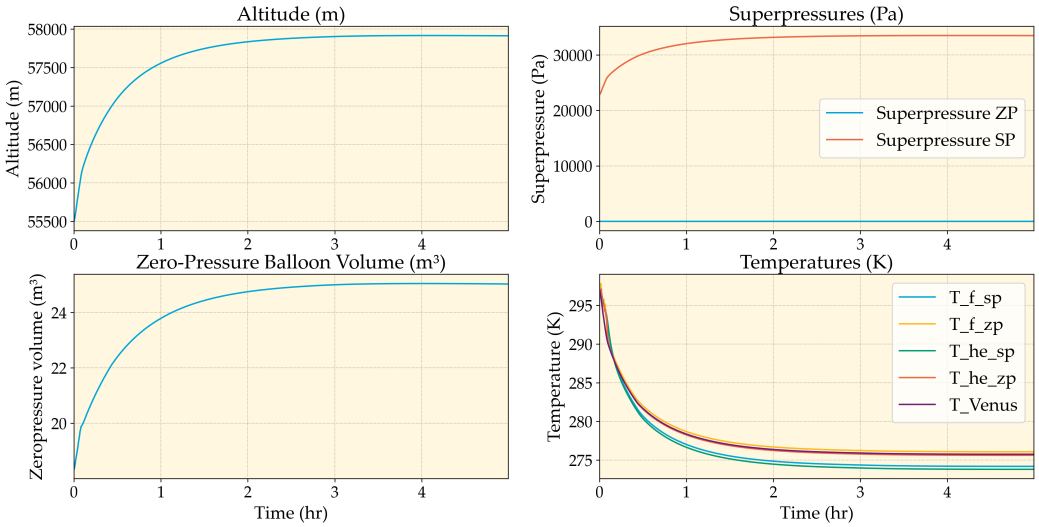

Figure 5.17: Balloon simulation starting at 50 km altitude, with a 2 $m \cdot s^{-2}$ downward wind during nighttime at the start of the mission.

From Figure 5.17, it is clear that even at a sustained 2 $m \cdot s^{-2}$ upward wind, the zeropressure does not reach its maximum inflation and stabilises itself below 58 km after rising almost 2.5 km in roughly 2 hours. From Figure 5.16 and Figure 5.17, it can also be seen that the balloon meets requirement **Req-SCM-1.3**, staying within a range of 48-58 km during normal operations when facing extreme sustained vertical winds.

In the case that the zeropressure does reach its maximum inflation, a superpressure will be created in the zeropressure balloon, however even for a sustained upward wind of 4 $m \cdot s^{-2}$, this will be limited to below 5000 Pa as can be seen in Figure 5.18, and is therefore not an issue according to Figure 5.14.

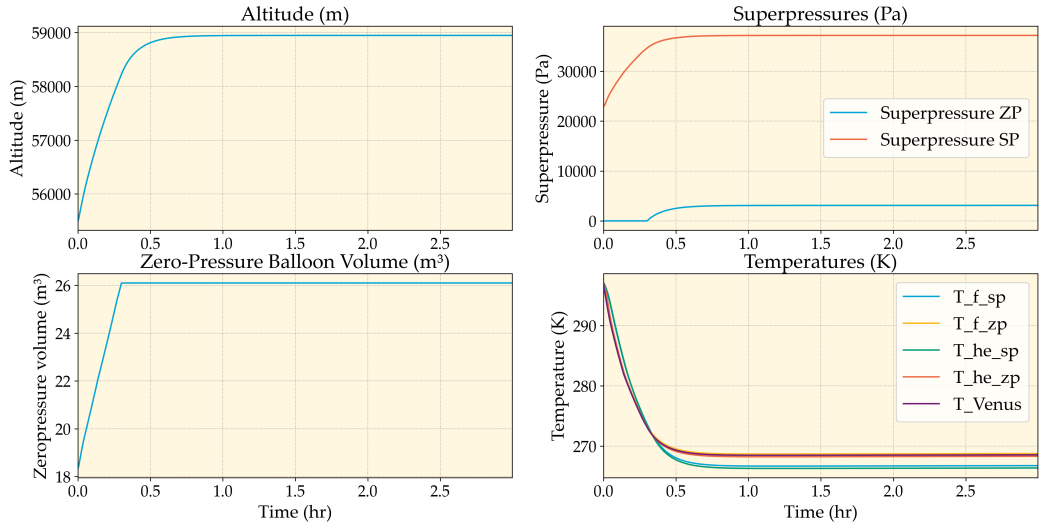

Figure 5.18: Balloon simulation starting at 55.5 km, with a 4 $m \cdot s^{-2}$ upward wind, showing the altitude, superpressure, balloon volume and temperatures over time.

Altitude Control

Using the simulation, it is also possible to analyse the altitude control performance of the balloon. Using the pressure regulation system designed in subsection 5.3.4, an ascent of the balloon is plotted in Figure 5.19. Note that while the slowest ascent would occur during the night, as the solar heating during the day helps the ascent, the difference is minimal and the balloon will, under normal operations, not perform an ascent during the night as it requires a significant amount of power to operate the valves. During normal operations, the venting will be done by opening the 2 valves lines in parallel as discussed in subsection 5.3.4.

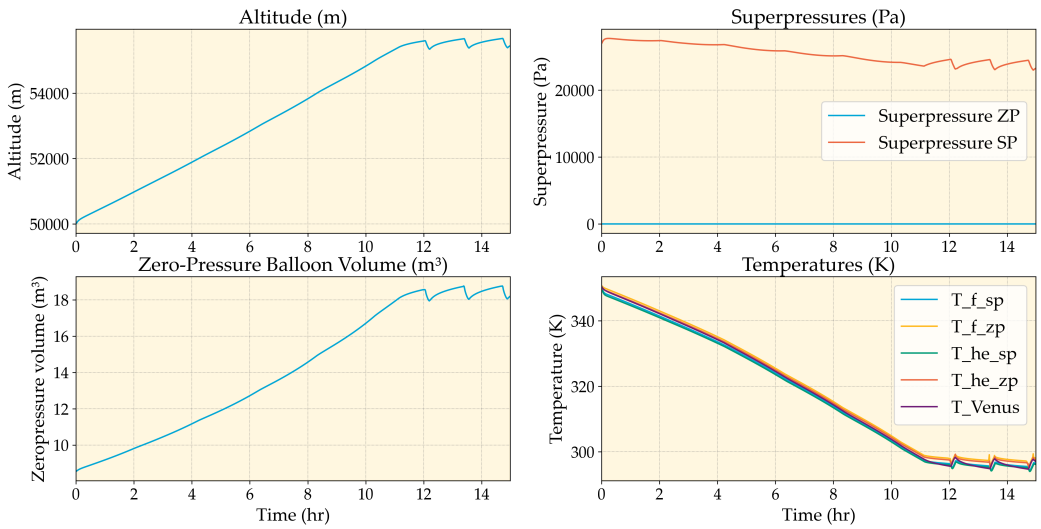

Figure 5.19: Venting of the balloon, showing the increase in altitude, the superpressures, balloon volume and temperatures of the balloon over time.

From Figure 5.19, it can be seen that the balloon ascents throughout the whole range within 12 hours, and therefore satisfying **Req-PRS-2**. It can also be noted that the superpressure in superpressure balloon does not drop significantly, even though the balloon is continuously venting. This can be explained by the accompanied drop in ambient pressure when ascending, making the pressure differential stay relatively constant. It can also be seen that the volume of the zeropressure balloon doubles when the altitude is increased from 50 to 55.5 km.

A similar graph can be mode for the descent phase during which helium will be pumped from the zeropressure back into the superpressure balloon to decrease the volume and buoyancy. Using the pump as specified in subsection 5.3.4, the descent can be plotted in Figure 5.20.

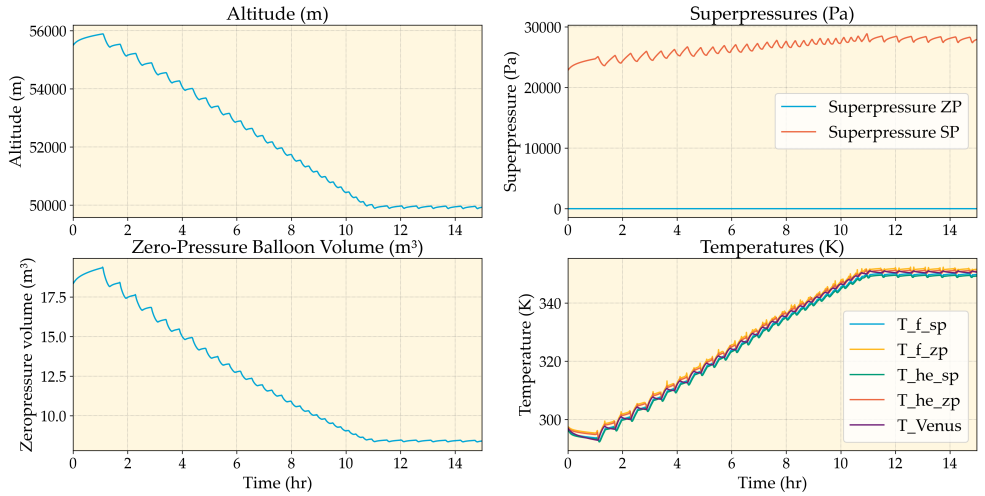

Figure 5.20: Pumping of the balloon, showing the decrease in altitude, the superpressures, balloon volume and temperatures of the balloon over time.

From Figure 5.20, it can be seen that the balloon starts pumping after 1 hour, and reaches the target altitude of 50 km roughly 10 hours later confirming that the descent rates also meets requirement **Req-PRS-1**. Note that descending during the night would be slightly faster, however similar to venting, operating during the night is under normal operations not possible as it requires a significant amount of power.

Incorrect Deployment Altitude

Apart from regular mission operations, the simulation can also be used to verify the balloon's behaviour in case of unexpected issues such as incorrect deployment altitude. The first case is deployment at an altitude above the operating range. Figure 5.21 shows the behaviour of the balloon after being deployed at an altitude of 65 km.

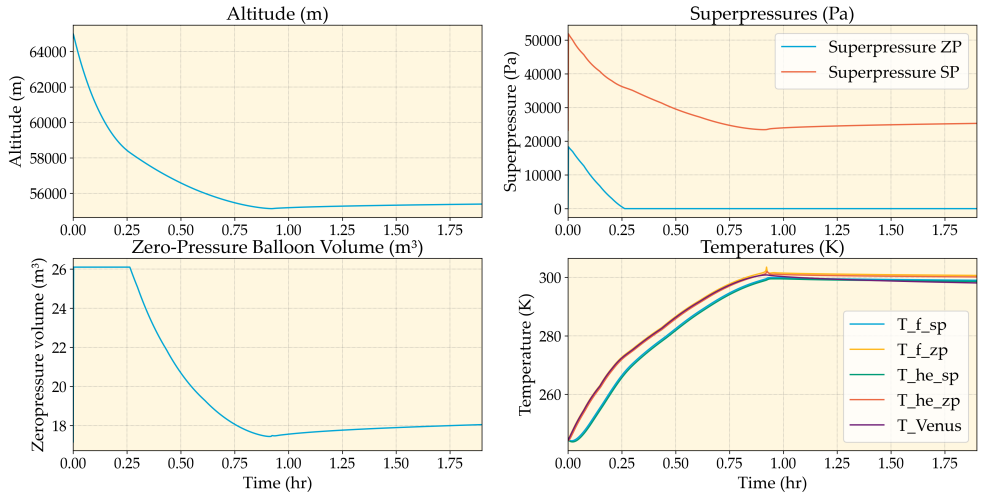

Figure 5.21: Simulation of the balloon deployed at an altitude of 65 km showing the decrease in altitude, superpressures, balloon volume and temperatures of the balloon over time.

From Figure 5.21, it can be seen that within one hour, the balloon is able to descent to within the operating range. While this incorrect deployment results in a higher then usual superpressure in the superpressure balloon, and even a superpressure in the zeropressure balloon, they are still significantly below the acceptable levels as discussed in subsection 5.3.2.

In the case that the balloon is deployed too late, and thus under 50 km, the behaviour seen in Figure 5.22 can be observed.

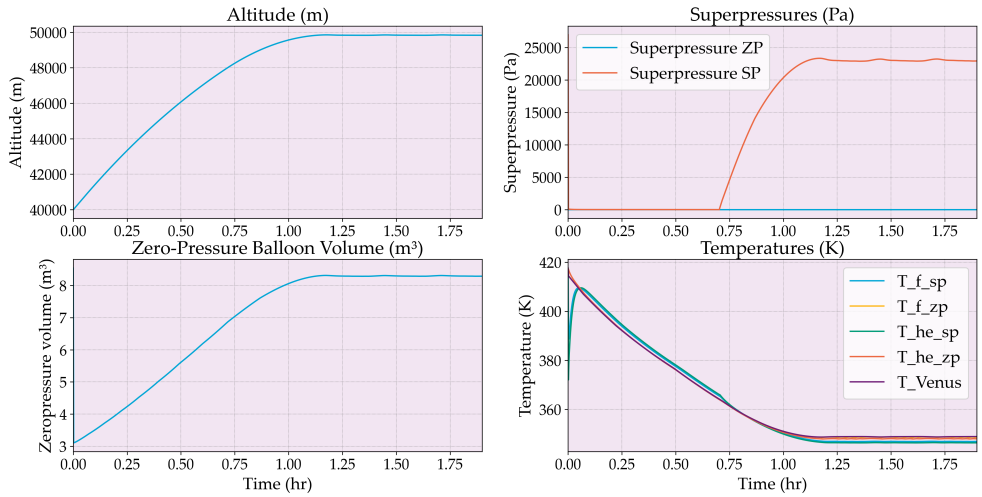

Figure 5.22: Simulation of the balloon deployed at an altitude of 40 km showing the increase in altitude, superpressure, balloon volume and temperatures of the balloon over time.

In Figure 5.22, it can be observed that the balloon rises until it reaches the operational altitude range within one hour. Due to the low altitude and thus the high ambient pressure, the superpressure balloon starts out below its maximum volume. However, it quickly expands until it reaches its designed volume and creates a superpressure within.

Verification and Validation

During the simulation, certain assumptions are made, first of all, the ones regarding the assumptions used in the VIRA model as covered in subsection 4.4.3. Apart from that, some additional assumptions are used throughout the design and simulation of the balloon, namely;

1. The ideal gas law is valid.
2. The balloons are filled with pure Helium. This is valid as helium purities of up to 99.9999% can be obtained if required [21].
3. The atmosphere consist of 96.5% CO_2 and 3.5% N_2, this was done to simplify calculations while still capturing the properties accurately as other elements take up less than 0.1% of the atmosphere [22]
4. For viscosity calculations of the atmosphere, an atmosphere consisting of 100% CO_2 has been assumed which was assumed to be valid as the atmosphere consists of 96.5% CO_2 [22].
5. When calculating the surface area of the superpressure balloon, the balloon is assumed to be a perfect sphere. While not exactly true, the superpressure will always be almost perfectly spherical due to the superpressure within.
6. When calculating the surface area and drag of the zeropressure balloon, the balloon is assumed to be a perfect sphere. In reality, the zeropressure balloon will almost never be spherical, however using a sphere to calculate cross section will only overestimate vertical drag, resulting in a conservative design.
7. The ratio of superpressure radius and zeropressure radius at maximum inflation is 0.5 [88].
8. The gravitational acceleration in Venus is assumed constant and equal to 8.87 $m \cdot s^{-2}$ [87]. While the balloon will fly at altitudes above 50 km, the difference in gravity compared to at ground level is small. Flying at such high altitudes also means that the gravity experienced will be lower than on the surface, resulting in a conservative design.
9. The drag coefficient of the system is assumed to be 0.5 [82].
10. The virtual mass coefficient of the system is assumed to be 0.5 [83].
11. During the simulation, helium leaking is not taken into account. While helium will leak continuously, on the timescale of the performed simulations, helium leakage does not change the results.
12. The latitude of the balloon is always assumed to be 0° when calculating the solar flux on the balloon. When the balloon eventually drifts towards the poles, the solar flux decreases, however using the maximum solar flux results in a conservative design.
13. The albedo of Venus is assumed to be 0.8.[68]
14. Circumnavigating Venus takes the balloon 6 days on average [89, 90]. While this changes throughout the mission, it does not have an effect on the simulations performed.
15. The balloon travels at a constant velocity around the equator. While the balloon will accelerate and slow down due to changing winds, and different wind speeds experienced at different altitudes, this will only marginally change the obtained results as the flux experienced will be very slightly different.

After setting up the simulation, results are compared with results obtained in "Thermodynamic Study for Venus Balloon" [87] and "Altitude-Controlled Light Gas Balloons for Venus and Titan Exploration" [82] and are confirmed to be similar. Apart from that, results from the simulation under a wide range of conditions seem to provide sensible results. The whole simulation has been visually inspected for mistakes, however no proper unit test have been conducted.

[21] https://zephyrsolutions.com/what-are-the-different-grades-of-helium-and-what-are-they-used-for/

[22] https://www.aeronomie.be/en/encyclopedia/venus-atmosphere-mainly-composed-carbon-dioxide-and-nitrogen

6 Instrument Design and Operations

With the Orpheus mission now equipped for buoyant flight within the Venusian clouds, including altitude-varying capabilities in a range from 50 to 55 km, and over a 60-day period, the precise scientific operations of the mission can be tailored. This culminates in a detailed *Scientific Operations Timeline* of 49 days which aims to maximise the obtained scientific data. To support the completion of these operations, all the necessary equipment is designed and presented in this chapter, including the *Sampling System* in charge of collecting sulphuric acid aerosols from the clouds, the *Fluidic Network* responsible of safely bringing the sampled material to the LMC_{OOL} and handling post-operation disposal, the LMC_{OOL} *Assembly* itself, and finally the *Secondary Payloads*.

In a first time, a list of refined payload requirements is presented in section 6.1. From the set requirements, an adequate strategy to successfully carry out the mission is elaborated, and results in a detailed scientific operations timeline, presented in section 6.2. To accomplish these operations, four subsystems are designed and presented logically: the Sampling System, the Fluidic Network, the LMC_{OOL} Assembly, and the Secondary Payloads, respectively presented from section 6.3 to section 6.6.

6.1. Payload Requirements

From the top-level user requirements established in section 2.2, a list of relevant payload requirements, adapted to an engineering design perspective, is derived. They are listed in Table 6.1, including some external requirements. The third column in the table shows which subsystem will be responsible of accomplishing the requirement, which therefore serves as a basis to start designing that subsystem.

Table 6.1: Payload Requirements Table. EVT: Earth to Venus Transfer, SCM: Scientific Mission, EXT: External.

Requirement ID	Requirement	Responsible Subsystem
Earth-Venus Transport		
Req-EVT-1	The system shall be compatible with the launcher.	
Req-EVT-1.1	The system shall withstand the vibrations during launch as specified by the launch provider.	All
Req-EVT-1.2	The system shall withstand the loads during launch specified by the launch provider.	All
Scientific Mission		
Req-SCM-2	The payload shall collect samples of the clouds.	
Req-SCM-2.1	The sampling system shall collect at least 20 ml of liquid from the sulphuric clouds.	Sampling System
Req-SCM-2.2	The payload shall take at least two samples.	Sampling System
Req-SCM-2.3	At least two of the samples shall be separated by a distance of at least 100 km.	Sampling System
Req-SCM-2.4	The samples shall be taken at altitudes between 50 and 55 km with an accuracy of 0.25 km.	Sampling System
Req-SCM-2.5	The samples shall be taken at <TBD> coordinates with an accuracy of <TBD> km.	Removed (see below)
Req-SCM-2.6	The sampling system shall not change the chemical composition of the sample before analysing it.	Sampling System, Fluidic Network

Continued from previous page

Requirement ID	Requirement	Responsible Subsystem
Req-SCM-2.7	The samples shall be disposed of in a manner that prevents any potential contamination of the Venusian environment.	Fluidic Network
Req-SCM-2.8	Samples shall be taken at three or more points of the Venusian day	Sampling System
Req-SCM-2.9	The sampling system shall achieve a sampling rate of at least 1 ml per day	Sampling System
Req-SCM-3	The payload shall include scientific instruments.	
Req-SCM-3.1	The payload shall include the LMC_{OOL}.	LMC_{OOL} Assembly
Req-SCM-3.2	The payload shall include at least one other instrument besides LMCool.	Secondary Payloads
Req-SCM-3.3	The LMC_{OOL} shall sample at a rate of 10 Hz during operations.	LMC_{OOL} Assembly
Req-SCM-3.4	All raw LMC_{OOL} data shall be sent back to Earth, without loss.	LMC_{OOL} Assembly, Communications
Req-SCM-7	The payload shall comply with the gondola system constraints.	
Req-SCM-7.1	The payload shall be compatible with CubeSat architecture.	All
Req-SCM-7.2	The total payload mass shall be below 2 kg.	All
Req-SCM-7.3	The payload shall not consume more than 4.8 Wh during eclipse time.	All
Req-SCM-7.4	The maximum peak power required for the payloads to operate shall not exceed 22 W.	All
Req-SCM-8	The LMC_{OOL} chips shall be protected to resist thermal degradation.	
Req-SCM-8.1	All the LMC_{OOL} chips temperatures shall not exceed 50°C from the assembly phase up to the mission End of Life.	LMC_{OOL} Assembly
Req-SCM-8.2	The LMC_{OOL} temperature shall stay at 25°C during its operation, with a 0.01°C accuracy.	LMC_{OOL} Assembly
External Requirements		
Req-EXT-1	The spacecraft shall meet COSPAR Category II contamination limits.	
Req-EXT-1.1	A planetary protection plan shall be compiled before the launch of the mission.	Fluidic Network
Req-EXT-1.2	An Impact Strategy Report shall be compiled before the launch of the mission.	Fluidic Network
Req-EXT-1.3	An End-of-Mission Report shall be compiled before the launch of the mission.	Fluidic Network
Req-EXT-3	The mission shall support European Strategic Autonomy	
Req-EXT-3.1	Any goods shall be purchased from European-based organisations.	All
Req-EXT-3.2	Any service shall be provided by European-based organisations.	All
Req-EXT-4	At least 50% of scientific instruments and subsystems shall be developed with commercial off-the-shelf (COTS) components.	All

A note on **Req-SCM-2.5:** "The samples shall be taken at <TBD> coordinates with an accuracy of <TBD> km." This requirement was discarded for two reasons. Firstly, it is repetitive. A motivation for this requirement is to increase sample diversity by choosing specific coordinates, which is already captured in **Req-SCM-2.3:** "At least two of the samples shall be separated by a distance of at least 100 km." In truth, sample diversity will rather come from the difference in sampling altitudes, also because Venus' upper atmosphere is relatively homogeneous across longitudes. Secondly, it would give an idea of the spatial resolution of the detected molecules, allowing to map where certain particles could be found. However, it was found that due to the high speed of the probe in combination with the relatively slow sampling rate, it is difficult to achieve a precision which would give meaningful results. At best, a resolution of 6337 km could be attained, which isn't very valuable. Additionally, the balloon is designed to fly with the wind, and can't aim for specific coordinates. Sizing a mechanism to allow for directed flight proves to be extremely complex and doesn't deliver many advantages. Still, a new requirement was created to "replace" **Req-SCM-2.5:**. That is **Req-SCM-2.8:** "Samples shall be taken at three or more points of the Venusian day." This requirement seeks to increase sample diversity by theorising that different moments of the Venusian day (such as noon, evening, or night) could introduce different chemical phenomenons and are thus good targets for this mission.

Another point on **Req-SCM-8:** "The LMC_{OOL} chips shall be protected to resist thermal degradation." This requirement has two sub-requirements (**Req-SCM-8.1** and **Req-SCM-8.2**) of maximum temperatures constraints but does not have a minimum temperature constraint. At this design stage, it was assumed that low temperatures shouldn't be a concern because of the LMC_{OOL}'s material nature (Silica), and because reactivity generally decreases as temperature decreases, justifying that no unwanted chemical phenomenon would occur. However, this must to be investigated and confirmed, specifically the behaviour of the bonded MIPs at low temperatures which could be constraining. The lowest temperature is reached during the transfer orbit from Earth to Venus and is -20°C. This could lead to the development of a new requirement: a low temperature constraint for the LMC_{OOL} Assembly, and the necessity for a heating device during transfer. As preventive measure, the behaviour of sulphuric acid at low temperatures is considered, as some buffer sulphuric acid will be already flooding the LMC_{OOL} chips during transfer. Sulphuric acid has a relatively high freezing point, which should be avoided as it could damage or interact with the sensitive chemistry at hand. Thankfully, this freezing point dips to -35°C when the acid is concentrated at 95%[1], which is therefore the chosen concentration for the buffer liquid that will already be present on the chips and in the system's fluidics at launch.

6.2. Scientific Operations Timeline

Now that the requirements are laid out, an operations timeline can be configured. To do so, a set of goals and constraints are identified, and an optimising script is written.

Goals

1. Maximise number of tests.
2. Maximise number of sampling altitudes.
3. Maximise sampling time.
4. Minimise number of ascent/descent to minimise risk of failure.
5. Two independent samples from different altitudes should be secured and tested as early as possible. Minimise this time.

These objectives aim to satisfy **Req-SCM-2** and its sub-requirements, as well as increase overall performance and sample diversity.

Constraints

1. The first LMC_{OOL} operation should be in-situ validation.

[1] `http://www.sulphuric-acid.com/techmanual/Properties/properties_acid_freezingpt.htm` Accessed 09/06/2025

2. The balloon path starts at 50 km.
3. The probe must stay at 50 km throughout the night.
4. The probe can only descent to lower altitudes for a fixed window around noon.
5. The first two Venusian day/night cycles experienced by the probe last 2×96 hours.
6. All following day/night cycles last 2×72 hours.
7. Each day cycle must include a night time uncertainty buffer of minimum 5 hours.
8. Time slots for computer checks of 2 hours must be included at critical mission stages.
9. Priority is put on operating the LMC_{OOL}. Secondary payloads only operate if excess power and data storage is available.

The first constraint is a reliability constraint and the second one stems from the entry dynamics and procedure, which release the balloon at 50 km.

Constraints 3 and 4 are power constraints. They stem from the maximum temperature requirements of LMC_{OOL} (**Req-SCM-8.1** and **Req-SCM-8.2**). As will be shown later, these entail that the LMC_{OOL} needs active cooling, especially at low altitudes where the Venusian atmospheric temperature increases drastically. Even when considering the best space-grade cooling modules for this application, this requires a consequent amount of power. At the lowest sampling altitude of 50 km, it reaches 18 W. Considering the power available from the gondola previously derived in subsection 5.2.3, this much power can only be delivered during a 40-hour window centred around the Venusian noon, where the solar flux is maximal. Specific cooling power requirements and maximum time windows of other sample altitudes are detailed later in Table 6.3. Worst, this means that the balloon-gondola system can not decrease altitude and must stay at 55 km during the night. As given per **Req-SCM-7.3**, the payload can only consume 4.8 Wh of energy during the night, which is not enough to power the cooling device for a meaningful time. This means Orpheus will never be able to go sample at low altitudes of the Venusian night where unique bio-chemistry potentially occurs. This is an important limitation of the design.

Constraints 4, 5, and 6 represent a rough estimate of the expected day/night cycles that the probe will experience. In practice, the probe will land at the equator, where wind takes around 96 hours to cross the whole day side, and it will start slowly drifting to lower latitudes, eventually stabilising at a -10° where it takes around 72 hours to cross the day. Due to the super-convection of Venus' atmosphere, these times also depend on the altitude and can vary of a few hours (96 and 72 are for 55 km). To model a preliminary timeline, It is assumed that the first two day and night cycles occur perfectly at the equator and last exactly 2×96 hours, while all other day and night cycles occur at the stable latitude and last exactly $\times 72$ hours. The time buffers incorporated by constraint 6 are there to account for this assumption. This is critical as the probe always needs to go up to 50 km before entering the night, and ascending always requires a few hours (Maximum 6.25 hours). In further developments, an autonomous system must be designed which will allow the onboard computer to constantly know the Venusian time fraction, and automatically make decisions regarding instrument operations. This can be implemented with a simple sun sensor.

Constraint 7 implements system checks at critical mission stages. This includes solar array deployments and computer checks just after arrival, instrument parts checks, valve checks before ascending, pump checks before descending, and back-to-day checks after exiting the night and re-establishing the communications link.

Constraint 8 barely has an effect as the picked secondary payloads (detailed in section 6.6) have low power consumptions and data storage capability is very high (see Figure 5.10).

To find the best operations timeline which satisfies the constraint and optimises the goals, a short simulation is written. It follows a brute force approach by cycling through all possibilities which satisfied the constraints, and giving a score to each configuration. The score is a sum of the 5 goal values, which are normalised. The configuration with the best score is picked. This culminates in an

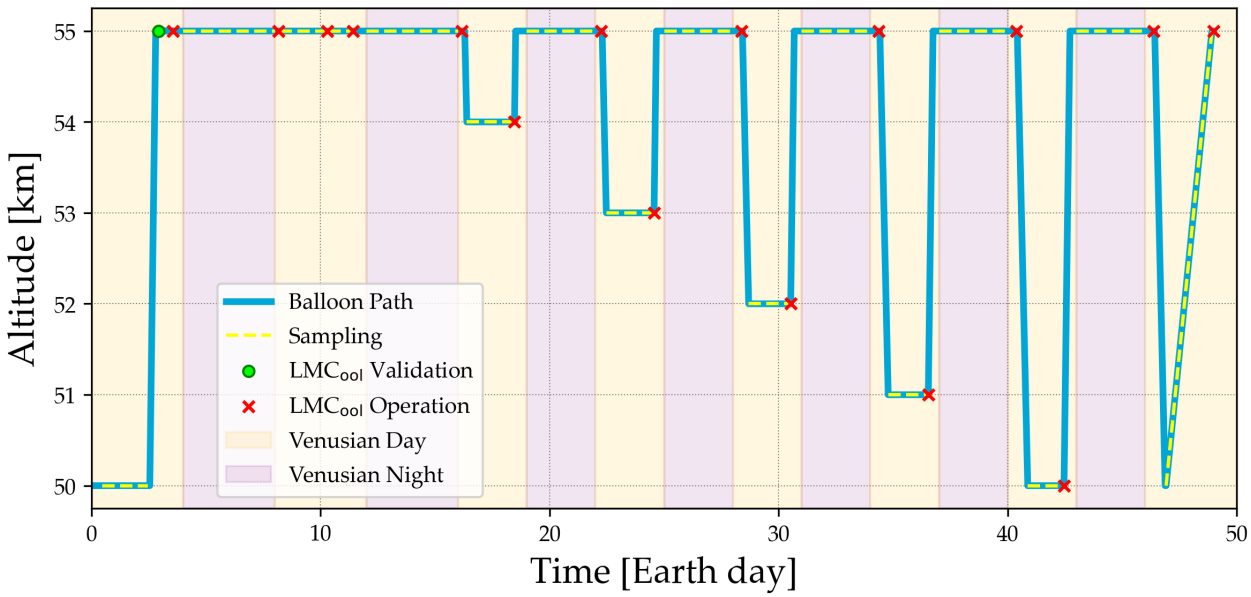

Figure 6.1: Timeline of the scientific operations.

optimised operations timeline shown in Figure 6.1. To validate this model, the score from random configurations is manually computed and cross-checked with the simulation results.

Table 6.2 describes each mission segment generated by the script in more detail. Additionally, the secondary payloads operate at the exact same time as the sampling occurs.

Table 6.2: Mission operations sequence.

Operation ID	Description	Duration [h]
Arrival and Commissioning		
Op-ARR-1	Solar array deployment with batteries	1
Op-ARR-2	Diagnostic and system checks	4
Op-ARR-3	Communications contact and telecommand validation	6
Test Segment 1		
Op-TS1-1	Clean sample 1. Day @ 50 km	48
Op-TS1-2	Valve checks and validation	2
Op-TS1-3	Venting and ascent 50 to 55 km	6.25
Op-TS1-5	LMC_{OOL} checks and validation	3
Op-TS1-5	LMC_{OOL} clean test 1 of sample 1	2
Op-TS1-6	Excess sample disposal	1
Op-TS1-X	Night time uncertainty buffer	0 - 22.75
Op-TS1-7	Clean sample 2. Night @ 55 km	96
Op-TS1-8	Back-to-day checks. Diagnostic and Earth contact	2
Op-TS1-9	LMC_{OOL} clean test 2 of sample 2	2
Op-TS1-10	Excess sample disposal	1
Test Segment 2		
Op-TS2-1	Sample 3. Day @ 55 km	48
Op-TS2-5	LMC_{OOL} test 3 of sample 3	2
Op-TS2-6	Excess sample disposal	1
Op-TS2-1	Sample 3. Day @ 55 km	24
Op-TS2-5	LMC_{OOL} test 3 of sample 3	2
Op-TS2-6	Excess sample disposal	1

Continued from previous page

Operation ID	Description	Duration [h]
Op-TS2-X	Night time uncertainty buffer	0 - 13
Op-TS2-7	Sample 4. Night @ 55 km	96
Op-TS2-8	Back-to-day checks. Diagnostic and Earth contact	2
Op-TS2-9	LMC_{OOL} test 4 of sample 4	2
Op-TS2-10	Excess sample disposal	1
Test Segment 3		
Op-TS3-1	Pump checks and validation	2
Op-TS3-2	Pumping and descent 55 to 54 km	2.2
Op-TS3-3	Sample 5. Day @ 54 km	48
Op-TS3-4	LMC_{OOL} test 5 of sample 5	2
Op-TS3-5	Venting and ascent 54 to 55 km	1.25
Op-TS3-6	Excess sample disposal	1
Op-TS3-X	Night time uncertainty buffer	0 - 11.55
Op-TS3-7	Sample 6. Night @ 55 km	72
Op-TS3-8	Back-to-day checks. Diagnostic and Earth contact	2
Op-TS3-9	LMC_{OOL} test 6 of sample 6	2
Op-TS3-10	Excess sample disposal	1
Test Segment 4 to 7		
Op-TS4	Repeat TS3 @ 53, 52, 51, 50 km	see Table 6.3
Op-TS5		
Op-TS6		
Op-TS7		
Test Segment 8		
Op-TS8-1	Pumping and descent 55 to 50 km	11
Op-TS8-2	Excess sample disposal	1
Op-TS8-3	Sample 15. During day ascent from 50 to 55 km	48
Op-TS8-4	LMC_{OOL} test 15 of sample 15	2
Op-TS8-5	Excess sample disposal	1
Mission Extension & Shutdown		
Op-MES-1	Discuss potential mission extension	-
Op-MES-2	Perform potential mission extension	-
Op-MES-1	Call mission shutdown	-
Op-MES-1	Perform End-of-Life procedures	-

Table 6.3: Test Segment 3 to 7 time divisions constrained by cooling power requirement.

Operation ID	Target Altitude [km]	Cooling Power [W]	Descent [h]	Sampling Window [h]	LMC_{OOL} Operations [h]	Ascent [h]
Op-TS3	54	1.5	2.2	48	2	1.25
Op-TS4	53	4.5	4.4	48	2	2.5
Op-TS5	52	9.75	6.6	42	2	3.75
Op-TS6	51	10.5	8.8	40	2	5
Op-TS7	50	18	11	36	2	6.25

6.3. Sampling System

Sampling is the process of capturing the liquid sulphuric acid from the clouds of Venus into a reservoir of 5 ml, from which the sampled liquid will be transferred onto the LMC_{OOL} architecture. Sampling is a passive process; droplets stuck in the open spaces of the mesh, coalesce and fall down along the height of the mesh into the funnel (components are explained in subsection 6.3.3) using gravity and capillary adhesion. In this section, the design constraints, concepts considered, components, mesh selection and the deployment of the sampler will be explained in detail.

6.3.1. Sampler Design

Multiple concepts are considered for the sampling system. The driving parameter for the design is the sampling volume, which is calculated using the following formula:

$$V_{samp} = \int_t u \cdot A \cdot \eta_{samp} \cdot C \, dt \tag{6.1}$$

Where u is the relative wind speed perpendicular to the sampling area $[m \cdot s^{-1}]$, A the sampling area $[m^2]$, η_{samp} the sampling efficiency and C $[ml \cdot m^{-3}]$ is the local sulphuric acid concentration, which is calculated using the Knollenberg model, as a function of altitude described in the midterm report [1]. It is decided to use 1 m^2 of sampling area as a starting point. Moreover, it is assumed that the relative wind speed would be 0.25 $m \cdot s^{-1}$ at all times, as the worst-case scenario value. Lastly, as per the literature study on mesh efficiencies [91, 92], a sampling efficiency of 20% was suggested and it is decided to use a margin of 100% to account for any other risk and use a final efficiency of 10%. This efficiency margin is decided to be redundant for the reliability of the sampler. With these considerations and **Req-SCM-2.1**, the sampling rate is 1 $ml \cdot day^{-1}$. It is calculated taking into account a sinusoidal trajectory and differing altitudes, the result can be seen in Figure 6.2. At the end of the mission, a volume of at least 49 ml will have been sampled, for which the LMC_{OOL} subassembly will conduct the scientific mission for 49 days.

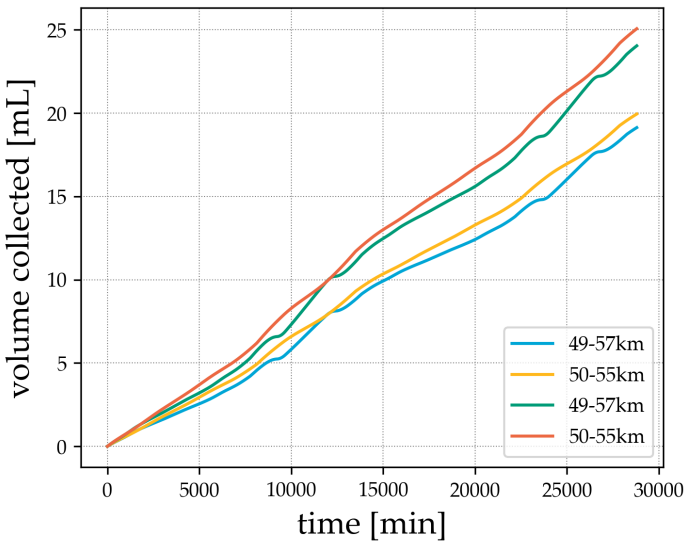

Figure 6.2: Volume sampled [ml] vs time [min] graph.

6.3.2. Sampling Strategy

It is decided to opt for a passive and continuous sampling strategy. Despite the absence of power during the night, it is still key to obtain some sample material at that time, as encouraged by **Req-SCM-2.8**. This motivates the choice for a passive sampling system. On top of this, constantly gathering sample material rather than targeting specific "sampling times" is preferred, because this avoids missing any potentially interesting particles that could appear outside of these sampling times. This motivates the choice for a continuous sampling strategy. Therefore, the mesh already conceptually sized in the midterm report [1] is further developed.

Having set the initial geometric constraints, 3 concepts were generated as can be seen in Figure 6.3:

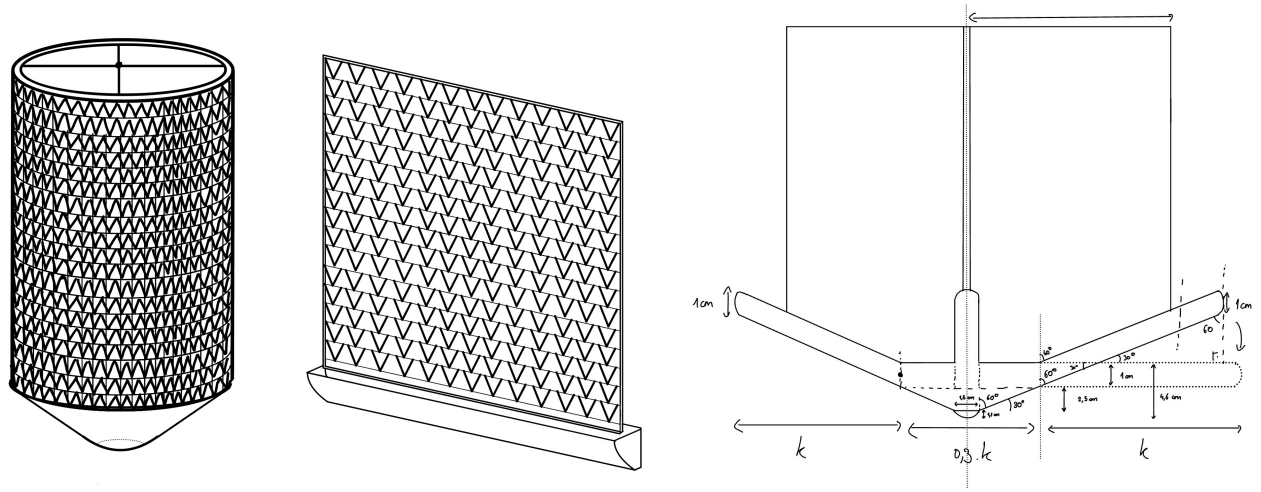

(a) Hollow cylinder concept. **(b)** Plate mesh concept. **(c)** Cross mesh concept.

Figure 6.3: Sketches of the proposed sampler concepts.

Hollow Cylinder

The hollow cylinder concept in Figure 6.3a is designed to have cross sectional area of 1 m^2. Its main advantage is the ease of deployment and low drag properties (compared to other flat mesh designs), however its mass is higher than other concepts and its advantages turned out to be impractical for use on Venus: the drag reduction is not significant due to the slow speed of the probe and the hollow cylinder structure means it is easy for it to be tangled by twisting compared to the other concepts.

Plate Mesh Concept

The plate mesh concept would sample by having a constant perpendicular cross-section with respect to the direction of motion, and it is ruled out due to the weather vane effect: When encountered with gusts from multiple directions, it risked rotating around the direction of motion, which would reduce the sampling efficiency and it does not provide any other significant advantages.

Cross Mesh Concept

The cross-mesh concept is the most promising concept out of the 3 proposals. It is reliable in sampling as it is possible to sample in multiple directions without the weather vane effect, it is much lighter compared to the hollow cylinder and compared to the other designs, its structural rigidity was superior by having a hollow cylinder at the centre. Moreover, it had the least risky deployment mechanism and hence this concept is chosen to be the sampler of the mission.

6.3.3. Sampler Components

The sampling system consists of 4 main subparts: the sampling mesh, mast, funnel and reservoir as can be seen in Figure 6.4. Furthermore, each subpart has multiple components within. At the initial design phase, components are designed with respect to the allocated mass budget for the sampler, which is 1 kg. For doing so, an iterative code was written to compute the masses of different geometries for different materials. The materials considered are Teflon®, Cu-Ni alloy, Hastelloy c276, fibreglass, Mg alloy and Polyetheretherketone (PEEK). Except for the corrosion-resistant materials (Teflon® and Hastelloy c276), it is required to coat the material with PTFE. A prototype balloon for a similar mission in Venus used a PTFE coating of 25.4 μm in thickness [65], and in our case it was decided to use a PTFE coating of 50 μm (0.05 mm) in thickness, making the design redundant. This coating was used for every part (except for the mesh which comes with its own PTFE coating).

Mesh

The mesh is comprised of 4 right trapezoids with a height of 1.4 m and width 34 cm. Mesh design will be explained in detail in subsection 6.3.4. Its primary function is to capture the droplets to be sampled

and make them coalesce.

Mast

The mast has 2 individual parts: a cross-shaped top part and a hollow tube that connects the 4 meshes in a cross shape and into the funnel. The cylinder is deployable in one way; that being said during the mission it will not be retracted. The deployment is explained in subsection 6.3.5, it works such that using the inertia of the system and the connection to the tethers, hollow cylinders are deployed to a height of 1.4 m. The function of the mast is to support the mesh and give the assembly structural rigidity. The mast top weighs 0.068 kg and the hollow cylinder weighs 0.176 kg, with a thickness of 2 mm. The mast top is made out of PEEK and the hollow clyinder out of Titanium, in order to acount for the loads throughout the mission.

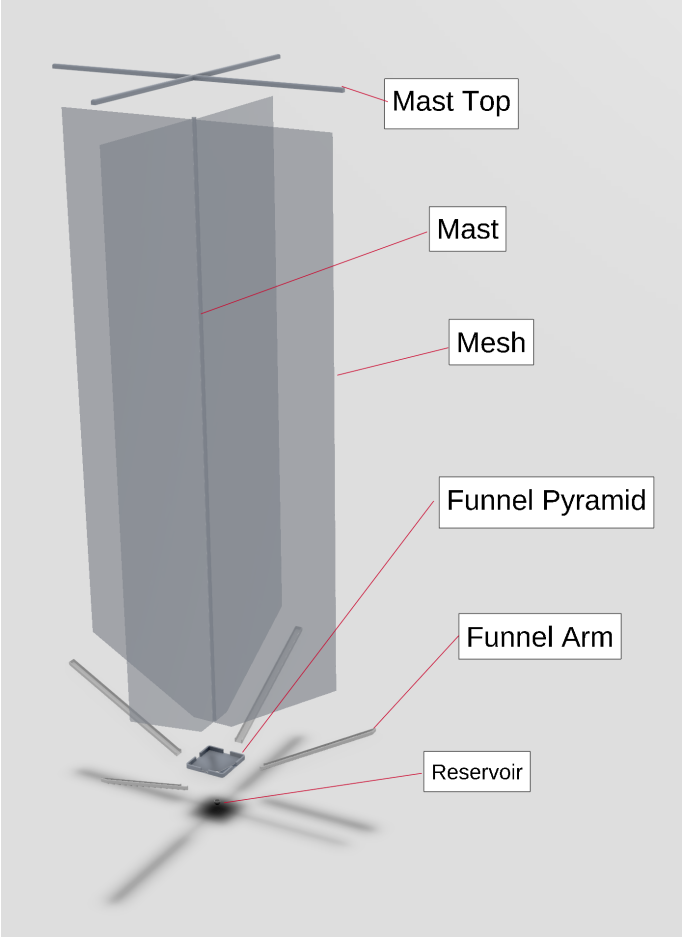

Figure 6.4: Exploded view of the deployed sampler assembly.

Funnel

The Funnel has 5 parts: a square-based pyramid structure in the middle with a height of 3.5 cm and a width of 10.2 cm as well as 4 arms that collect the liquid from the mesh into the pyramid. Arms are 33.5 cm in length and 2 cm in width. The pyramid sides are angled at 60°, which comes from a rule of thumb from a chemical engineering handbook [93], so that the sampled sulphuric acid, which is highly viscous, can flow along the funnel. Material used for both the pyramid and the arms is polyetheretherketone (PEEK). The pyramid weighs 0.042 kg and the arms weigh 0.028 kg individually, which makes the complete funnel assembly weigh 0.154 kg.

Reservoir

The reservoir is a half-ellipse with a wall thickness of 2 mm, diameter 15 mm, and height 11 mm. It has a volume of 5 ml and is made out of Teflon® (PTFE), weighing only 5.1 g. It goes directly below the funnel and connects the sampled liquid to the LMC_{OOL} subsystem via pipes, which is explained in detail in section 6.4.

Table 6.4: Mass and material summary of the components.

Entry	Mass [kg]	Material
Mesh	0.380	PTFE-coated fabric
Funnel	0.154	PEEK
Mast	0.244	PEEK / Titanium
Reservoir	0.0051	Teflon® (PTFE)
Total	**0.7831**	

End-of-Life Strategy

The materials used for the sampler assembly are PEEK, PTFE, Titanium and aramid fabrics. At the end of the mission, the sampling system will descend onto the Venusian surface along with the probe. Venusian surface temperature is on average 465°C and it is enough to melt the PEEK (whose melting point is 343°C) and PTFE (whose melting point is 327°C). For titanium and aramid fabrics on the other

hand (with melting points 1725°C and 500°C respectively) it is expected that once the PTFE coating covering them melts, they will corrode by the sulphuric acid-rich environment.

6.3.4. Mesh Selection

Multiple mesh types were researched, such as the Raschel mesh, which is used for collecting water out of thin air in countries such as Peru, Namibia and Oman [94]. Kirigami (origami structures with cut-out elements) meshes and regular rectangular meshes were also researched, and it was decided to use a rectangular mesh. A rectangular mesh has at least twice the collecting efficiency compared to a kirigami mesh (10 $ml \cdot h^{-1}$ for rectangular vs 4 $ml \cdot h^{-1}$ for the kirigami mesh), as was tested out by the MIT Morning Star Team [95]. Moreover, the fact that the mesh had to be corrosion resistant ruled out the Raschel mesh option, as the PTFE coating necessary would take the advantage it had over the rectangular mesh: By coating the Raschel mesh with PTFE, its elastic nature would be changed and it would function like a rectangular mesh. After deciding on the mesh type, European providers for a flexible, PTFE-coated mesh were researched. The PTFE coated aramid fabric (article 8074 RV) produced by Kastilo GmbH[2] of Germany was the most suitable option: with a thickness of 0.19 mm and density of 2000 $kg \cdot m^{-3}$ it is the lightest and most flexible option. Moreover, the company was contacted for corrosion characteristics and it was confirmed that the mesh was corrosion resistant against hydrochloric acid (HCl). The mesh comes in rolls, as can be seen in Figure 6.5. By being flexible, it also allows for a relatively simple solution for deployment.

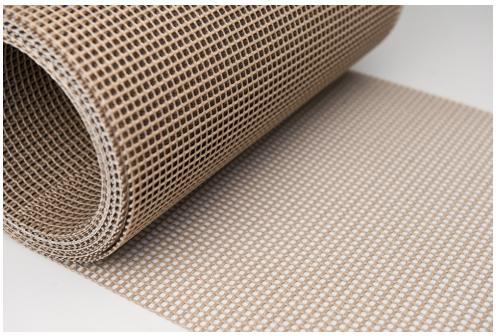

Figure 6.5: The PTFE-coated aramid fabric 8074 RV.

6.3.5. Deployment of the Sampler

The sampler is designed such that it fits in the widest cross-section of the entry capsule and minimises its height. When retracted, the maximum height of the assembly is approximately 10 cm. It is designed such that it only deploys and does not retract again. During deployment of the entire probe, the sampler is deployed using its inertia; the hollow cylinder will have stopper hinges to fully deploy and as it will be connected to the tethers, it will only carry the weight of the sampler assembly, which is approximately 7N. The deployment raises the tip to a height of 1.4 m. During this process, the mesh unfolds in a rectangular pattern, in which its top is connected to the top of the mast. At the end of the unfolding, the bottom of the mesh provides the reaction force necessary to raise the funnel arms by 60° with respect to the normal, which is connected to the tip of the funnel arm by a PTFE-coated lightweight PEEK connector.

6.3.6. Sensitivity Analysis

The sampling performance depends on multiple parameters as explained in subsection 6.3.1. The sampler is designed with respect to a realistic worst-case scenario which uses the lowest-performing parameters – relative wind speed and efficiency - hence sampling below the requirement, 20 ml in total which is 0.4 $ml \cdot day^{-1}$, is highly unlikely. On the contrary, oversampling is possible and expected. Initial estimates from the atmospheric model showed that the relative wind speed could go up to 1.5 $m \cdot s^{-1}$, which would increase the volume sampled to 6 $ml \cdot day^{-1}$. By using an open funnel, the oversampling problem is mitigated, as the sample would simply overflow without interfering with other subsystems. Moreover, the sampling efficiency must be calculated using testing. The design is similar to meshes proposed by Elshennawy [92], which calculated the sampling efficiency to be 20%. The efficiency is expected to be higher than the value used, which is 10%, hence the volume sampled is expected to increase as well.

[2] `https://www.kastilo.de/index.php/en/products/ptfe-coated-fabrics` Accessed 09/06/2025

6.4. Microfluidic Network

Here, the Microfluidic Network is presented. It's role is to safely bring the sampled material from the reservoir under the mesh to the LMC_{OOL} chips and handle post-operation disposal. In this system, reliability and redundancy is key, single point failures must be avoided. To create a successful network which can provide the support for the scientific operations set in section 6.2 while ensuring this level of reliability, some strategies are implemented, eventually leading to a Piping & Instrumentation Diagram (P&ID). Following this, the necessary components are picked and put together in an assembly, shown in a 3D render.

6.4.1. Strategies and P&ID

The Piping and Instrumentation Diagram is shown in Figure 6.6, and it is explained hereafter.

Starting from the top at the funnel and the 5ml reservoir, Figure 6.6 show that they are equipped with an acidity sensor, a simple instrument which can give good insight on the composition of the samples.

Between the reservoir and the LMC_{OOL} Assembly, a 5 ml Load Chamber is placed. Its role is to secure sample material as soon as it is detected in the reservoir. As commonly appreciated in the aerospace industry, it is good to secure samples as fast as possible, to prevent potential upcoming failures from compromising the science objectives. In the reservoir, passively collected sample could be subjected to sloshing and spilling, and would be exposed to the unknown environment outside the gondola. A capacitive sensor is placed on the reservoir which activates the first pumps and secures sample material. Check valves are always placed after pumps to prevent backward reflux. Thankfully, this mechanism isn't very power incentive, one pump operates at 0.05 W. This means that the 4.8 Wh allocated for the payload during eclipse can serve this purpose and secure sample even during the night, as intended by the scientific operations timeline. In the best case, night sampling can therefore last for 4.8 / 0.05 = 96 h. This also explains why a volume of 5 ml is picked. Following from **Req-SCM-2.9**, a flow rate of 1 ml per day leads to 4 ml over 96 hours, and a buffer of 1 ml is included.

Moving down, Figure 6.6 shows that the Fluidic Network is composed of two main lines. This serves two purposes. Firstly, it supports **Req-SCM-2.2** by providing two clean routes for sample material and ensures there is no cross-contamination during the first two tests. This is also reflected in the LMC_{OOL} Assembly, which is similarly composed of two LMC_{OOL} Arrays, (see upcoming section 6.5). Some minor cross-contamination might occur on the sampling system or in the loading chamber if residues of a sample are left behind. While this is inevitable, the consequences are not dramatic for the mission. It would simply lead to some inaccuracy in the location determination of detected molecules, which was already proven to be inaccurate. Detecting any life-related molecule anywhere is already valuable scientific data in itself.

Secondly, having two path lines for sample material allows for more redundancy. An On/Off Valve is placed between the two routes, which allows to keep access to both lines in the LMC_{OOL} Assembly in the eventually of a single point failure.

On the right, a Validating Chamber is placed. It will take care of the first LMC_{OOL} operation: in-situ validation. It is also sized to be 5 ml, so it can essentially be a duplicate of the Load Chamber, facilitating manufacturing and assembly. It will carry concentrated sulphuric acid with a validating molecule. To limit potential interactions between the validating material and the samples, an inherently inert and stable molecule is picked. It is chosen to be Perfluorooctanesulfonic acid (PFOS) [96], a member of the PFAS family. The concentration of PFOS should be of precisly 5 $mg\ L^{-1}$, allowing for precise instrument validation and tuning. Note that this means PFOS can not be used as a target molecule, but it is of no interest for life-related science anyway.

For redundancy and to mitigate single point failures, the Validating Chamber has two arms connected to the main fluidic route. They are connected via 3-Way Valves which close the main sampling path during validation. After validation, the 3-Way Valves switch and close the validating Chamber for the

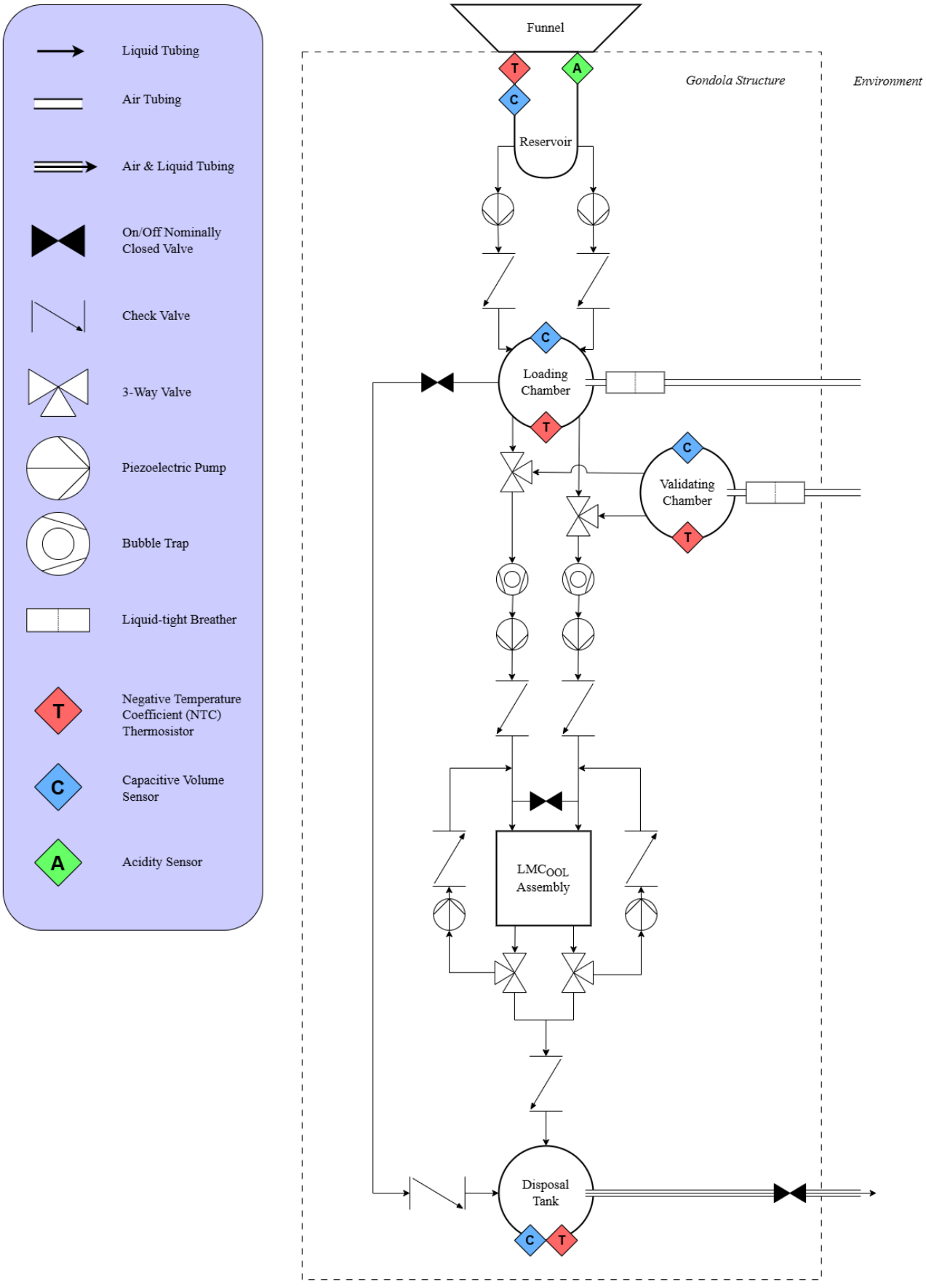

Figure 6.6: Fluidic network piping and instrumentation diagram.

rest of the mission.

To further limit cross-contamination between testing cycles, an open loop system is picked over a closed loop system, as a closed loop system would recycle and mix previously collected samples with new samples. However, open loop systems require buffer volumes (liquid or air) to avoid creating vacuums. In this design, it was decided to use air over liquid. Instead of carrying and managing additional liquid mass, the system can simply remain open to the ambient Venusian atmosphere, which naturally provides the required gas pressure without the need for active pressurization or dedicated storage. This explains why the three tanks have air tubing open to the Venusian environment. For the Load Chamber and the Validation Chamber, these tubes are equipped with liquid tight breathers to restrict any liquid from infiltrating the fluidics. The Disposal Tank has a simple On/Off Valve as it needs to be able to dump liquid in the environment. However, to avoid any considerable pressure differences during transfer, all the fluidic tubes and the Loading Chamber will be filled with pure 95% concentrated sulphuric acid. The Disposal Tank has to remain empty by nature, so it will be filled with Argon at 1 bar, similarly to the rest of the gondola.

Following below the two chambers is where the main fluidics will operate. Bubble Traps, preventing any air from entering the LMC_{OOL} Assembly, are placed right before the main pumps which will regulate the flow at 5 $\mu L\ min^{-1}$. After the LMC_{OOL} Assembly, 3-Way Valves and a second set of pumps circling backwards are placed. In this configuration, playing with the 3-Way Valves and the On/Off Valve above allows to redirect the sample material to any LMC_{OOL} Array and offers maximum redundancy. This can also be used to cross-check results between the two arrays.

Finally, after testing, the samples are brought to the Disposal Tank through a last Check Valve. On top of this, a line is added directly from the Loading Chamber to the Disposal Tank on the left, with a On/Off Valve and a Check Valve. In this manner, liquid which is continuously and passively sampled but is of no interest for the scientific mission can be disposed of rapidly.

Lastly, in case a lot of sample material is collected, for example if the sampling rate is greater than anticipated or if the mission is extended, sulphuric acid will accumulate in the system and might start taking too much place or weighing too much. A disposal mechanism is incorporated to get rid off liquid before a critical point is reached. This consists of a simple On/Off Valve and the action of gravity.

This release of material into the Venusian atmosphere raises potential concerns with respect to the COSPAR planetary protection guidelines. However, following a thorough review of the COSPAR Category II regulations applicable to Venus [29], the proposed design remains compliant. Although the presence of PTFE and PFOS in the microfluidics poses a potential contamination concern, these substances are already present all over the coating of the probe and cannot be removed. Nevertheless, all procedures are considered acceptable under current COSPAR guidelines. Still, the disposal tank volume is maximised to ensure a maximum of material can be kept before disposing becomes an absolute necessity.

For end-of-life procedures, the probe is designed to descend into the lower Venusian atmosphere. Under the extreme conditions encountered near the surface, characterized by temperatures exceeding 460°C and pressures above 90 bar [95], structural disintegration and chemical degradation of the system will occur rapidly. Any complex molecules, including potential contaminants, are expected to break down into simple stable species already abundant on Venus, primarily carbon monoxide. Even PTFE components will decompose once temperatures exceed 260°C [96], ensuring full degradation of fluorinated materials.

A Negative Temperature Coefficient (NTC) Thermosistor and a Capacitive Sensor is placed on each tank to constantly measure their temperature and their internal volume of liquid. These data points are constantly taken and sent to the onboard computer, where automatic decisions will be made to secure, test, validate, drain, and dispose of liquid. Some of the data is also sent back to Earth.

6.4.2. Assembly and Components

Here, all the off-the-shelf components required from the P&ID are picked. A 3D Model of the Microfluidic Network is shown in Figure 6.7. Most of the microfluidic instruments come from the medical industry, which must provide very precise performance levels. This makes them good candidates for the aerospace industry, however, it is important to keep in mind that most of these components must be verified, tested and space-qualified during the further development stages of Orpheus. Table 6.5 summarises all the specifications of the parts.

One of the main objectives of this design stage was to make the Microfluidic Network fit in a single CubeSat ($10 \times 10 \times 10\ cm$). In this way, the Microfluidic Network, including the LMC_{OOL} Assembly, will be able to be proposed on other relevant mission. This could prove to be a great return on investment compared to sizing a one-time mission.

Overall, The Bartel Microtechnik company was generally considered to pick components because they are European, give all the necessary specifications of their parts, and have parts compatible between them. Outsourcing microfluidic to a centralised company is also easier for project logistics.

Although the price of individual parts can seem low (in the range of tens of euros), a large price buffer is included. It comes from four considerations: Unknown prices of components, Research and design of the parts, Financing researchers and engineers, Qualifying parts for space (extensive verification and validation). Buffers are also included for mass and power to account for neglected or unavailable values.

Table 6.5: Microfluidics components.

Component	Amount	Mass [g]	Peak Power [W]	Price [€]
PTFE Tubing	60 cm	0.28	0	Unavailable
BP7 Piezolectric Pump	6	2	0.05	55[3]
sm-cv Check Valve	8	0.49	0	53.50[4]
On/Off normally-closed	3	0.75	0.3	99[5]
3-Way Valve	4	84.32	1.25	99[6]
mp-bt Bubble Trap	2	6.94	0	49.50[7]
Liquid-Tight Breathers	0	0	0	None
Capacitive sensor SOLITRAC 31	4	20	0.4	Unavailable
Acidity Sensor	1	0.8	Unavailable	Unavailable
PTFE Chambers	2	23.65	0	Unavailable
PTFE Disposal Tank	1	301	0	Unavilable
NTC thermosistor	4	neglect	neglect	Unavailable
Buffers	-	20	2	2.5M

The PTFE Tubing transports liquid and air from component to component. Effort was put in configuring the network such that the total tubing length is minimised and there is no tangling. The tubes can be purchased from Creative Biolabs® Microfluidics [97], they have an inner diameter of 0.3 mm and an outer diameter of 0.6 mm.

A piezoelectric diaphragm pump is necessary to deliver the low 5 $\mu L\ min^{-1}$ flow rate. The BP7 Bartel Pump from German company Bartels microtechnik [98] is chosen as the best option. It is available for 55€ at Darwin Microfluidics[3]. Although this pump fits in the design and works, it is slightly oversized,

[3] https://darwin-microfluidics.com/products/bartels-bp7-micropump/

[4] https://bartels-mikrotechnik.de/product/sm-cv-check-valve/ Accessed 09/06/2025

[5] https://shop.memetis.com/shop/mvl-22-nc-08-14p-peek-sil-normally-closed-microvalve-classic-6

[6] https://bartels-mikrotechnik.de/product/active-3-2-valve-with-medium-separation-by-buerkert/ Accessed 09/06/2025

[7] https://bartels-mikrotechnik.de/product/mp-bt-bubble-trap/

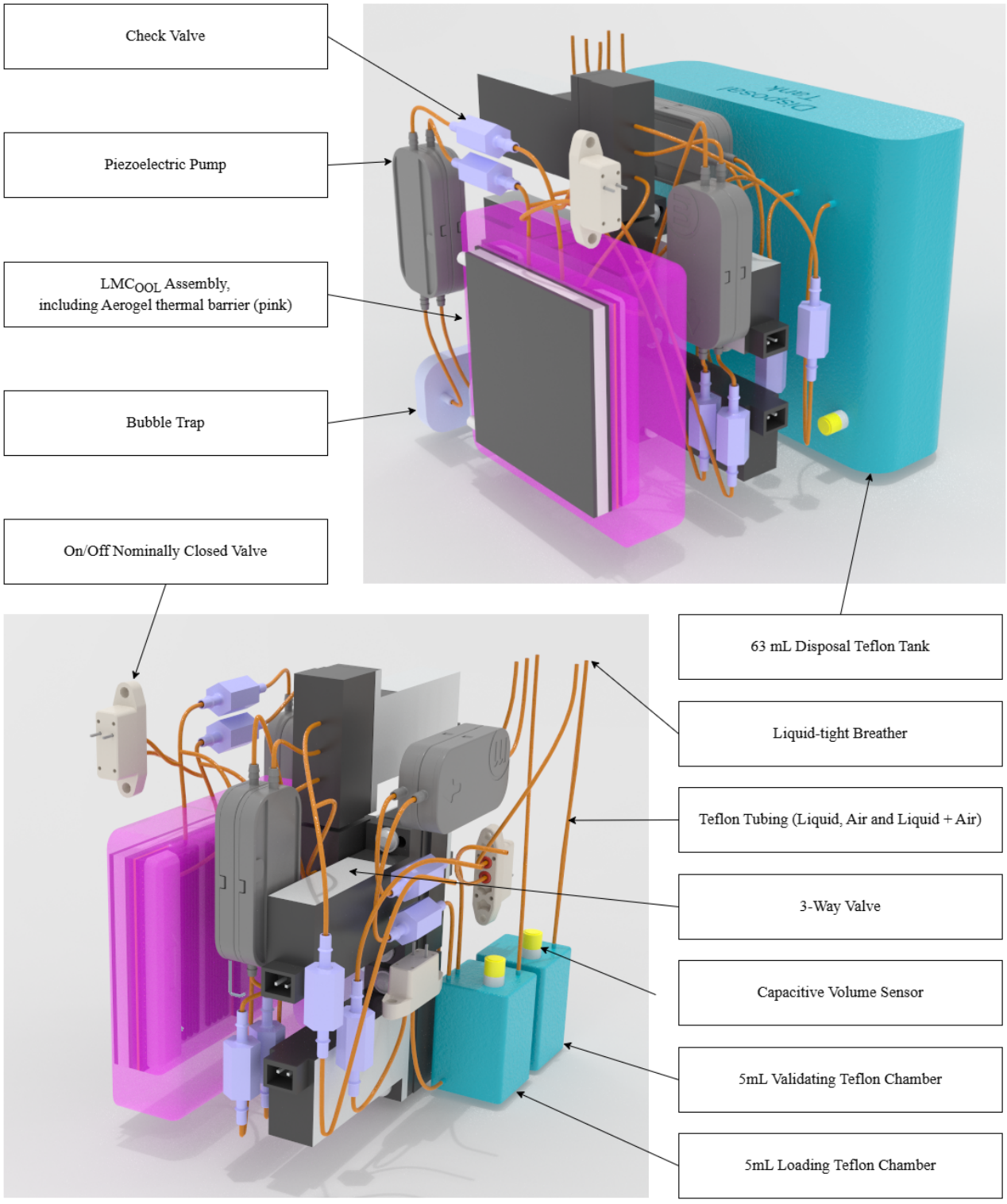

Figure 6.7: 3D Model of the microfluidic network.

and the possibility to make a smaller space-qualified custom version should be investigated, possibly in collaboration with Bartel microtechnik.

Check valves allow the fluids to flow only in one direction, avoiding reflux when placed after pumps for example. Initially, duckbill valves were considered, but finally the more simple sm-cv Check Valve from Bartels microtechnik [99] was taken, it largely satisfies the necessary conditions and has the advantage of having customisable fluid connectors. It is readily available for 53.50€[4].

Regarding the normally closed On/Off Valves, a 2/2-way, monostable microvalve is needed. The MVL-22-NC-08-14P-PEEK-SIL from German company memetis GmbH [100] is selected for its media-separated design, which is compatible with sulphuric acid and prevents contamination. It can be sterilized by autoclaving, features a PEEK housing and a silicone membrane, and is available for 99€[5].

For the 3-Way Valve, the Active 3/2-Solenoid Valve with medium separation by Bürkert (and sold by Bartel microtechnik) [99] was selected. This valve has a fast reaction time of 3 ms, and its medium-separated design prevents fluid contact with the valve mechanism, making it ideal for life science applications. It has great durability and long-lasting performance in chemically aggressive environments. However, it is quite big for this application $26 \times 9 \times 41$ cm^3 and consumes a non-negligible 1.25 W. Although it was able to fit within the assembly and close the power budget, attempts to create a smaller custom version would be a good investment. For now, it is available for 150€[6].

The bubble trap choice was simple, Bartel microtechnik provide a very compact mp-bt Bubble Trap [99] that works well in combination with their BP7, which is already picked as a pump. It is passive and relies on a hydrophobic Polyethylene terephthalate (PET) membrane to selectively remove air from the flow. It is readily available for 49.50€.

Regarding the Liquid-Tight Breathers, they were deemed unnecessary after designing the secondary payloads. Indeed, the secondary payloads include a sensor box (presented later in section 6.6) which require a liquid-free environment, provided by acid-resistant membranes. It is therefore decided that the air tubing will strategically fetch air from this environment. To avoid contaminating the sensor box from the inside, the membrane will also be integrated in the tubing between the Chambers and the gas sensor box, only allowing air flow. More on this membrane in section 6.6.

Capacitive Sensors are a crucial element of the system. They constantly determine the volume of liquid in the three tanks, allowing the onboard computer to make decisions and making the probe autonomous. The best capacitive sensor found for Orpheus is the VEGA SOLITRAC 31 [101]. However, it is too big for the 5 ml Chambers and needs to be scaled down. For now, a custom scaled down version is assumed. Alternatively, other volume sensing options could be considered for this application, such as laser, conductive, or radar sensing.

Acidity Sensors typically work as pH sensors, which determine the acidity of a solvent with respect to water by measuring the activity of hydrogen ions. In the Venusian environment, with the 98% concentration sulphuric acid and less than 2% water traces, this mechanism won't be possible, so a custom acidity sensor needs to be created for Orpheus. In the event that is not possible, this instrument shall be removed and would leave place for additional secondary payloads, see section 6.6. For now, a classic pH sensor which has the correct dimensions for the reservoir is picked as a reference. Namely, the CS526-L Digital ISFET pH Sensor from Campbell® Scientific. This is an American instrument and efforts should be put to make a custom European version.

The Loading and Validating Chambers are made out of PTFE. This material choice was made because it is extremely resistant to sulphuric acid and safe shielding of the gondola interior is crucial. Also, it easy to manufacture and print. These 5 ml rectangular recipients can be custom made at TU Delft. Once constructed, the Loading Chamber will be filled with 95% sulphuric acid and the Validatig Chamber with 95% sulphuric acid and some PFOS at 5 $mg\ L^{-1}$.

Similarly to the smaller chambers, the disposal tank will be made of PTFE and can be 3D printed at

TU Delft. It is 60 ml and will be filled with pure Argon gas at 1 bar (@ 25°C).

Available Negative Temperature Coefficient thermosistors are given by Measurements Specialties, specifically the 10K3CG Gold terminated leadless model [102]. If unavailable, the Japanese alternative by TDK electronics is an option [103], although not European.

6.5. $\mathbf{LMC_{OOL}}$ Assembly

In this section, the LMC_{OOL} assembly is presented. Its objective is to provide a suitable environment for the LMC_{OOL} chips to operate. An exploded view (Figure 6.8) and a diagram (Figure 6.9) are available on the next pages. Table 6.6 is a summary of all the components forming the assembly. The key specifications of each component are discussed, as well as their availability on the market.

Most of these parts can be locally manufactured by TU Delft, and putting a price on them can be difficult. Similarly to the Microfluidics Network, a high price buffer is included and justified by: unknown prices of available components, research and design of the parts, Remuneration of scientists and engineers, qualification of each part for aerospace environment (extensive verification and validation). Once again, buffers are included if some masses or powers are neglected or unavailable.

There are 2 LMC_{OOL} *Arrays* of 2×4 LMC_{OOL} *Chips*. The arrays are separated and sealed to ensure the first 2 tests can be completed with 2 different samples, avoiding cross-contamination. Any following test will inevitably show some sort of contamination, even small, from the previous batches. Additionally, due to the nature of LMC_{OOL}, if a molecule has already been detected, any new detection is unreliable as it could come from a previous batch. Also, if the antibodies of a specific target molecule become saturated and a maximum concentration detection is reached, new detection of these molecules can not happen. However, these concerns are minor since detecting any target molecule in the first place would already be a very valuable scientific outcome. Each LMC_{OOL} Chip has 6 spots for antibodies. On all chips, 1 spot is reserved for PFAS antibodies fulfilling the validation requirement and each of the 5 other spots is allocated antibodies specific to a target molecule from the list established in section 2.4. On each chip, a Vertical Cavity Surface Emmitting Laser (VCSEL) integrated Photodiode (ViP) and a NTC thermosistor are bonded. The LMC_{OOL} chips are provided by LioniX[8].

The ViP is a combination of a VCSEL which delivers the 850 nm light waves to the chip and an integrated Photodiode which can detect the phase difference intensity once the light waves have traversed the asymetric Mach-Zehnder Interferometer. The photodiodes are electronically connected to the onboard computer to send the measured scientific data. The ViP is very small at $165 \times 165 \times 130$ μm. It can be delivered by TRUMPF in Germany [104].

For the NTCs, the same ones as for the Microfluidic Networks are used. They are strategically placed before and after the cooling coils and on each chip. They are all connected to a centralised PID controller which is in turn connected to the Thermoelectric Cooler (TEC) module, allowing for precise temperature control within the assembly. Again, the 10K3CG Gold terminated leadless NTC provided by Measurement Specialities [102] is used. If unavailable, the Japanese alternative by TDK electronics is still an option [103], although not European. The silica substrate is a 40×10 mm^2 and 0.5 mm thick plate. It aids in gluing the LMC_{OOL} Chips together into an array and provides structural support. It can be provided by LioniX[8] on top of the LMC_{OOL} Chips.

[8] `https://www.lionix-international.com/` Accessed 09/06/2025

Table 6.6: LMC_{OOL} assembly components.

Component	Number	Mass [g]	Peak Power [W]	Price [€]
LMC_{OOL} Chips	16	1	0	0
VCSEL integrated Photodiode	96	neglect	0.033	Unavailable
NTCs	12	neglect	neglect	Unavailable
Silica Substrate	2	0.464	0	0
PTFE covers	2	1	0	Unavailable
Cooling Coils	14.4cm	3.3	0	Unavailable
Aluminium Cold Plate	1	4.32	0	Unavailable
Thermoelectric Cooler (TEC)	1	150	18	13[9]
Skogar® Aerogel Thermal Barrier	1	14.4	0	Unavailable
Aluminium Casing	1	12.96	0	Unavailable
S8U Adhesive	-	neglect	0	Unavailable
Buffers	-	20	0.02	2.5M

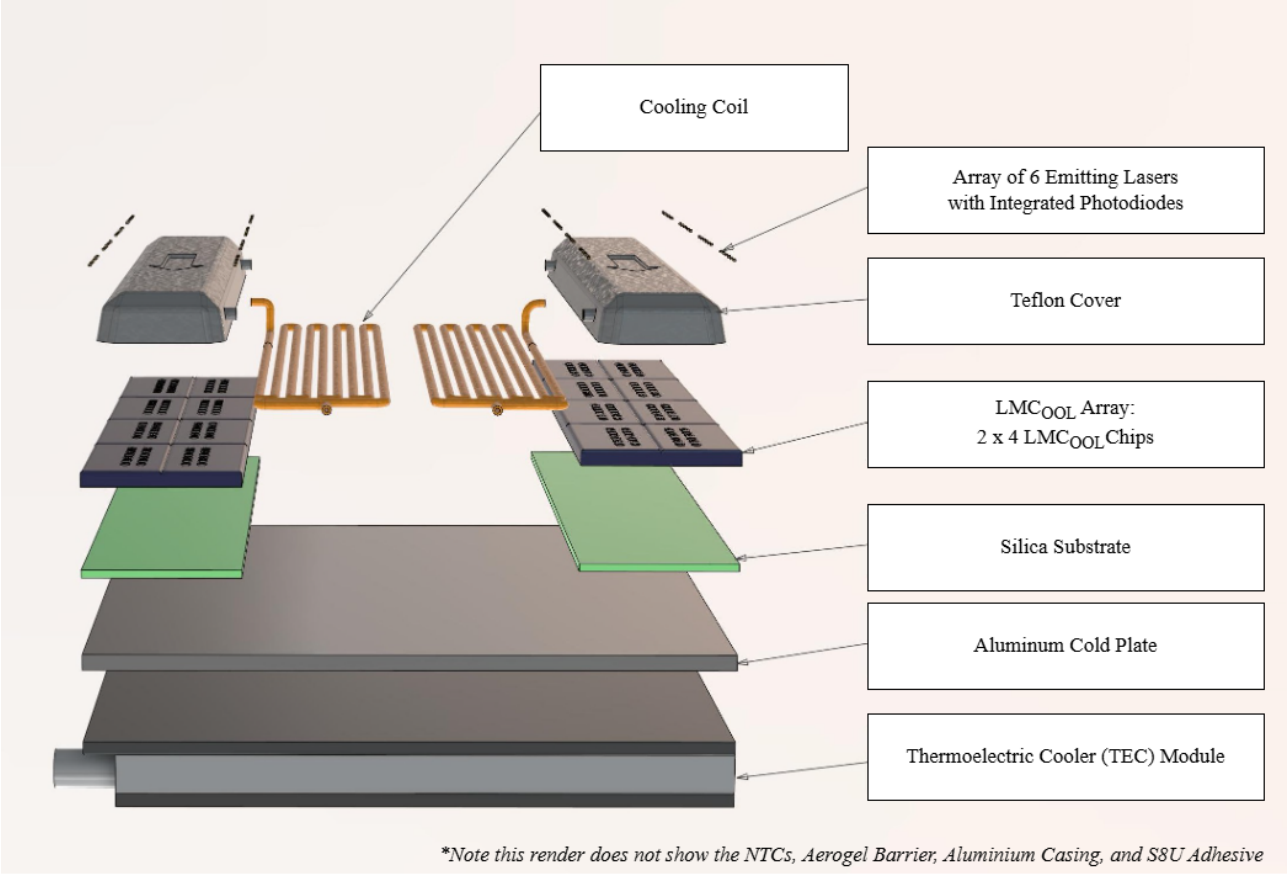

Figure 6.8: 3D model & exploded view of the LMC_{OOL} assembly.

[9] https://www.digikey.com/en/products/detail/european-thermodynamics-ltd/ADV-127-135200-S/13566782

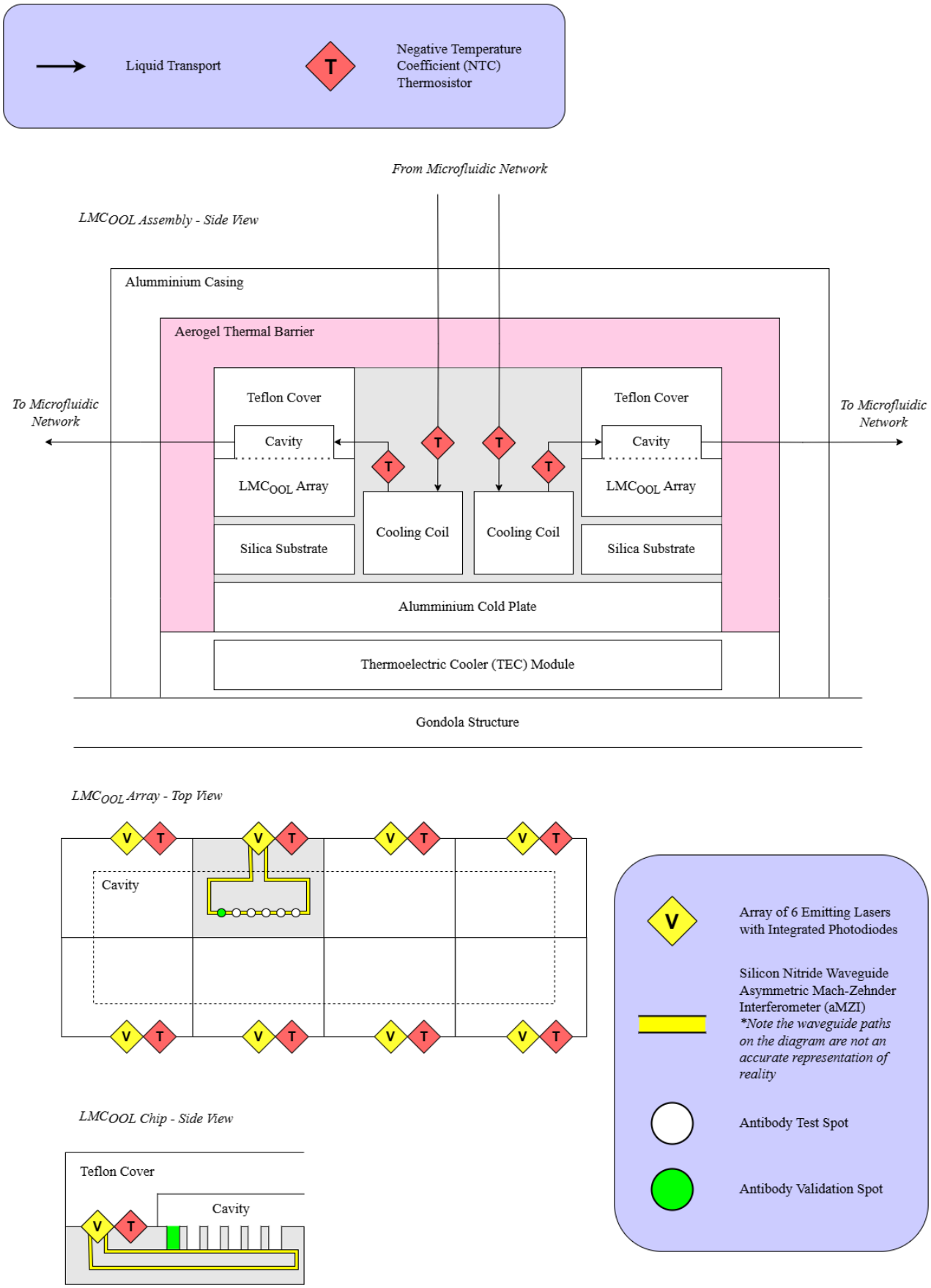

Figure 6.9: LMC_{OOL} assembly, array, and chip diagram.

Next, there are two PTFE covers, glued on top of the LMC_{OOL} arrays, and they serve two roles. Firstly, they guide the sample liquid on the chips with its integrated cavity. The cavity's volume is around 0.1 ml, allowing for proper smearing of the sample over the antibody spots. Secondly, it prevents sulphuric acid from leaking and degrading the other components. This part can be custom made and 3D printed at TU Delft or another Dutch university in collaboration with the project. It's envelope dimensions are $8 \times 40 \times 3$ mm.

There are two Cooling Coils. They cool the sample liquid as it slowly flows at 5 $\mu L\ min^{-1}$ before reaching the LMC_{OOL} Arrays. There are made from the same tubing as in the fluidic network [97]. They are 7.2 cm long and can contain 20 μL at a time. This ensures 4 min of cooling which is sufficient considering the volumes at hand. The tubes, like the Microfluidic Network, will initially be flooded with 95% concentrated sulphuric acid, acting as a buffer liquid. This also concerns the PTFE cover inner tubes and the LMC_{OOL} array cavities themselves.

The aluminium cold plate is 1 mm thick and serves 2 purposes. Firstly, it is a component which holds other components together and provides structural strength. Secondly, is serves as a thermal guide between the LMC_{OOL} chips and the TEC. As a good conductor, aluminium transfers heat rapidly and gets rid of local thermal sinks, creating a homogenous thermal flow which improves the TEC efficiency.

The Thermoelectric Cooler (TEC) is chosen to be the ADV-127-135200-S TEC [105]. It is a single-stage module that transfers heat using the Peltier effect, where electric current drives heat flow from one side of the module to the other, enabling precise cooling with $0.01°C$ accuracy and fulfilling **Req-SCM-8.2**. It is $40 \times 40 \times 4.2$ mm and weighs 150 g. The TEC datasheet graphs [105] give the necessary current and voltage required to power it in order to achieve a certain temperature gradient, when the hot side temperature is fixed. For example, when the hot side is at $75°C$ (Venusian atmosphere at 50 km), a temperature gradient of $50°C$ is required to cool the LMC_{OOL} Arrays down to $25°C$. At the best efficiency, which is easily attainable by tuning the voltage, a $50°C$ gradient at $75°C$ requires a 2 A current and a 9 V current, thus a power of $2 \times 9 = 18$ W is needed.

The Aerogel Thermal Barrier serves as an insulator between the LMC_{OOL} Chips and the hot environment, essentially creating a small fridge which passively decreases the TEC power requirements. The Skogar® 6 mm thermal barrier is chosen, it is reinforced and achieves a low conductivity of 0.012 $Wm^{-1}K^{-1}$. Fitting it all around the LMC_{OOL} Assembly (except on the TEC side) allows to decrease the heat coming from the environment down to 1 W. This is conservatively ignored when picking the TEC to implement a safety margin on the temperature cooling rates.

Regarding the Aluminium Casing, even if it is not exposed to the Venusian environment, it will be coated with PTFE on the outside. This is a safety measure to prevent sulphuric acid from propagating to the rest of the gondola in the eventuality that it starts leaking in the assembly. An aluminium casing can be manufactured at TU Delft. It's outer dimensions are $40 \times 40 \times 20$ mm and it is 1 mm thick.

All the previously mentioned components will be glued together using the S8U Adhesive [106]. This recently developed adhesive shows excellent characteristics, specifically strong adhesion to Silica SiO_2 and has a low thickness ≤ 15 μm.

6.6. Secondary Payloads

As mentioned in chapter 2, besides LMC_{OOL}, the gondola also carries secondary payload. A camera and most notably an array of small electronic gas sensors. This section will introduce them, along with reasoning why they were chosen and how they will support the scientific objectives of the mission.

6.6.1. Gas Sensor Array

The main secondary payload is shown schematically in Figure 6.10. The design is a PTFE box in a *rectangular torus* shape. Each of the four sides has 2 elliptic openings with a gas-permeable membrane. In the box, 12 gas sensors are mounted. Since the sensors analyse gas concentrations in the atmosphere,

this instrument is placed outside of the pressurized gondola. This design allows it to be placed in between the gondola and the funnel from the sampling system. The funnel passes through the box to deliver the sulphuric acid samples to LMC_{OOL}. The gas-permeable membrane allows gases to pass through, while keeping out the harmful sulphuric acid. As mentioned in section 2.4, the 6 different gases to be measured are H_2S,SO_2,CO,H_2CO, PH_3 and NH_3. For verification of the measurements, Orpheus carries 2 sensors for each of the selected gases. The total weight of this secondary payload, including the box is estimated to be 0.247 kg. From a power perspective, the array will perform a measurement every 15 minutes and consumes 1.8 W during the measurement. The sensors are not suited for ultra-precise measurements, but their small size, low cost and low power makes them ideal for our purposes.

The gas sensor array was chosen because it provides context to the molecules to be detected by LMC_{OOL}. In combination with the more complex LMC_{OOL} target molecules, the detection of certain gases can offer insight into the chemical processes in the atmosphere. For example, Hexamethylenetetramine is known to be a common reaction product from the combination of formaldehyde and ammonia. Thus, if both reactants and reaction product are present, this could confirm the reaction and ultimately tell us something about the chemical cycles in Venus' atmosphere. Another example is a carbon cycle proposed in [9], the formation of Polycyclic Aromatic Hydrocarbons, and sugar derivatives, both of which are part of LMC_{OOL}'s target molecules as well. PAHs are included themselves, and sugars are included as part of nucleosides, where a (deoxy)ribose sugar group is bound to a nucleic base.

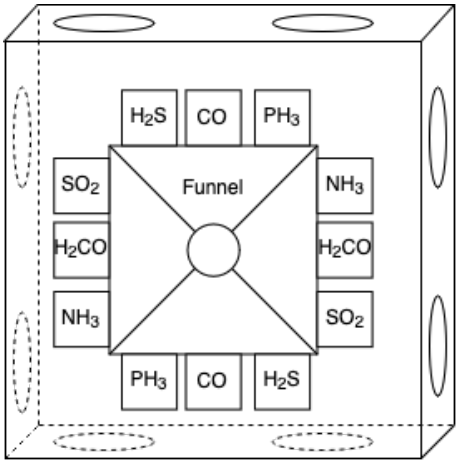

Figure 6.10: Gas sensor array.

The array consists of 12 sensors, each with a mass of 0.01 kg and power consumption of 0.15 W during operation. They are available as IoT components and therefore not space-grade. As a result, some effort should go into ensuring correct operation in Venus and survival in space. Tests for temperature, radiation, and behaviour in vaccuum should be performed. This type of gas sensors are commonly sold commercially[10]. The main drawback of this type of sensor, is that they are susceptible to cross-sensitivity with other gases. While difficult to prevent, testing should be performed to quantify the behaviour of the sensors.

6.6.2. Camera

Next to the gas sensor array, a wide angle camera will be carried by the gondola as well. Scientifically it does not provide much value, as photos of the Venusian environment exist from previous missions, and due to the data-rata, resolution is limited. Still, it is a useful tool to verify that the balloon is successfully deployed, and it could provide useful info if an unexpected issue occurs. Next to that, from A PR standpoint it is useful as well as pictures are one on of the best ways to keep the public updated and excited for a space mission. Finally it provides a general overview of the environment in which the probe is in, for example about cloud structures and other atmospheric phenomena.

The selected camera is the kissCAM V2[11], a flight-proven, space-grade camera module. It provides colour images in standard (640 x 480 pixels) or high definition (1280 x 960 pixels) resolution, weighing 0.01 kg and consuming about 0.2 W. Despite it being space-grade, some care should still be taken when integrating it in the probe, as it needs to withstand the Venusian atmosphere as well.

[10] https://www.tinytronics.nl/en/sensors/air/gas/mq-7-gas-sensor-module Accessed: 09/06/2025
[11] https://www.satcatalog.com/component/kisscam-v2/Accessed: 07/06/2025

7 Mission performance

Now that a detailed design has been developed, an overview of the design performance is given in this chapter. This can be used to check whether the design complies with the set parameters. Section section 7.1 revises every mission requirement and provides the part of the report in which the relevant performance is discussed. Following, section 7.2 provides an overview of all the relevant budgets for the mission. This includes the mass and the cost. In section 7.3, the risks are updated and discussed. Finally, in section 7.4, the reliability of the mission is calculated, and the availability, maintainability and safety of the design is discussed.

7.1. Compliance Matrix

To finalise the verification and validation process for the current mission phase, a requirement compliance matrix is needed, and can be seen in Table 7.1. It contains all the finalised requirements with their corresponding ID. On the rightmost column, the section of this report in which proof of compliance is given for every requirement is stated. Green means that the requirement is met. In case a particular requirement has not been investigated yet, but could potentially be met, *TBD* is displayed in orange. In case the design does not meet a certain requirement, the section is displayed in red, accompanied by the actual value. For these cases, an explanation for every individual case is given after the table, in the feasibility analysis. In some cases, a requirement has been removed, which is also stated in the rightmost column. Only the sub-requirements (child) are considered, not the parents. For example, **Req-EVT-1** consists of three children requirements, so it is not specifically given proof of compliance.

Table 7.1: Requirements compliance table. EVT: Earth-Venus Transport, VEE: Venus Entry, SCM: Scientific Mission, BFM: Balloon Fabric Material, PRS: Pressure Regulation System, EXT: External Requirements, INT: Internal Requirements, SAR: Safety and Reliability.

Requirement ID	Requirement	Proof in
Earth-Venus Transport		
Req-EVT-1	The system shall be compatible with the launcher.	-
Req-EVT-1.1	The system shall withstand the vibrations during launch as specified by the launch provider.	TBD
Req-EVT-1.2	The system shall withstand the loads during launch specified by the launch provider.	TBD
Req-EVT-1.3	The dimensions of the system shall comply with the fairing dimensions of the RFA One launch vehicle.	Section 4.3.1, 1 x 1.15 m
Req-EVT-2	The system shall comply with the set engineering budget during the transfer to Venus.	-
Req-EVT-2.1	The system shall have a maximum mass of 320 kg.	Section 7.2.1, 118.1 kg
Req-EVT-2.2	The spacecraft shall provide a Delta-V of at least 1.6 $km \cdot s^{-1}$.	Section 4.3.3, 1.84 $km \cdot s^{-1}$
Req-EVT-2.3	The spacecraft shall provide an average power of at least 47 W at 1 AU.	Section 4.3.6, 66 W
Req-EVT-2.4	The spacecraft shall provide a downlink transmission data rate of 1.4 $kbps$.	Section 4.3.7, 1.4 $kbps$
Req-EVT-3	The spacecraft shall comply with the minimum required performance parameters.	-

Continued from previous page

Requirement ID	Requirement	Proof in
Req-EVT-3.1	The spacecraft shall provide a thrust of at least 200 N.	Section 4.3.3, 200 N
Req-EVT-3.2	The spacecraft shall achieve a pointing accuracy higher than 0.5° (3σ) in all axes during the transfer to Venus.	Section 4.3.2, 0.5°
Req-EVT-3.3	The spacecraft shall achieve orbital insertion with an altitude error of no more than <TBD> km relative to the target orbit.	TBD
Req-EVT-3.4	The spacecraft shall achieve orbital insertion with an inclination error of no more than <TBD>° relative to the target orbit.	TBD
Req-EVT-3.5	The spacecraft shall achieve orbital insertion with a right ascension of the ascending node error of no more than <TBD>° relative to the target orbit.	TBD
Req-EVT-4	The system shall withstand the operational environment during the transfer to Venus.	-
Req-EVT-4.1	The system and its components shall be able to withstand the radiation of the space environments.	Section 4.3.4, MLI blankets
Req-EVT-4.2	The system shall withstand the thermal environment.	Section 4.3.4, $[-20, 23°C]$
Req-EVT-4.2.1	The system shall withstand a total temperature range of [243, 333 K] for the duration of the transfer to Venus.	Section 4.3.4, $[-20, 23°C]$ encountered
Req-EVT-4.2.2	The system shall withstand the thermal load during for the duration of the transfer to Venus.	TBD
Venus Entry		
Req-VEE-1	The system shall perform a controlled entry.	-
Req-VEE-1.1	The capsule shall remain in an orientation with the heat shield facing the flow.	Section 4.4.2
Req-VEE-1.2	The capsule shall not tumble uncontrollably.	Section 4.4.2
Req-VEE-1.3	The system shall not enter via a flight path angle that causes excessive thermal or mechanical loads.	Section 4.4.1
Req-VEE-2	The system shall withstand the operating environment during entry.	-
Req-VEE-2.1	The system shall withstand the peak heat flux during entry.	Section 4.4.4
Req-VEE-2.2	The system shall withstand the total heat load during entry.	Section 4.4.4
Req-VEE-2.3	The system shall withstand peak entry deceleration loads.	Section 4.4.5 and 5.2.2
Req-VEE-2.4	The system shall withstand the vibrations during entry into the Venusian atmosphere.	TBD
Req-VEE-2.5	The system shall withstand gust loads due to atmospheric wind.	TBD
Req-VEE-3	The capsule shall successfully deploy the probe in an operational state.	-
Req-VEE-3.1	The system shall deploy two parachutes without damage.	Section 5.1.5
Req-VEE-3.2	The system shall open the balloon up to the atmosphere at a velocity no higher than 16 $m \cdot s^{-1}$.	Section 5.1.1, 15.8 ms^{-1}
Req-VEE-3.4	The system shall vent no less than 99.5 % of stored Helium into the balloon before reaching 50 km altitude.	Section 5.1.1, 51km

Continued from previous page

Requirement ID	Requirement	Proof in
Req-VEE-3.5	The system shall dismount from the probe without any further contact.	Section 5.1.6
Scientific Mission		
Req-SCM-1	The platform shall provide the necessary operational support functions to enable full execution of the scientific payloads' measurement.	-
Req-SCM-1.1	The system shall transmit 2.9 $kbps$ of data to the orbiting spacecraft.	Section 5.2.4, 2.9 $kbps$
Req-SCM-1.2	The platform shall achieve a pointing accuracy higher than <TBD> ° (3σ) in all axes.	Removed
Req-SCM-1.3	The platform shall remain at an altitude range of 47-58 km with an accuracy of 0.25 km.	Section 5.3.6, 50-55.5 km
Req-SCM-1.4	The platform shall be autonomously controlled throughout the duration of the scientific mission.	TBD
Req-SCM-1.5	All scientific payload components shall be accommodated within the allocated volume and interfaces of the platform.	Section 5.2.1
Req-SCM-2	The payload shall collect samples of the clouds.	-
Req-SCM-2.1	The sampling system shall collect at least 20 ml of liquid from the sulphuric clouds.	Section 6.3.1, 49 mL
Req-SCM-2.2	The payload shall take at least two samples.	Section 6.2, 16 samples
Req-SCM-2.3	At least two of the samples shall be separated by a distance of at least 100 km.	Section 5.3.2 and 6.2
Req-SCM-2.4	The samples shall be taken at altitudes between 50 and 55 km with an accuracy of 0.25 km.	Section 5.3.3
Req-SCM-2.5	The samples shall be taken at <TBD> coordinates with an accuracy of <TBD> km.	Removed
Req-SCM-2.6	The sampling system shall not change the chemical composition of the sample before analysing it.	Section 6.4
Req-SCM-2.7	The samples shall be disposed of in a manner that prevents any potential contamination of the Venusian environment.	Section6.4
Req-SCM-2.8	Samples shall be taken at three or more points of the Venusian day	Section 5.3.2 and 6.2
Req-SCM-2.9	The sampling system shall achieve a sampling rate of at least 1 mL per day	Section 6.3, 1 mL
Req-SCM-3	The payload shall include scientific instruments.	-
Req-SCM-3.1	The payload shall include the LMC_{OOL}.	Section 6.5
Req-SCM-3.2	The payload shall include at least one other instrument besides LMCool.	Section 6.6
Req-SCM-3.3	The LMC_{OOL} shall sample at a rate of 0.5 Hz or more during operations.	Section 6.5, 0.5 Hz
Req-SCM-3.4	All raw LMC_{OOL} data shall be sent back to Earth, without loss.	Section 5.2.4
Req-SCM-4	The system shall withstand the conditions of the Venusian atmosphere for the entire mission duration.	-
Req-SCM-4.1	The system shall withstand the H_2SO_4 clouds for the entire mission duration.	Section 5.3.2, Section 5.2.2, Teflon®

Continued from previous page

Requirement ID	Requirement	Proof in
Req-SCM-4.1.1	During measurement phases, critical components inside the system shall be protected.	Section 5.2.2
Req-SCM-4.2	The system shall withstand all trace elements of the Venusian atmosphere for the entire mission duration.	Section 5.2.2, Teflon®
Req-SCM-4.3	The system shall withstand a temperature range of 280-350 K for the entire mission duration.	Section 5.2.2, Batteries
Req-SCM-4.4	The system shall withstand wind gusts up to 2 $m \cdot s^{-1}$ at the target altitude for the duration of the whole mission.	Section 5.3.6, 2 $m \cdot s^{-1}$
Req-SCM-4.5	The system shall withstand the UV radiation at and above the target altitude of the Venusian atmosphere for the entire mission duration.	Section 5.2.2, 5.3.2
Req-SCM-4.6	The system shall withstand the pressure at the target altitude of the Venusian atmosphere for the entire mission duration.	Section 5.3 and 5.2.2
Req-SCM-4.7	The system shall have a lifetime of at least 45 days.	Section 5.3.2, 58 days
Req-SCM-5	The system shall comply with the set engineering budget during the mission on Venus.	-
Req-SCM-5.1	The platform and payload combined shall have a maximum mass of 20 kg.	Section 7.2.1, 18.88 kg
Req-SCM-5.2	The platform shall provide a power of at least 35 W.	Section 5.2.3
Req-SCM-5.3	The platform shall be able to store at least 12.5 MB of data in between transmission periods.	Section 4.3.7, 25 MB
Req-SCM-5.4	The platform shall have an energy storage capacity of at least 80 Wh.	Section 5.2.3
Req-SCM-6	The spacecraft shall provide the necessary operational support functions to enable full execution of the scientific payloads' measurement.	-
Req-SCM-6.1	The spacecraft shall provide an average power of at least 55.5 W at 0.72 AU.	Section 4.3.6, 115.7 W
Req-SCM-6.2	The spacecraft shall provide a data rate of at least 1 $kbps$ to transmit scientific data.	Section 5.2.4, 2.9 $kbps$
Req-SCM-6.3	The spacecraft shall be able to store at least 25 MB of data in between transmission periods.	Section 4.3.7, 50 MB
Req-SCM-7	The payload shall comply with the gondola system constraints.	-
Req-SCM-7.1	The payload shall be compatible with CubeSat architecture.	Section 6.4
Req-SCM-7.2	The total payload mass shall be below 2 kg.	Chapter 6, 1.74 kg
Req-SCM-7.3	The payload shall not consume more than 4.8 Wh during eclipse time.	Section 6.4, 4.8 Wh
Req-SCM-7.4	The maximum peak power required for the payloads to operate shall not exceed 28 W.	Chapter 6.5, 22 W
Req-SCM-8	The LMC_{OOL} chips shall be protected to resist thermal degradation.	-
Req-SCM-8.1	The LMC_{OOL} temperature shall not exceed 50° C from the assembly phase up to the mission End of Life.	Section 6.5, 40° C
Req-SCM-8.2	The LMC_{OOL} temperature shall stay at 25° C during its operation, with a 0.01° C accuracy.	Section 6.5, 25° C
Balloon Fabric Material		

Continued from previous page

Requirement ID	Requirement	Proof in
Req-BFM-1	The material of the superpressure balloon shall endure a super pressure of at least 50 000 Pa.	Section 5.3.2, 129076 Pa
Req-BFM-2	The balloon material shall accommodate integrated openings for venting, pumping, and inflating the lifting gas.	Section 5.3.2
Req-BFM-3	The balloon shall not tear due to dynamic pressure loads during deployment.	Section 5.3.2
Req-BFM-4	The balloon shall not leak more Helium than 900 $cm^3 \cdot m^{-2} \cdot day^{-1}$.	Section 5.3.2, 700 $cm^3 \cdot m^{-2} \cdot day^{-1}$
Req-BFM-5	The balloon material shall have a solar absorptivity of 0.15 or less.	Section 5.3.2, 0.15
Req-BFM-6	The balloon material shall have an infrared emissivity of 0.5 or more.	Section 5.3.2, 0.51
Pressure Regulation System		
Req-PRS-1	The altitude control system shall allow the balloon to descent the whole range within at most 12 hours	Section 5.3.6, 10 hours
Req-PRS-2	The altitude control system shall allow the balloon to ascent the whole range within at most 12 hours	Section 5.3.6, 12 hours
Req-PRS-3	The pressure system shall have a total mass of less than 2 kg	Section 5.3.4, 1.2 kg
Req-PRS-4	The pressure system shall be able to handle a temperature range of 280-350K	Section 5.3.4, 0-80°C
Req-PRS-5	The pressure system shall be able to handle a pressure difference between the superpressure and zeropressure balloon of at least 50,000 Pa	Section 5.3.4, 180,000 Pa
External Requirements		
Req-EXT-1	The spacecraft shall meet COSPAR Category II contamination limits.	Section 8.3
Req-EXT-1.1	A planetary protection plan shall be compiled before the launch of the mission.	Section 8.3
Req-EXT-1.2	An Impact Strategy Report shall be compiled before the launch of the mission.	Section 8.3
Req-EXT-1.3	An End-of-Mission Report shall be compiled before the launch of the mission.	Section 8.3
Req-EXT-2	Mission updates shall be shared with interested parties.	TBD
Req-EXT-2.1	At least 80% of collected mission data shall be made publicly available within 3 months of the mission's end.	TBD
Req-EXT-2.2	The engineering team shall provide media organisations with monthly periodic updates regarding progress and the scientific findings of the mission.	TBD
Req-EXT-2.3	The mission team shall provide the launch provider with updated integration schedules and interface documentation at the latest <TBD>.	TBD
Req-EXT-2.4	Clients shall be informed and included in any major mission decision-making process.	Status Meetings conducted
Req-EXT-3	The mission shall support European Strategic Autonomy	-
Req-EXT-3.1	Any goods shall be purchased from European-based organisations.	Not met

Continued from previous page

Requirement ID	Requirement	Proof in
Req-EXT-3.2	Any service shall be provided by European-based organisations.	Section 3.2, 4.1
Req-EXT-4	At least 50% of scientific instruments and subsystems shall be developed with commercial off-the-shelf (COTS) components.	Section 4.3
Internal requirements		
Req-INT-1	Mission costs shall not exceed €150M (FY2025), excluding launch and operation.	Section 7.2.2, ~ €65M
Req-INT-2	The detailed mission design shall be completed in 45 workdays.	Gantt Chart [1]
Req-INT-3	The detailed mission design shall be completed by 10 students.	Cover page
Safety and Reliability		
Req-SAR-1	Reliability of the complete system shall be at least 95%	Section 7.4, 75%
Req-SAR-2	The system shall include safety measurements.	TBD
Req-SAR-2.1	The system shall be able to detect anomalies during all mission phases to a degree of accuracy of 95%.	TBD
Req-SAR-2.2	The system shall be able to autonomously resolve detected anomalies within <TBD> where possible.	TBD
Req-SAR-2.3	The system shall autonomously enter a predefined safe mode within upon detection of a critical anomaly that cannot be resolved within <TBD> minutes.	TBD
Req-SAR-2.4	The spacecraft shall be able to absorb impact with space debris that is smaller than <TBD> whilst orbiting Earth.	TBD
Req-SAR-2.5	The spacecraft shall be able to perform manoeuvrers to avoid a mission-threatening impact with external objects during transport from Earth to Venus.	TBD

Feasibility Analysis

As can be seen from Table 7.1, many of the set requirements have been satisfactorily met with the current design. Because the design still needs further development and refinement, some of the requirements have been labelled with *TBD*, expressing that the constraint will be considered in future stages, like sharing updates with interested parties. Other more technical ones, like including safety measures in the spacecraft, have not yet been considered due to restricted time, as they do not represent a crucial step in the basic functioning of the system. They will be investigated later, as specified in section 8.3.

Removed requirements

Two requirements have been removed during the detailed design phase. The first one, **Req-SCM-1.2**: The platform shall achieve a pointing accuracy higher than <TBD> $^\circ$ (3σ) in all axes, has been deemed unnecessary to fulfill the communication purposes between probe and spacecraft. Analysing the case in which the antenna is not pointed at all, communication between the systems is still possible, so the requirement is no longer considered.

The second one, **Req-SCM-2.5**: The samples shall be taken at <TBD> coordinates with an accuracy of <TBD> km, has been removed because it has been found that there is not scientific reason to sample at a specific coordinate instead of another one.

Not met requirements

Three requirements have not been met so far. **Req-SCM-4.3**, about the probe withstanding Venusian

temperatures, is not met due to the battery. While the environment temperature is expected to reach 350 K, the batteries are rated for only 333 K. Therefore, extra development and testing will need to be made to ensure space-rated components, as discussed in section 8.4.

Req-EXT-3.1, regarding the purchase of goods from European-based organisations, is only partially met. While efforts have been made to pick most of the components from Europe, the valve from the pressure regulation system in the balloon is from an American company. This choice has been made due to the component's long flight heritage and success rate, and because it is a convenient choice that does not jeopardise the mission, even if the requirement is not entirely met. Additionally, some of the communication components are also not European, but have been chosen for the same reasons. Efforts will be made to pick European components in further stages.

Finally, the reliability of the mission is only 75% and not 95% or higher, as required in **Req-SAR-1**. The low reliability is mostly due to the LMC_{OOL} technology and the sampling system. These are very novel concepts that need a lot of verification, validation and testing, which are planned for future stages of the design. Hence, it is expected that after performing those activities, the reliability will increased to meet the requirement.

7.2. Resource Allocation

The budgets considered for this section are the mass and the cost budget. For the power budget each section related to the power subsystem design can be referred to in tables Table 4.5, Table 4.6 and Table 5.5. Regarding the volume budget it has been deemed to not be required at this stage of the design process when the detailed dimensions of many components have already been calculated and presented in the rest of the report[1].

7.2.1. Mass Budget

Since many components have been identified and the ΔV budget has been finalized following the selection of the transfer and insertion orbits, the current design phase can already provide a fairly accurate estimate of the final mass of the system. Nevertheless, a margin is always included to account for uncertainties and potential variations in subsystem design at this stage. This margin depends on the maturity of each subsystem, the level of confidence in the design data, and the potential for changes as the design evolves. The requirement that most relates to the mass budget is **Req-EVT-2.1**. The value for the margin was generated qualitatively in agreement with the responsible of each subsystem.

Table 7.2: Mass budgets with margins for the spacecraft (left) and entry vehicle (right).

Subsystem	**Mass [kg]**	**Margin (%)**
Structures	3.21	50
EPS	1.51	20
CD&H	0.65	10
TT&C	5.17	10
Propulsion	35.05	10
ADCS	4.83	10
Total	50.42	
Total+Margin	56.90	

Subsystem	**Mass [kg]**	**Margin (%)**
Entry Capsule	36.03	10
Balloon	10.67	10
Pressure System	1.18	10
Sampling System	0.78	10
LMC_{OOL}	0.70	25
Secondary Payload	0.26	10
Structure	2.43	30
EPS	1.90	20
CD&H	0.62	20
TT&C	0.24	20
Total	54.81	
Total+Margin	61.16	

[1]The purpose of a budget is as a tool for design process in the case of the volume budget it is no longer useful for the remainder of the design if the mission

The total mass for the whole mission comes to be **118.1** kgincluding margins which is far less than what was estimated for the baseline report. The main reason behind this discrepancy was that only in later design stage it was decided that he launcher was going to be used to propellant the spacecraft into the transfer orbit, saving valuable fuel required for propulsion. Furthermore the insertion of the orbiter is without the entry capsule and the probe since they detach before the firing of the main thrusters, this also lowers the amount of fuel required for insertion.

7.2.2. Cost Budget Estimation

The main purpose for completing a budget breakdown is to present results that prove that the mission meets or exceeds **Req-INT-1** concerning the total cost of the mission including operation and launch costs.

When performing an estimation of the costs for a space mission the first decision to be performed is whether to use a bottom up approach or a top down approach. The former refers to the process of dividing the system and subsystems in individual components to which a cost can be assigned and summing all of them together leads to a final cost estimation. The latter refers to the use of parametric relationships that relate high-level parameters like total power required or subsystem mass to a cost estimation, this has the disadvantage of being more uncertain but it requires less detailed information on the subsystem level design. The main problem with the bottom-up approach is that it depends on knowing every component in the system. If any parts are unknown, the estimate must rely on rough guesses, which defeats the purpose of the method's supposed accuracy. In this report, even though many subsystem components were selected, their costs were often unavailable, making the bottom-up approach difficult to apply effectively.

Spacecraft

For the spacecraft, the cost estimating relationships described in SMAD related to small spacecraft with masses less than 500 kg was used [35]. This takes subsystems individual masses and computes their costs in dollars from the 2010 financial year. Values must be converted to Euros from dollars and to 2025 which was taken as a reference for the requirement definition [107] [108] . Unfortunately, many of the masses for the subsystems in our spacecraft fall far below the recommended input range. However an absolute error for each subsystem cost is provided by SMAD and on top of this a margin of 30 % is considered to make our estimate as reliable as possible. In Table 7.3, costs relating to engineering design and project management are grouped under Program Level, whilst manufacturing, integration, assembly and testing are referred to IA&T.

Table 7.3: Cost breakdown by subsystem in FY2010 and FY2025 euros, showing base cost, uncertainty-inclusive cost, and cost with margin. Conversion assumes 1 USD = 0.85 EUR [107].

Subsystem	Base Cost [k€]	+ Uncertainty [k€]	+ Margin [k€]
Structure	407	1340	1743
Thermal Control	285	386	502
ADCS	1806	2752	3577
EPS	1686	2460	3197
Propulsion	647	1438	1869
TT&C	847	1382	1796
C&DH	595	1321	1717
IA&T	872	872	1134
Program Level	1436	1436	1868
Total (FY2010)	**8,580**	**13,384**	**17,405**
Total (FY2025)	**12,709**	**19,823**	**25,776**

Probe and Entry Capsule

For the probe and entry capsule a hybrid approach can be utilised to come to the most accurate possible estimation. Since the main gondola essentially contains all subsystems that a regular spacecraft would the same SMAD relations that are described for the spacecraft can be used [35]. A larger margin of 50% was chosen to account for the fact that the cost estiamting relationships were for a spacecraft vehicle.

Table 7.4: Gondola subsystem costs in thousands of Euros, converted from USD assuming 1 USD = 0.85 EUR. All values rounded to nearest €1K [107].

Subsystem	Base Cost [k€]	+ Uncertainty [k€]	+ Margin [k€]
Structure	381	1,314	1,971
EPS	1,800	2,574	3,861
TT&C	420	954	1,431
C&DH	592	1,319	1,978
IA&T	444	444	666
Program Level	731	731	1,097
Total (FY2010)	4,368	7,336	10,997
Total (FY2025)	6,471	10,864	16,301

On top of the gondola manufacturing, the cost producing and testing the LMC_{OOL} instrument which includes the creation of novel receptors to target specific molecules described in subsection 2.4.2 and testing the its performance in sulphuric acid environment. The cost estimate provided in the baseline report of 5 million EUR was deemed reasonable by Dr. Ligterink, one of the groups tutors and a foremost expert on LMC_{OOL}.

The balloon system also represents a significant source of costs, particularly related to testing, as it must be demonstrated that it can withstand the harsh Venusian environment for the required duration without substantial leakage. Costs for NASA's Ultra Long Duration Balloons (ULDBs), designed for flight durations of up to 100 days, are approximately $ 1M or € 850k [2] accounting for inflation from and euro conversion. These balloons do not include variable-altitude capabilities. Assuming a conservative margin to account for the increased complexity of the variable altitude design and the requirement to sustain flight within the this value could be expected to increase to € 3M as a final value.

Estimating an accurate cost for the entry vehicle is very challenging, information about specific costs of entry systems for interplanetary missions is extremely scarce or completely unavailable to the public domain. Furthermore most entry capsules are designed to fulfil extremely specific mission requirements. Therefore only an order of magnitude estimate can be performed. Considering that for the mission the entry capsule is inserted into Venus directly without being slowed down, the extreme heat loads will drive costs upwards. A German space company, ATMOS Space CARGO, estimates the cost of its highly complex re-entry capsules focused on earth re-entry at € 4.5M [3]. Due to the increased complexity of re-entry at Venus, this figure represents a lower bound; costs could reach as high as € 15M.

Combining all these elements leads to a estimate for the total mission cost excluding missions operations and launch to **€ 65M** . Still at this design stage this number does not represent an accurate estimate but it is conservative enough to provide a ballpark for the costs to be expected in the further mission phases.

7.3. Technical Risk Assessment

In this section, risks associated with the Orpheus mission (development and execution) are defined and presented. Minimising the effect of risks can be done in 2 ways, namely prevention and mitigation.

[2] `https://www.lpi.usra.edu/decadal/sbag/topical_wp/EliotFYoung.pdf` Accessed: 17/06/2025
[3] `https://payloadspace.com/atmos-space-cargo-is-go-for-reentry/` Accessed: 16/06/2025

Prevention is reducing the risk before an event and mitigation is after. These strategies are explained in Table 7.7 and the associated risks are explained in Table 7.5. Lastly, risk maps pre-mitigation and post-mitigation are presented in Table 7.6 and Table 7.8.

7.3.1. Risk Parameter Definition

Risk is defined as the probability of an event/element multiplied by the impact of the event/element. Both probability and impact are scored on a scale from 1 to 5, hence the risk is scored on a scale from 1 to 25. Probability is calculated taking into account the data coming from the similar past missions as well as the current technological readiness level. The probability of an event/element is categorised into the 5-point scale and is defined more in detail below:

1. **Improbable (P < 1%):** The technology has been proven to be space-ready and reliable by similar missions.
2. **Remote (1% ≤ P < 30%):** The technology has been extrapolated from existing space-ready technology, with few failures in past missions.
3. **Occasional (30% ≤ P < 50%):** The technology is based on existing, non-space-ready technology, or a number of previous missions have experienced failures related to it.
4. **Probable (50% ≤ P < 70%):** The technology works in a laboratory, or previous missions show that this is a common failure cause.
5. **Frequent (P ≥ 70%):** The technology only works in theory, or a significant percentage of failures in past missions are caused due to this.

Furthermore, the impact is also scored on a scale from 1 to 5, with 5 having the most severe effect. The same terminology from the Baseline Report [2, Chapter 5] was used and the following definitions were put in place:

1. **Negligible:** Minor inconvenience, failure will not affect performance.
2. **Low:** Degradation of the secondary mission objectives, or a small reduction of performance.
3. **Moderate:** Secondary mission failure, or some reduction of performance.
4. **Critical:** Mission success is questionable, or significant reduction of performance.
5. **Catastrophic:** Mission failure or severe reduction of performance.

7.3.2. Initial Risk Identification and Risk Map

Risks will use identifiers in the form of TR-XX-nn, as was done in the Baseline Report [2, Chapter 5]. TR stands for "Technical Risk" and the 'XX' indicates the mission phase:

1. **MA:** Manufacturing
2. **PR:** Preparation for launch
3. **CR:** Cruise to Venus
4. **MI:** Mission operations
5. **EOL:** End-of-life
6. **GE:** General technical risks

The "nn" suffix is the number of risks inside the given phase.

Table 7.5: Technical risk assessment: P = "Probability", I = "Impact", and R = "Risk" (R = I · P).

ID	Risk	P	I	R	Responsible
TR-MA-01	Delays during manufacturing	5	1	5	Peter
TR-MA-02	Defects in manufacturing	2	3	6	Wout
TR-MA-03	Subsystems do not fit together as intended	2	3	6	Tristan
TR-MA-04	Manufacturing costs exceed budget	4	4	16	Firine
TR-MA-05	Unavailability of parts due to geopolitical tension	3	2	6	Carla
TR-PR-01	Spacecraft does not fit in launcher	1	4	4	Wout

Continued from previous page

ID	Risk	P	I	R	Responsible
TR-CR-01	Launcher unavailable due to geopolitical tensions	3	3	9	Peter
TR-CR-02	Spacecraft cannot handle launcher vibrations	1	5	5	Firine
TR-CR-03	Spacecraft cannot handle launch loads	1	5	5	Firine
TR-CR-04	Launcher blows up during ascent	1	5	5	Peter
TR-CR-05	Low Earth orbit insertion by launcher fails	1	5	5	Peter
TR-CR-06	Spacecraft put on incorrect transfer trajectory	2	3	6	Carla
TR-CR-07	Spacecraft gets hit by space debris	1	4	4	Wout
TR-CR-08	Spacecraft gets hacked	1	3	3	Carlos
TR-CR-09	Onboard electronics damaged by geomagnetic storm	1	3	3	Firine
TR-CR-10	Required trajectory corrections are too large	1	5	5	Carla
TR-CR-11	Venus orbit insertion fails	2	5	10	Carla
TR-CR-12	Spacecraft is not correctly separated	1	4	4	Tristan
TR-CR-13	Spacecraft incapable of getting correct entry attitude	3	5	15	Tristan
TR-MI-01	Probe burns up during Venus entry	2	5	10	Thijs
TR-MI-02	Probe loses control during Venus entry	3	4	12	Alphan
TR-MI-03	Lack of aerodynamic performance (Probe does not fly)	3	4	12	Thijs
TR-MI-04	Sampling system fails	4	5	20	Carlos
TR-MI-05	Not enough fluid is sampled	4	3	12	Carlos
TR-MI-06	LMC_{OOL} cannot handle Venus environment	4	5	20	Ward
TR-MI-07	LMC_{OOL} returns false positives or negatives	3	5	15	Ward
TR-MI-08	Assembly to bring liquid to LMC_{OOL} fails	2	5	10	Alphan
TR-MI-09	Other science equipment fails	3	3	9	Carlos
TR-MI-10	Sulphuric acid protection fails	2	4	8	Firine
TR-MI-11	Probe is unable to navigate to required locations	3	2	6	Thijs
TR-MI-12	Data collected is corrupted	2	4	8	Giulio
TR-MI-13	Sulphuric acid leaks into the spacecraft after sampling	3	5	15	Alphan
TR-MI-14	Major lifting gas leak	2	5	10	Peter
TR-MI-15	Balloon not sufficiently inflating during deployment	3	5	15	Thijs
TR-MI-16	Balloon ripping apart during deployment	2	5	10	Thijs
TR-MI-17	Gas leak from SP to ZP	2	3	6	Peter
TR-MI-18	Balloon deployment at incorrect altitude	4	4	16	Wout
TR-MI-19	Battery not lasting throughout the entire eclipse time	2	3	6	Carlos
TR-MI-20	Tether snap	2	5	10	Carlos
TR-MI-21	Pressure regulation system failure	3	3	9	Wout
TR-MI-22	Balloon rises/sinks outside of designed altitude range	2	3	6	Wout
TR-EOL-01	Disposal not properly performed	2	2	4	Giulio
TR-EOL-02	Contamination of Venus	1	5	5	Giulio
TR-GE-01	Power system fails	2	5	10	Giulio
TR-GE-02	Communication system fails	3	5	15	Giulio
TR-GE-03	Thermal control fails	2	4	8	Ward
TR-GE-04	Onboard computer fails	2	5	10	Tristan

Table 7.6: Pre-mitigation risk assessment matrix, where the impact can be seen on the y-axis and the likelihood can be seen on the x-axis. Green = desirable, blue = acceptable, yellow = undesirable, orange = unacceptable and red = catastrophic.

Impact						
	5	TR-CR-02 TR-CR-03 TR-CR-04 TR-CR-05 TR-CR-10 TR-EOL-02	TR-CR-11 TR-GE-01 TR-GE-04 TR-MI-01 TR-MI-08 TR-MI-14 TR-MI-16 TR-MI-20	TR-CR-13 TR-GE-02 TR-MI-07 TR-MI-13 TR-MI-15	TR-MI-04 TR-MI-06	
	4	TR-CR-07 TR-CR-12 TR-PR-01	TR-GE-03 TR-MI-10 TR-MI-12	TR-MI-02 TR-MI-03	TR-MA-04 TR-MI-18	
	3	TR-CR-08 TR-CR-09	TR-CR-06 TR-MA-02 TR-MA-03 TR-MI-17 TR-MI-19 TR-MI-22	TR-CR-01 TR-MI-09 TR-MI-21	TR-MI-05	
	2		TR-EOL-01	TR-MA-05 TR-MI-11		
	1					TR-MA-01
		1	2	3	4	5
		Likelihood				

The pre-mitigation technical risks are visualised above in the risk map in Table 7.6. It can be seen that there are 4 catastrophic and 8 unacceptable risks which need to be mitigated/prevented at least until they are of category "undesirable" or better. The strategies for doing so are discussed in Table 7.7, which is related to the necessary design changes made and the mission execution.

Table 7.7: Technical risk mitigation strategy. R_O: original risk value, P_{PM}: probability of risk post mitigation, I_{PM}: impact of risk post mitigation, R_{PM}: risk value post mitigation.

ID	**Mitigation/Prevention strategy**	R_O	P_{PM}	I_{PM}	R_{PM}
TR-MA-01	**P:** Have backup manufacturers.	5	3	1	3
TR-MA-02	**P:** Perform extensive verification and validation tests.	6	1	3	3
TR-MA-03	**P:** Ensure proper communication between engineering teams.	6	1	3	3
TR-MA-04	**M:** Warn stakeholders when budget will be exceeded so that more funding can be arranged.	16	4	2	8
TR-MA-05	**P:** Use European parts when possible; assure alternate providers (Europe preferred).	6	2	1	2
TR-PR-01	**P:** Maintain updated 3D models; measure parts pre-integration; limit redesigns to components.	4	1	3	3
TR-CR-01	**P:** Prefer European launch providers; assure alternate launcher option.	9	2	2	4

Continued from previous page

ID	Prevention (P) / Mitigation (M) strategy	R_O	P_{PM}	I_{PM}	R_{PM}
TR-CR-02	**P:** Thorough vibration testing; frequent contact with launch provider.	5	1	5	5
TR-CR-03	**P:** Thorough load testing; frequent contact with launch provider.	5	1	5	5
TR-CR-04	**P:** Choose proven launch vehicle.	5	1	5	5
TR-CR-05	**P:** Choose proven launch vehicle.	5	1	5	5
TR-CR-06	**P:** Choose proven launch vehicle.	6	1	3	3
TR-CR-07	**M:** Include debris integrity calculation; perform avoidance maneuvers if necessary.	4	1	3	3
TR-CR-08	**P & M:** Implement cybersecurity and reboot system.	3	1	2	2
TR-CR-09	**P:** Shield critical electronic components.	3	1	2	2
TR-CR-10	**M:** Have backup mission routes, including Venus crash option.	5	1	4	4
TR-CR-11	**P & M:** Prepare for worst-case orbit and alternate insertion strategies.	10	2	4	8
TR-CR-12	**P:** Test attachment system; maintain contact with launch and interface engineers.	4	1	4	4
TR-CR-13	**P:** Use flight-proven ADCS; delay reentry burn for passive alignment.	15	2	4	8
TR-MI-01	**P:** Thermal protection with safety margins; extensive V&V.	10	1	5	5
TR-MI-02	**M:** Design safe mode; ensure stability and resistance to tumbling.	12	2	3	6
TR-MI-03	**M:** Collect max data during failure; prioritize critical data; simulate/test early.	12	2	3	6
TR-MI-04	**P:** Reduce moving parts; ground test; use safety margins and validate in-situ.	20	3	5	15
TR-MI-05	**P & M:** Prioritize critical data; use multi-use sampling system.	12	3	2	6
TR-MI-06	**P:** Ensure receptors resist H_2SO_4.	20	2	5	10
TR-MI-07	**P & M:** Use redundant chips; consult LMC_{OOL} for false positive/negative stats.	15	3	2	6
TR-MI-08	**P & M:** Reduce moving parts; redundancy and passive flow.	10	2	5	10
TR-MI-09	**P:** Use proven, off-the-shelf components.	9	1	3	3
TR-MI-10	**P & M:** Shield critical components from H_2SO_4 ; act early to avoid disintegration.	8	2	4	8
TR-MI-11	**P & M:** Choose homogeneous landing areas; still perform measurements.	6	3	2	6
TR-MI-12	**P & M:** Enable software updates and reboots; validate received data.	8	2	2	4
TR-MI-13	**P & M:** Coat sample transport paths; separate from internal H_2SO_4 .	15	2	4	8
TR-MI-14	**P:** Multiple coating layers for balloon; thorough testing.	10	1	5	5
TR-MI-15	**P & M:** Passive inflation; test early; measure before sampling altitude loss.	15	2	4	8
TR-MI-16	**P & M:** Test and prioritize early sampling.	10	1	4	4
TR-MI-17	**P & M:** Coat SP balloon; vent or re-inflate SP/ZP balloons.	6	1	2	2

Continued from previous page

ID	Prevention (P) / Mitigation (M) strategy	R_O	P_{PM}	I_{PM}	R_{PM}
TR-MI-18	**P & M:** Test deployment system; design for off-nominal altitudes.	16	3	2	6
TR-MI-19	**P & M:** Add eclipse and battery margins; shut down non-critical systems.	6	1	3	3
TR-MI-20	**P:** Use strong tether materials; thorough testing.	10	1	5	5
TR-MI-21	**P:** Test pressure regulation system.	9	2	3	6
TR-MI-22	**P & M:** Use closed loop for altitude control; off-nominal tolerance.	6	1	2	2
TR-EOL-01	**P & M:** Separate sample disposal from system EOL; redundancy.	4	1	2	2
TR-EOL-02	**M:** Warn scientific community about contamination.	4	1	3	3
TR-GE-01	**P & M:** Redundancy; proven parts; design safe mode.	5	1	4	4
TR-GE-02	**P & M:** Redundancy; proven parts; design safe mode.	15	2	5	10
TR-GE-03	**P & M:** Redundancy; proven parts; design safe mode.	8	1	4	4
TR-GE-04	**P & M:** Reboot, redundancy, proven parts, implement EOL failsafe.	10	2	4	8

Table 7.8: Post-mitigation risk assessment matrix, where the impact can be seen on the y-axis and the likelihood can be seen on the x-axis. Green = desirable, blue = acceptable, yellow = undesirable, orange = unacceptable and red = catastrophic.

Impact						
	5	TR-CR-02 TR-CR-03 TR-CR-04 TR-CR-05 TR-MI-01 TR-GE-01 TR-MI-14 TR-MI-20	TR-MI-04 TR-MI-06 TR-MI-08 TR-MI-13 TR-GE-02			
	4	TR-CR-12 TR-MI-16	TR-CR-11 TR-MI-10 TR-GE-04 TR-MI-15			
	3	TR-CR-08 TR-CR-09 TR-MI-19	TR-MA-02 TR-MA-03 TR-CR-06 TR-MI-09 TR-MI-18	TR-CR-01		
	2	TR-MA-05 TR-EOL-01	TR-MI-11 TR-MI-07 TR-MI-12	TR-MI-21	TR-MA-04	
	1		TR-CR-13	TR-MA-01		TR-MI-14 TR-MI-20
		1	2	3	4	5
		Likelihood				

As can be seen in the post-mitigation risk map in Table 7.8, after the mitigation/prevention strategies, risks classified as "catastrophic" and "unacceptable" are eliminated and their risks are reduced.

7.4. Reliability, Availability, Maintainability, and Safety Characteristics

As the mission definition advances into more detailed phases, it is paramount to not only look into performance metrics for success, but also into the system's reliability, availability, maintainability and safety (RAMS) characteristics. Just as in the preceding sections on resources, costs, and risks, RAMS's characteristics further investigate the mission's feasibility. This section thus outlines how RAMS principles have been integrated into the design, and what aspects still need to be considered in future development stages.

Reliability

Reliability concerns the ability of the system to perform what is expected of it during nominal operation conditions, during the mission duration. Given the nature of the mission, it is essential that the system is reliable, as no maintenance or repair is possible once it is launched.

One of the system requirements, **Req-SAR-1**, states that the minimum reliability of the complete system must be at least 95%. To check that this is met, the reliability of the separate subsystems must be considered. The methodology followed for this purpose is to consider the technology readiness level of the different parts, and relate that to the estimated reliability. The technology readiness levels with their corresponding explanation are presented in Table 7.9, along with the assumed reliability in the right column. These values have been based on NASA's systems engineering guidelines [109], which relate TRLs to system maturity and associated reliability estimations, combined with engineering reasoning.

Table 7.9: Estimated reliability by technology readiness level [4].

Technology Readiness Level (TRL)	Est. Reliability
TRL 1: Basic principles observed	0.50
TRL 2: Technology concept formulated	0.55
TRL 3: Experimental proof-of-concept	0.65
TRL 4: Component validated in lab	0.75
TRL 5: Component validated in relevant environment	0.85
TRL 6: System/subsystem model demonstrated in relevant environment	0.93
TRL 7: System prototype in operational environment	0.96
TRL 8: System flight-qualified through test and demonstration	0.98
TRL 9: Actual system flight-proven through mission operations	0.99

Five subsystems are considered: the spacecraft, the entry capsule, the probe, the sampling system, and the instruments. The probe includes both the balloon and the gondola, but excludes the payload. Table 7.10 presents each subsystem with their technology readiness level, an explanation of the redundancy included in the design, and the estimated reliability. This estimation is done by considering the relations in Table 7.9. Moreover, in case the design incorporates redundancy, Equation 7.1 is used, where r is the reliability of a single component and n is the number of components in parallel (redundant to each other) [110].

$$R_p = 1 - (1 - r)^n \tag{7.1}$$

Both the spacecraft and the entry capsule have a TRL of 9, because they incorporate space-proven materials and components, and similar designs have been widely used in previous missions. The

[4] https://www.nasa.gov/wp-content/uploads/2017/12/458490main_trl_definitions.pdf, [Accessed 13/06/2025]

probe has a TRL of 6, because past missions, such as Vega, have used the balloon concept on Venus. However, the balloon-in-balloon architecture has not yet been used on Venus, but has been thoroughly tested multiple times on Earth [84, 88]. The sampling system uses a novel design, but the selected mesh is off-the-shelf, considerably reducing development risks. Its technology readiness level is 6, as it has been tested in a relevant environment: submerged for 24 h in 1 mole of HCl, with a change of its mechanical properties of less than 5%. Finally, for the payload only LMC_{OOL} is considered, as it is the main focus of the mission. This instrument has been validated in the lab, however, it has not been tested in sulphuric acid, which leaves its TRL at 4.

Table 7.10: Estimated reliability of the components in the Orpheus mission.

Subsystem	TRL	Redundancy	Reliability
Spacecraft	9	Two types of ADCS sensors and actuators. Multiple pyrogenic valves in parallel. Two antennas for Earth communication.	0.9997
Entry capsule	9	None.	0.9900
Probe	6	Extra valves in pressure regulation system. Balloon in balloon → reduced venting to environment.	0.9902
Sampling System	6	None.	0.9300
Instruments	4	Two possible paths to bring sample to LMC_{OOL}. Two sensors for each targeted molecule. Double pump system.	0.8240
Total			**0.75**

The total reliability is the multiplication of the individual reliabilities of each subsystem. Considering **Req-SAR-1**, a total of 75% is not satisfactory. From Table 7.10, it can be seen that the spacecraft, the entry capsule and the probe meet the requirement, either by being a proven concept, by incorporating solid redundancy, or both. However, the sampling system, and especially the LMC_{OOL}, need further development and testing. The testing campaign must ensure that the components used can survive in a space environment and maintain nominal operations on Venus when required. Recommendations on future testing activities are given in section 8.4.

Availability

Because there is no possible maintenance in orbit or on Venus, the system is not expected to have downtime due to repairs. Hence, its availability, which is the probability that the system can function when needed, should be as designed for, given that reliability is high.

However, the system will not be able to function continuously during the entire mission duration, as already stipulated in the design. While the sampling can take place at all times, communication becomes difficult during eclipse, which could be considered a lack of availability. For example, communication during the night is not expected to happen due to the limited power of the probe and the short contact window with the orbiter. Nevertheless, these situations are taken into account and designed for. Hence, the availability will not be interrupted by maintenance.

Maintainability

Maintainability refers to the ease with which a system can be inspected and repaired to restore functionality after a failure. In conventional systems, high maintainability ensures minimal downtime and efficient resource use. However, for a space mission to Venus, in-situ maintenance is infeasible. Once the spacecraft departs Earth, physical human intervention becomes impossible.

As a result, maintainability in this mission context shifts from physical repairs to designing for fault tolerance, redundancy and autonomous recovery. This is reflected in the system's requirements (**Req-SCM-1.4**, **Req-SCM-1.4**, **Req-SAR-2.2**, **Req-SAR-2.3**, **Req-SAR-2.4**, **Req-SAR-2.5**), regarding autonomy, anomaly detection and resolution, safe mode entering, and damage tolerance and avoidance.

These requirements ensure that single-point failures or dangerous situations do not jeopardise the entire mission. Hence, reliability again plays an important role in the mission integrity: since no repairs can be performed after launch, the system must be robust, thoroughly tested, and designed to autonomously handle potential failures throughout the mission.

Because the mentioned requirements have still not been designed for, further design and development, as well as testing and validation, are needed to ensure a robust system. The necessary steps to finalise the design can be seen in section 8.3.

Safety

Safety within the Orpheus mission includes ensuring the well-being of staff involved in the manufacturing and testing of the design, preventing the system from harming itself during operations, and avoiding contamination of the Venusian environment.

Manufacturing will take place partly in-house, in the TU Delft laboratories as outlined in section 3.2, and partly in a subcontracted company. This choice has been made to adhere to sufficient safety measures, as the propulsion system requires careful storage and handling, especially due to the helium tanks. For this reason, experts specialised in the topic will take care of that subsystem, ensuring adequate safety.

Once the mission is launched, safety concerns the ability of the system to survive. One of the main considerations is requirement **Req-SAR-2**: The system shall include safety measurements. It includes anomaly detection and resolution, space debris impact avoidance and safe mode entering. These requirements will ensure that the spacecraft can continue the mission given dangerous situations. However, the current design does not account for safety measures, as it needs further development. They will be considered in later stages, as described in section 8.3.

Furthermore, as the probe will enter the Venusian atmosphere, planetary protection guidelines must be considered. Venus falls into COSPAR Category II, which means that it does not have strict biological contamination constraints. However, efforts still need to be put into minimising the risk of bringing biological traces from Earth that could be detected by LMC_{OOL} and confused with being original from Venus. Therefore, sterilisation protocols and cleanroom integration procedures should be followed.

8 Future Mission Development

As this phase of the design concludes, the basic principles for a successful mission have been set. However, many necessary steps are still needed to reach a fully operational mission. This chapter hence outlines the critical post-DSE activities required to finalise the design. They include further development of certain subsystems, detailed simulations, and verification and validation procedures to increase reliability. These steps will bridge the gap between design and mission realisation.

Section 8.1 details the production plan necessary for the manufacturing of the current design, required by all the parties involved in the assembly of the system. Sections 8.2 and 8.3 outline all the future activities needed to finalise the design, both in the form of a Gantt chart and as a diagram. Finally, recommendations are given in section 8.4.

8.1. Production Plan

Once a design is finalized, a production plan becomes essential for the proper manufacturing of each system component. However, since the current design is still under development, only the critical steps completed up to this point are discussed here.

With such a complex mission, encompassing many different subsystems, it is essential to have an overview of the different methodologies and spaces used to produce each mission segment. Therefore, this production plan is divided into the different systems: the spacecraft, the entry capsule, the balloon, and the instruments. Special focus is put on the latter two elements, as they compose the least commonly manufactured parts, and hence need a more detailed explanation.

Spacecraft

The spacecraft body will follow a traditional microsatellite design, making use of existing knowledge and infrastructure at TU Delft. The primary structure will be developed and integrated in the Delfi Space Laboratory, as it provides the necessary infrastructure to build and test satellites.

The propulsion subsystem, on the other hand, will be outsourced to Air Liquide Advanced Technologies, as discussed in section 3.2. This decision ensures that all the dangerous substances involved in the propulsion system are stored and handled properly.

All other subsystems of the spacecraft will utilise commercial off-the-shelf components to reduce development and testing costs, hence simplifying the manufacturing part. They will be assembled into the main body in-house at TU Delft. Since the parties involved in the manufacturing process have previous experience in the Aerospace industry, only the technical drawings displaying the design will be provided to the relevant parties and it is assumed that this will provide sufficient knowledge to successfully complete the manufacturing of the spacecraft.

Capsule

The entry capsule shares many subsystems with the spacecraft bus, allowing commonality in materials and manufacturing methods. For this reason, production will occur in the TU Delft laboratories mentioned above.

However, the current design of the capsule includes a unique feature: a donut-shaped helium tank. This is used to store the helium needed to inflate the balloon once on Venus, and due to the arrangement of the capsule components, a torus was found to be the optimal way to fit in the tank, maximising its volume. Because it is not a commonly used shape in a tank, its development and manufacturing will have to be outsourced to an external party, instead of being done at TU Delft. One potential partner

has been found to be MT Aerospace, a company from Germany specialised in satellite tanks. With the proposed design and their expertise, the development and production of the helium tank will be possible.

The heat shield will be developed using ablative materials, made to resist extreme temperatures. The deceleration systems, such as the parachute and the separation mechanisms, will be integrated and tested in parallel with the balloon inflation system.

Gondola

The production of the gondola will involve welding all the sides but the top, inserting the internal structure and components, and welding the top wall to seal the gondola. The assembly will be mounted using cubesat components in order to reduce the price, complexity, and production time. Once the walls are welded in place, the cuboid will be depleted of air and filled with argon gas. The opening through which this process will be done is the same opening through which the wires will be fed outside of the gondola, so it must be airtight. As for the outside, solar panels will be hinged to the gondola, and the antennas will be mounted using brackets.

One possible complication in the manufacturing process is the weld being porous, which is the most common weld defect with titanium alloys[1]. To prevent this, the assembly should be thoroughly cleaned before the weld. In case it is found that welded Ti-6Al-4V does not meet the system requirements, Al5456-H343 has been selected as a backup material for the gondola. It is one of the aluminium alloys with the highest strength retention after welding, apart from having excellent weldability, and standing out due to the low porosity of its welds [62]. Note that the overall mass of the probe would go up if the gondola was made of Al5456-H343, so changing to this material should only be done in the case Ti-6Al-4V can not work in any way.

Balloon

The balloon is manufactured similarly to the prototype balloon developed by the Jet Propulsion Laboratory, California Institute of Technology, and NASA [65]. Sixteen gores will be laser cut from the laminate material designed in subsection 5.3.2 and joined to create a spherical balloon shape [65]. There will be circular laminate end caps at to top and bottom of the balloon connecting all the gores. This is done for both the super pressure and zero pressure balloon. The different gores are bonded with a urethane-coated , Vectran® based, structural tape on the inside of the balloon. The tape is thermally welded to the aliphatic urethane layer on the inside of the laminate using a heat seal platen [65]. The outside of the bond is covered by an FEP cover tape that prevents sulphuric acid penetration into the balloon. This is bonded using a special adhesive that is resistant to sulphuric acid as was done in the previously mentioned prototype [65]. This can be painted on by hand. In future stages of the design, all adhesives will be chosen with specialised European based manufacturing companies such as Saint Gobain [2].

To connect the balloons to the pumping system and to the gondola, holes have to be cut in the bottom end caps. As can be seen in Figure 5.15, each balloon needs 3 ports to connect Helium tubes from the Pressure Regulation System (PRS) to the balloon. The helium tube configuration is sketched in Figure 8.1b and a concept of the a connection port is sketched in Figure 8.1a. The three ports connecting the super pressure balloon and the PRS go through the zero pressure balloon. This has a dual purpose of both connecting the tubing from the PRS to the super pressure balloon and clamping the zeropressure and superpressure balloon together. The other three connections between the zeropressure balloon and the PRS are to the side of the bottom end cap such that these do not interfere with the super pressure balloon.

[1] https://www.twi-global.com/technical-knowledge/job-knowledge/weldability-of-materials-titanium-and-titanium-alloys-024 Accessed 16/06/2025

[2] https://saint-gobain.com/en Accessed : 18/06/2025

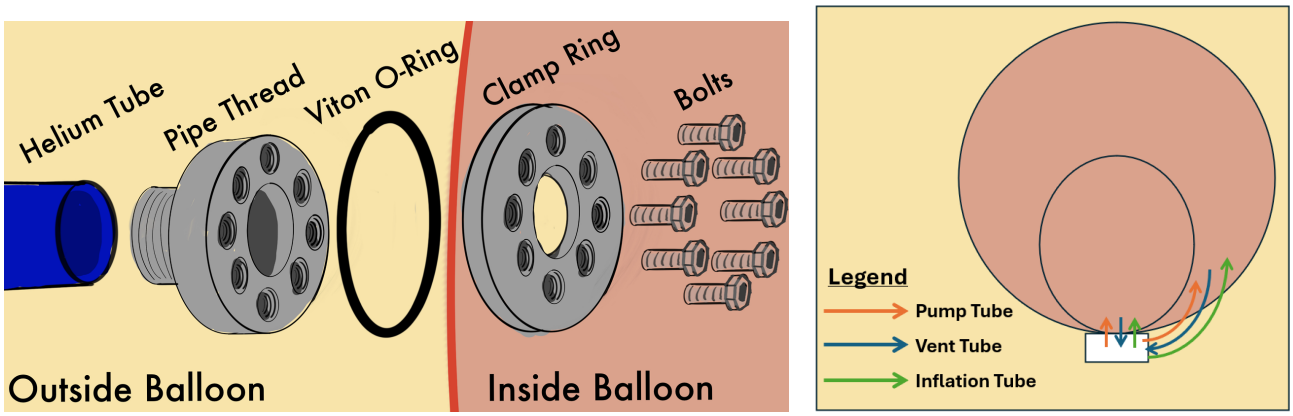

(a) Balloon tube connection concept (not to scale).

(b) Balloon tube configuration diagram (not to scale).

Figure 8.1: Balloon tubing diagrams.

The balloon PRS connection port concept is sketched in Figure 8.1a and it contains multiple crucial parts, inspired from the previously discussed prototype [65]. The "Pipe Thread" part is a male sided pipe thread on the left side where the helium tube is attached. On the balloon facing side, there is an array of blind threaded holes (8 are drawn here) such that the bolts are not exposed to the outside. The pipe thread itself can be machined from a sulphuric acid resistant metal alloy like Hastelloy, which is a nickel alloy used in a previous Venus balloon prototype [65]. The "Viton O-Ring" ensures a tight seal and prevents any sulphuric acid aerosols from penetrating the connection port. Viton is a rubber that has excellent resistance against concentrated sulphuric acid and many other chemicals [3]. The "Clamp Ring" can be bonded to the balloon interior of the laminate with structural epoxy such that it can transfer the load from the pipe thread into the laminate [65]. It can be machined from a lighter material like an aluminium alloy as it is not exposed to the corrosive Venusian atmosphere. The "Bolts" join the Clamp Ring to the Pipe Thread through the centre of the Viton O-Ring. Since the bolt threads in the Pipe Thread do not fully go through the part, the bolts are not exposed to the outside and therefore these can be made of a strong stainless steel [65]. To prevent damage on the interior of the balloon from friction with the bolts and clamp ring, these components will be covered in protective padding.

Instruments

Firstly, the LMC_{OOL} Chips are produced by LioniX[4] in the Netherlands. Flip-chip bonding is then employed to integrate the VCSELs integrated Photodiodes and NTCs on the substrate, submicron precision is necessary to place them correctly at the electrical-optical interface. This can be achieved via machine vision and fiducial marks.

The next critical step is the implementation of MIPs. Unique research and manufacturing is needed for each specific MIP, which can be timely and costly. Deposition of the MIPs on the waveguides first requires selective etching of the silica cladding. Then, precise functional monomer solutions are sequentially smeared to successfully bond the MIPs. This step can also necessitate accurate laser-assisted photopolymerisation.

Next, The LMC_{OOL} Assembly is integrated together with the use of S8U Adhesive following the recently developed polyimide foil technique [106]. Special care must be taken to seal the Aerogel Thermal Barrier which provides important insulation during the mission.

After acquiring each components, the fluidic network can then be built and integrated in the CubeSat configuration. First, the parts are attached to the CubeSat Aluminium Slabs with S8U, rivets or nuts & bolts. Then, they are interconnected together with the tubing in a detailed sequence to avoid tangling

[3] https://www.missionrubber.com/fkm-chemical-resistance-guide/
[4] https://www.lionix-international.com/

or interface issues. Tubing interfaces are secured with capillary ferrules, compression fittings, and O-ring seals.

Finally, before the cable is connected to the gondola, the sampling system is coaxially slided on. Then, after the gondola is fixed, the mesh is folded in a zizag fashion and fits in the 5 cm thick mast top, which is then secured.

8.2. Project Design & Development Logic

While the design presented in this report is detailed, several critical steps remain before the mission can be fully realised. To clarify the sequence of activities and their dependencies, a Project Design & Development Logic has been created, and is shown in Figure 8.2.

The diagram starts with the preliminary design developed during the DSE as input. Each major task, displayed in dark grey, is part of a logic loop, highlighted in red, that must be completed before moving on to the next task. In some cases, major tasks are broken down into three levels of detail. The second level is shown in light grey, and the last one in plain text. If only two levels exist, plain text comes right after the main task in dark grey.

8.3. Project Gantt Chart

The project Gantt chart, in Figure 8.3, displays the future tasks necessary to bring the design to an actual mission, relating it to the Project Design & Development Logic and including dates. It starts in July 2025, right after the end of the DSE, and it concludes in mid-2033, with the end-of-life operations of the system on Venus. The planning of the design development, manufacturing and assembly, and testing are included, as well as the launch and operations.

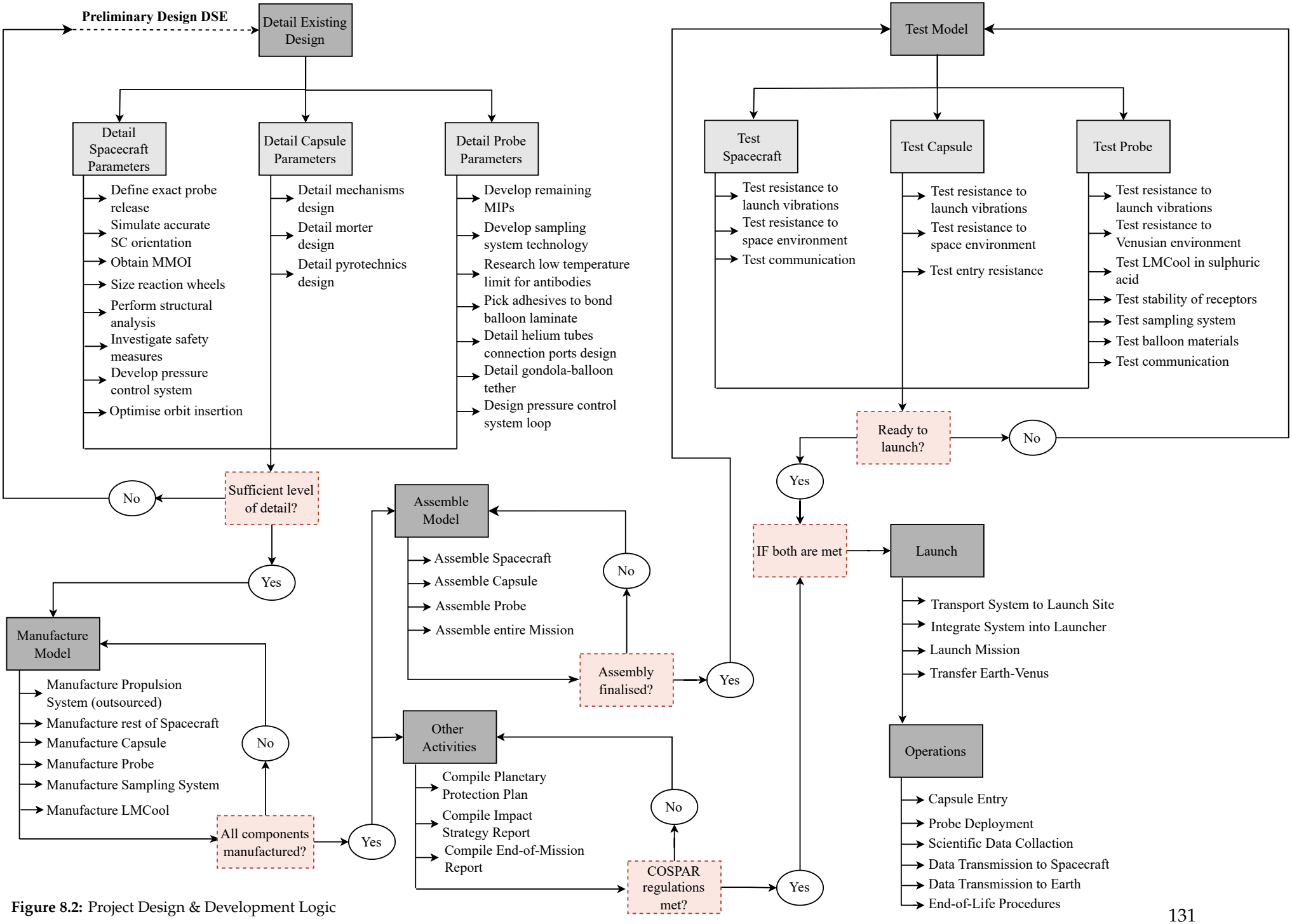

Figure 8.2: Project Design & Development Logic

Life on Venus? - Orpheus

TASK #	TASK TITLE	START DATE	DEADLINE
5	**Post-DSE Activities**		
5.1	Detail Existing Design	Jul 2025	Sep 2027
5.1.1	Detail Spacecraft Parameters		
5.1.1.1	Define exact probe release		
5.1.1.2	Simulate accurate orientation of spacecraft during orbit		
5.1.1.3	Obtain accurate MMOI from spacecraft simulation		
5.1.1.4	Size reaction wheels based on accurate MMOI and orientation		
5.1.1.5	Perform structural analysis on spacecraft		
5.1.1.6	Investigate autonomous safety measures		
5.1.1.7	Develop pressure control system for propulsion		
5.1.1.8	Optimise orbit insertion accounting for Venus movement around Sun		
5.1.2	Detail Capsule Parameters		
5.1.2.1	Detail mechanisms design		
5.1.2.2	Detail design of morter that shoots the capsule		
5.1.2.3	Detail pyrothechnics design used to separate capsule		
5.1.3	Detail Probe Parameters		
5.1.3.1	Develop MIPs for remaining molecules		
5.1.3.2	Develop Sampling System Technology		
5.1.3.3	Research lower temperature limit for antibodies		
5.2	Manufacture Model	Oct 2027	Feb 2029
5.2.1	Manufacture Propulsion System (outsourced)		
5.2.2	Manufacture rest of Spacecraft		
5.2.3	Manufacture Capsule		
5.2.4	Manufacture Probe		
5.2.5	Manuacture Sampling System		
5.2.6	Manufacture LMCool		
5.3	Assemble Model	Mar 2029	Jan 2030
5.3.1	Assemble Spacecraft Components		
5.3.2	Assemble Capsule Components		
5.3.3	Assemble Probe Components		
5.3.4	Assemble entire Mission		
5.4	Test Model	Mar 2030	Jun 2032
5.4.1	Test Spacecraft		
5.4.1.1	Test resistance to launch vibrations		
5.4.1.2	Test resistance to space environment		
5.4.1.3	Test communication		
5.4.2	Test Capsule		
5.4.2.1	Test resistance to launch vibrations		
5.4.2.2	Test resistance to space environment		
5.4.2.3	Test entry resistance		
5.4.3	Test Probe		
5.4.3.1	Test resistance to launch vibrations		
5.4.3.2	Test resustance to Venusian environment		
5.4.3.3	Test LMCool in sulphuric acid		
5.4.3.4	Test stability of receptors in space and acidic environments		
5.4.3.5	Test sampling system in sulphuric acid		
5.4.3.6	Test balloon materials in relevant environment		
5.4.3.7	Test communication		
5.5	Others	Jul 2032	Nov 2032
5.5.1	Compile Planetary Protection Plan		
5.5.2	Compile Impact Strategy Report		
5.5.3	Compile End-of-Mission Report		
5.6	Launch	Dec 2032	May 2033
5.6.1	Transport System to Launch Site		
5.6.2	Integrate System into Launcher		
5.6.3	Launch Mission		
5.6.4	Transfer Earth-Venus		
5.7	Operations	May 2033	Jul 2033
5.7.1	Capsule Entry		
5.7.2	Probe Deployment		
5.7.3	Scientific Data Collection		
5.7.4	Data Transmission to Spacecraft		
5.7.5	Data Transmission to Earth		
5.7.6	End-of-life Procedures		

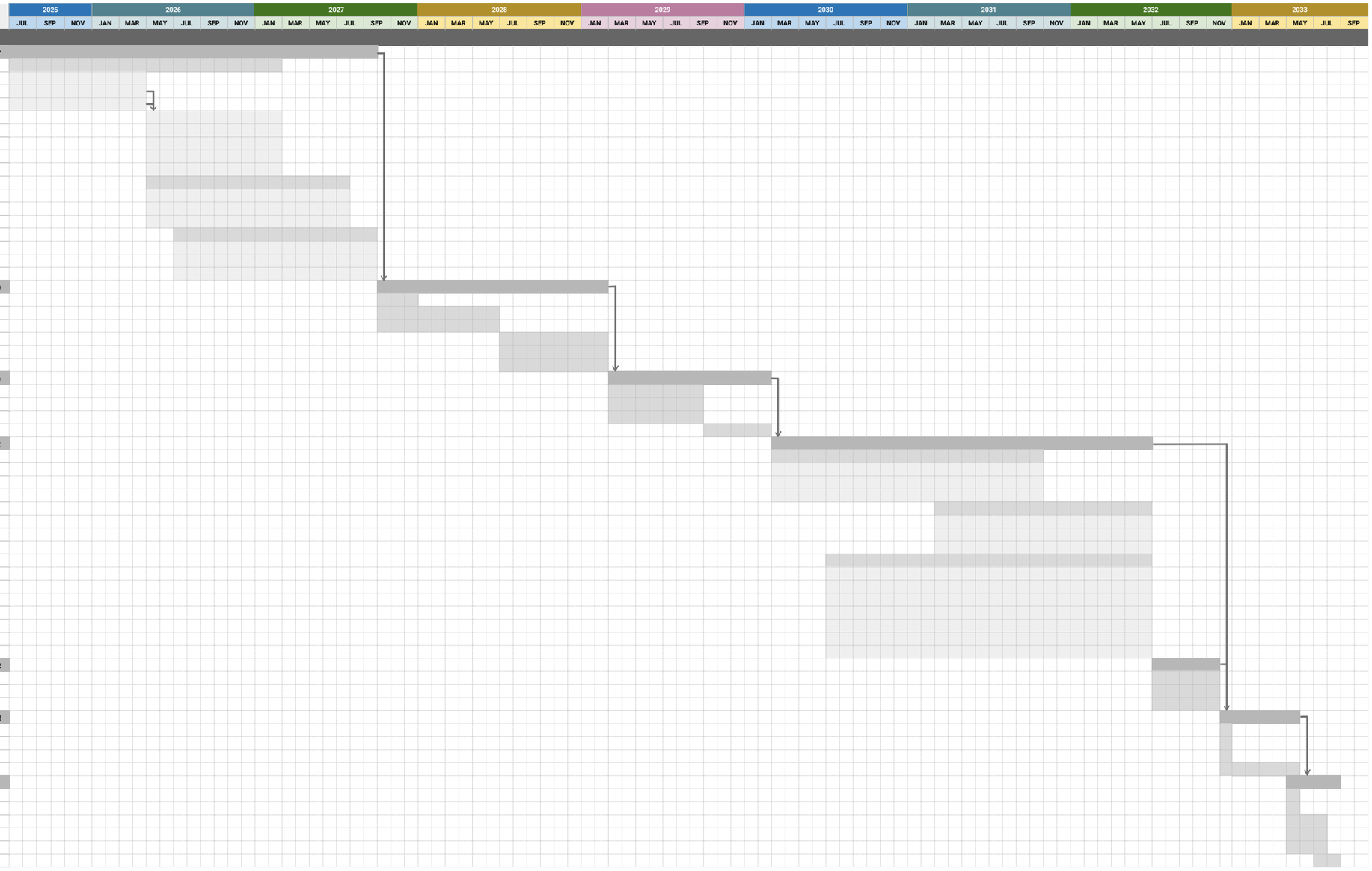

Figure 8.3: Project Gantt Chart (Post-DSE activities).

8.4. Recommendations

Based on the current design progress and the challenges identified during the process, this chapter provides a set of key recommendations that should guide any future development. These suggestions address the technical side of the mission, the communication part, and the sustainability considerations, and are intended to support the successful realisation of the mission.

Given that many requirements have been left as TBD, considerable technical development still needs to occur to fulfill them. Regarding the spacecraft design, structural analysis must be performed to ensure it survives every segment of the mission, including launch. The addition of safety measures to the spacecraft, such as space debris avoidance systems, is highly recommended to increase the chance of success. For the capsule, refining of the pyrotechnics used to eject it from the spacecraft is needed. Moreover, an accurate astrodynamics simulation is necessary to decide the exact capsule release timing and ensure communication is possible at all planned times, as well as optimising even further the orbit insertion into Venus. The exact orbit insertion timing should be calculated to determine the detailed probe operations.

Looking at the balloon, the materials used for its design must be extensively tested before manufacturing. Some of the recommended tests include being tightly folded for a long time, being submerged in sulphuric acid, cycling loading tests, leakage tests and FEM stress analysis for seams. The tether connecting the balloon to the gondola must also be detailed further. The sampling system does not currently have satisfactory reliability, hence it is recommended to test it in a relevant environment to increase its technology readiness level. The LMC_{OOL} technology, being such a novel concept, also does not have the required reliability. For this reason, extensive testing is paramount. The chip's resistance to launch vibrations must be evaluated, and it has to be tested in sulphuric acid. Moreover, the MIPs for the remaining molecules still have to be developed. Finally, it is recommended to embed a system that will autonomously detect the time of day, which will help in making the instrument's operations fully automatic.

To ensure that the mission complies with COSPAR regulations, multiple reports must be compiled before the launch. These include a planetary protection plan, an impact strategy and end-of-mission reports. It is also recommended to set up a communication plan to share the scientific insights with the general public, as specified in the mission requirements. Publicly sharing information about the mission development could potentially be used to obtain sponsors, hence reducing the cost of the mission.

Sustainability is an area that can be further improved. A Life Cycle Assessment is a key aspect to be considered in the more developed stages of the project. Furthermore, it is recommended to investigate alternatives to some of the design's components, such as the use of helium and batteries. Some of the proposed battery alternatives include solid-state, batteries with recycling agreements, modular, and low-cobalt. Another ambit that should be considered is to coordinate with similar missions to reduce the redundant infrastructure use during manufacturing, testing, launch, and operations. Finally, it is encouraged to detail the end-of-life operations of both the orbiter and the probe.

These are the main recommendations given at this specific stage of the design, which are essential for the project's long-term success. However, as progress is made, these recommendations must be re-evaluated to confirm that they are still relevant, and additional steps will probably be necessary along the way. A more complete overview of the technical recommendations can be found in Figure 8.2.

9 Conclusion

Orpheus presents a complete mission description for an innovative life-finding concept aimed at investigating the potential for life in the cloud layers of Venus at altitudes of 50-55 km. It distinguishes itself as a private, European and low-budget mission, uses a high-accuracy payload, developed to fit in a 1U cubesat module. The mission is planned to launch on December 6th, 2032 on top of the European RFA One rocket. Inside the fairing will be a small spacecraft, roughly the size of a microwave, connected to an entry capsule that contains the atmospheric probe. The **€65M** spacecraft will have a total launch mass below 120 kg.

RFA will deliver Oprheus into an interplanetary transfer orbit to Venus. After 160 days, the entry capsule will enter Venus' atmosphere while the spacecraft enters an elliptic Venus orbit, ready to transmit the scientific data. The 61 kg entry capsule slows itself down using a heatshield and parachutes until it reaches an altitude of 60 km, after which the balloon is inflated, and the solar panel, antenna and sampling mesh are deployed. When the deployment is complete, sampling starts and the scientific mission can commence. The LMC_{OOL} payload assembly will be carried as a gondola under a variable altitude balloon. This platform allows for measurements across different atmospheric layers, maximising the scientific return. Compared to similar life-detection missions like the Morning Star mission of MIT, the LMC_{OOL} provides comparable scientific value while being dramatically lighter and more compact, weighing only a fraction of the instrumentation typically required. This technology could enable scalable, low-cost missions to Venus and other high-priority targets like Enceladus, Mars, or gas giant moons, where payload mass and power constraints are critical. By replacing bulky lab equipment with a single integrated photonic biosensor, future missions could deploy multiple low-mass probes across diverse environments, massively increasing the chances of detecting life while reducing risk and cost.

The mesh will passively collect sulphuric acid droplets from the Venusian clouds, at an expected rate of 1 ml per day. It is collected in a tank, and will be analysed for biosignatures. Throughout the balloon's planned lifetime of 58 days, LMC_{OOL} will perform 16 tests at 6 different altitudes, investigating the presence of complex (biotical) chemistry. 46 molecules including amino acids, nucleobases, lipids, and small organics are selected for in-situ analysis.

Although much work has been done, further development of the concept is needed to make it a reality. The mission profile needs to be further refined with a life cycle assessment for sustainability, extensive safety measures and a more detailed operations & logistics concept. Two requirements were removed due to redundancy—such as the pointing accuracy no longer being critical for communication—while unmet requirements, including the battery's limited thermal tolerance and the current 75% mission reliability caused by the novel LMC_{OOL} and sampling systems, indicate the need for further development and validation. The orbiter needs more work on structural analysis and its interface with the capsule. For the balloon, more focus on the material strength and permeability is needed. The payload needs more research into receptor chemistry. Next to that, extensive testing and validation for use in a space environment has to be performed.

Bibliography

[1] Alcántara, C., Bugenhagen, F., de Mandt, P., Depoorter, W., van den Heuvel, T., Pérez, C., Ruiz, G., Schaerlaecken, W., Souillart, T., and Umman, A., "Orpheus. Life on Venus? Midterm Report," Tech. rep., TU Delft, 2025.

[2] Alcántara, C., Bugenhagen, F., de Mandt, P., Depoorter, W., van den Heuvel, T., Pérez, C., Ruiz, G., Schaerlaecken, W., Souillart, T., and Umman, A., "Orpheus - Life on Venus? Baseline Report," Tech. rep., TU Delft, 05 2025.

[3] Paardekooper, S.-J., "Project Guide: Design Synthesis Exercise - Life on Venus?" 01 2025.

[4] Seager, M. D., Seager, S., Bains, W., and Petkowski, J. J., "Stability of 20 Biogenic Amino Acids in Concentrated Sulfuric Acid: Implications for the Habitability of Venus' Clouds," *Astrobiology*, Vol. 24, No. 4, 2024, pp. 386–396.

[5] Greaves, J. S., Richards, A. M. S., Bains, W., Rimmer, P. B., Clements, D. L., Seager, S., Sousa-Silva, C., Petkowski, J. J., and et al., "Phosphine gas in the cloud decks of Venus," *Nature Astronomy*, Vol. 5, 2021, pp. 655–664.

[6] Seager, S., Petkowski, J. J., Seager, M. D., Grimes, J. H., Zinsli, Z., Vollmer-Snarr, H. R., El-Rahman, M. K. A., Wishart, D. S., Lee, B. L., Gautam, V., Herrington, L., Bains, W., and Darrow, C., "Stability of nucleic acid bases in concentrated sulfuric acid: Implications for the habitability of Venus' clouds," *Proceedings of the National Academy of Sciences*, Vol. 120, No. 25, 2023, pp. e2220007120.

[7] Petkowski, J. J., Seager, S., Grinspoon, D. H., Bains, W., Ranjan, S., Rimmer, P. B., Buchanan, W. P., Agrawal, R., Mogul, R., and Carr, C. E., "Astrobiological Potential of Venus Atmosphere Chemical Anomalies and Other Unexplained Cloud Properties," *Astrobiology*, Vol. 24, No. 4, 2024, pp. 343–370, PMID: 38452176.

[8] Duzdevich, D., Nisler, C., Petkowski, J. J., Bains, W., Kaminsky, C. K., Szostak, J. W., and Seager, S., "Simple Lipids Form Stable Higher-Order Structures in Concentrated Sulfuric Acid," *Astrobiology*, Vol. 25, No. 4, April 2025, pp. 270–283.

[9] Spacek, J., Rimmer, P., Owens, G. E., Cady, S. R., Sharma, D., and Benner, S. A., "Production and Reactions of Organic Molecules in Clouds of Venus," *ACS Earth and Space Chemistry*, Vol. 8, No. 1, 01 2024, pp. 89–98.

[10] Seager, S., Petkowski, J. J., Carr, C. E., Grinspoon, D., Ehlmann, B., Saikia, S. J., Agrawal, R., Buchanan, W., Weber, M. U., French, R., Klupar, P., and Worden, S. P., "Venus Life Finder Mission Study," 2021.

[11] Prak, A., Leeuwis, H., Heideman, R., Leinse, A., and Borst, G., "Integration of Optical Waveguides and Microfluidics in a Miniaturized Antibody Micro-Array System for Life Detection in the NASA/ESA ExoMars Mission," *Proceedings of SPIE - The International Society for Optical Engineering*, 02 2011.

[12] Booth, G., *Naphthalene Derivatives*, John Wiley & Sons, Ltd, 2000.

[13] Parnell, J., Cullen, D., Sims, M. R., Bowden, S., Cockell, C. S., Court, R., Ehrenfreund, P., Gaubert, F., Grant, W., Parro, V., Rohmer, M., Sephton, M., Stan-Lotter, H., Steele, A., Toporski, J., and Vago, J., "Searching for Life on Mars: Selection of Molecular Targets for ESA's Aurora ExoMars Mission," *Astrobiology*, Vol. 7, No. 4, 2007, pp. 578–604, PMID: 17723091.

[14] Glavin, D. P., Dworkin, J. P., Alexander, C. M. O., Aponte, J., Baczynski, A. A., Barnes, J. J., Bechtel, H. A., and Berger, E. L., "Abundant ammonia and nitrogen-rich soluble organic matter in samples from asteroid (101955) Bennu," *Nature Astronomy*, Vol. 9, No. 2, 2025, pp. 199–210.

[15] Callahan, M. P., Smith, K. E., Cleaves, H. J., Ruzicka, J., Stern, J. C., Glavin, D. P., House, C. H., and Dworkin, J. P., "Carbonaceous meteorites contain a wide range of extraterrestrial nucleobases," *Proceedings of the National Academy of Sciences*, Vol. 108, No. 34, 2011, pp. 13995–13998.

[16] Martins, Z., Botta, O., Fogel, M. L., Sephton, M. A., Glavin, D. P., Watson, J. S., Dworkin, J. P., Schwartz, A. W., and Ehrenfreund, P., "Extraterrestrial nucleobases in the Murchison meteorite," *Earth and Planetary Science Letters*, Vol. 270, No. 1, 2008, pp. 130–136.

[17] Monnard, P.-A. and Deamer, D. W., "Membrane self-assembly processes: Steps toward the first cellular life," *The Anatomical Record*, Vol. 268, No. 3, 2002, pp. 196–207.

[18] Chen, I. A., Roberts, R. W., and Szostak, J. W., "The Emergence of Competition Between Model Protocells," *Science*, Vol. 305, No. 5689, 2004, pp. 1474–1476.

[19] Poater, J., Duran, M., and Solà, M., "Aromaticity Determines the Relative Stability of Kinked vs. Straight Topologies in Polycyclic Aromatic Hydrocarbons," *Frontiers in Chemistry*, Vol. Volume 6 - 2018, 2018.

[20] Oba, Y., Takano, Y., Naraoka, H., Furukawa, Y., Glavin, D. P., Dworkin, J. P., and Tachibana, S., "Extraterrestrial hexamethylenetetramine in meteorites—a precursor of prebiotic chemistry in the inner solar system," *Nature Communications*, Vol. 11, No. 1, 2020, pp. 6243.

[21] Vinogradoff, V., Duvernay, F., Danger, G., Theulé, P., and Chiavassa, T., "New insight into the formation of hexamethylenetetramine (HMT) in interstellar and cometary ice analogs," *A&A*, Vol. 530, 2011, pp. A128.

[22] Arosio, P., Barolo, G., Müller-Späth, T., Wu, H., and Morbidelli, M., "Aggregation Stability of a Monoclonal Antibody During Downstream Processing," *Pharmaceutical Research*, Vol. 28, No. 8, 2011, pp. 1884–1894.

[23] Ma, H., Ó'Fágáin, C., and O'Kennedy, R., "Antibody stability: A key to performance - Analysis, influences and improvement," *Biochimie*, Vol. 177, 2020, pp. 213–225.

[24] Navaneeth, A. G. and Karthikeyan, S., "A comprehensive investigation of the biophysical approach for aptamer functionalized nanoparticles in cancer therapy: a review," *RSC Pharmaceutics*, Vol. 1, No. 5, 2024, pp. 879–903.

[25] Svenson, J. and Nicholls, I. A., "On the thermal and chemical stability of molecularly imprinted polymers,"

Analytica Chimica Acta, Vol. 435, No. 1, 2001, pp. 19–24, MIP 2001.

[26] Sims, M. R., Cullen, D. C., Rix, C. S., Buckley, A., Derveni, M., Evans, D., Miguel García-Con, L., Rhodes, A., Rato, C. C., Stefinovic, M., Sephton, M. A., and Court, R. W., "Development status of the life marker chip instrument for ExoMars," *Planetary and Space Science*, Vol. 72, No. 1, 2012, pp. 129–137, Mars Habitability.

[27] UK Civil Aviation Authority, "Environmental Assessment Report for SaxaVord Spaceport - RFA One Launch Licence," 2024, Accessed: 2025-06-18.

[28] Bossio, D., *Analysis of RFA ONE first stage recovery methods*, Master's thesis, Politecnico di Milano, School of Industrial and Information Engineering, 2023, Master's Thesis.

[29] Bureau, C., "COSPAR Policy on Planetary Protection," Tech. rep., COSPAR, June 2020.

[30] French, R., Mandy, C., Hunter, R., Mosleh, E., Sinclair, D., Beck, P., Seager, S., Petkowski, J. J., Carr, C. E., Grinspoon, D. H., and Baumgardner, D., "Rocket Lab Mission to Venus," *Aerospace*, Vol. 9, No. 8, 2022, pp. 445.

[31] Kemble, S., *Interplanetary Mission Analysis and Design*, Springer, 2006.

[32] Price, K. M., Pidgeon, D., and Tsao, A., "Mass and Power Modeling of Communication Satellites," Nasa contractor report cr-189186, NASA Lewis Research Center, Cleveland, OH, December 1991, Chapter 7.

[33] Delft University of Technology, "AE1222-II: Aerospace Design and Systems Engineering Elements I," `https://brightspace.tudelft.nl`, 2020, Course reader.

[34] Cortes Borgmeyer, S., "Chemical Bi-Propellant Thruster Family," .

[35] Wertz R. James, David F. Everett, J. J. P., *Space Missions Engineering: the new SMAD*, Microcosm Press, NA 2011.

[36] Wiley J. Larson, J. R. W., *Space Mission Analysis and Design*, K1uwer Academic PubUsbers, 1999.

[37] 2NDSpace, "CORE Solar Panels," Tech. rep., 2NDSpace, 2024.

[38] Plemel, R. A., Warhaut, M., and Martin, R., "ESA Station Tracking Network (ESTRACK) Augmented by the Second Deep Space Antenna at Cebreros/Spain," *SpaceOps 2006 Conference*, 2006.

[39] Mitchell, G., "Investigation of Hamming, Reed–Solomon, and Turbo Forward Error Correcting Codes," 2009, See page 15. Available at: `https://apps.dtic.mil/sti/tr/pdf/ADA505116.pdf`.

[40] Ugochi, D. H. and Ezenugu, I. A., "Analysis of Antenna Point Loss in Satellite Communication Link," *Science and Technology Publishing (SCI & TECH)*, Vol. 3, No. 10, Oct 2019, pp. 643–648, SCITECHP420156. ISSN: 2632-1017. Available at: `https://www.scitechpub.org/wp-content/uploads/2021/03/SCITECHP420156.pdf`.

[41] Wakefield·, R. M., "ANALYSIS OF THE HEAT-SHIELD EXPERIMENT ON THE PIONEER-VENUS F.NTRY PROPES," .

[42] Mooij, E., *Re-entry Systems*, Springer Aerospace Technology, 2024.

[43] V. Carandente1, R. Savino1, M. I. and Boffa, C., "Aerothermal Analysis of a Sample-Return Reentry Capsule," 2013.

[44] Musso, G., "Concurrent design study: Venus Atmosphere Sample Analysis mission," 2022.

[45] John A. Dec, R. D. B., "An Approximate Ablative Thermal Protection System Sizing Tool for Entry System Design," 2006.

[46] Riccio, A., Raimondo, F., Sellitto, A., Carandente, V., and R. Scigliano, D. T., "Optimum design of ablative thermal protection systems for atmospheric entry vehicles," 2017.

[47] Venkatapathy, E., Prabhu, D., Allen, G., Milos, F., and Gasch, M., "Next Generation Thermal Protection Systems for Outer Planet Missions," `https://www.hou.usra.edu/meetings/OPAG2021Aug/eposter/6008.pdf`.

[48] Homero Paula Silva1, Luiz Cláudio Pardini, E. B., "Shear Properties of Carbon Fiber/Phenolic Resin Composites Heat Treated at High Temperatures," `https://www.researchgate.net/publication/306050208_Shear_Properties_of_Carbon_FiberPhenolic_Resin_Composites_Heat_Treated_at_High_Temperatures`, 2016.

[49] Maurizio Natali, L. T. and Rallin, M., "Evaluation of the Thermal Diffusivity of Carbon/Phenolic Composites (CPCs) through Oxy-Acetylene Torch (OAT) Test—Part 1: Experimental Characterization and Preliminary Validation," `https://www.mdpi.com/2073-4360/16/5/577`, 2024.

[50] S.D. Dorfman, "Final Report System Design of the Pioneer Venus Spacecraft," Tech. rep., NASA Ames Research Center, 07 1973, Volume 1, Executive Overview.

[51] Murphy, K. J., "Orion Crew Module Aerodynamic Testing," Tech. rep., NASA Langley Research Center, Hampton, Virginia, 2011.

[52] Kontinos, D., "Post-Flight Evaluation of Stardust PICA Forebody Heatshield Material," Tech. rep., ELORET Corporation, Sunnyvale, 2008.

[53] Fowler, C. P., Orifici, A. C., and Wang, C. H., "A review of toroidal composite pressure vessel optimisation and damage tolerant design for high pressure gaseous fuel storage," *International Journal of Hydrogen Energy*, Vol. 41, No. 47, 2016, pp. 22067–22089.

[54] Eko, A. J., Epaarachchi, J., Jewewantha, J., and Zeng, X., "A review of type IV composite overwrapped pressure vessels," *International Journal of Hydrogen Energy*, Vol. 109, 2025, pp. 551–573.

[55] Roh, H., Hua, T., and Ahluwalia, R., "Optimization of carbon fiber usage in Type 4 hydrogen storage tanks for fuel cell automobiles," *International Journal of Hydrogen Energy*, Vol. 38, No. 29, 2013, pp. 12795–12802.

[56] Jonathan Morgan, E. V., "Thermal Protection System Design of Aerocapture Systems for Uranus Orbiters," Tech. rep., NASA Ames Research Center, Moffett Field, 2023.

[57] Matthew L. Zwicker, R., "Pack Density Limitations of Hybrid Parachutes," Tech. rep., Airborne Systems North America, Santa Ana, 2013.

[58] 2NDSpace, "2NDSpace SOLO ICD 2.0," Tech. rep., 2NDSpace, 02 2024.

[59] *The GeneSat-1 Microsatellite Mission: A challenge in Small*

Satellite Design, 2006, Paper: SSC06-IV-8.

[60] Young, W. C. and Budynas, R. G., *Roark's Formulas for Stress and Strain*, McGraw-Hill, 2001, 7th edition.

[61] Yan, G., Tan, M. J., Crivoi, A., Li, F., Kumar, S., and Nicholas Chia, C. H., "Improving the mechanical properties of TIG welding Ti-6Al-4V by post weld heat treatment," *Procedia Engineering*, Vol. 207, 2017, pp. 633–638.

[62] NASA, *Materials Data Handbook*, NASA Marshall Space Flight Center, 1972.

[63] Delft, T., "Lecture notes - Crippling - Johnson-Euler parabola - buckling of a stiffened panel," .

[64] LIROS, "Rope Catalogue 20024/2025," Tech. rep., LIROS, 2025.

[65] Hall, J., Fairbrother, D., Frederickson, T., Kerzhanovich, V., Said, M., Sandy, C., Ware, J., Willey, C., and Yavrouian, A., "Prototype design and testing of a Venus long duration, high altitude balloon," *Advances in Space Research*, Vol. 42, No. 10, 2008, pp. 1648–1655.

[66] Moroz, V., Ekonomov, A., Golovin, Y., Moshkin, B., and San'ko, N., "Solar radiation scattered in the Venus atmosphere: The Venera 11,12 data," *Icarus*, Vol. 53, No. 3, 1983, pp. 509–537.

[67] Spectrolab, I., "PV UTJ Cell 5-20-10 Datasheet," Tech. rep., Spectrolab, Sylmar, California, October 2010.

[68] Cutts, J., Baines, K., Dorsky, L., Frazier, W., Izraelevitz, J., Krishnamoorthy, S., Pauken, M., Wallace, M. S., Byrne, P., Seager, S., Wilson, C., and O'Rourke, J., "Exploring the Clouds of Venus: Science Driven Aerobot Missions to our Sister Planet," *2022 IEEE Aerospace Conference (AERO)*, 2022, pp. 1–20.

[69] "Teflon™ FEP properties bulletin," .

[70] for Space Data Systems (CCSDS), C. C., "Lossless Data Compression," Tech. Rep. CCSDS 121.0-B-3, Consultative Committee for Space Data Systems, November 2022, Blue Book, Issue 3.

[71] Roth, Y., Doré, J.-B., Ros, L., and Berg, V., "Turbo-FSK: A New Uplink Scheme for Low Power Wide Area Networks," *HAL Open Science*, 2016, HAL Id: hal-01289883.

[72] Häusler, B., Pätzold, M., Tyler, G., Bertior, V.-P., Bird, M., Dehant, V., Hinson, D., and Simpson, R., "Venus Atmospheric, Ionospheric, Surface and Interplanetary Radio-Wave Propagation Studies with the VeRA Radio-Science Experiment," *ESA Special Publication*, Vol. 1295, 2006.

[73] Balanis, C. A., *Antenna Theory: Analysis and Design*, Wiley, Hoboken, NJ, 4th ed., 2016, See Sections 4.2 (Dipole Radiation Patterns) and 9.5 (Circular Polarization) for crossed-dipole azimuthal omnidirectionality.

[74] Apostol, P., Izraelevitz, J., Goel, A., and Allenspach, M., "Planning and optimal control of a Venus variable altitude aerobot," *Acta Astronautica*, Vol. 232, 2025, pp. 330–341.

[75] "Aluminized Teflon™ Film," .

[76] Jung, H., Jang, C. H., Yeo, I. S., and Song, T.-H., "Investigation of gas permeation through Al-metallized film for vacuum insulation panels," *Elsevier*, 2012.

[77] Masterflex, "Chemical Resistance Chart," Tech. rep., Masterduct Group, 2018.

[78] Dupont, "Polyimide Film Safety in Handling and Use," Tech. rep., Dupont, n.d.

[79] Norgard, "Polyimide Films," Tech. rep., Saint Gobain Tape Solutions, 2018.

[80] Kuraray, "Vectran," Tech. rep., Kuraray, 2014.

[81] Hall, J., Kerzhanovich, V., Yavrouian, A., Plett, G., Said, M., Fairbrother, D., Sandy, C., Frederickson, T., Sharpe, G., and Day, S., "Second generation prototype design and testing for a high altitude Venus balloon," *Advances in Space Research*, Vol. 44, No. 1, 2009, pp. 93–105.

[82] Hall, J. L., Cameron, J., Pauken, M., Izraelevitz, J., Dominguez, M. W., and Wehage, K. T., "Altitude-Controlled Light Gas Balloons for Venus and Titan Exploration," *AIAA Aviation 2019 Forum*, 2019.

[83] Drew, D. and Lahey, R., "The virtual mass and lift force on a sphere in rotating and straining inviscid flow," *International Journal of Multiphase Flow*, Vol. 13, No. 1, 1987, pp. 113–121.

[84] Hall, J. L., Pauken, M., Schutte, A., Krishnamoorthy, S., Aiazzi, C., Izraelevitz, J., Lachenmeier, T., and Turner, C., "Prototype Development of a Variable Altitude Venus Aerobot," *AIAA AVIATION 2021 FORUM*, 2021.

[85] Precision, S., "Eccentric Diaphragm Pumps for Gases Datasheet," Tech. rep., Schwarzer Precision, n.d.

[86] Controls, M., "MV602L SOLENOID VALVE DATASHEET," Tech. rep., Marotta Controls, n.d.

[87] Lei, Y. P., "Thermodynamic Study for Venus Balloon," *Advanced Materials Research*, Vol. 433, 2012, pp. 45–50.

[88] Izraelevitz, J., Pauken, M., Krishnamoorthy, S., Goel, A., Aiazzi, C., Dorsky, L., Cutts, J., Hall, J. L., Turner, C., and Lachenmeier, T., "Subscale Prototype and Hangar Test Flight of a Venus Variable-Altitude Aerobot," *2022 IEEE Aerospace Conference (AERO)*, 2022, pp. 1–11.

[89] Preston, R. A. et al., "Determination of Venus Winds by Ground-Based Radio Tracking of the VEGA Balloons," *Science*, Vol. 231, No. 4744, 1986, pp. 1414–1416.

[90] Sagdeev, R., Linkin, V., Blamont, J., and Preston, R., "The VEGA Venus balloon experiment," *Science (New York, N.Y.)*, Vol. 231, 04 1986, pp. 1407–8.

[91] Fernandez, D. M., Torregrosa, A., Weiss-Penzias, P. S., Zhang, B. J., Sorensen, D., Cohen, R. E., McKinley, G. H., Kleingartner, J., Oliphant, A., and Bowman, M., "Fog Water Collection Effectiveness: Mesh Intercomparisons," *Aerosol and Air Quality Research*, Vol. 18, No. 1, 2018, pp. 270–283, © Taiwan Association for Aerosol Research.

[92] Elshennawy, A. A., Abdelaal, M. Y., Hamed, A. M., and Awad, M. M., "Evaluating Mesh Geometry and Shade Coefficient for Fog Harvesting Collectors," *Water Resources Management*, Vol. 37, No. 41, 2023, pp. 6107–6126, Online publication date: November 14, 2023.

[93] Green, D. W. and Maloney, J. O., editors, *Perry's Chemical Engineers' Handbook*, McGraw-Hill, New York, 7th ed., 1997.

[94] Klemm, O., Schemenauer, R. S., Lummerich, A., Cereceda, P., Marzol, V., Corell, D., van Heerden, J., Reinhard, D., Gherezghiher, T., Olivier, J., Osses, P., Sarsour, J., Frost, E., Estrela, M. J., Valiente, J. A., and Fessehaye, G. M., "Fog as a Fresh-Water Resource: Overview and Perspectives," *Ambio*, Vol. 41, No. 3, Feb. 2012, pp. 221–234.

[95] Seager, S., Carr, C. E., Grinspoon, D., Petkowski, J.,

Ehlmann, B., Bywaters, K., King, I., de Jong, M., Saikia, S., Zacny, K., Agrawal, R., Iakubivskyi, I., and Buchanan, W., "Venus Atmosphere and Cloud Particle Sample Return for Astrobiology: NIAC Phase I Study Final Report," Tech. Rep. 80NSSC22K0759, NASA Innovative Advanced Concepts (NIAC), Jan. 2023, Contract period: 04/01/2022 to 12/31/2022.

[96] Wee, S. and Aris, A., "Revisiting the "forever chemicals", PFOA and PFOS exposure in drinking water," *npj Clean Water*, Vol. 6, 2023, pp. 57.

[97] Creative Biolabs, *Microfluidic Accessories–Tubing (CAT#: MFMM-1123-JS11) Datasheet*, Creative Biolabs, 2025, Used for microfluidic liquid control and pump-to-chip connections; research use only.

[98] Bartels Mikrotechnik GmbH, *The Bartels Pump BP7 - Tubing Datasheet*, Bartels Mikrotechnik GmbH, 2024, Double-diaphragm piezoelectric micropump for liquid/gas with tubing interface; operating range 1-140mbar, 0-70C, internal volume 30uL, burst pressure 1.5bar, weight 2g.

[99] Bartels Mikrotechnik GmbH, *Microfluidic Accessories Catalogue, v1.12*, Bartels Mikrotechnik GmbH, June 2025, Catalogue of tubing, valves, filters, connectors and other microfluidic accessories for mp6-series pumps.

[100] memetis GmbH, *Normally Closed Microvalve Classic (MVL-22-NC-08) Datasheet, v1.6*, memetis GmbH, February 2025, Shape-memory-alloy actuated 2/2-way microvalve; media-separated; suitable for liquids and gases; footprint: 20×5×8.24 mm; internal volume: approx. 5.6–6.5 µL; switching time: <70 ms; leakage: $<1\times10^{-3}$ mbar·L/s; rated for 10 million cycles.

[101] VEGA Grieshaber KG, *Specification sheet SOLITRAC 31*, 4 ... 20 mA/HART - four-wire Radiometric sensor for continuous level and interface measurement.

[102] TE Connectivity / Measurement Specialties, *10K3CG Gold Leadless Chip Thermistor (GA10K3CG3) Datasheet*, TE Connectivity, Sh unik global, March 2019.

[103] TDK Electronics, *Chip NTC Thermistor Commercial Catalog (NTCG Series)*, TDK Electronics AG, Sept. 2024, Commercial-grade SMD NTCG series in sizes 0402–2012; reflow-solderable, RoHS-compliant.

[104] TRUMPF Photonic Components GmbH, "Datasheet: 850 nm Single-Mode VCSEL TO46," May 2023, Ordering number: ULM850-B2-PL-S46FTT.

[105] Adaptive Thermal Management (European Thermodynamics Ltd), *ADV-127-135200-S Thermoelectric (Peltier) Module Datasheet*, European Thermodynamics Ltd, 2022, Single-stage Peltier module: 127 couples, 4A max, 15.4V max, Q_{max} = 34.2 W @ 25 °C, ΔT_{max} = 65 °C, 40×40 mm, sealed silicone lead-wires.

[106] Salvo, P., Verplancke, R., Bossuyt, F., Vanfleteren, J., and Puers, R., "Adhesive bonding by SU-8 transfer for assembling microfluidic devices," *Microfluidics and Nanofluidics*, Vol. 13, 2012, pp. 987–991.

[107] European Central Bank, "Euro foreign exchange reference rates," 2025, Accessed: 2025-06-17.

[108] U.S. Bureau of Labor Statistics, "Consumer Price Index (CPI) for All Urban Consumers," April 2024, Accessed: 2025-06-17.

[109] NASA, "NASA Systems Engineering Handbook," Tech. Rep. NASA/SP-2007-6105 Rev2, NASA Headquarters, Washington, D.C., 2007.

[110] Blanchard, B. S. and Fabrycky, W. J., *Systems Engineering and Analysis*, Pearson Education, 5th ed., 2011.